Single-molecule Fluorescence Studies of KirBac1.1

Emma E. Sadler

DPhil Candidate

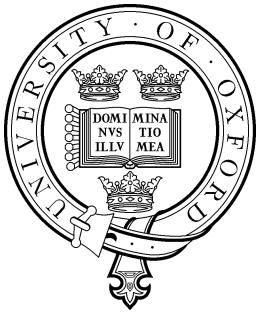
Condensed Matter Physics, Clarendon Laboratory

Life Sciences Interface Doctoral Training Centre

St Hilda's College

Supervisors: Stephen J. Tucker and Achillefs N. Kapanidis

Submitted in partial fulfilment of the requirements for the degree of Doctor of Philosophy



30th March 2015

Declaration

The work described in this thesis was carried in the laboratories of Dr Stephen Tucker, and Dr Achillefs Kapanidis, both of the Clarendon Laboratory, Department of Physics, University of Oxford, between July 2011 and December 2014. All work within this thesis is entirely my own unless otherwise stated in the text. This work has not been previously submitted for any other degree at the University of Oxford, or any other university.

Emma E. Sadler

(December 2014)

Acknowledgements

I must first thank my supervisor, Stephen Tucker, for his support and patience throughout the last few years, not least during the process of putting together this manuscript. I also thank my secondary supervisor Achillefs Kapanidis for use of the fluorescence microscope facilities and informative discussions.

The 'Snowdon' microscope set-up was built by Geraint Evans and Johannes Hohlbein, and is maintained by Geraint with the assistance of Timothy Craggs, who both gave me useful advice regarding data analysis. I also thank Johannes Hohlbein for teaching me how to perform smFRET studies, and in conjunction with Joseph Torella he also wrote the fluorescence burst analysis code.

Lejla Zubcevic spent many hours teaching me wet lab techniques, and providing other forms of support, including her friendship, both during the initial stages of my DPhil and my distantly past MPhys project.

The TREK-2 protein was a gift from Liz Carpenter's lab in the SGC, and was purified by Alexandra MacKenzie, whom I also thank for her friendship and tea-drinking solidarity.

I owe much to my colleagues and office-mates not already mentioned, both past and present: Lauriane Angué, Giovanna Bucci, Geraint Evans, Federico Garza de Leon, Peter May, Conor McClenaghan, Mathew Stracy, Chetan Sharma, Amadeus Stevenson, and Firdaus Wahab tucked away in our corner of the Clarendon; Prafulla Aryal and Matthias Schmidt over in Biochemistry; and Marc Szabo and Eve Weatherill in the CRL.

My experiences and friendships at the DTC have been invaluable, but I am particularly grateful for the continued support and advice of Elspeth Garman, a truly incredible woman and a real inspiration.

I thank everyone at CORC and SHBC for the opportunities to take out my frustrations on the water, and for the opportunity to discover I'm stronger than I thought I could be in more ways than just brute force.

I know my family have always been and always will be there for me when I need them. I wouldn't have come all this way without my parents and grandparents.

My wonderful friends have shared many steps of this journey with me, and helped me to stay sane, whether in 'real' life or more distantly: Emma Grisdale; Sam Tusk; Melissa North; and I particularly thank Kimberly Ralph for proofreading this thesis as well.

And last but not least, a certain Jack J^3 Miller: $9x - 7i > 3(3x - 7u)$. I suppose I have to read yours now...

List of Figures

1.1 Equivalent RC circuit for the membrane-ion channel system 3
1.2 A typical action potential in a mammalian neuron 6
1.3 A model cell and its ionic gradients 7
1.4 A stereotypical Kir current trace 8
1.5 KirBac1.1 crystal structure [74] 13
1.6 Location of the helix bundle crossing in KirBac1.1 [74] 14
1.7 Proposed gating mechanism of KirBac, from crystal structures [13] 15
1.8 Atomic mechanisms of Förster Resonance Energy Transfer 21
1.9 Nanodisc structure 36

2.1 Expression of codon-optimised KirBac1.1 with cysteine point mutations . . 48
2.2 Size-exclusion chromatography of codon-optimised detergent-solubilised KirBac1.1 with cysteine mutations 49
2.3 SDS-PAGE of cysteine only KirBac1.1 50
2.4 I-V trace of a WT KirBac1.1 channel in DHB 51
2.5 Fluorescence gel of doubly labelled KirBac1.1 52
2.6 Fluorescence spectrophotometry of doubly labelled KirBac1.1 53

3.1 Confocal-in-solution microscopy with ALEX 57
3.2 Photograph of Snowdon: confocal-in-solution with ALEX set up 58
3.3 Diffusion in the confocal observation volume 60
3.4 A stereotypical E-S histogram 62
3.5 Proximal and distal labelling stoichiometry of tetrameric KirBac1.1 62
3.6 Location of the cysteine labelling mutations in KirBac1.1 63
3.7 Preliminary smFRET observations of KirBac1.1 66
3.8 Doubly labelled dsDNA control for microscope alignment 68
3.9 Optimised smFRET signals for all three cysteine only KirBac1.1 70

4.1 Location of the cysteine and activatory point mutations in KirBac1.1 73
4.2 Expression of KirBac1.1 with activatory point mutations 74
4.3 I-V trace of a functional KirBac1.1 (V145L) channel 75
4.4 Exemplary smFRET histogram from experiments 77
4.5 Exemplary graph of smFRET shifts (artificial data) 78
4.6 smFRET shifts for R151C ± V145L solubilised in detergent micelles . . . 80
4.7 smFRET shifts for R151C solubilised in detergent micelles upon a change in pH 83
4.8 smFRET shifts for G249C solubilised in detergent micelles upon a change in pH 85
4.9 Dye-only control smFRET measurements for pH variation 86

5.1 Nanodisc structure 90

5.2 Membrane scaffold protein (MSP) structure 92
5.3 Size-exclusion chromatography of nanodisc-reconstituted KirBac1.1 96
5.4 SDS-PAGE of KirBac1.1 reconstituted into nanodiscs 97
5.5 Exemplary smFRET observation of KirBac1.1 reconstituted into nanodiscs 99
5.6 smFRET shifts for R151C ± V145L reconstituted into nanodiscs 101
5.7 smFRET shifts for G249C ± V145L reconstituted into nanodiscs 103
5.8 smFRET shifts for R151C reconstituted into nanodiscs upon a change in pH 105
5.9 smFRET shifts for G249C reconstituted into nanodiscs upon a change in pH 107
5.10 smFRET shifts for R151C ± PIP_2 reconstituted into nanodiscs 109
5.11 smFRET shifts for G249C ± PIP_2 reconstituted into nanodiscs 111
5.12 Summary of smFRET shifts for nanodisc-solubilised KirBac1.1 112
5.13 Histogram of a smFRET aggregation event 115
5.14 Size-exclusion chromatography of purified TREK-2 120
5.15 Exemplary size-exclusion chromatography of TREK-2 reconstitution 122
5.16 Size-exclusion chromatography of TREK-2 nanodisc reconstitution 123
5.17 SDS-PAGE of TREK-2 nanodisc reconstitution 124

6.1 Structural changes of KirBac1.1 measured by Wang *et al.* (2012) [123] . . . 137
6.2 KirBac1.1 structure: F146 and R151 highlighted 140
6.3 KirBac1.1 structure: plane slices 141
6.4 Cartoon of two possible gating models 143
6.5 Helix bundle crossing "twist-to-shrink" model 144

A.1 Alignment of original and codon-optimised KirBac1.1 sequences 151
A.2 *E*-S* histogram for R151C ± V145L (detergent-solubilised samples) 152
A.3 *E*-S* histogram for R151C with a change in pH (detergent-solubilised samples) 153
A.4 *E*-S* histogram for G249C with a change in pH (detergent-solubilised samples) 154
A.5 *E*-S* histogram for G249C ± V145L (nanodisc-reconstituted samples) . . . 155
A.6 *E*-S* histogram for R151C with a change in pH (nanodisc-reconstituted samples) 156
A.7 *E*-S* histogram for R151C ± PIP_2 (nanodisc-reconstituted samples) 157
A.8 *E*-S* histogram for G249C ± V145L (nanodisc-reconstituted samples) . . . 158
A.9 *E*-S* histogram for G249C with a change in pH (nanodisc-reconstituted samples) 159
A.10 *E*-S* histogram for G249C ± PIP_2 (nanodisc-reconstituted samples) 160
A.11 Obtaining the γ correction factor from smFRET histograms 162

List of Tables

2.1 Restriction digest mixture . . . 41
2.2 Ligation mixture . . . 41
2.3 PCR reaction mixture . . . 42
2.4 PCR heating cycle . . . 42
2.5 Sources of molecular biology reagents . . . 44
2.6 KirBac1.1 purification buffers . . . 46
2.7 KirBac1.1 labelling reaction mixture . . . 46
2.8 KirBac1.1 labelling buffers . . . 47

3.1 Inter-fluorophore distances for KirBac1.1 cysteine mutants . . . 64

4.1 KirBac1.1 point mutations . . . 72
4.2 Cysteine/gating mutation combinations used for smFRET measurements . . 76
4.3 smFRET shifts for R151C ± V145L solubilised in detergent micelles. . . . 79
4.4 smFRET shifts for R151C solubilised in detergent micelles upon a change in pH . . . 82
4.5 smFRET shifts for G249C solubilised in detergent micelles upon a change in pH . . . 84
4.6 Summary of the smFRET results from detergent-solubilised KirBac1.1 . . . 88

5.1 MSP purification wash buffers . . . 93
5.2 Nanodisc assembly mixture . . . 93
5.3 Nanodisc assembly buffer recipes . . . 93
5.4 smFRET shifts for R151C ± V145L reconstituted into nanodiscs . . . 101
5.5 smFRET shifts for G249C ± V145L reconstituted into nanodiscs . . . 103
5.6 smFRET shifts for R151C reconstituted into nanodiscs upon a change in pH 105
5.7 smFRET shifts for G249C reconstituted into nanodiscs upon a change in pH 107
5.8 smFRET shifts for R151C ± PIP_2 reconstituted into nanodiscs . . . 109
5.9 smFRET shifts for G249C ± PIP_2 reconstituted into nanodiscs . . . 110
5.10 Summary of the smFRET results from nanodisc-reconstituted KirBac1.1 . . 113
5.11 Summary of smFRET shifts for detergent- and nanodisc-solubilised protein 116
5.12 Summary of p-values for detergent- and nanodisc-solubilised protein . . . 117
5.13 Nanodisc assembly mixtures: TREK-2 reconstitution trials . . . 120
5.14 Nanodisc assembly buffer recipes . . . 120

A.1 Correction factors: detergent-solubilised R151C . . . 163
A.2 Corrected smFRET values: detergent-solubilised R151C ± V145L . . . 163
A.3 Corrected smFRET values: detergent-solubilised R151C pH = 7.5 and pH = 5.5 . . . 163
A.4 Correction factors: detergent-solubilised G249C . . . 164

A.5 Corrected smFRET values: detergent-solubilised G249C pH = 7.5 and pH = 5.5 164
A.6 Correction factors: nanodisc-reconstituted R151C 165
A.7 Corrected smFRET values: nanodisc-reconstituted R151C ± V145L 165
A.8 Corrected smFRET values: nanodisc-reconstituted R151C pH = 7.5 and pH = 5.5 165
A.9 Corrected smFRET values: nanodisc-reconstituted R151C ± PIP_2 165
A.10 Correction factors: nanodisc-reconstituted G249C 166
A.11 Corrected smFRET values: nanodisc-reconstituted G249C ± V145L 166
A.12 Corrected smFRET values: nanodisc-reconstituted G249C pH = 7.5 and pH = 5.5 166
A.13 Corrected smFRET values: nanodisc-reconstituted G249C ± PIP_2 166

Contents

Declaration of authorship i

Acknowledgements ii

Abstract 1

1 Introduction 2
- 1.1 Ions and the cell . . . 2
  - 1.1.1 The action potential . . . 5
  - 1.1.2 The origin of the resting membrane potential . . . 5
  - 1.1.3 Dysfunction and disease . . . 8
- 1.2 Potassium channels . . . 9
- 1.3 Kir channels: inwardly rectifying potassium channels . . . 9
  - 1.3.1 Selectivity: the filter . . . 9
  - 1.3.2 Gating . . . 10
- 1.4 KirBac: a prokaryotic analogue to Kir channels . . . 11
  - 1.4.1 Structure: architecture . . . 12
  - 1.4.2 Structure: gating . . . 12
  - 1.4.3 A proposed gating mechanism . . . 15
  - 1.4.4 Examinations of the gating mechanism of KirBac1.1 . . . 16
- 1.5 Fluorescence microscopy . . . 19
  - 1.5.1 Förster Resonance Energy Transfer (FRET) . . . 19
  - 1.5.2 Fluorescence studies of membrane proteins . . . 20
  - 1.5.3 Bulk (ensemble) averaging *vs* single molecule measurements . . . 26
  - 1.5.4 One molecule at a time . . . 27
  - 1.5.5 Achieving single molecule resolution . . . 30
  - 1.5.6 Alternating-Laser Excitation (ALEX) . . . 32
- 1.6 Towards single-molecule fluorescence studies of KirBac1.1 . . . 34
- 1.7 Nanodiscs . . . 35
  - 1.7.1 Advantages and disadvantages of nanodiscs . . . 35
  - 1.7.2 Nanodiscs in solution . . . 38
- 1.8 Thesis overview . . . 38

2 Expression, purification, and labelling of KirBac1.1 39
- 2.1 Introduction . . . 39
  - 2.1.1 Site-directed point mutations of KirBac1.1 . . . 39
- 2.2 Methods . . . 40
  - 2.2.1 Molecular biology . . . 40
  - 2.2.2 Protein biochemistry . . . 44
- 2.3 Results . . . 47

2.3.1 Molecular biology . . . 47
2.3.2 Protein biochemistry . . . 47
2.4 Conclusions . . . 54

3 Measurement of smFRET in KirBac1.1 55
3.1 Introduction . . . 55
3.2 Methods . . . 56
3.2.1 Confocal-in-solution smFRET . . . 56
3.2.2 Fluorescence-Aided Molecule Sorting (FAMS) . . . 61
3.2.3 Data analysis . . . 64
3.3 Results: smFRET observations . . . 65
3.3.1 First observations . . . 65
3.3.2 Optimisation of signal . . . 67
3.3.3 Resolution achieved . . . 67
3.4 Conclusions . . . 69

4 Monitoring conformational changes in KirBac1.1 using smFRET 71
4.1 Introduction . . . 71
4.1.1 Chapter summary . . . 72
4.2 Activatory gating mutations . . . 72
4.2.1 Selection and creation of mutations . . . 72
4.2.2 Expression levels of gating mutants . . . 74
4.2.3 Functional studies of KirBac1.1 (V145L) . . . 74
4.2.4 Labelling and smFRET . . . 75
4.2.5 Results: exemplary raw data . . . 76
4.2.6 Results: exemplary smFRET shift data . . . 76
4.2.7 Results: R151C as the reporter site . . . 79
4.2.8 Discussion: activatory mutations . . . 80
4.3 Inhibition by H^+ . . . 81
4.3.1 Sample preparation . . . 81
4.3.2 Results: R151C as the reporter site . . . 82
4.3.3 Results: G249C as the reporter site . . . 83
4.3.4 pH does not affect the fluorescent dyes . . . 85
4.3.5 Discussion: inhibition by H^+ . . . 86
4.4 Inhibition by PIP_2 . . . 87
4.5 Summary of findings . . . 87

5 Nanodisc reconstitution 89
5.1 Introduction . . . 89
5.1.1 Chapter summary . . . 91
5.2 Methods . . . 91
5.2.1 Membrane scaffold protein (MSP) . . . 91
5.2.2 Nanodisc assembly . . . 93
5.2.3 smFRET of KirBac1.1 in nanodiscs . . . 94
5.3 Results: reconstitution of KirBac1.1 into nanodiscs . . . 95
5.4 smFRET from KirBac1.1 reconstituted in nanodiscs . . . 98
5.5 Modulation of smFRET of KirBac1.1 in nanodiscs . . . 98
5.6 Effect of the V145L activatory gating mutation . . . 100
5.6.1 Results: R151C as the reporter site . . . 100
5.6.2 Results: G249C as the reporter site . . . 102

5.7 Inhibition by H^+ . . . 104
5.7.1 Results: R151C as the reporter site . . . 104
5.7.2 Results: G249C as the reporter site . . . 106
5.8 Inhibition by PIP_2 . . . 108
5.8.1 Results: R151C as the reporter site . . . 108
5.8.2 Results: G249C as the reporter site . . . 110
5.9 Summary of results for nanodisc-reconstituted KirBac1.1 . . . 111
5.10 Comparison of the modulatory factors . . . 113
5.11 Comparison of solubilisation methods . . . 114
5.12 Reconstitution of TREK-2 into nanodiscs . . . 118
5.12.1 Introduction . . . 118
5.12.2 Methods . . . 119
5.12.3 Results . . . 121
5.12.4 Discussion and conclusions . . . 125

6 Conclusions and future directions **126**
6.1 Summary of findings . . . 126
6.2 Cautions and caveats . . . 128
6.2.1 Detergent micelles *vs* nanodiscs . . . 128
6.2.2 Eukaryotic *vs* prokaryotic channels . . . 130
6.2.3 Relevance of crystal structures to native conformation . . . 130
6.2.4 Limitations of smFRET data . . . 132
6.3 Implications of smFRET studies of KirBac1.1 . . . 134
6.3.1 Possible structural interpretations . . . 134
6.3.2 Comparison with the findings of Wang *et al.* . . . 136
6.3.3 Inconsistencies with Wang *et al.*: possible reasons . . . 138
6.4 Concluding remarks and future directions . . . 147
6.4.1 KirBac1.1 . . . 147
6.4.2 Other channels . . . 148

A Appendices **150**
A.1 KirBac1.1 amino acid sequence . . . 150
A.2 Original *vs* codon-optimised KirBac1.1 . . . 150
A.3 Exemplary *E**-*S* histograms . . . 152
A.3.1 Detergent-solubilised KirBac1.1 . . . 152
A.3.2 Nanodisc-reconstituted KirBac1.1 . . . 155
A.4 Corrected smFRET values . . . 161
A.4.1 Calculation of corrected smFRET efficiencies . . . 161
A.4.2 Detergent-solubilised KirBac1.1: corrected values . . . 163
A.4.3 Nanodisc-reconstituted KirBac1.1: corrected values . . . 165

Bibliography **183**

Abstract

Inwardly rectifying potassium (Kir) channels are essential for controlling the excitability of eukaryotic cells, forming a key part of the inter-cellular signalling system in multi-cellular organisms. However, as prokaryotic (KirBac) channels are less technically challenging to study *in vitro* and have been shown to be directly homologous to eukaryotic channels, they are often studied *in lieu* of their mammalian counterparts. A vital feature of Kir and KirBac channels is their mechanism for opening and closing, or their gating: this study predominantly features observations of open and/or closed channel populations. A well-characterised member of the KirBac family, KirBac1.1, has been successfully expressed, purified into detergent micelles, and doubly labelled with fluorescent maleimide dyes in order to enable observation of confocal-in-solution Förster Resonance Energy Transfer (FRET) at the single molecule level. Results demonstrate single-molecule FRET signals from KirBac1.1 and therefore represent the first single-molecule FRET observations from a KirBac channel. Perturbation of the open-closed dynamic equilibrium was performed *via* activatory point mutations, changes in pH, and ligand binding. A protocol for reconstitution into nanodiscs was optimised in order to more closely approximate native conditions, and the single-molecule FRET observations repeated. This thesis presents a comparison between measurements made using the detergent solubilisation system and those made using nanodiscs.

Keywords: excitable membranes; potassium channels; Kir; KirBac; dynamic equilibrium; detergent; FRET; single-molecule; confocal; nanodiscs.

Chapter 1

Introduction

1.1 Ions and the cell

The two phospholipid leaflets of the cell membrane create a hydrophobic environment which presents an almost insurmountable barrier to permeating ions; mediating proteins are therefore required to enable the movement of ions across the membrane, one class of which is the ion channels. Ions are implicated in all basic processes of life, as they are the quanta of the physical processes which regulate both electrical activity and salt balance. Dysfunctional ion channels are therefore responsible for many diseases and physiological abnormalities in a wide range of species from *Escherichia coli* to *Homo sapiens* [7]. In addition, membrane proteins make up nearly a third of all human proteins [122], and about half of all current drug targets [48, 129]. This makes reaching an understanding of their function imperative.

Ionic currents are necessary for the electrical signalling that is a key feature of many cells, multicellular systems, and tissues, for example, the action potential in neurons and cardiac myocytes [37, 134]. Ion channels are conductive, and typically obey Ohm's law. Coupled with the fact that the cell membrane can be thought of as an insulating dielectric separating two regions of different voltages, and hence is effectively a capacitor, the membrane-ion channel system can therefore be modelled as an RC circuit, illustrated in Figure 1.1, with the corresponding discharge relation:

$$V = V_0 e^{\frac{-t}{RC}} = V_0 e^{\frac{-t}{\tau}} \tag{1.1}$$

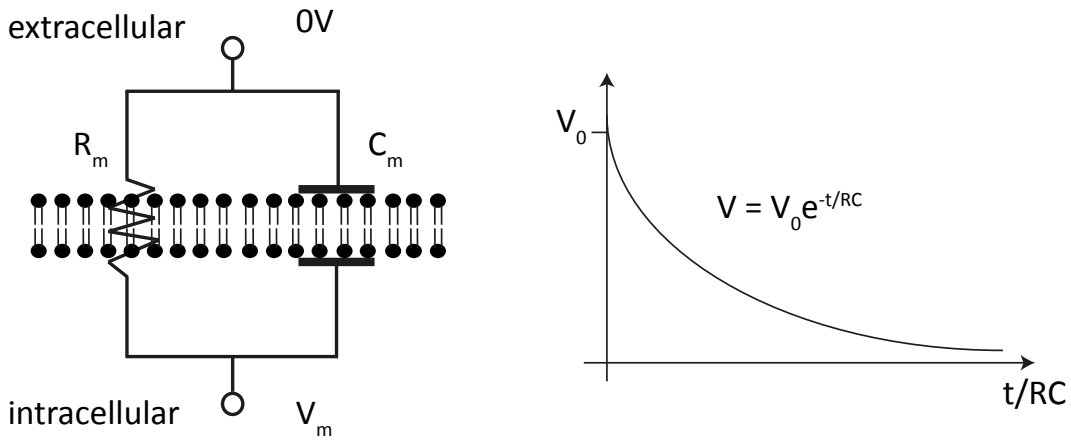


FIGURE 1.1: The membrane-ion channel system is effectively a capacitor (where the lipid bilayer acts as the insulating dielectric) and a resistor (the ion channel) connected in parallel, and can therefore be modelled as an RC circuit with an exponential decay relation. This simple concept underlies the time-dependent response of the membrane to an action potential.

where time constant $\tau = RC$

This voltage and current decay determines many properties of an electrically excitable membrane: in particular, the response time of the membrane to a change in voltage is determined by the time constant of the equivalent RC circuit, and this response time is one of the most important features of the action potential [68].

However, a cell membrane is not an isolated system: its electrical activity is coupled to the chemical consequences of ion movements *via* the electrochemical potential, and there are electrostatic interactions when charges of the same polarity are brought into close proximity. The relevant driving forces are for the ions to diffuse down their chemical gradient to equilibrate the concentrations throughout the system, and for the ions to minimise their electrostatic energy. However, these forces ultimately act in opposition: ions moving to equilibrate the chemical gradient leads to an accumulation of identical ions, the consequence of which is obviously electrostatic repulsion. The electrochemical equilibrium is therefore the equilibrium which corresponds to minimising the electrical and chemical energies of the ions, and will be the point at which the ion fluxes produced by the two opposing processes are equal and opposite (but where ionic *movement* is still occurring). The equation expressing this relationship is derived from the Boltzmann equation of statistical mechanics, which describes the probability distribution for a population of particles

throughout several states of different energies:

$$\frac{p_2}{p_1} = \frac{g_2}{g_1} \exp\left(-\frac{(u_2 - u_1)}{k_B T}\right) \tag{1.2}$$

for a two state system, where p_n is the probability of finding a particle in the *nth* state, which has an associated energy u_n and degeneracy g_n.

Expressed in the more physiologically relevant terms of concentration and charge rather than probability and electrical energy, and with some rearrangement, this yields the Nernst equation:

$$V_{eq} = \frac{RT}{zF} \ln \frac{[C]_2}{[C]_1} \tag{1.3}$$

where z is the ion valence, F is the Faraday constant, $[C]_1$ and $[C]_2$ are the internal and external ionic concentrations, respectively, and V_{eq} is the (membrane) voltage at equilibirum.

V_{eq} is known as the *equilibrium potential* or *resting potential* and its value will be different for each ion in the system: the overall equilibrium potential of the system is the sum of the equilibrium potentials corresponding to each ion species, and is expressed as:

$$V_{total} = \frac{RT}{F} \sum_i \frac{P_i}{z_i} \ln \frac{[C]_2^i}{[C]_1^i} \tag{1.4}$$

where i denotes the ionic species, and P_i is the relative permeability for each ionic species.

V_{total} is also known as the *reversal potential*, as perturbation either side of the equilibrium value will reverse the direction of ion flux.

Control of the ionic concentration either side of the cell membrane is essential for correctly functioning physiological processes within a cell, not only with respect to those which depend on maintaining a correct salt concentration, such as salt/fluid homeostasis in the kidney, but also electrical activity, for example, the action potential, and both intra- and intercellular signalling.

1.1.1 The action potential

The action potential is an electrical signalling phenomenon which has its basis in the conductive properties of the cell membrane. The membrane, and some of its integral proteins, can be treated as components in an equivalent circuit, and their behaviour described by cable theory. This system can be quantitatively described by four non-linear ordinary differential equations relating currents to conductances: these equations comprise the Hodgkin-Huxley model [7, 68, 70].

A key feature of the Hodgkin-Huxley model is that these conductances are a function of both time and voltage, so the system is therefore sensitive to voltage perturbations. An action potential is generated upon application of a voltage perturbation above a certain threshold value, whereby the the conduction elements which control the depolaristaion of the membrane are activated. The conduction elements responsible for repolarisation are activated more slowly, so the membrane voltage will reach a peak before repolarisation occurs. The recovering potential will usually 'overshoot' the resting membrane potential, and a refractory period will follow during which another action potential cannot be generated, regardless of the magnitude of the stimulus [7, 68]. This process is illustrated in Figure 1.2.

The action potential requires a relatively stable resting membrane potential to be established and maintained, although this is achieved through a buffering-type feedback mechanism, as *too* stable a resting potential will result in an inability to generate an action potential event.

1.1.2 The origin of the resting membrane potential

The equilibrium potential for one ionic species is often calculated using the Nernst equation, but as the presence of ion pumps results in an ionic concentration gradient across the cell membrane, it is necessary to instead use the Goldman-Hodgkin-Katz (GHK) equation. For a system containing K^+, Na^+, and Cl^-, a reasonable description of physiological conditions, the GHK equation is:

$$E_m = \frac{RT}{F} \ln\left(\frac{P_{Na}[Na]_{out} + P_K[K]_{out} + P_{Cl}[Cl]_{in}}{P_{Na}[Na]_{in} + P_K[K]_{in} + P_{Cl}[Cl]_{out}}\right) \tag{1.5}$$

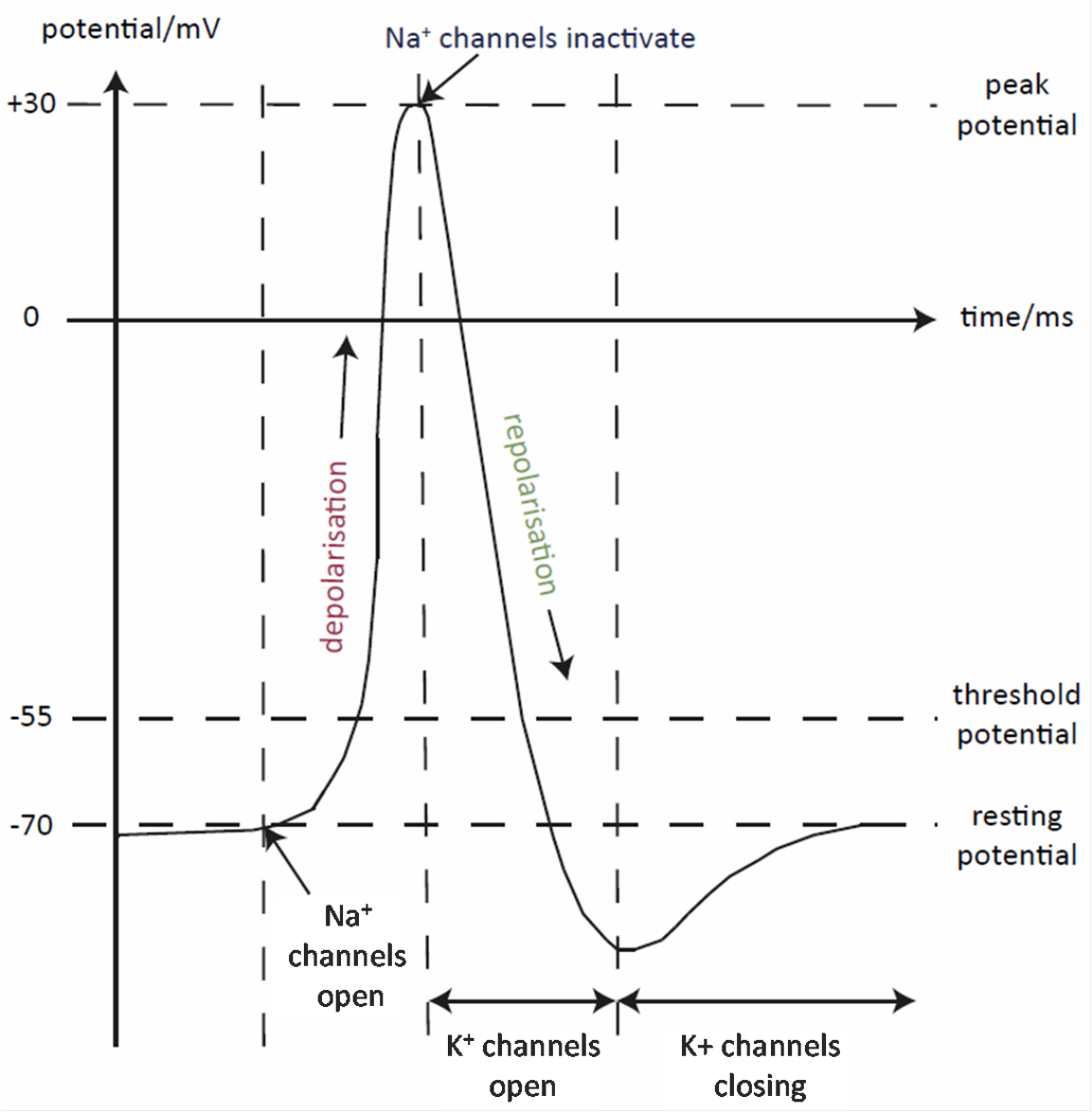


FIGURE 1.2: The action potential occurs in response to a stimulating voltage above a certain threshold: the cell membrane becomes depolarised by the rapid opening of sodium channels (depolarising conduction elements) until a peak voltage is reached, whereupon the sodium channels are inactivated and potassium channels (repolarising conduction elements) are slowly activated, repolarising the membrane. This repolarisation slightly overshoots the resting potential of the membrane, and a refractory period ensues during which no further actions potentials can be generated. The values shown are typical for a mammalian neuron, and will be constant, regardless of the magnitude of the stimulus. The timescale of these events is typically 1-10 ms, but varies depending upon ion channel and cell type.

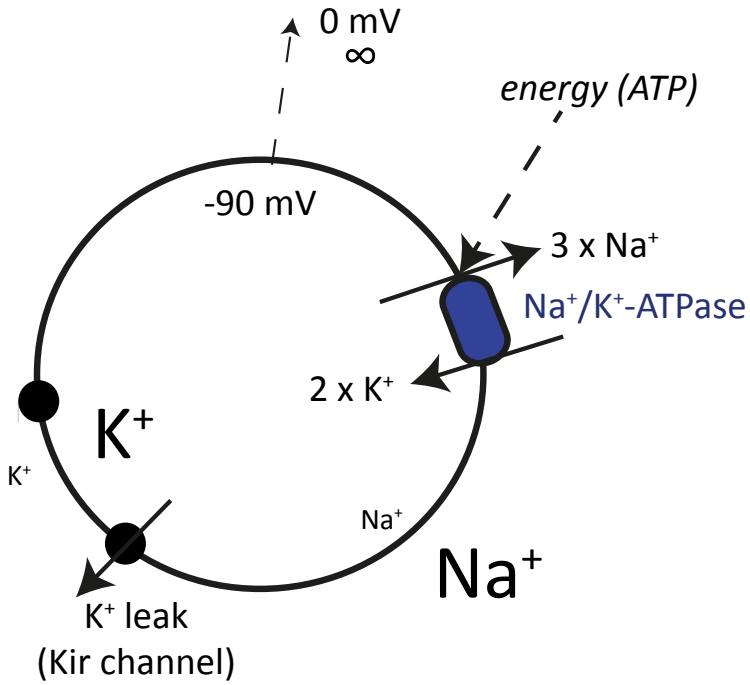


FIGURE 1.3: Outward sodium flux is energetically coupled *via* the Na^+/K^+-ATPase pump to inward potassium flux, whereby three sodium ions leave the cell for every two potassiums ions that enter. This results in an extracellular excess of sodium, an intracellular excess of potassium, and a resting membrane potential of -90 mV. However, potassium 'leak' channels are also present in the membrane, and these are vital for establishing and maintaining the overall resting potential.

where P_i is the permeability for ion species i.

In vivo, this typically results in an excess of *extra*cellular sodium and *intra*cellular potassium. These fluxes are energetically coupled *via* ATP hydrolysis through the conducting components themselves: the ion pumps. These pumps are usually selectively permeable, and in this case, the potassium pump is coupled to the sodium pump in a way which ensures that two potassium ions enter the cell for every three sodium ions that leave, resulting in a resting membrane potential of -90 mV. This equilibrium is illustrated in Figure 1.3.

However, these pumps are not the only integral membrane proteins present. Particularly notable are the potassium 'leak' channels, which allow a small amount of outward flux: an important subset of these are the inwardly rectifying potassium (Kir) channels (shown in Figure 1.3), and a typical I-V curve for one of these channels is shown Figure 1.4. The defining feature of an inwardly rectifying channel is that the inward potassium current produced by a stimulating hyperpolarisation from the potassium equilibrium potential is greater in magnitude than the outward current produced by a depolarisation of the same

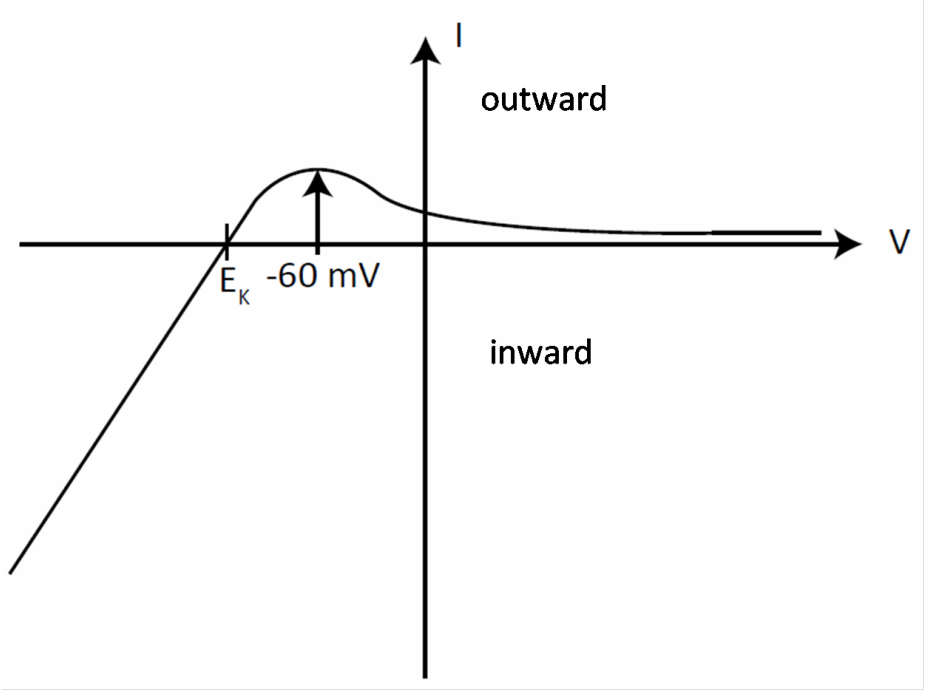


FIGURE 1.4: Although Kir channels are inwardly rectifying, it is the small amount of outward current that acts to establish and maintain the resting membrane potential *via* acting as a buffer for small voltage changes. The potassium reversal potential, E_K, is typically around -90 mV, and the peak outward current occurs near -60 mV.

size, even if extra- and intracellular [K^+] are equal [7]: *i.e.*, the potassium current is said to be *rectified*. However, it is the small outward leak current which establishes – and acts as a buffer to maintain – the potassium reversal potential E_K, and therefore the resting membrane potential.

1.1.3 Dysfunction and disease

The importance of Kir channels is emphasised when considering those implicated in disease. Human Kir2.1 is responsible for the IK_1 current in the heart, which assists repolarisation in preparation for a new action potential; a loss of function in this channel causes Long QT Syndrome, a potentially fatal arrhythmia, whereas a gain-of-function (GoF) mutation may produce a pathologically short QT interval [85, 117]. Other mutations in Kir2.1 cause Andersen-Tawil syndrome, a multi-system disorder, of which one symptom among many is Long QT Syndrome [7].

A group of loss-of-function (LoF) mutations of Kir1.1, primarily (although not exclusively) expressed in the kidney tubules, lead to a form of Bartter syndrome, a disorder of

salt transport and homeostasis which causes hypokalaemia, but also hypercalciuria, resulting in bone loss and kidney stones, as well as arrhythmia [7, 69].

The ATP-sensitive channel Kir6.2 is highly expressed in the pancreatic β cells, and polymorphisms in this channel can lead to neonatal diabetes, another potentially fatal disorder which also causes severe developmental delays in the best case scenarios [65, 99].

Such cases highlight the importance of understanding the coupling of the structure and function of such channels.

1.2 Potassium channels

As stated in the previous section, the vast majority of ion channels are *selectively* permeable, meaning that the conductance with respect to particular ionic species is much higher than for all other ions. This thesis specifically examines inwardly rectifying potassium-selective (Kir) channels, a subset of the vast range of potassium-selective channels. However, as eukaryotic channels are difficult to express and purify, this work focuses on Kir channels originally derived from prokaryotes (KirBac channels), which have been shown to be structurally and functionally homologous to their eukaryotic counterparts [34].

Most potassium channels share similar conduction characteristics and structural features: their selectivity preference is usually $K^+ \sim Rb^+ > Cs^+ \gg Na^+/Li^+$ [47]; and their main structural feature is a long pore which can accommodate multiple ions.

1.3 Kir channels: inwardly rectifying potassium channels

1.3.1 Selectivity: the filter

As stated above, most potassium-selective channels have similar conduction characteristics with respect to ionic preference, thought to be primarily determined by the selectivity filter. One of the most conspicuous structural features of the channel is the long pore: in the case of the inwardly rectifying channels and their relatives, this is formed by a homomeric tetramer and includes a distinguishing sequence (TXGYG or TXGFG) in the region generally accepted to be the selectivity filter [21, 24, 37, 47, 74].

Although Kir channels are inwardly rectifying potassium channels[1] , as discussed above, it is the small degree of outward current which establishes the resting membrane potential and acts as a buffering mechanism for its maintenance, thereby giving these channels a key role in controlling the electrical excitability of the cell. Kir channels known to be implicated in cellular excitability are also known to be strong rectifiers [7], meaning that they allow little outward ion current, and are also mainly active at membrane voltages near to the equilibrium potential [68]. It is currently accepted that this inward rectification occurs because the pore becomes blocked from the intracellular side of the membrane in a voltage-dependent manner by positive cations, most notably Mg^{2+} and cationic polyamines such as spermine [24, 34, 50, 74, 75, 83, 88, 89, 134].

1.3.2 Gating

All ion channels exist in a *dynamic equilibrium* between at least a conducting and a non-conducting state, with one or more conformational changes required to shift between the states. In many channels, these will correspond to "open" and "closed" states, which describes the absence or or presence of constrictions in the ionic pathway along the length of the channel. *Gating* is the term for the process by which these transitions occur, but is also used colloquially to refer to modulatory factors which may affect the gating process.

In a given population of channels, external perturbatory factors can cause global conformational changes which act to 'gate' individual channels, or shift the population equilibrium between the fractions of conducting and non-conducting states for the population [37]. However, while an individual channel may be rapidly switching between the conducting and non-conducting states (gating), the overall fraction of channels in each state throughout the population will remain constant: this is the defining feature of the dynamic equilibrium, in this case relating specifically to the gating mechanism.

As many pathologies are caused by dysfunctional Kir channels [7, 13, 59], it is important to understand their structure and mechanism, and in particular the gating mechanism, including its regulation. However, eukaryotic Kir channels are challenging to express and

[1] Interestingly, their eukaryotic counterparts, the KirBac channels, do not rectify under physiological conditions, although they can be made to do so *via* mechanisms such as point mutations [34].

purify, so it is desirable to find viable alternatives if a high yield and experimental throughput is required. Therefore, this thesis is based upon work performed using one of the prokaryotic counterparts of Kir channels, KirBac1.1; details of its structure, and gating mechanism and regulation are discussed in the next section.

1.4 KirBac: a prokaryotic analogue to Kir channels

It has been shown that KirBac genes, first derived from the Gram-negative bacterium *Burkholderia pseudomallei*, are analogous to eukaryotic Kir genes [34]. The two classes also share significant structural homology [24, 74, 113], implying that studies of KirBac channels could provide insight into the mechanisms of eukaryotic Kir, while being easier to perform by virtue of being easily expressible in bacterial systems such as *E. coli*. It has also been shown that members of the KirBac superfamily are *functionally* as well as structurally and genetically homologous to mammalian Kir [95, 113]: a study to show that KirBac1.1 is a *potassium-selective* channel was published in 2004 [50, 95, 113], followed by a study in 2009 showing that it can be made to act as an *inwardly rectifying* potassium channel [34].

There are some similarities between the prokaryotic and eukaryotic channels with respect to their functional regulation: both KirBac and mammalian Kir channels are inhibited by acidic intracellular pH [50, 61, 101, 102], although KirBac1.1 may require a non-physiologically acidic pH (≤ 5) for any effect to become apparent [50]. However, there are subtle, but significant, differences in the behaviour of eukaryotic and prokaryotic channels with respect to negatively charged lipids and similar ligands [50]. One of the most prolific lipid ligands of eukaryotic Kir channels is phosphatidylinositol 4,5-bisphosphate (PIP_2), which has been shown to have a regulatory effect on members of almost every ion channel family, and specifically an *activatory* effect on all of the eukaryotic Kir channels [50, 61, 101, 102]. However, while PIP_2 is the most common lipid in the eukaryotic membrane, making up $\sim$1% of the total lipids, it and its relatives are often absent from prokaryotic membranes [50], so it would not necessarily be expected to play a role in KirBac regulation. Interestingly, it has however been shown that PIP_2 has an *inhibitory* effect

on KirBac1.1 [34, 42, 52, 123]: this is thought to be due to subtle structural differences at the base of the transmembrane domain (discussed below) [42, 52, 62, 123].

1.4.1 Structure: architecture

The X-ray crystal structure of KirBac1.1 solved to a resolution of 3.65 Å was published in 2003 [74], and is shown in Figure 1.5. KirBac1.1, in common with other potassium channels (for example KcsA [135] and KirBac3.1 [73]), has a transmembrane pore formed from four – identical, in the case of Kir and KirBac – subunits arranged colinearly around a central axis which is coincident with the long pore [37, 74, 134], but with a two-fold axis of symmetry, forming a "dimer of dimers" [74]. The transmembrane region is primarily formed of alpha helices: each subunit, or monomer, contains an inner helix, the pore loop, and an outer helix [74]. The pore loop contains the 'signature' selectivity filter sequence TXGYG, highly conserved among potassium channels [47], with the four pore loops of each of the four monomers arranged in such a way that these sequences form the selectivity filter of the channel; selectivity is thought to be conferred by the geometry of the carbonyl groups of these residues providing a substitute for the hydration shell of the potassium ion [21, 24, 47, 88, 135]. The cytoplasmic domain is dominated by beta sheet and amino acid loops motifs which resemble an immunoglobulin-like β sheet fold [37, 59], and some of which are recognised as the interaction sites for ligands such as G proteins, ATP, H^+, and PIP_2, as well as obviously forming the bulk of the hydrophilic portion of the protein which is in contact with the intracellular solution [13, 24, 67].

1.4.2 Structure: gating

A vitally important structural feature with respect to the dynamics and function of KirBac1.1 is the helix bundle crossing (HBC), the point near the intracellular face of the membrane where the inner and outer helices meet and form a constriction in the conduction pathway, and thought to be the point at which the main gating mechanism acts [13, 37, 74, 134]: its location is shown in Figure 1.6. It has been proposed that one of the key components of this gating mechanism is the slide helix situated near the intracellular

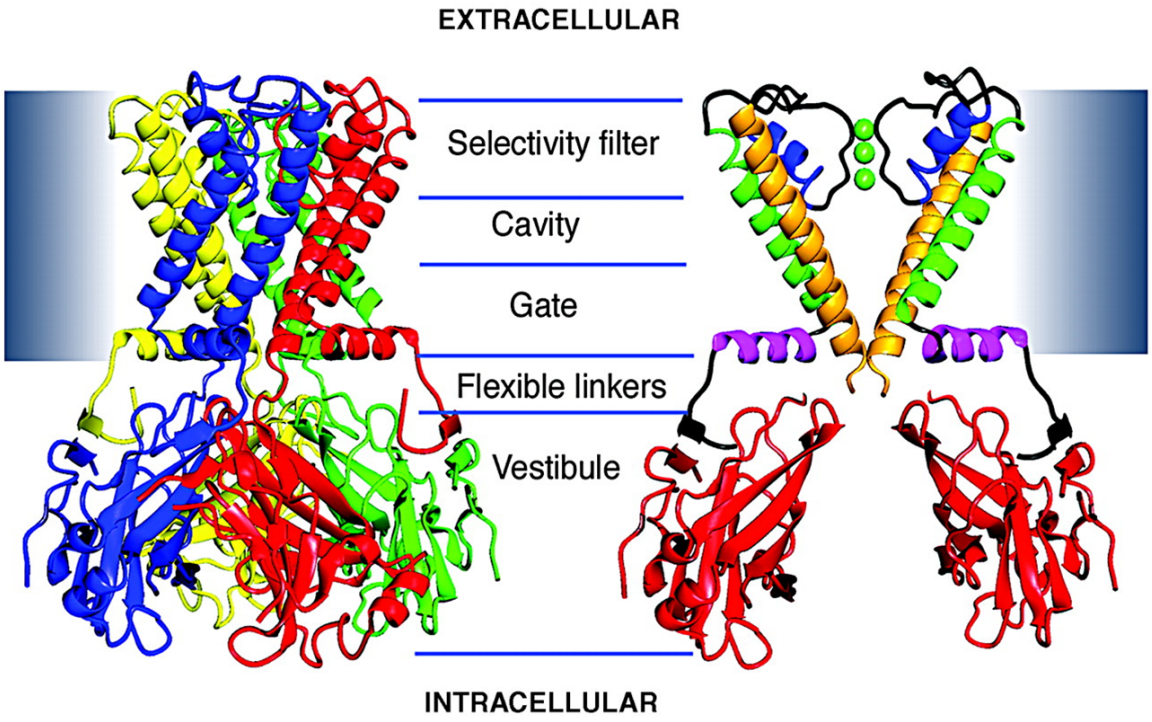


FIGURE 1.5: The structure of KirBac1.1 (from Kuo *et al.* [74]). The membrane is represented by the shaded area. In the left-hand image, each monomer has been shaded a different colour to illustrate the overall tetrameric structure, and in the right-hand image, only two of the four monomers are shown to more clearly illustrate the relative positions of various elements of secondary structure. Each secondary structural motif in the right-hand image is shaded a different colour: slide helix (pink); outer helix (green); pore helix (blue); inner helix (yellow); and C-terminal domain (red). The labels in the centre correspond to the characteristic sections along the path of the ions as they traverse the membrane.

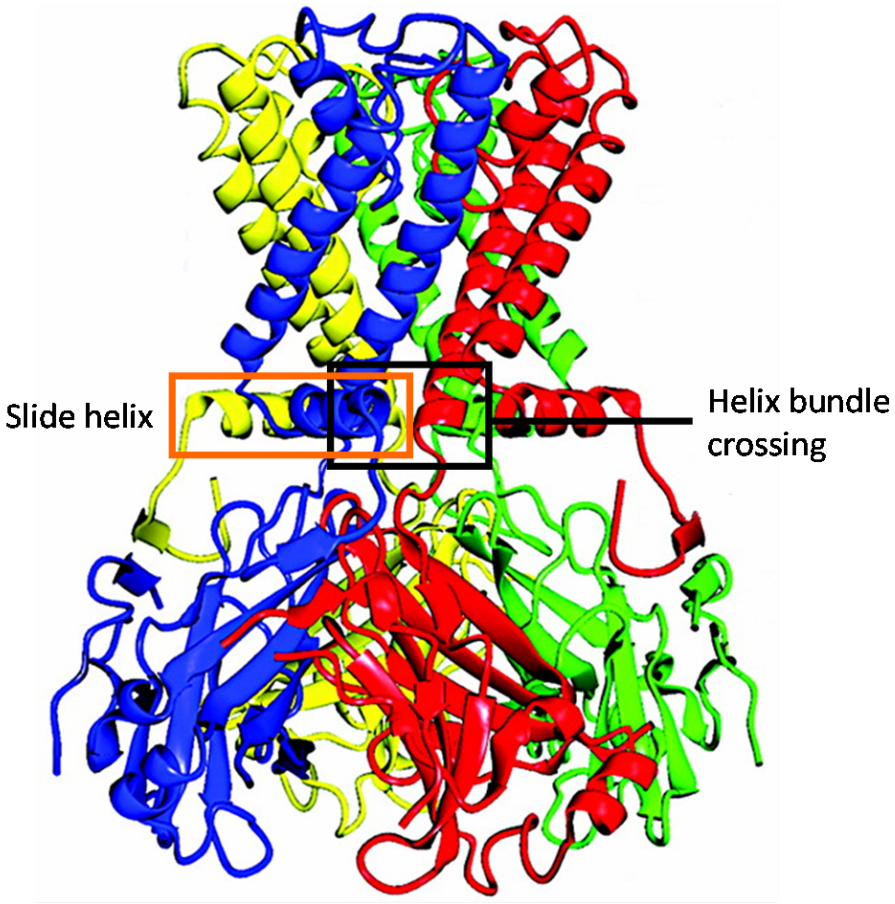


FIGURE 1.6: The helix bundle crossing in KirBac1.1, located at the point near the intracellular face of the membrane where the inner and outer helices meet and form a constriction in the conduction pathway, and thought to be one of the key features implicated in the gating mechanism (adapted from [74]).

face of the membrane at the HBC and running parallel to the face of the membrane: the lateral movement of the four slide helices displaces the outer helices, which in turn causes the inner helices to bend, thereby opening the conduction pathway in a manner reminiscent of a camera aperture or iris [13, 74]. In this way, conformational changes at the HBC are transduced along the entire conduction pathway *via* a cascade of coupled conformational changes. Indeed, the slide helix appears to be conserved in most potassium-selective channels [37], implying that it plays a crucial functional role. In addition, many regulatory mutations, in particular activatory mutations, have been found in close proximity to the slide helix and HBC [95, 136].

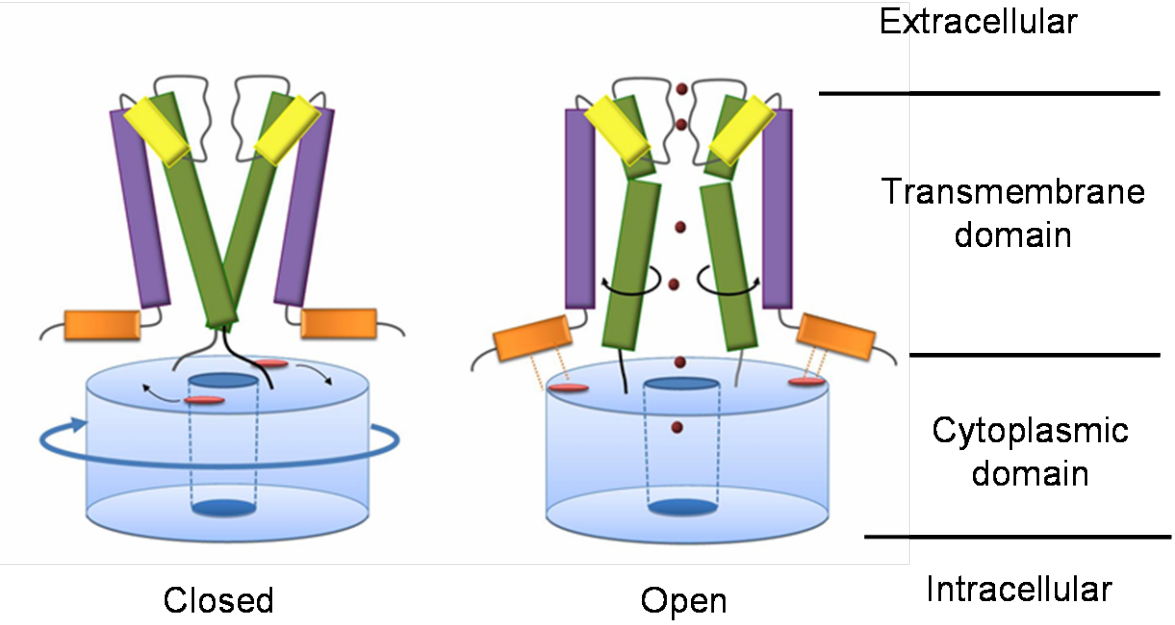


FIGURE 1.7: A cartoon of the proposed gating mechanism of KirBac channels, adapted from Bavro *et al.* [13]; slide helices are shown in orange, outer helices in purple, pore helices in yellow, and inner helices in green. In the closed image, the pore is occluded by the helix bundle crossing, whereas in the open image, the inner helices have acquired a kink and twisted outwards, while the slide helices have moved laterally outwards, opening the pore. The red dots symbolise potassium ions, and their presence indicates that the channel will accommodate permeant ions and is therefore considered to be conductive.

1.4.3 A proposed gating mechanism

Recent X-ray crystallography studies have provided more information about the global conformational changes which are concomitant with the movement of the slide helix. Bavro *et al.* [13] solved the structure of KirBac3.1 thought to be "locked" in the open state to a resolution of 3.05 Å, and compared these results with the structures obtained for KirBac3.1 in the closed state; the open state was confirmed by the observation of regions of electron density in the selectivity filter which were consistent with presence of ions, implying a conductive state. This is one of the first crystallographic observations of an open KirBac channel, and was achieved by mutating key residues which were postulated to stabilise the open state [13]. It has been notoriously difficult to crystallise Kir and KirBac channels in their open state, as it appears that they preferentially crystallise in the closed state, despite having a high open probability in functional studies: it is thought that this is because a closed HBC must correspond to the lowest energy state when the protein is extracted from the membrane, solublised in detergent micelles, and then crystallised into

the far from native-like unit cell [136].

In Bavro *et al.*'s study, a 23° rotation of the cytoplasmic domain relative to the transmembrane domain was observed, and this was concomitant with a lateral movement of the slide helix away from the central long axis. The authors hypothesised that this produced a cascade of conformational changes throughout the rest of the structure: a kink is induced in the inner helices, which produces a rotation in the helices towards the intracellular side of the membrane relative to this point, while the outer helices are displaced outwards, following the motion of the inner helices. This series of movements results in an increase in the pore diameter, thus opening the conduction pathway [13]. When the channel is closed, the constriction of the pore by the inner helices occludes the conduction pathway, thus preventing the permeation of ions. This mechanism is illustrated in Figure 1.7: the lateral movement of the slide helices and the kink in the inner helices is clearly depicted in this cartoon.

1.4.4 Examinations of the gating mechanism of KirBac1.1

The structural rearrangements of KirBac3.1 upon opening and closing proposed by Bavro *et al.* based upon their X-ray crystal structures [13] are consistent with those observed in other potassium channels which have been captured in the open state, such as KcsA [119]. However, the conclusions drawn from the observations by Bavro *et al.* are very different from those drawn by Clarke *et al.*, who also obtained X-ray crystal structures of KirBac3.1 hypothesised to be in the open state [37]. While Clarke *et al.* proposed that the configuration in which the cytoplasmic domain was twisted relative to the transmembrane domain corresponded to a *non-conductive* state of the selectivity filter [37], Bavro *et al.* observed that this twisted configuration was in fact associated with regions of electron density in the ionic pathway which implied that the channel was in the *conductive* state, also noting that the pore pathway was open and unconstricted [13]. Despite these conflicting conclusions, one can still infer that if a twist in the cytoplasmic domain affects the conformation of the transmembrane helices, and therefore the gating state, the helices must be physically coupled to the cytoplasmic domain, meaning that there are linker regions between the helix bundle crossing, the slide helix, and the cytoplasmic domain loops which would act to sta-

bilise the interactions, and potentially to stabilise a particular conformational state [13], as well as provide an interface for ligand interactions [118].

A different method for tracing conformational changes in KirBac channels has been explored by Wang *et al.*, who used Förster Resonance Energy Transfer (FRET) to map the tilting and rotation of secondary structural elements within the cytoplasmic domain of KirBac1.1 upon PIP_2 binding, and thus propose a model of the conformational changes implicated in ligand-induced Kir gating [123]. The authors observed a narrowing of the cytoplasmic pore coupled to PIP_2 binding (implying that PIP_2 binding precipitated a closed state) which was also associated with the tilting of a section of one of the β sheets in the cytoplasmic domain, changes which are consistent with previous observations from eukaryotic Kir channels [62, 127].

However, while PIP_2 has an inhibitory effect on KirBac channels, it has an activatory effect upon eukaryotic Kir channels. This could be partially accounted for by structural differences between Kir and KirBac channels: a study of Kir2.2 revealed that PIP_2 binds to several linker residues which are absent from KirBac1.1 [62], and PIP_2 has also been shown to bind to an equivalent feature in Kir3.2, producing a twist in the cytoplasmic domain which leads to activation [127]. Indeed, this twisted and activated Kir structure is qualitatively similar to that observed in KirBac1.1 in the *open* state (in which PIP_2 was absent) by Wang *et al.* [123], implying that a similar mechanism can produce different effects due to subtle divergences in structural details. It is therefore clear that it is necessary to further investigate the importance of this rotation and lateral motion of the cytoplasmic domain and slide helices, respectively, with respect to the gating mechanism, both of eukaryotic Kir, and prokaryotic KirBac channels.

Since the current study was initiated, new crystallographic studies from the MacKinnon laboratory have shown a rotation in the cytoplasmic C-terminal domain of Kir3.2 (referred to as GIRK2) upon gating by a constitutively active mutation, binding of PIP_2 or the G$\beta\gamma$ subunit [127, 128]. A rotation and splaying of the inner helices is induced *via* transduction of a small anticlockwise rotation in the cytoplasmic C-terminal domain through an interaction network formed by clusters of residues located in the G loop, slide helix, and transmembrane helices. A similar interaction network which is also thought to transduce

conformational changes from the cytoplasmic to the transmembrane domains, and hence stablise the open state, has been proposed by Bollepalli *et al.* based on their Molecular Dynamics (MD) simulations derived from examinations of X-ray crystal structures of Kir1.1. However, the authors expressed their concern that a crystal structure does not necessarily reflect the native state of a protein [28].

In addition, it is interesting that PIP_2 and the activatory mutation of Kir3.2 have an additive effect upon gating, whereby both effects produce a greater degree of rotation in the cytoplasmic domain than one perturbating factor alone [127, 128]. There is also evidence from MD simulations of KcsA that subtle conformational changes and voltage-induced displacement of potassium ions in the selectivity filter means that the filter itself can act as a secondary gate *via* two peptide linkages reorienting to stabilise a nonconductive state. This mechanism has been tentatively proposed as being responsible for C-type (slow) inactivation and related phenomena in potassium channels [21].

However, X-ray crystallography and studies utilising X-ray data can only provide a static view in a non-native environment of what is an inherently dynamic system: conformational changes not only depend on the environment (a lipid membrane *vs* a detergent micelle in the case of channels), but Brownian motion. Crystallographic methods rely on non-physiological thermodynamics and are therefore unlikely to be compatible with observing the dynamic range of channel behaviours that arise from the physiological variation in thermodynamics and give rise to their dynamic behaviour. Although there is a considerable volume of MD studies which incorporate both a model membrane and Brownian oscillations, it is still desirable and necessary to study global conformational changes if not *in vivo*, then at least in real time under conditions which more closely approximate the native environment than a crystallised unit cell.

Fluorescence microscopy, and in particular single-molecule fluorescence, described in detail below, is a versatile method which enables real time conformational measurements of a wide range of proteins, including membrane proteins such as ion channels, thereby coupling functional activity to structural changes. This thesis exploits single-molecule fluorescence microscopy in order to address the coupling of gating to regulation in KirBac1.1.

1.5 Fluorescence microscopy

Fluorescence is a form of luminescence: a photon is absorbed by a fluorophore, which is excited to a state of higher energy and then decays radiatively, emitting a photon of a lower energy, and therefore a longer wavelength. There exist a wide range of possible fluorophores suitable for biophysical studies, from naturally occurring amino acids such as tryptophan [121], to fluorescent proteins such as GFP, to small organic molecules. These are typically directly attached to the protein of interest covalently, and the protein is then said to be *labelled*. The fluorescence of a labelled protein sample can be measured in several different ways, the simplest being a fluorescence spectrometer, or fluorimeter, which illuminates a sample solution in a cuvette, and measures the fluorescence emission, in much the same manner as a spectrophotometer would measure absorption/extinction.

A variety of fluorescence microscopes can also be used. The most common arrangement is an epifluorescence microscope, where the donor is excited and its emission detected through the same optical path. The emission signal is separated from the excitation signal using filters or dichroic mirrors which exploit the fact that the emission wavelength will be longer than the excitation wavelength. The excitation source is usually a laser to ensure high spatial and temporal coherence of the beam, *i.e.* the beam is focused to a very small area and will have a constant, specified wavelength and phase.

1.5.1 Förster Resonance Energy Transfer (FRET)

Förster Resonance Energy Transfer (FRET) is the non-radiative transfer of molecular excitation energy from an excited donor fluorophore to an acceptor fluorophore *via* a dipole-dipole interaction, resulting in the excitation of the acceptor [78]. The acceptor fluorophore can then decay radiatively, emitting a photon of a longer wavelength, as energy loss occurs through subtle quantum electrodynamic processes. This process is illustrated in Figure 1.8 (A). As shown by the Jablonski energy level diagram in Figure 1.8 (B), the energies of the both the excitatory photon and the non-radiative decay of the donor fluorophore must precisely match the fluorophore energy levels of the donor and acceptor, respectively. There must therefore be a significant degree of overlap in the excitation and emission spectra of

the donor and acceptor fluorophores, as seen in Figure 1.8 (C) which shows the spectra of the commonly used commercially available FRET pair AlexaFluor488 (donor) and AlexaFluor555 (acceptor): the large degree of overlap between AlexaFluor488 emission and AlexaFluor555 excitation indicates that this is a compatible FRET pairing.

However, the transfer of fluorescence energy is very sensitive to the distance between the fluorophores [72], with FRET efficiency E depending on the sixth power of the inter-fluorophore distance r:

$$E = \frac{1}{1 + (\frac{r}{R_0})^6} \tag{1.6}$$

where R_0 is the Förster radius for the FRET pair, the distance at which FRET is 50% efficient and which has to be determined empirically for each FRET dye pair under the relevant experimental conditions.

This exquisite sensitivity to the inter-fluorophore distance underlies FRET's power as a tool for studying proteins; indeed, the technique is often referred to as a "molecular ruler" for its facilitation of the detection and quantification of sub-nanometre distance changes [72, 78]. If the donor and acceptor dyes are attached to the protein of interest in felicitous locations, it is possible to detect distance changes *within* the protein itself, *i.e.* between chosen structural features/domains as the protein undergoes conformational changes. This thereby opens up the possibility of real-time observations coupling a protein's structure to its functional activity.

1.5.2 Fluorescence studies of membrane proteins

Quenching

There are several feasible methods for exploiting FRET in studies of ion channels and other membrane proteins. One is to examine the fluorescence intensity of the donor fluorophore, and its reduction in fluorescence intensity, or *quenching*, as its excitation energy is transferred to an acceptor. This is commonly performed using a fluorimeter, and as such, is considered a bulk measurement technique. However, it can still be used to make useful observations: Gether *et al.* [55] and Swaminath *et al.* [114] both used a thiol-reactive

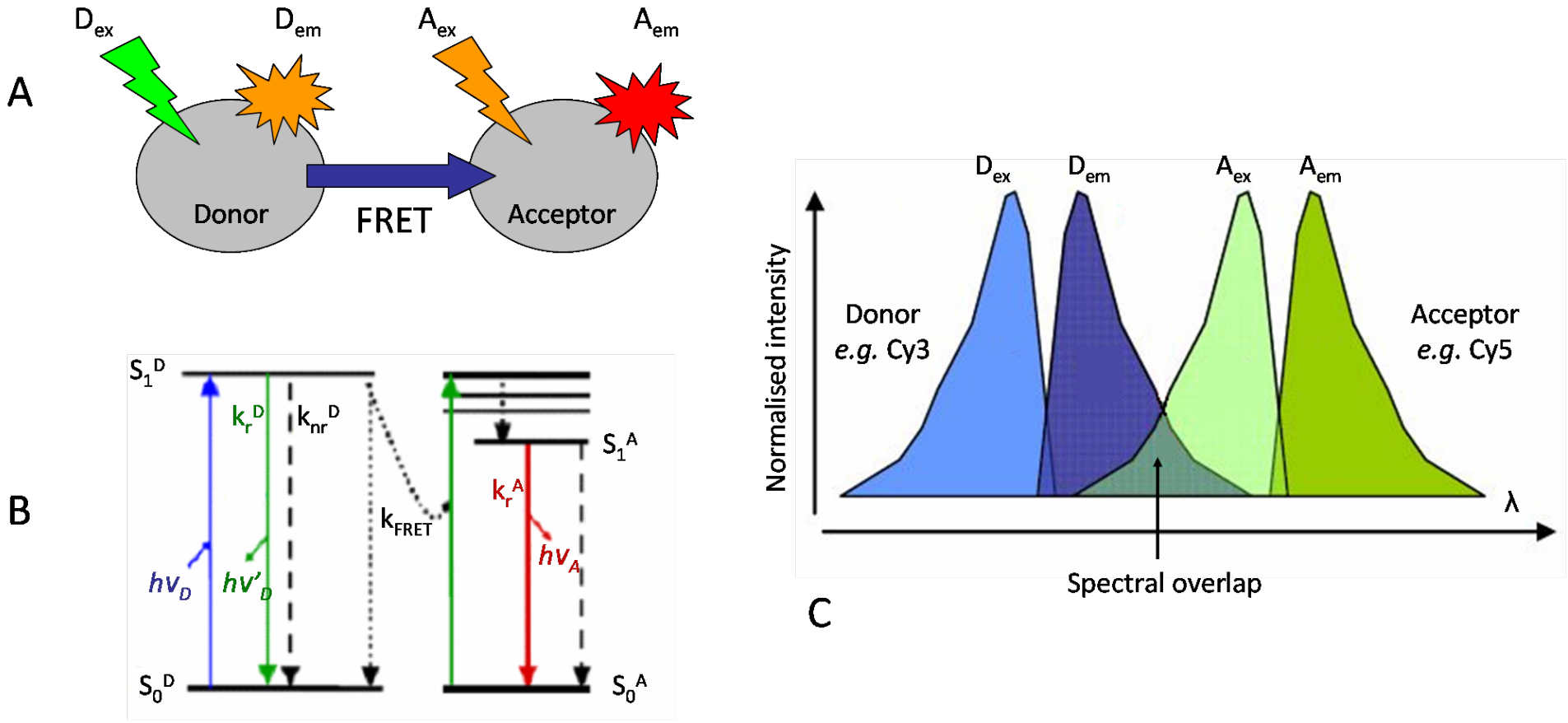


FIGURE 1.8: (A): A cartoon of donor-acceptor FRET. The donor fluorophore absorbs a photon and becomes excited. The donor fluorophore then can either decay radiatively, emitting a photon, or can decay non-radiatively, and transfer its excitation energy to an acceptor fluorophore, which can then decay radiatively and emit a photon. Energy loss occurs through subtle quantum electrodynamic processes, so the wavelength of the photons will increase as an event proceeds.
(B): Jablonski diagram detailing the triplet and singlet states of the donor and acceptor fluorophores, which can be accessed upon excitation by an incident photon. The energies of the excitatory photons must be precisely matched to the energies of these states for excitation, fluorescence transfer, and emission to take place (adapted from [72]).
(C): The emission/excitation spectra of a donor and acceptor fluorophore, shown as a plot of normalised intensity against wavelength. The spectral overlap between donor emission and acceptor excitation indicates that this is a compatible FRET pair.

amide to obtain time traces of donor quenching, and thus determine the kinetics, of agonist binding to the G protein-coupled receptor (GPCR) β-2 adrenergic receptor inducing a conformational change. The details of which transmembrane segments were involved in this conformational change were largely unknown before Gether *et al.*'s experiments [55].

However, the target protein itself is often fluorescent, primarily due to the indole rings of tryptophan residues (although tyrosine and phenylalanine also have appreciable fluorescence) [121]. Using tryptophan as the donor fluorophore has the advantage that it is a naturally occurring amino acid, rather than a synthetic organic molecule, and furthermore, it is relatively rare in wild type proteins. Its fluorescence is sensitive to its environment, which is the property commonly exploited in these studies: Weitzman *et al.* used tryptophan quenching due to iodide and acrylamide measured by solution fluorimetry in order to map solvent accessibility of *E. coli* lac permease, and thus identify putative binding sites [126]. Similar experiments on lac permease, but using a different thiol-reactive amide enabled Wu *et al.* to map solvent accessible sites [130, 131].

Li *et al.* carried out studies which were related with respect to the fluorescence principles, but obtained time courses of the quenching in order to determine the association and dissociation constants of the three subunits of the GPCR $GABA_B$ solubilised in detergent micelles [82]. It is also possible to use tryptophan as a fluorescence quencher: Yao *et al* observed the quenching of a bimane molecule by a tryptophan molecule located in an adjacent helix. The bimane was attached to the end of a transmembrane helix thought to play a key role in stabilising the inactivated structure of the β-2 adrenergic receptor, hence enabling examination of the conformational changes which occur upon ligand binding, and thereby determining association/dissociation constants for the ligand binding reaction [132]. Similar studies have been performed upon the vacuolar H^+-ATPase proton pump, where quenching of dicyclohexylcarbodiimide (PCD) fluorescence at felicitously chosen sites enabled Findlay *et al.* to verify the lipid bilayer accessibility of a glutamate residue thought to be essential to the proton pumping mechanism [54]. However, a significant disadvantage of using tryptophan in fluorescence studies is that its wavelength and brightness is highly sensitive to local influences such as the proximity of protonated residues and temperature [121]: is therefore desirable to exploit other fluorescent molecules.

Acceptor sensitisation

An alternative FRET-based methodology is acceptor sensitisation. This entails measuring the fluorescent lifetime of the donor, or more accurately, the *decrease* in the fluorescent lifetime of the donor, which is indicative of fluorescence transfer to the acceptor: the closer the donor and acceptor, the greater the degree of fluorescence transfer, and the greater the amount by which the donor excited state lifetime is shortened. This can be a surprisingly powerful way of detecting heterogeneity in a protein which exists in more than one conformational state, and has been exploited for several different ion channels. For example, Ghanouni *et al.* used bulk solution fluorimetry to obtain donor lifetime measurements of the fluorescin maleimide-labelled G protein-coupled domain of β-2 adrenergic receptor and thereby detected conformational changes of the domain upon agonist binding [56].

A variant upon FRET using lanthanide fluorescence transfer, known as LRET, coupled with *in situ* electrical measurements, was used by Cha *et al.* to detect the distance changes between subunits of the *Shaker* K^+ channel *via* lanthanide donor lifetime measurements and hence distinguish between two competing models of the conformational changes which occur during gating: translation, and rotation [33]. LRET also has an advantage over FRET with respect to the label's emission anisotropy: as the linker between the protein and the lanthanide atom is much smaller than for organic molecules, the rotation of the lanthanide label is much reduced [105].

However, a particularly powerful use of acceptor-sensitised donor lifetime measurements from bulk solution spectroscopy was demonstrated by Blunck *et al.*, who proposed the existence of a secondary gate located at the selectivity filter in KcsA based on their observation of two populations with distinct tetramethylrhodamine (TMRM) decay lifetimes. These data implied an open state which was not consistent with the known open fraction of the sample and hence the existence of an additional gating site was postulated [25].

Photodestruction

Another way to utilise acceptor sensitisation of donor fluorophores is to examine the ratio of the donor photobleaching rate in the presence and absence of an acceptor: as described above, fluorescence transfer decreases the excited state lifetime of a donor fluorophore,

and this will also reduce the rate of irreversible photodestruction of the donor fluorophore. Therefore, measuring the rate of donor photodestruction is an indirect measurement of donor lifetime, and hence FRET efficiency and donor-acceptor distance. Glauner *et al.* exploited this to measure voltage-dependent distance changes in the voltage-sensing S4 domain in voltage-clamped *Shaker* channels, and thereby measure the degree of tilt and rotation of the helix [57], whereas Riven *et al* applied the same principle to detect conformational changes in GIRK upon G$\beta\gamma$ subunit binding [104]. However, rather than performing bulk fluorimetry in solution, both of these studies in fact used Total Internal Reflection Fluorescence (TIRF) spectroscopy to image channels expressed in the membrane of *Xenopus* oocytes [57, 104], although as signal was collected from the entire illumination region, these were still ensemble-based studies.

Pairing structure and function

The studies from Glauner *et al.* and Riven *et al.* illustrate that it is possible to fluorescently label a protein in a way which will cause minimal interference with its native function [57, 104]. The protein can then be expressed in *Xenopus* oocyte membranes or reconstituted into lipid bilayers, enabling the use of techniques such as voltage-clamp electrophysiology to acquire observations of how the channel's electrical activity might be coupled to its structural activity. Indeed, Cha *et al.* incorporated electrical recordings into their study of the *Shaker* channel's S4 helix [33]. In their study of the same domain, Sonnleitner *et al.* paired their observations of the dimming of TMRM fluorescence with electrical recordings of the *Shaker* channel expressed in *Xenopus* oocyte membranes to detect structural changes in the voltage sensor associated with changes in applied voltage, demonstrating the relationship between the structure and function of this motif [112]. Cheng *et al.* (2007) also expressed the labelled transient receptor potential cation channels TRPV1-Cerulean and TRPV2-eYFP in *Xenopus* membranes to examine heteromer formation by coupling FRET data obtained using wide-field TIRF illumination microscopy with single channel electrical recordings [35]. Although this was still an ensemble-averaged measurement with respect to the fluorescence microscopy, and modelling simulations were applied in order to obtain "single molecule" traces, the concomitant acquisition of electrical measurements

meant that this comprised an elegant demonstration of the coupling between structure and electrical activity in ion channels.

Although the presence of more than one labelled protein might appear to be an intractable problem, it is possible to perform Monte-Carlo-based analysis upon donor photobleaching traces acquired through bulk measurements to obtain FRET values for 'single molecules'. This has been performed in several studies by the Martinac lab in order to examine the open state of the mechano-sensitive protein MscL, for which no X-ray crystal structures of the open state exist [38, 39, 40]. However, as the Monte-Carlo simulations are required in order to make inferences relating to the activity of individual proteins, this is not a true single-molecule experiment, despite the elegant way in which the limitations of ensemble-based measurements were circumvented.

Kir/KirBac

The Nichols group[2] have recently published several interesting studies of Kir and KirBac channels which used FRET-based techniques. Wang *et al.* (2013) exploited GFP/CFP FRET as both a reporter and a way to quantitatively measure formation of the Kir6.2/SUR1 complex [124], but these data were acquired using *bulk* fluorescence spectroscopy of the protein samples in solution. Wang *et al.* (2012), examined FRET changes upon PIP_2 binding of doubly labelled KirBac1.1 reconstituted into liposomes and then imaged *via* fluorescence spectroscopy in solution. This enabled the authors to calculate corresponding distance changes and map them to a known crystal structure in order to propose a detailed model for the conformational changes upon PIP_2 binding, and thereby a molecular model for ligand gating in Kir channels [123]. However, while these are both elegant experiments, it is important to note that these studies, in common with those described above, represent bulk fluorescence measurements based on ensemble-averaging techniques, rather than single-molecule observations.

[2]Washington University in St Louis (WUSTL), St Louis, Missouri

1.5.3 Bulk (ensemble) averaging *vs* single molecule measurements

The distinction between bulk measurements and single-molecule observations is particularly important in relation to proteins which occupy more than one conformational state, and even more so when these conformational states are coupled to their function. While it is clear from the studies described above that ensemble experiments can provide important insights into conformational heterogeneity, some properties are going to be obscured due to the averaging which is intrinsic to a bulk measurement. For example, if a door can exist in two stable states, open or closed, but continually moves between these states, spatiotemporal averaging using certain constraining parameters could produce an apparent single state in which the door is constantly half open.[3]

In a more pertinent example, it can be seen from the studies described above that although a bulk solution measurement such as that made of KcsA by Blunck *et al.* (2006) [25] can demonstrate the presence of two conformational states, and that there is a constant fraction of channels in each state, it cannot be determined whether this is because each individual protein remains stable (*static heterogeneity*), or because each protein molecule is in fact switching between the two states (*dynamic heterogeneity*) with constant rates. As it is known from electrophysiological studies that ion channels in fact rapidly 'flicker' between their conducting and non-conducting (assumed to correspond to open and closed, respectively) states [64], it is vitally important to understand the conformational transitions responsible for thier dynamic heterogeneity, which therefore requires a technique capable of examining single molecules.

Some studies have attempted to observe channels at the single molecule level: as well as measuring bulk fluorescence from the membrane, Sonnleitner *et al.* eliminated channels by photobleaching which resulted in only one fluorescent protein in the TIRF field of view at any time [112]. However, as this requires the photodestruction of many labelled channels, this is neither the most efficient, nor most elegant way of achieving single molecule resolution. In a study from 2008, Blunck *et al.* relied on KcsA channels labelled with TMRM inserting into a supported lipid bilayer far enough from each other to be able to fit point spread functions to each channel, and hence obtain single-molecule FRET mea-

[3] Paraphrased from Senyon Choe [36].

surements of the conformational changes associated with channel opening by fitting the resulting fluorescence and bleaching traces to a hidden Markov model [26]. While this does result in single-molecule observations, and in the relatively native-like environment of a lipid bilayer, in contrast to the more crudely solubilised samples used in fluorimetry, there exist more elegant techniques to obtain single molecule data.

1.5.4 One molecule at a time

Bulk measurements, or ensemble-averaging methods, have produced powerful insights into the mechanism of many membrane proteins, including ion channels. Many familiar techniques are ensemble-averaged methods, and range from calorimetry (classical thermodynamics is a bulk-measurement process), to FRET-based fluorimetry [77].

The term 'ensemble averaging' refers to the fact that the signals and measurements obtained from these experiments are unsynchronised time-averaged distributions which contain contributions from every molecule in the sample, and therefore stochastic variations may be obscured [77]. The vast majority of biological molecules show structural heterogeneity, but often these multiple states cannot be distinguished by ensemble-averaging techniques, even though these methods confer the advantage of low measurement noise. It is therefore necessary to explore single-molecule techniques, which can examine distributions of the relevant physical properties within the sample population, in contrast to averages for the whole system. This is the salient feature which enables single molecule measurements to observe distinct subpopulations within an overall population distribution, and is of particular importance when considering proteins thought to occupy several different conformational and functional states, such as the open and closed populations of ion channels (not to mention subconductance states). These subpopulations can be missed in temporally- or spatially-averaged ensemble measurements, particularly if they correspond to a state which is rare or short-lived.

Molecular heterogeneity

The existence of multiple states of a molecule is known as *molecular heterogeneity*. Molecular heterogeneity can be divided into two types: *static* and *dynamic* heterogeneity. *Static heterogeneity* refers to a collection of several subpopulations of the same protein in different conformational states, or with and without a bound ligand, which are stable over time, and do not interconvert. In *dynamic heterogeneity*, these subpopulations interconvert, but will have reached a stable, but dynamic, equilibrium. It is important to note that in these cases interconversion reactions are still occurring at equilibrium, but the rates of the forward and backward reactions are equal. It is often desirable to measure the distribution of reactants and products present, but this cannot be determined by ensemble-averaging techniques [115]. When examined in single-molecule studies, if the subpopulations are interconverting on a timescale longer than that of the observation period, their distributions can be detected, but if the interconversion timescale is faster than that of the experiment, subpopulation distributions cannot be distinguished and instead a weighted time-averaged mean will be obtained, as for an ensemble-averaged experiment. This is an important consideration when designing confocal-in-solution experiments, as the timescale of observation is determined by the time taken by a freely diffusing molecule to traverse an observation volume, usually on the order of femtolitres, defined by the optics of the system. This can result in an observation time too short to make useful observations, but can often be circumvented by tethering the molecule of interest to a surface and using Total Internal Reflection Fluorescence (TIRF) wide-field microscopy [115] or by changing the diffusion constant of the protein in solution (although this confers the potential to affect the protein's function).

Single-molecule techniques can also be applied to systems which are not in equilibrium, and are a particularly powerful approach for determining the details of reaction pathways. The ability to measure subpopulations means that one can extract the dwell times of each state in a reaction scheme, and thereby determine better estimates of rate constants than can be obtained *via* ensemble-averaging techniques. This is not least because a population distribution histogram can enable detection of previously unknown intermediates, substeps, and very rare alternative pathways [77, 115]. It is also possible to track a single molecule

through its reaction pathway, although this has the potential to be a frustrating experience as, like radioactive decay, chemical reactions are a Poisson process and it is not possible to predict when an individual molecule will undergo a reaction [115].

Synchronicity and stoichiometry

The issue of synchronicity is also pertinent when considering protein systems which contain a degree of dynamic heterogeneity: although many process will be occurring concurrently, they will not be occurring simultaneously in a system which has reached equilibrium, *i.e.* they will occurring asynchronously. This is to be expected, as even if the system was initially perfectly synchronised, the sample is subject to thermal fluctuations driven by Brownian motion, as well as the aforementioned Poisson statistics for its reaction rates. As ensemble-averaging methods capture all of these asynchronous temporal fluctuations, the statistical distributions of the physical properties being measured will be broadened [77]. Furthermore, in a system where proteins occupy more than one conformational or functional state, the fluctuations in the timescale of the transitions between the states often act to obscure the transitions themselves [112]. It is possible to briefly remove the system from equilibrium, essentially 'resetting the clock', but this will still result in only a very short observation time, as thermal fluctuations will rapidly return the system to asynchronicity, and some systems cannot be synchronised by controllable external perturbations [29]. However, if one observes single molecules, the problem of aynchronicity is abolished: a single molecule will always be synchronised with itself.

Another interesting point to consider is the relevance of experiments to the stoichiometry of the cellular processes *in vivo*. Many physiological processes involve very few molecules, and the resulting stochasticity is a vital component of their *in vivo* mechanisms, but this could be obscured by bulk or ensemble measurements. Single molecule observations have the potential to replicate this minimal stoichiometry much more closely [77], and hence have the potential to more accurately capture the conditions within live cells.

1.5.5 Achieving single molecule resolution

Just as for bulk fluorescence studies, there are several different methodologies which can be exploited to achieve single-molecule resolution. As previously described [38, 39, 40], although Monte-Carlo simulations appear to be an ingenious way of breaking the single-molecule barrier, this technique achieves its resolution *via* random sampling of the bulk population, and is therefore not a true single-molecule approach.

The most common approaches for performing single-molecule fluorescence experiments are TIRF and confocal-in-solution fluorescence microscopy. Both techniques are usually performed using epifluorescence microscopes: the excitation light is focused on the sample using the objective, which is also where the emission light enters the optical system, *i.e.* the emission and excitation beams share a common optical pathway, and filters are used to separate the two sources.

Total Internal Reflection Fluorescence (TIRF) microscopy

Total Internal Reflection Fluorescence (TIRF) microscopy exploits the exponentially decaying evanescent field produced when an electromagnetic wave is incident upon the interface between two media of different optical properties, such as glass and water [4, 9]. This produces a wide-field illumination of shallow depth, and is therefore ideal for examining membrane proteins *in situ*. TIRF has been used in several studies of membrane proteins: Akyuz *et al.* [3] and Erkens *et al.* [53] both examined the conformational dynamics of the glutamate transporter Glt_{Ph}; and Wang *et al.* (2014) attempted to distinguish between two models for the opening of the mechano-sensitive ion channel MscL [125]. However, rather than expressing or reconstituting the protein into a membrane, all three studies tethered single molecules to a slide coverslip (*via* the biotin-avidin system) to achieve the relatively static conditions required for observing a single molecule under TIRF. Whereas Akyuz *et al.* directly tethered detergent micelle-solubilised Glt_{Ph} to the coverslip, Erkens *et al.* tethered a lipid bilayer into which Glt_{Ph} had been reconstituted, and thereby obtained slightly different results which they hypothesised may have been due to lipid mediation which would have been absent in a detergent-solubilised system [3, 53]. Wang *et al.* reconstituted MscL into tethered liposomes, although they also had to overcome the potential complica-

tion of more than one protein inserting into liposome, which would render the experiment an ensemble-averaged study. The authors circumvented this issue by using a very low stoichiometry of fluorescently labelled proteins in their reconstitution protocol (5% labelled *vs* 95% unlabelled), and filtering the resulting FRET data to include only those bursts which appeared to result from a single donor/single acceptor system [125].

As TIRF enables experiments to be performed with the membrane protein in a near-native environment, either reconstituted in a lipid membrane, or expressed in a cell membrane, is possible to pair TIRF experiments with electrical recordings, and hence obtain an understanding of how structural and conformational changes are coupled to the electrical activity of the membrane. Borisenko *et al.* performed elegant experiments to examine the formation of gramicidin channels, which was detected *via* both a FRET signal and electrical conduction through the membrane [29, 71]. The Wallace group[4] has paired optical measurements of calcium flux obtained using TIRF microscopy with single-channel recordings of membrane proteins reconstituted into droplet-hydrogel bilayers (DHBs). The pioneering use of the DHB technique was outlined in a publication which presented simultaneous optical observations of calcium flux and single-channel electrical recordings of the α-haemolysin (α-HL) pore [66], and the technique was subsequently extended to measure the dose-dependent response of α-HL to the pore blocker γ-cyclodextrin [32]. The DHB method has since been applied to other pore-forming channels, such as in the group's study of the subconductance states of alamethicin, which also enabled them to examine the coupling between the channel's conformational state and electrical activity [63].

Confocal-in-solution microscopy

Another pathway to single molecule resolution is confocal fluorescence microscopy, also known as confocal-in-solution microscopy. Confocal microscopy uses pinhole apertures and focused laser beams to define a very small observation volume, usually on the order of femtolitres. The pinholes eliminate out-of-focus illumination and thereby enable extremely high resolution ($<\lambda/2$) reconstruction of three dimensional images [109, 120]. Single-molecule confocal-in-solution observations are achieved by exploiting diffusion in solution.

[4]Chemistry Research Laboratory, Department of Chemistry, University of Oxford

The concentration – and diffusion constant – of the sample under observation is chosen such that only one labelled molecule will be traversing the observation volume at a time, where the labels can be excited and emission detected within the short time taken for the protein to cross the confocal volume. This means that although many proteins can be examined *sequentially*, none are being observed *simultaneously* or *concurrently*, and the data can be collated to examine the distribution of states in the form of FRET histograms. A powerful example of this is Fluorescence-Aided Molecule Sorting (FAMS) developed by Kapanidis *et al.* [72, 78, 109], and comprehensively applied by Kapanidis and colleagues to soluble protein systems such as DNA and RNA polymerase to examine the distribution of their conformational states, particularly in relation to the proofreading mechanism [72, 78, 107]. Confocal-in-solution fluorescence microscopy has also been performed upon membrane proteins, although much more rarely, due to their insolubility and instability in water. A notable example is the GPCR β-2 adrenergic receptor: Peleg *et al.* formulated histograms resulting from fluorescence bursts obtained from doubly labelled β-2 adrenergic receptor solubilised in detergent micelles to determine the effect of ligand binding upon the distribution of conformational states, and upon the conformational heterogeneity of these states [96].

1.5.6 Alternating-Laser Excitation (ALEX)

Single-molecule fluorescence microscopy is often used in conjunction with Alternating-Laser Excitation (ALEX). ALEX entails rapid switching between two (or more) excitation lasers, and therefore allows the excitation of at least two fluorophores with different excitation wavelengths [72]. As well as enabling simultaneous monitoring of several different intra-protein distances through FRET, ALEX also enables observations of the interactions between different proteins, or between different domains of a single protein, such as the assembly of a multimeric protein such as an ion channel, or global conformational changes within a protein. In fact, many single-molecule FRET studies, including some of those described above, are performed in conjunction with ALEX in order to properly differentiate FRET signals from the donor and acceptor, vital for constructing population histograms and thereby distinguishing subpopulations [72]. The ability to detect subpopulations means that

confocal-in-solution FRET paired with ALEX is a powerful method of examining dynamic heterogeneity within a sample, and therefore of examining systems whose nature means that they exist in a dynamic equilibrium which is sensitive to outside perturbation. This has been exploited to great effect by Santoso *et al.* who examined the proofreading mechanism of the Klenow fragment of *E. coli* DNA polymerase I by observing the shift between the 'fingers-open' and 'fingers-closed' configurations upon titration of either a matching or mismatching nucleotide, hence inferring the dissociation coefficients, and therefore the strength of the proofreading mechanism [107].

ALEX has been exploited in the study of ion channels, for example in the previously mentioned Glt_{Ph} study by Erkens *et al.* [53]. However, Akyuz *et al.* also examined the Glt_{Ph} transporter under similar (TIRF) conditions, but using a single excitation laser and a series of filters to separate out the donor and acceptor emission and excitation [3], so it is perhaps not immediately obvious what ALEX could add. The distinction between the two studies is subtle, but significant: whereas Akyuz *et al.* used several constraints on the trajectories of single protein molecules to reject those which appeared to be labelled with more than one donor and acceptor [3], Erkens *et al.* exploited ALEX's propensity for easily determining labelling stoichiometry to ensure that only those proteins with a single donor and single acceptor were considered in their analysis [53]. Already having obtained accurate stoichiometric measurements then facilitated their elegant modelling of the branching ratios, rate constants, and dwell times of the conformational transitions of the three monomers [53].

1.6 Towards single-molecule fluorescence studies of KirBac1.1

This thesis presents confocal-in-solution smFRET with two-colour ALEX studies of the inwardly rectifying prokaryotic potassium channel KirBac1.1. The distribution of the conformational states can be observed, and hence the dynamic equilibrium between the open and closed states determined, both with and without external perturbatory factors, such as point mutations, a change in pH, or ligand binding. However, KirBac1.1 is a membrane protein, and hence presents some difficulties for confocal-in-*solution* experiments. While the method used to solubilise KirBac1.1 during purification, *i.e.* solubilisation into detergent micelles, can be transferred directly to fluorescence experiments, this is a far from optimal solution. Detergent micelles have non-ideal optical properties [18], which could produce artefacts in the observed FRET signals, and micelles are prone to aggregation and thermal instability [11]: KirBac1.1 in detergent micelles has a 'bench life' at room temperature of <1 hour (E.S. personal observations). However, even if these problems were overcome, the protein would still be in a non-native environment, in which one cannot be certain that the behaviour exhibited is what would be observed if the protein were expressed or reconstituted in a more native-like environment, such as a lipid bilayer. This can be illustrated by comparing the results of the studies of Glt_{Ph} by Akyuz *et al.* and Erkens *et al.*: whereas Akyuz *et al.* observed rapid flickering between the conformational substates, Erkens *et al.* did not observe this form of dynamic heterogeneity [3, 53]. It is hypothesised that this is because while Akyuz *et al.* made their observations of tethered detergent micelle-solubilised transporters, Erkens *et al.* reconsituted the Glt_{Ph} into tethered lipid bilayers. The lack of rapid conformational dynamics in the former study is thought to be due to the absence of a lipid mediation effect stabilising the substates [3, 53].

There are a handful of membrane proteins that have been shown to be equally functional in both lipid and detergent reconstitution; for example, a comparison has been made between the sodium-tyrosine transporter Tyt1 in both proteoliposomes and detergent-solubilised crude membrane extract [100]. However, these are considered to be exceptionally rare and noteworthy instances. It is therefore imperative to develop an alternative to

detergent micelle-based solubilisation of membrane proteins if meaningful observations of ion channels are to be made. There already exist several methods for overcoming the solubilsation problem, including reconstitution into liposomes and supported lipid bilayers, as described above, but this thesis explores a relatively new development: nanodiscs.

1.7 Nanodiscs

Nanodiscs [5] are effectively a small section of bilayer membrane: they consist of two amphipathic alpha-helical membrane scaffold proteins (MSP), each wrapped around one leaflet of a lipid bilayer in the fashion of a 'belt', as illustrated in Figure 1.9 [14, 18]. The scaffold protein was developed from apolipoprotein A-I (apoA-I), which with high density lipoprotein (HDL) particles is involved in reverse cholesterol transport [8, 87, 90], and indeed, nanodiscs do strongly resemble discoidal HDL particles [87]. The scaffold protein is now available in a range of defined and controllable sizes following the work of Denisov *et al.* to produce a library of modifications to the apoA-I sequence by insertion of amphipathic alpha helix repeats [44, 87]. There was some speculation about which model of lipoprotein particle structure nanodiscs obeyed: the apoA-I molecule was thought to either wrap in a "double belt" [81, 84, 91, 108], or a "hairpin loop" [116] configuration. This debate was settled by structural data acquired using a variety of methods, including EPR [84], fluorescence spectroscopy [91], FRET [81, 84], and NMR [108], all of which emerged in favour of the double belt model [87].

1.7.1 Advantages and disadvantages of nanodiscs

Nanodiscs were originally developed using dipalmitoylphosphatidylcholine (DPPC) and palmitoyloleoylphosphatidylcholine (POPC) as the reconstitutory lipids [14, 87], but have since been shown to be stable with other lipids [103]. This means that it is therefore possible to optimise the lipid constitution for the target protein of interest.

Nanodiscs present significant advantages even over other model membrane systems, such as liposomes and fixed bilayers, not to mention detergent micelles. The protein belts

[5] Developed by the Sligar group of the University of Illinois at Urbana-Champaign.

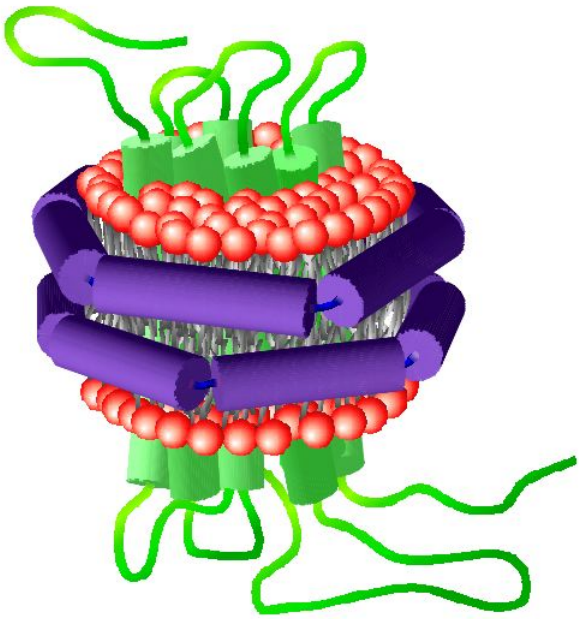


FIGURE 1.9: A cartoon of a nanodisc containing a reconsituted membrane protein with six transmembrane alpha helices. The "double belt" amphipathic alpha-helical membrane scaffold proteins are shown in purple, the lipids in red, and the reconstituted membrane protein in green (from S. Sligar's webpage).

stabilise the nanodisc, meaning that a reconstituted protein sample could be stable at room temperature for several days [14]. This is a vast improvement on detergent-solubilised samples, which will aggregate or degrade within a matter of hours [11].

Nanodisc size has been shown to be monodisperse within a sample, and consistent between sample preparations [14, 87, 103] due to the fact that the apoA-I belt efficiently defines the size of the nanodisc [14, 87]. This makes the nanodisc an optimal model lipid system for examining small molecule binding: binding of small molecules to liposomes is known to be affected by the size of the liposome [23], and the monodisperse nature of nanodiscs hence makes them a more reliable model for investigations of this nature [87]. Because the protein and the model lipid system in which it has been reconstituted are intrinsically linked, it is vital to understand the interaction between ligand molecules and nanodiscs before the results of a study of the interaction between the ligands and their target protein can be rigorously interpreted. Unsurprisingly, given the use of adapted apoA-I protein as the membrane scaffold protein, nanodiscs closely resemble HDL particles, the structure and behaviour of which is already well understood [87]. This provides an advantage for understanding the interactions between nanodiscs, their environment, ligands, and

the proteins which they corral. It is also thought that nanodiscs reflect the phase transition behaviour of the membrane more accurately than other lipid models [44, 110]: the lipid membrane of a cell is a dynamic system due to its intrinsic fluidity, and this will of course have an influence on the conformational behaviour of integral membrane proteins [20].

The primary disadvantage of nanodiscs is that reconstitution procedures would have to be optimised for every target protein used. However, this is a relatively minor consideration and nanodiscs have been used as a tool for investigating many membrane proteins. One of the most prolific protein targets so far is cytochrome P450: Bayburt *et al.* used cytochrome P450 as one of their initial targets when pioneering the technique, using atomic force microscopy (AFM) to undertake structural studies of the assembled system [14]. Several studies of cytochrome P450's binding kinetics have since been performed [10, 43, 45, 49], in some cases supplemented by solid-state NMR [43], and stopped-flow spectroscopy [45]. Bacteriorhodopsin was another of the initial targets for nanodisc reconstitution, and a study by Bayburt *et al.* in 2003 showing that bacteriorhodopsin was stable and functional in nanodiscs [17] was followed in 2006 by a combined solution spectroscopy *via* circular dichroism and small-angle X-ray scattering study to examine its multimeric assembly [15]. The GPCR β-2 adrenergic receptor has been reconstituted into nanodiscs and its ligand binding properties investigated [79], and its interaction with rhodopsin was later examined by density gradient centrifugation of the nanodisc reconstitution sample [16]. New insights have also been gained into the functional state of the bacterial chemoreceptor: originally thought to require at least a trimeric configuration, it was shown that dimers reconstituted into nanodiscs were still functional, hence redefining the minimum functional stoichiometry [27]. Furthermore, it has also been shown by electrophysiology and barium flux assays that not only can functional ion channels such as KcsA be reconstituted into nanodiscs (or at least the very similar "discoidal lipoprotein", or Lipodisq^{TM} system), but that the functional channels can then be transferred to lipid bilayers, without intermediate vesicle fusion [11].

1.7.2 Nanodiscs in solution

Importantly for this thesis, nanodiscs can be treated like detergent micelles, enabling solution-based experiments to be performed [18]. In particular, this would facilitate confocal-in-solution single-molecule FRET (smFRET) studies, bring the advantage of the sample having a longer 'bench life' [14, 87], and produce results thought to more closely reflect the protein's behaviour in its native membrane environment. The primary experimental focus is to reconstitute KirBac1.1 into nanodiscs, acquire confocal-in-solution smFRET measurements, and thereby establish whether this is a viable system for future KirBac, and other ion channel experiments.

1.8 Thesis overview

The aim of this thesis is to examine the gating regulation of the prokaryotic potassium channel KirBac1.1 using confocal-in-solution smFRET microscopy with two-colour ALEX. Chapter 2 describes optimisation of the expression, the purification into detergent micelles, and fluorescent labelling of KirBac1.1. Chapter 3 describes the optimisation of smFRET of KirBac1.1, and presents initial observations of smFRET signal from KirBac1.1. In Chapter 4, this signal is perturbed using modulatory factors (change in pH, activatory mutation, addition of PIP_2 as a ligand) to both confirm that the smFRET observed in the previous chapter is a true signal rather than an artefact, and to make a comparison with current findings about the conformational changes involved in KirBac gating. The same pertubatory experiments are performed in Chapter 5, but with the channel reconstituted into nanodiscs rather than solubilised in detergent micelles, and a comparison made with the results obtained using detergent. The latter part of Chapter 5 demonstrates reconstitution of a member of the two-pore inwardly rectifying potassium channel family, TREK-2, into nanodiscs. Finally, Chapter 6 consists of a discussion of the results of this thesis, with a brief consideration of possible directions for future studies.

Chapter 2

Expression, purification, and labelling of KirBac1.1

2.1 Introduction

This chapter describes the expression, purification, and labelling of KirBac1.1. The KirBac1.1 gene initially intended for use in this thesis was a gift from Shizhen Wang and Colin Nichols (WUSTL, MO), but the high G-C content of the gene made it very difficult to produce site-directed point mutations using standard procedures, so a codon-optimised version of the gene was synthesised which had a much reduced G-C content (56.42%, *cf.* 67.53% in the original version). Success in producing mutations with this 'new' construct was achieved on the first or second attempt at modification, and all experiments were therefore performed using the codon-optimised construct.

2.1.1 Site-directed point mutations of KirBac1.1

In order to perform smFRET microscopy, the protein of interest, in this case KirBac1.1, must be labelled with fluorescent molecules. One of the simplest ways to do this is *via* cysteine-maleimide labelling, whereby the thiol side chain of a cysteine residue reacts with the maleimide group of the label molecule to form a covalent bond. However, wild type KirBac1.1 contains no cysteine residues, so while this means that there are no extraneous cysteines to consider during labelling reactions, cysteines must be artificially introduced

using site-directed point mutations.

The three cysteine mutants used in this study (R151C, G249C, and A273C) have been shown by the Nichols group to be functionally indistinguishable from the wild-type protein, and to be accessible to labelling reactions [123]. All of these mutants were used in the ensemble-based FRET study by Wang *et al.* which mapped conformational changes in the cytoplasmic domain upon PIP_2 binding, and hence inhibition [123], so have already proven their utility as markers of conformational changes in KirBac1.1 associated with gating. In addition, each of the three mutants is located in a distinct region of the protein: R151C near the helix bundle crossing and C-linker [13, 123]; G249C in the cytoplasmic domain near the G loop [13, 123]; and A273C in the middle of the immunoglobulin fold of the cytoplasmic domain [59, 123]. This means that combining the data acquired from the different mutants provides a report on global conformational changes of the entirety of the cytoplasmic domain, and hence the majority of the solvent-accessible parts of KirBac1.1.

2.2 Methods

2.2.1 Molecular biology

Site-directed point mutations

The sequence of the original KirBac1.1 gene from the Nichols group formed the basis for codon-optimised KirBac1.1 to be synthesised by Genscript Ltd.: the codon-optimised gene had reduced G-C content (56.42%, *cf.* the original of 67.53%), and also contained a 6-His tag and TEV protease[1], NcoI, and HindIII cleavage sites. The codon-optimised gene was subcloned from the pUC57 vector into pQE60Lac for expression in BL21-Gold (DE3)pLysS Competent Cells (Agilent UK).

Primers for cysteine and gating modulation point mutations were designed and synthesised by Sigma-Aldrich. These point mutations were incorporated into the gene using a modified version of the QUIKChange site-directed mutagenesis method (see below).

[1]Tobacco Etch Virus nuclear inclusion a endopeptidase, a sequence-specific protease.

Subcloning

RESTRICTION DIGEST: The target plasmid is cut out of the original vector and the target vector is cut with the same restriction enzymes. In this case, the codon-optimised KirBac1.1 was transferred from pU57 to pQE60Lac using the restriction enzymes NcoI and HindIII[2]. Both reactions were made as follows in Table 2.1 and incubated at 37° for one hour. The mixtures for the original and target vector solutions are identical.

22 μL	plasmid DNA (50-100 ng/μL)
5 μL	10x buffer E
2 μL	enzyme 1 (10 units/μL)
2 μL	enzyme 2 (10 units/μL)
19 μL	molecular biology H_2O
50 μL	total

TABLE 2.1: Restriction digest mixture

GEL PURIFICATION: The digested samples were run on an agarose gel and gel purification performed according to the QiaQuick Gel Purification protocol (Qiagen). Samples were eluted with 25 μL molecular biology H_2O.

LIGATION: The ligation mixture was set up as follows in Table 2.2 and incubated at room temperature for >3 hours. A control measurement is made using H_2O instead of the insert DNA.

10 μL	insert DNA (gene of interest at 50-100 ng/μL))
2.5 μL	vector DNA (50-100 ng/μL)
1.5 μL	10x T4 DNA ligase buffer
1 μL	T4 DNA ligase enzyme (3 units/μL)
15 μL	total

TABLE 2.2: Ligation mixture

TRANSFORMATION AND DNA EXTRACTION: The ligation mixture was directly transformed into DH5α cells (Invitrogen) using heat shock transformation (see below), the resulting mixture plated on antibiotic plates, typically LB (Luria Broth) (Sigma Aldrich) agar (Sigma Aldrich) and carbenicillin (Apollo Scientific Ltd.) (0.05% w/v) and incubated overnight, then single colonies chosen to inoculate 4 mL LB with carbenicillin (0.05%) liquid cultures.

[2]In Chapter 5 the same procedure was used to transfer the membrane scaffold protein gene to pET28a for expression in *E.coli*

A small-scale alkaline lysis procedure (the process colloquially known as “miniprep”) was performed to extract DNA (outlined below).

Polymerase Chain Reaction (PCR)

Polymerase Chain Reaction (PCR) was used to incorporate point mutations into the KirBac1.1 gene. The reaction mixture is given in Table 2.3 and the heating cycle in Table 2.4

5 μL	10x Pfu ultra buffer
1 μL	10 mM dNTPs
1.25 μL	10 μM forward primer
1.25 μL	10 μM reverse primer
1 μL	gene template (50-100 ng/μL)
3 μL	100% DMSO
1 μL	Pfu ultra enzyme (2.5 units/μL)
36.5 μL	dH_2O
50 μL	total

TABLE 2.3: PCR reaction mixture

95°C	1’	
95°C	50”	
60°C	50”	x 18
68°C	12’	
68°C	7’	
4°C	∞	

TABLE 2.4: PCR heating cycle

The reaction mixtures were transferred to microcentrifuge tubes (Eppendorf), 1 μL DpnI (10 units/μL, Thermo Scientific) added to each sample, and the samples incubated at 37°C for 1 hour. Product clean-up was performed to remove unincorporated dNTPs and short-failed products using a QiaQuick PCR Purification Kit (Qiagen). Five volumes PB buffer (250 μL) was added, and each sample transferred into a QiaQuick spin column. Samples were centrifuged at 20,000 g for 30 sec, the flowthrough discarded, 750 μL PE buffer added, samples centrifuged for another 30 sec, and the flowthrough discarded again. Another 1 min centrifugation was followed by transferring each sample to a clean microcentrifuge tube. The DNA was eluted with 25 μL molecular biology water: after a 5 min incubation, the samples underwent 30 sec centrifugation.

The entire DNA solution was added to 100 μL DH5α cells, and a heat shock transformation performed (outlined below). The transformed solution was plated onto LB agar with carbenicillin (0.05% w/v) and incubated at 37°C overnight.

A single colony was chosen and used to inoculate 4 mL LB with carbenicillin (0.05% w/v), which was then incubated at 37°C and 210 rpm overnight.

The "miniprep" procedure for DNA extraction (see below) was performed and the resulting samples sequenced by Source BioScience[3].

Heat shock transformation

Plasmid DNA was added to the chosen cell strain and incubated at 4°C for 30 min. Heat shock was performed at 42°C for 45 sec, then the cells were incubated at 4° for 2 min. 250 μL LB was added and the mixture incubated at 37°C for 15-20 min before plating or inoculating liquid culture.

NB: when a kanamycin-resistant plasmid was used, this incubation period was increased to 60 min to sufficient time for the antibiotic resistance gene to be expressed.

DNA extraction

DNA extraction was performed using the QiaPrep Spin Miniprep kit (Qiagen), a small-scale form of alkaline lysis extraction. Both this procedure, and the resulting DNA solution, is colloquially known as a "miniprep".

DH5α cells would have undergone heat shock transformation with the plasmid of interest and grown for 16 hours at 37°C and 210 rpm in 4 mL LB with carbenicillin (0.05% w/v). The cells were harvested by centrifugation at 2,000 *g*, then resuspended in 250 μL P1 buffer and the suspension transferred to a clean microcentrifuge tube. 250 μL P2 buffer was added, the sample mixed well, then 350 μL buffer N3 added, and the sample immediately mixed then centrifuged at 20,000 *g* for 10 min. The supernatant was added to a Qiaprep spin column and centrifuged for 1 min, then the flowthrough discarded. 750 μL PE buffer was added, the sample centrifuged for 30 sec and the flowthrough discarded, then

[3]Local Sanger sequencing laboratory based at the Department of Biochemistry, University of Oxford.

centrifuged for a further 1 min before the Qiaprep column was transferred to a clean micro-centrifuge tube. DNA was eluted by adding 50 μL molecular biology water, incubating for 3 min, then centrifuging for 45 sec. The samples could then be sent for sequencing (Source BioScience) or further procedures performed.

Sources of molecular biology reagents

	Reagent	Brand
	Molecular biology H_2O	Fisher BioReagents
	DH5α cells	Invitrogen
Subcloning	10x Buffer E	Promega
	NcoI (10 u/μL)	Promega
	HindIII (10 u/μL)	Promega
	T4 DNA ligase buffer and enzyme (3 u/μL)	Promega
PCR	100% DMSO	Finnzymes
	10 mM dNTPs	Thermo Scientific
	DpnI (10 u/μL)	Thermo Scientific
	pfu ultra buffer and enzyme (2.5 u/μL)	Agilent

TABLE 2.5: Sources of molecular biology reagents

2.2.2 Protein biochemistry

Growth of cultures and induction of protein expression

KirBac1.1 in pQE60Lac was transformed into BL21-Gold (DE3)pLysS and used to inoculate 50 mL LB with carbenicillin (0.05% w/v) starter cultures, which were incubated overnight at 37°C and 210 rpm. 2 L LB with carbenicillin (0.05% w/v) cultures were then inoculated with 15 mL/L of this starter culture, and incubated at 37°C and 190 rpm until OD_{600} = 1.1. Induction was then performed using 1 mM isopropyl-β-D-1-thiogalactopyranoside (IPTG) (Apollo Scientific Ltd) and the cultures incubated overnight at 19°C and 190 rpm. Cell pellets were harvested by centrifugation at 16,000 *g* for 40 min.

Dot blot expression test

~5 mL fully induced cell culture was centrifuged at 2,000 *g*, the pellet resuspended in KirBac1.1 purification buffer (composition below) with 2% Triton-X (VWR), and the mixture agitated gently for 30 min. 10 μL of each sample was pipetted directly onto a piece of

Western blot membrane (Pall Life Sciences). The membrane was incubated in blocking buffer (Hen Egg White Lysozyme (Fluka) in Tris-Buffered Saline with Tween®20, pH 8.0 (TBS-T) (Sigma Aldrich)) for 1-2 hours, then washed for 3 x 10 min in TBS-T. The membrane was then incubated in TBS-T with ~5μL Anti-His antibody (Invitrogen) for 1 hour, then washed for 3 x 10 min in TBS-T. Novex®AP Chromogenic Substrate (Invitrogen) was added to cover the membrane, and incubated for 30 min. The membrane was washed with water to arrest the development reaction, and left to dry.

KirBac1.1 purification

Pellets were resuspended in 25 mL resuspension buffer per 2 L original culture (buffer compositions below) with one tablet/50 mL EDTA-free Protease Inhibitor Cocktail tablet (Roche), Hen Egg White Lysozyme (HEWL) (Fluka), and DNaseI (Sigma Aldrich). Cells were lysed with 6-8 passes through a French press homogeniser (Stansted Fluid Power Ltd.), n-Dodecyl-β-D-maltoside (DM) (Affymetrix Anatrace Products) was added to a final concentration of 30 mM, and the mixture incubated at 4°C for 1-2 hours for solubilsation to occur.

The solubilised lysate was centrifuged at 70,000 *g* for 40 min to extract cell debris. The supernatant was added to cobalt resin[4] (Amintra CoHIS Resin, Expedeon) which had been equilibrated with 20 volumes Wash A buffer, and incubated at 4°C for 1-2 hours to facilitate binding for affinity purification. The unbound fraction was collected and the resin washed with 20 volumes Wash B buffer before elution with 10 volumes Elution buffer (after a 20 min incubation). The elute was then concentrated to <0.5 mL using a 50 kDa cut-off centrifugal filter device (Millipore) and filtered with a 0.22 μm membrane (VWR). The concentrated and filtered sample was then loaded onto a size exclusion column[5], specifically Fast Protein Liquid Chromatography (FPLC) (Superdex 200 10/300, GE Healthcare) equilibrated with 50 mM Tris-HCl pH = 7.8, 150 mM KCl, and 5 mM DM, to separate and collect the tetrameric fraction. All buffers for size-exclusion chromatography had been filtered using a 0.22 μm membrane and degassed by vacuum pump for >3 hours.

[4]Suspension of beads with hexaaquacobalt(II) $[Co(H_2O)_6]^{2+}$.

[5]Size-exclusion chromatography: fractionation of an aqueous protein sample based on differential elution speed through a gel column.

KirBac1.1 purification buffers

Buffer recipes for KirBac1.1 purification are given below in Table 2.6.

	Tris-HCl pH = 7.8	KCl	
Resuspension buffer	50 mM	150 mM	10 mM $MgCl_2$ 250 mM sucrose 5 mM β-mercaptoethanol
Wash A	50 mM	150 mM	
Wash B	50 mM	150 mM	5mM DM + 10 mM imidazole pH = 8.0
Elution	50 mM	150 mM	5 mM DM + 500 mM imidazole pH = 8.0

Table 2.6: KirBac1.1 purification buffers

Fluorescent labelling of KirBac1.1

Tetrameric KirBac1.1 was concentrated to ~2 mg/mL, and the fluorescent dyes Cy3B Maleimide (GE Healthcare) and AlexaFluor®647 Maleimide (Invitrogen) added. The reaction mixtures are given in Table 2.7.

	Volume/μL
Protein	200
Cy3B	1.0
AlexaFluor®647	0.5

Table 2.7: KirBac1.1 labelling reaction mixture

This mixture was incubated in the dark at room temperature for 1 hour, then added to cobalt resin (equilibrated with 20 volumes Wash A buffer, see below), and incubated at 4°C for 1 hour. Affinity purification was performed by washing with 20 volumes of Wash B buffer, followed by elution with 10 volumes Elution buffer (after a 15 min incubation). The elute was run through an equilibrated NAP-5© column (GE Healthcare) and six 0.5 mL fractions collected. Samples from each fraction were loaded onto an SDS-PAGE[6] gel (NuPAGE 4-12% Bis-Tris, Novex) which was then visualised using a fluorescence gel scanner (Pharos FX™ Molecular Imager (BioRad) with The Discovery Series™ Quantity One v4.6.9) in both Cy3B (532 nm excitation, 605 nm bandpass filter) and AlexaFluor647 (635 nm excitation, 695 nm bandpass filter) channels to determine in which fractions labelled protein was present.

[6]PolyAcrylamide Gel Electrophoresis: separation of biological molecules based on electrical motility, which depends on molecular weight, size, charge, and the acrylamide concentration of the gel. An XCell SureLock™ (Novex) tank was used.

KirBac1.1 labelling buffers

Buffers for labelling KirBac1.1 are given below in Table 2.8.

	HEPES pH = 7.5	KCl	
Wash A	20 mM	150 mM	
Wash B	20 mM	150 mM	5 mM DM + 10 mM imidazole pH = 8.0
Elution	20 mM	150 mM	5 mM DM + 500 mM imidazole pH = 8.0

Table 2.8: KirBac1.1 labelling buffers

2.3 Results

2.3.1 Molecular biology

A codon-optimised KirBac1.1 gene was synthesised by Genscript Ltd: the 'wild type' has a G-C content of ~68%, whereas the codon-optimised construct has a G-C content of ~56%, and was additionally engineered to include NcoI, HindIII, and TEV cleavage sites, and a C-terminal 6-His tag. The engineered gene was delivered in the pUC57 vector, and successfully subcloned into pQE60Lac using the NcoI and HindIII cleavage sites. All point mutations were added to the new codon-optimised protein, including the cysteine substitutions which are essential for labelling and subsequent fluorescence experiments. This was successfully performed using standard PCR on either the first or second attempt, representing a vast improvement in the ease of making mutations compared to the G-C rich wild type.

2.3.2 Protein biochemistry

Expression

Protein expression was tested by making a dot blot of the whole cell lysate. The Anti-His antibody selectively binds to the 6-His tag, so a positive result will only be obtained if KirBac1.1 is being expressed in the *E. coli* culture: this is represented by a distinct and sizeable purple spot on the blotting membrane. As can be seen in Figure 2.1, there were satisfactory levels of expression for all three cysteine-only mutants, so purification optimisation was undertaken. Expression of the codon-optimised KirBac1.1 was indistinguishable from the

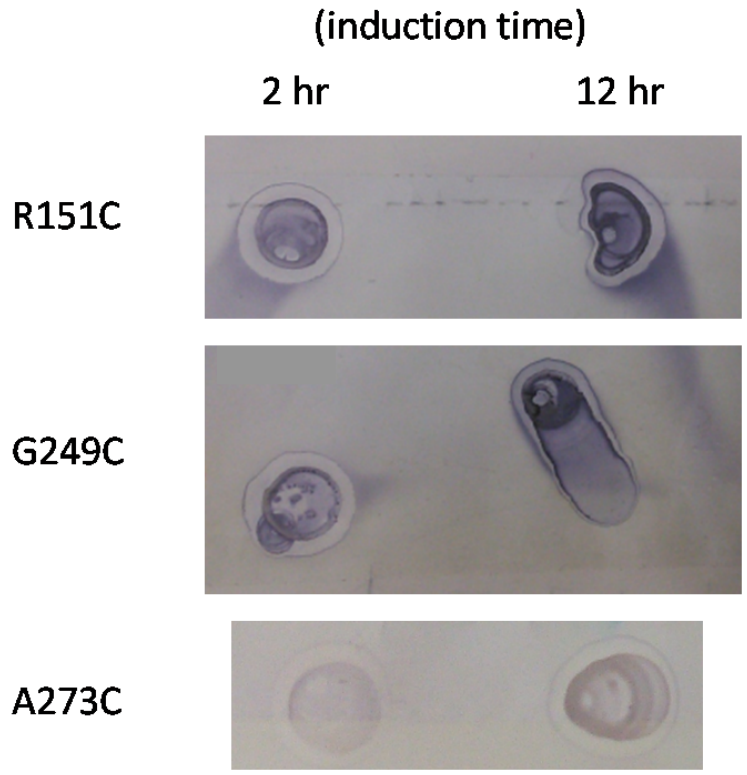


FIGURE 2.1: A dot blot expression test for the three cysteine-only mutations in KirBac1.1. The purple spots indicate a satisfactory level of expression for all mutants, so purification optimisation was undertaken.

original 'wild type', so all further experiments were performed using the codon-optimised KirBac1.1 protein.

Purification

Purification procedures were optimised to arrive at the protcols described above. All samples were solubilised into detergent micelles, and size-exclusion chromatography performed to confirm the dominance of assembled tetrameric protein in the purified samples. This demonstrated that all three cysteine-only constructs can be purified in tetrameric form (peak at ~12 mL), shown in Figure 2.2.

SDS-PAGE (Invitrogen) with Coomassie™ staining was performed to visualise the purification process, and confirmed that there was a substantial amount of pure protein obtained. This is presented in Figure 2.3, although as SDS-PAGE is a denaturing process, it is not possible to visualise the quaternary structure of the protein. (A) illustrates the purification process for one mutant (R151C), while (B) confirms the presence of all three mutants in a final purification product.

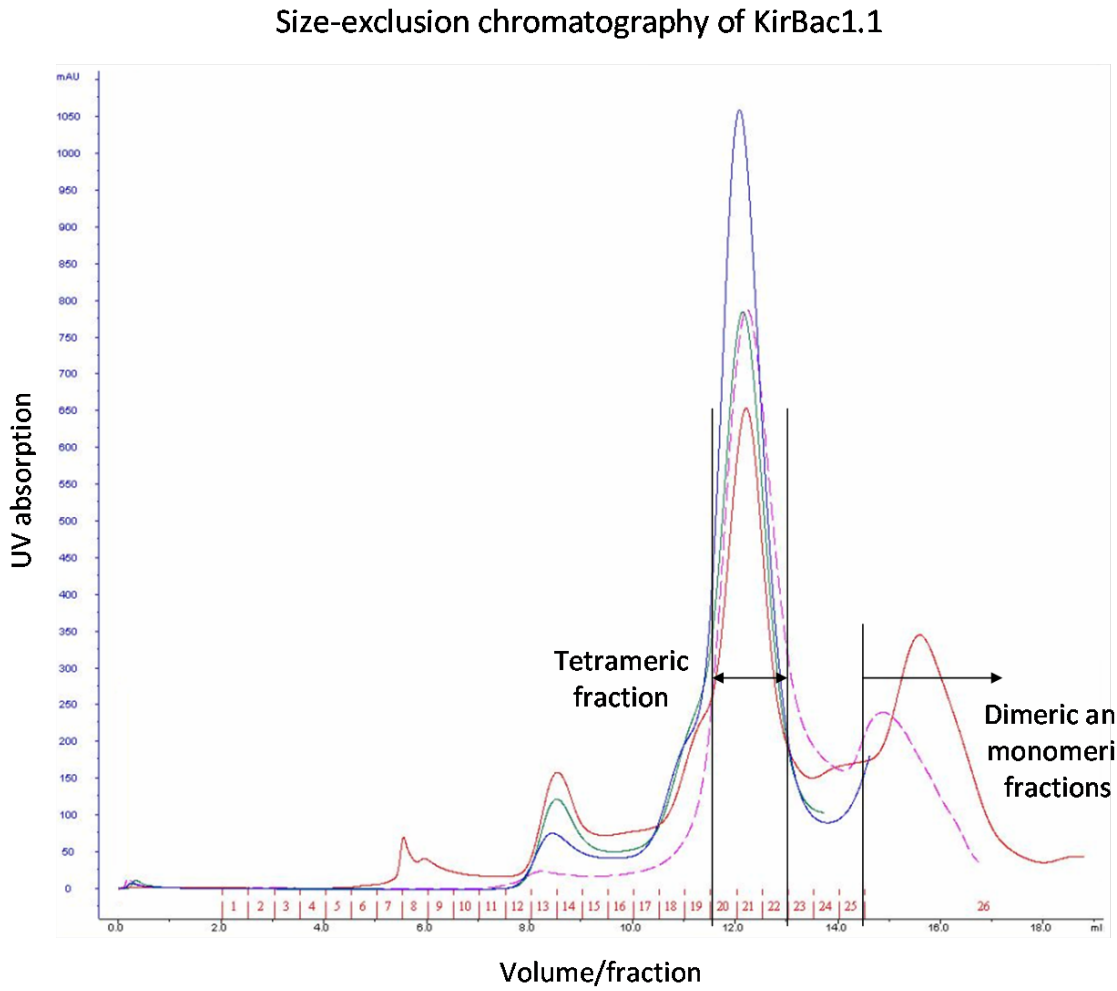


FIGURE 2.2: Size-exclusion chromatography of codon-optimised detergent-solubilised KirBac1.1 with cysteine mutations. The three cysteine-only point mutations (blue: R151C, red: G249C, green: A273C) all express and purify as tetrameric proteins (peak at ~12 mL). The dashed pink trace is a wild-type KirBac1.1 control known to be relatively stable in tetrameric form under the usual purification conditions, confirming that the cysteine mutants are tetrameric in detergent-solubilised purification.

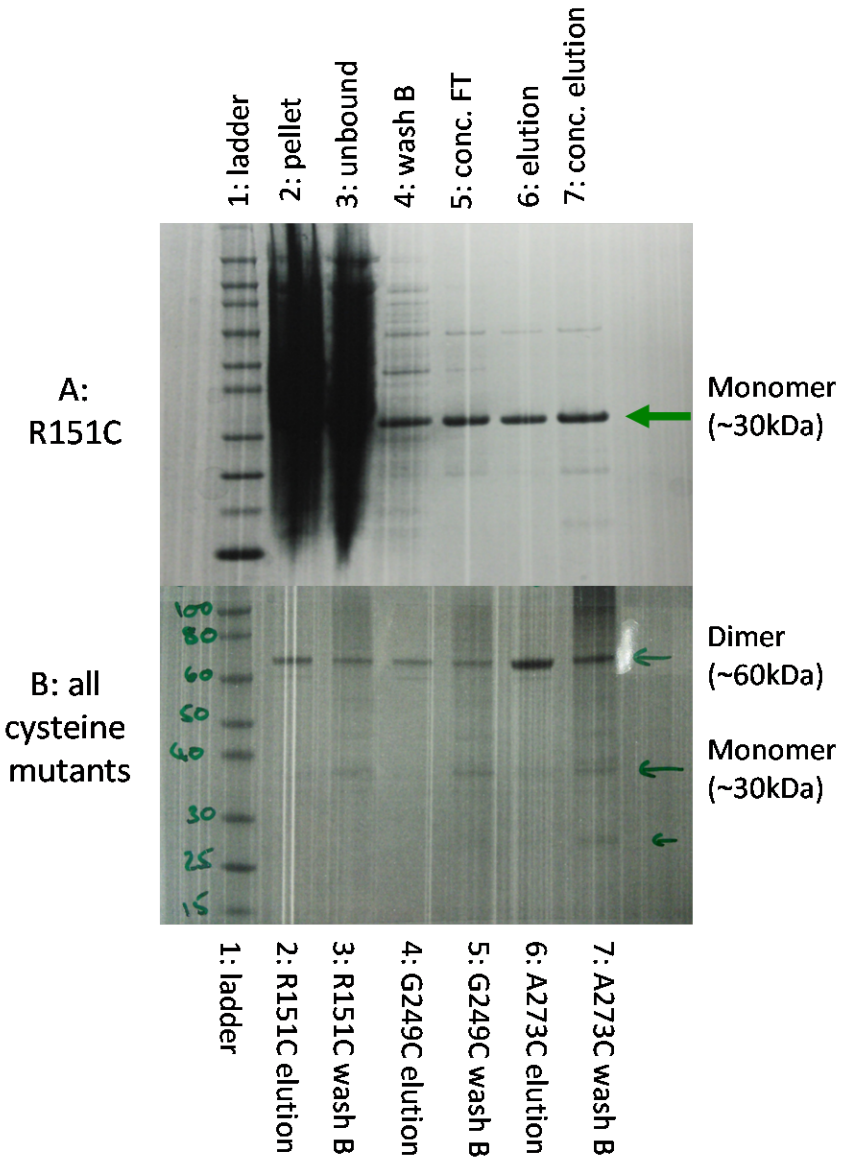


FIGURE 2.3: (A) SDS-PAGE illustrating the various stages of a KirBac1.1 purification (R151C): (1) ladder; (2) pellet; (3) unbound fraction; (4) wash B; (5) concentration flowthrough; (6) elution fraction; (7) concentrated elution fraction. The band corresponding to a KirBac1.1 monomer is visible at ~30 kDa.
(B) All three cysteine mutants: (1) ladder; (2) R151C elution fraction; (3) R151C wash B; (4) G249C elution fraction; (5) G249C wash B; (6) A273C elution fraction; (7) A273C wash B. The arrows indicate that most of the protein is in dimeric or monomeric form in this (denaturing) gel (~60 kDa and ~30 kDa, respectively).

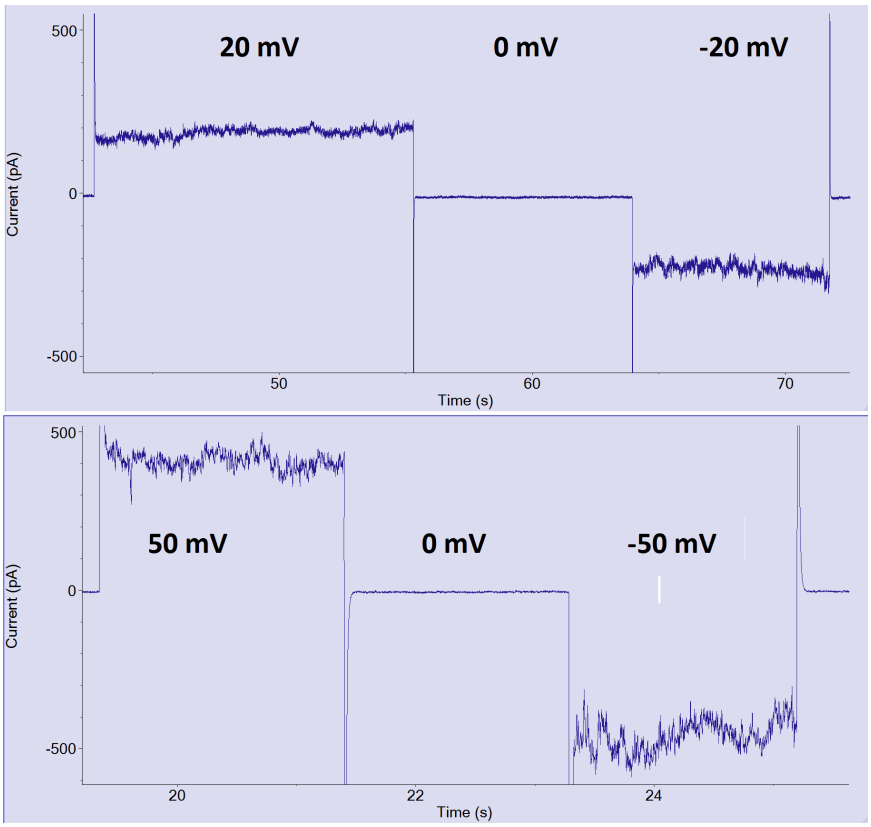


FIGURE 2.4: An electrophysiological recording of wild type KirBac1.1 at 20 mV (top) and 50 mV (bottom). The change in current direction upon reversal of the polarity of the voltage, suggests that a functional channel may be present. These experiments were performed by Marc Szabo in the Wallace laboratory.

Purified KirBac1.1 is functional

The construct of KirBac1.1 used in this study has been examined in electrophysiological studies using patch clamp within the droplet-hydrogel bilayer (DHB; performed by Marc Szabo in the Wallace Laboratory): results are illustrated in Figure 2.4. The change in current direction upon reversal of voltage polarity is suggestive of the presence of a functional channel.

Fluorescent labelling of KirBac1.1

Labelling procedures were optimised to obtain the protocol outlined above. Samples were loaded onto an SDS-PAGE gel (NuPAGE 4-12% Bis-Tris, Novex) which was then visualised using a fluorescence gel scanner, as described above. This enabled the determination of which fractions contained labelled protein, as well as verifying labelling success. Gels showing a positive result for all three cysteine reporter mutants are shown in Figure 2.5. A

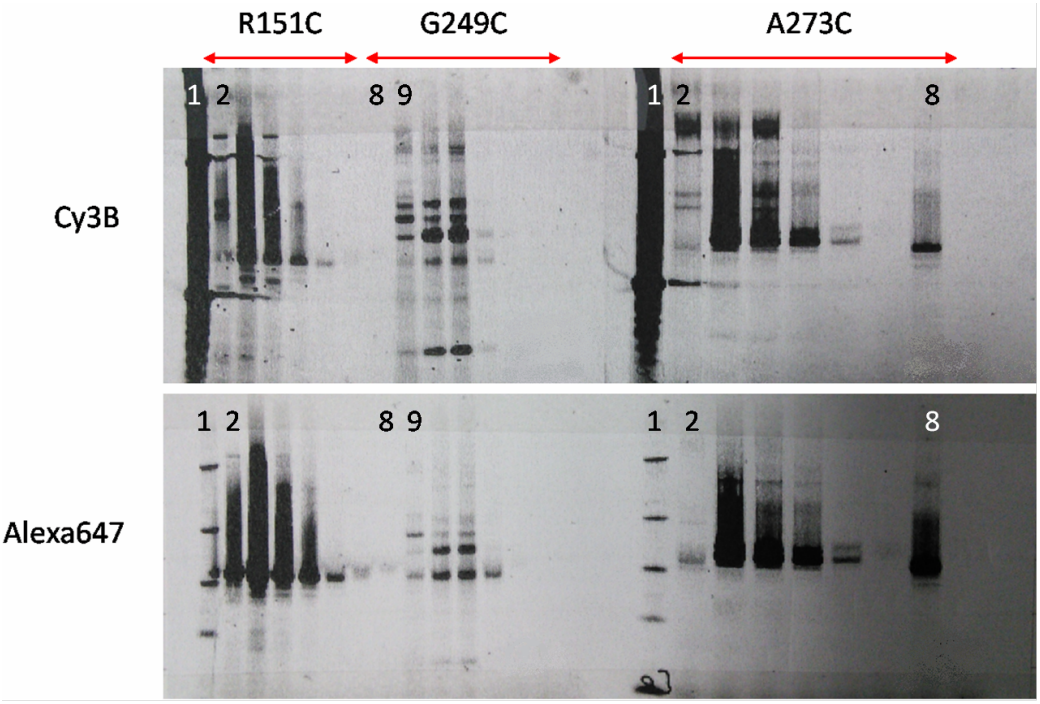


FIGURE 2.5: A gel showing a positive result for labelling all three cysteine reporter mutant KirBac1.1 constructs. A band is visible in the same location (corresponding to the correct protein molecular weight) in both scanning wavelengths. However, this takes the form of a double, rather than a single band: this is thought to be due to cleavage or part of the N-terminal or C-terminal domain, neither of which would affect protein function.
KEY Left (top: Cy3B; bottom: AlexaFluor®647): (1) ladder; (2-8) R151C; (9-15) G249. Right (top: Cy3B; bottom: AlexaFluor®647): (1) ladder; (2-8) A273C. The fractions used in later experiments are taken from lanes (3) and (11), corresponding to the second fraction from the NAP-5© column stage of the labelling protocol.

band must be visible in the same location on the gel, corresponding to the monomer molecular weight, in both scanning wavelengths. The second lane for each mutant (lanes (3) and (10) in the gels) is the fraction used in later experiments, corresponding to the second fraction from the NAP-5© column stage of the labelling protocol. A double band is visible for most samples, thought to be due to cleavage of part of the C-terminus or N-terminus, and it is assumed that neither loss would affect protein functionality with respect to the gating mechanism.

Samples were also visualised using a fluorescence spectrophotometer (Cary Eclipse, Agilent) to confirm successful labelling: a typical spectrum is given in Figure 2.6. Excitation at 532 nm (Cy3B, donor excitation) produced emission from Cy3B at 575 nm, indicating successful labelling with the donor fluorophore, and emission from AlexaFluor®647 at 673 nm owing to FRET, indicating successful labelling with the acceptor fluorophore. Excitation at 635 nm (AlexaFluor®647, acceptor fluorophore) produced emission from

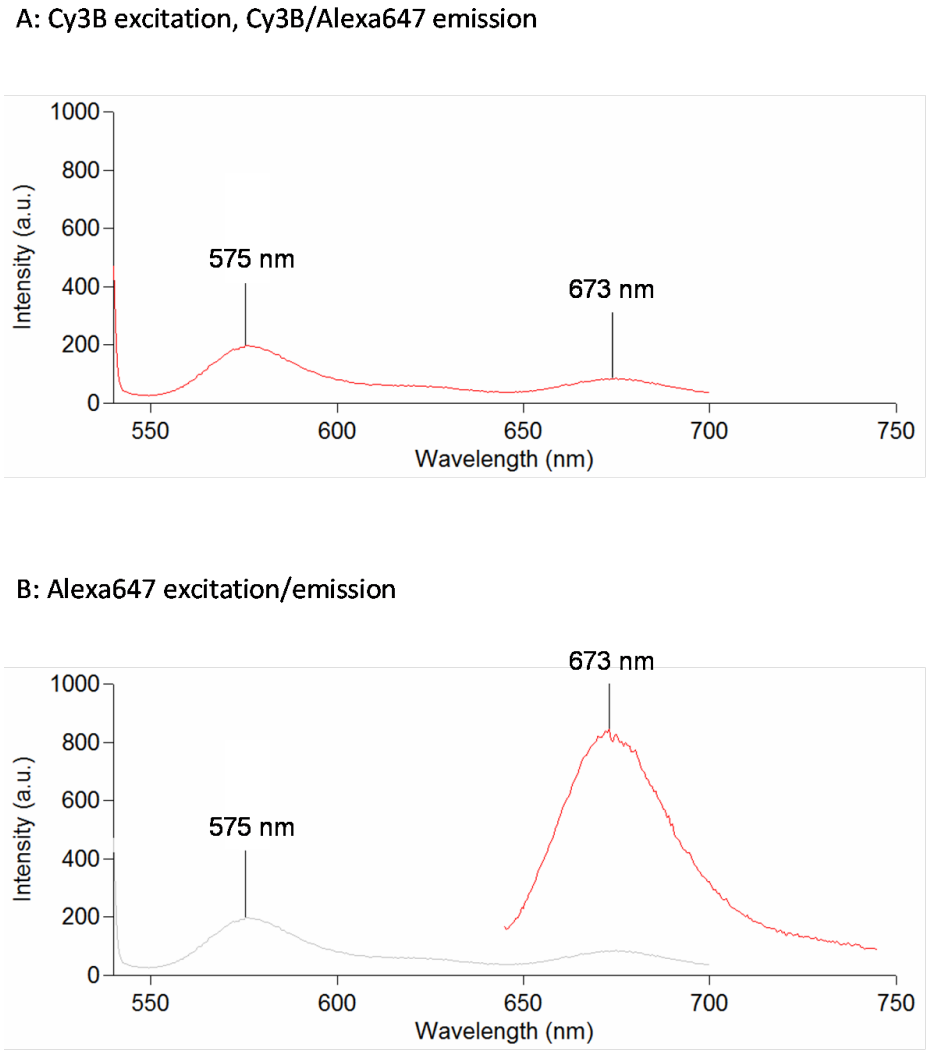


FIGURE 2.6: (A) Excitation at 532 nm (Cy3B, donor fluorophore): emission at 575 nm from direct decay of the donor fluorophore; and emission at 673 nm from decay of the acceptor fluorophore, *via* FRET.
(B) Excitation at 635 nm (AlexaFluor®647, acceptor fluorophore): emission at 673 nm from direct decay of the acceptor fluorophore (red trace).

AlexaFluor®647 at 673 nm, indicating successful labelling with the acceptor fluorophore. The greater intensity of the acceptor-only peak is consistent with the observation that AlexaFluor®647 appeared to react more easily than Cy3B, reflected in the ratios in the labelling reaction mixture (above).

2.4 Conclusions

The codon-optimised KirBac1.1 gene was successfully subcloned into the pQE60Lac vector, and the three cysteine reporter mutations inserted. All three mutants were expressed, purified, and doubly labelled with Cy3B maleimide and AlexaFluor®647 maleimide. The (now doubly labelled) detergent-solubilised protein samples were therefore considered ready for use in smFRET experiments, described the next two chapters of this thesis.

However, as KirBac1.1 is a homomeric tetramer, there are four cysteine residues, *i.e.* four possible labelling sites, per assembled channel. In the ideal, substoichiometric labelling case in which each assembled channel is labelled with one donor and one acceptor, this would result in two possibilities for the inter-fluorophore distance: the fluorophores would be located on either adjacent or diagonally opposite subunits. The differences between the inter-fluorophore distances are within the detectable range of the FRET pair, so could be distinguished as distinct populations with different FRET efficiency. Being able to clearly resolve these populations is a good starting point to establish controls before perturbing the dynamic equilibrium of the gating state, and hence the transfer efficiency of the fluorescence populations. The optimisation of this is the subject of the next chapter, wherein the procedure and optimisation thereof for making smFRET recordings of KirBac1.1 is described.

Chapter 3

Measurement of smFRET in KirBac1.1

3.1 Introduction

The previous chapter described the successful expression, purification, and fluorescent labelling of KirBac1.1, in preparation for smFRET experiments. This was accomplished for all three cysteine reporter point mutations: R151C, near the helix bundle crossing; G249C, near the cytoplasmic G-loop; and A273C, located in the immunoglobulin-like cytoplasmic β sheet fold. This chapter focuses on the optimisation of the smFRET procedures in order to achieve satisfactory resolution of the fluorescence populations.

KirBac1.1 is a homomeric tetramer, so there are four possible sites for cysteine maleimide labelling if a single cysteine point substitution is made. Even in the ideal substoichiometric case where the assembled tetrameric channel has been labelled with one donor and one acceptor, this results in two possibilities for inter-fluorophore distances: the proximal case, where adjacent subunits are labelled; and the distal case, where subunits diagonally opposite each other are labelled. This will result in two distinct fluoroscence populations of differing transfer efficiency in the sample population. The ability to distinguish these distinct populations is a useful test of data quality, and has been previously used by Benoît Roux's group[1] in their LRET study of the *Shaker* channel to verify the precision of their intra-protein distance measurements [105]. It is therefore desirable to be able to reliably and repeatably resolve these populations as it is the eventual aim of this study to perturb the

[1] Department of Biochemistry and Molecular Biology, The University of Chicago

dynamic equilibrium of the population *via* gating perturbations, thereby producing a shift in the FRET values, and it is necessary to be confident that these shifts can be accurately quantified.

This chapter therefore describes the approach taken to achieve resolution of the proximal and distal fluorescence populations. Even after optimising the labelling protocol, this required adjusting the concentration and threshold parameters of the confocal-in-solution experiments, but smFRET signals were observed which reliably and repeatably demonstrated the presence of the proximal and distal populations. These measurements were to form the basis of controls when attempts were made to modify the gating equilibria of the channels, and thereby the smFRET signals, described in the next chapter.

3.2 Methods

3.2.1 Confocal-in-solution smFRET

Confocal microscopy

All single-molecule fluorescence experiments were performed at room temperature (18-22°C) on doubly labelled codon-optimised KirBac1.1 in observation buffer (20 mM HEPES pH=7.5, 150 mM KCl, 0.5 mM EDTA) using confocal-in-solution microscopy with Alternating-Laser Excitation (ALEX) at 10 kHz between 532 nm (120 μW continuous wave (CW), Samba, Cobalt) and 635 nm (30 μW CW, CUBE, Coherent), as described in Santoso *et al.* [107], and illustrated schematically in Figure 3.1. A photograph of the set-up used in this study (built and maintained by Geraint Evans of the Kapanidis group), is shown in Figure 3.2.

The two beam paths from the alternating lasers are combined using a dichroic mirror (DM1) and directed through a series of lenses and pinholes which act to define the observation volume. Aqueous samples are pipetted directly onto a coverslip resting on top of an oil immersion objective (60x, NA=1.35, Olympus UPLSA 60XO) focused to 20 μm above the coverslip surface. Fluorophores attached to freely diffusing molecules are excited as they pass through the observation volume, and the resulting photon streams from fluores-

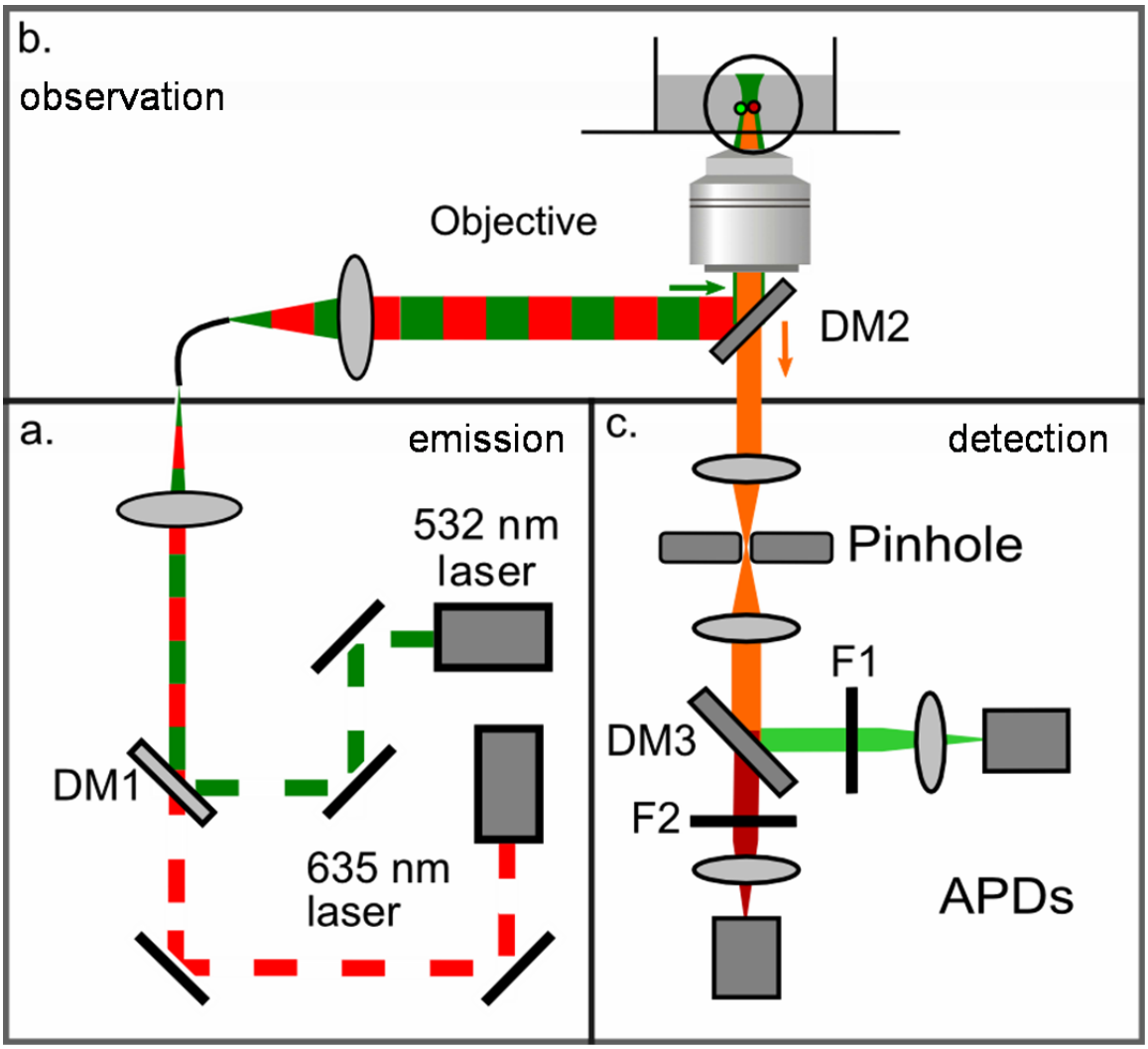


FIGURE 3.1: A schematic representation of confocal microscopy with Alternating-Laser Excitation (ALEX). The beam paths are combined using the dichroic mirror DM1, and directed to the objective, where freely diffusing molecules pass through a femtolitre volume defined by the focused laser beams and confocal optics. The fluorophores are excited by the laser light and the resulting signal from fluorescent decay and emission is directed to further beam splitters (the dichroic mirrors DM2 and DM3) and detected by avalanche photodiodes (APDs), after furthering filtering extraneous wavelengths using filters F1 and F2.
This is in fact the schematic arrangement for Snowdon, the microscope used in this thesis (figure courtesy of Geraint Evans). (a) is the emission sector, (b) the observation sector, and (c) the detection sector of the set-up. A photograph of the excitation sector is shown in Figure 3.2.

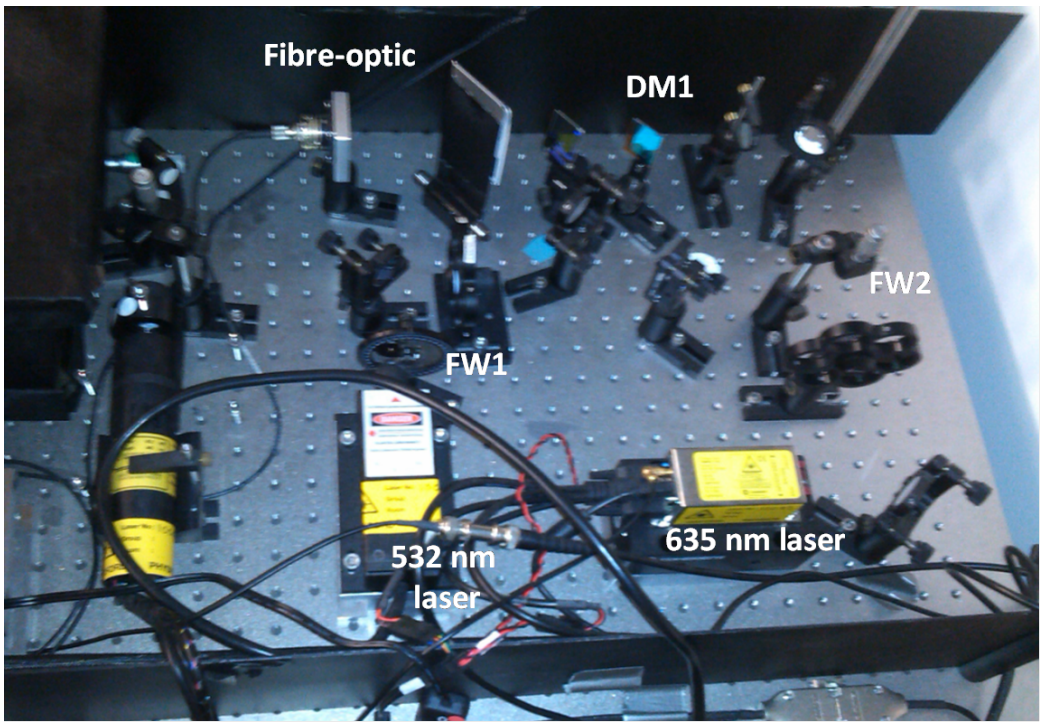


FIGURE 3.2: Photograph of the excitation sector of Snowdon, the confocal-in-solution with ALEX microscopy set-up used in this study. This set-up was built by Geraint Evans, of the Kapanidis group. A schematic diagram of the whole microscope is shown in Figure 3.1. DM1 is the dichroic mirror which combines the beams from the two lasers, FW1 and FW2 are the filter wheels which control the powers of the 532 nm and 635 nm beams, respectively, and the fibre-optic is the mechanism by which the beams enter the observation sector of the microscope.

cent decay and emission are directed through two beam splitting dichroic mirrors, the first to separate out the longer wavelength fluorescence emission from the excitation laser light (DM2), and the second (DM3) to split the donor and acceptor beams to send them to separate avalanche photodiodes (APDs; SPCM-AQR-14, PerkinElmer). F1 and F2 are filters which exclude extraneous wavelengths, as the dichroics allow passage of a *band* of frequencies, rather than a single wavelength. Photon arrival times are recorded and analysed using custom-written software in LabVIEW (National Instruments) and MATLAB (MathWorks, Natick), which detects photon bursts and fits one or more Gaussian distributions to the results (see below).

It is the pinhole of the confocal optics (set to 200 μm), shown in the detection sector (c) of Figure 3.1 and illustrated in more detail in Figure 3.3, which defines the observation volume, the size of which is on the order of femtolitres. Taking into account the diffusion constant of the labelled molecules in solution, this means that it is overwhelmingly probable that there will be one (or zero) fluorescently labelled molecule(s) traversing the observation volume at a given time. This makes confocal-in-solution microscopy a single-molecule technique, despite the fact that there would be many billions of molecules in the solution: although data may be obtained from many molecules *sequentially*, and the data may be collated for subsequent analysis, none of these molecules are being observed *concurrently* or *simultaneously*.

Alternating-Laser Excitation (ALEX)

The emission and excitation lasers are both driven by a LabVIEW Virtual Instrument which ensures that data collection is coupled with information about which laser is active at the instant of observation. The laser illumination excites the fluorescent labels, which then decay either directly or *via* non-radiative transfer to a partner[2], producing a fluorescence signal which can be detected in either the donor-emission (D_{em}) or acceptor-emission (A_{em}) channel, respectively.

[2]More correctly, this is a *radiationless* mechanism, which consists of near-field emission/absorption of photons on a length scale smaller than the wavelength of the photons, hence the photons are undetectable, and considered to be *virtual* photons. It has been shown through quantum electrodynamics (QED) that this is the short-range equivalent of radiative transfer [5, 6].

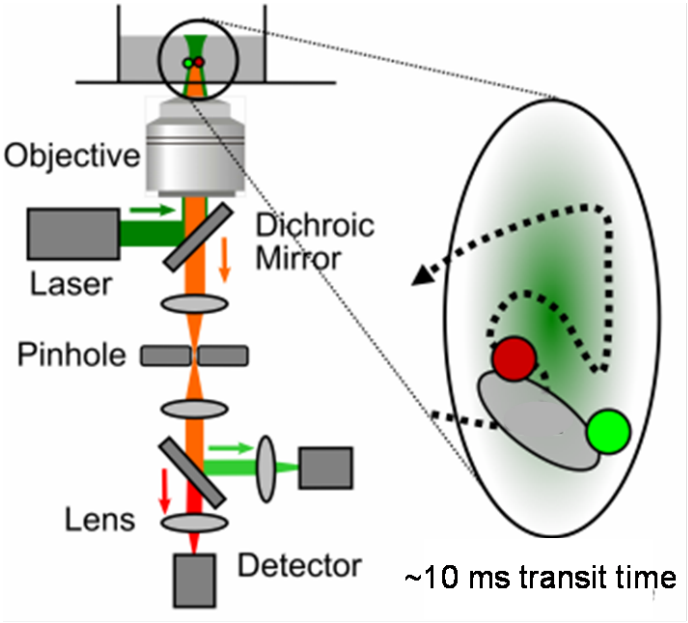


FIGURE 3.3: The pinhole of the confocal optics defines an observation volume on the order of femtolitres. The diffusion constant of the solution is such that this means that it is overwhelmingly probable that only one fluorescently labelled molecule will be traversing the observation volume at a time, effectively making this a single molecule technique.

Alternating-laser excitation (ALEX) produces four photon streams [72]: $F_{Dex,Dem}$, $F_{Dex,Aem}$, $F_{Aex,Dem}$, and $F_{Aex,Aem}$, where $F_{Xex,Yem}$ is the photon count detected in the Y-emission wavelength upon excitation with the X-excitation laser[3]. Fluorescence bursts corresponding to molecules detected diffusing through the observation volume are identified using the algorithm described in Kapanidis (2008) [109] and Lee *et al.* [78] (and described below in the *Data analysis* section). Apparent FRET efficiency (E^*) and Stoichiometry (S) are calculated for each burst using the equations:

$$E^* = \frac{F_{Dex,Aem}}{F_{Dex,Aem} + F_{Dex,Dem}} \tag{3.1}$$

$$S = \frac{F_{Dex,Aem} + F_{Dex,Dem}}{F_{Dex,Aem} + F_{Dex,Dem} + F_{Aex,Aem}} \tag{3.2}$$

E^* and S depend on the transfer of fluorescence between the fluorophores, which in turn is highly dependent on the distance between them:

$$E^* = \frac{1}{1 + (\frac{r}{R_0})^6} \tag{3.3}$$

[3] X and Y denoting either the donor (D) or acceptor (A) wavelength.

where r is the distance between the fluorophores, and R_0 is the Förster radius[4] of the dye pair. This exquisite sensitivity upon donor-acceptor separation underlies FRET's great power as a molecular ruler, and therefore as a marker of conformational changes.

3.2.2 Fluorescence-Aided Molecule Sorting (FAMS)

The data from the fluorescence bursts are collated into a two-dimensional histogram of FRET efficiency E^* and Stoichiometry S, as described in Kapanidis *et al.* [72], and illustrated in Figure 3.4. It is possible to discern distinct populations of donor-only, acceptor-only, and donor-acceptor labelled molecules; this is known as Fluorescence-Aided Molecule Sorting. As E^* (FRET efficiency) is dependent upon donor-acceptor distance, if there are populations of doubly labelled molecules which have different donor-acceptor distances, these will also appear as distinct populations on the histogram: a higher E^* (FRET) value is characteristic of a shorter D-A separation, *i.e.* more efficient FRET, and *vice versa*. This could correspond to a sample which contains several different labelled proteins, or the same protein with multiple subpopulations in dynamic equilibrium between different conformational states.

Doubly labelled KirBac1.1

As previously described, there are two fluorescence populations in the doubly labelled KirBac1.1 sample, even without considering any perturbation of the dynamic equilibrium, due to the proximal and distal labelling schemes, whereby two adjacent, or two diagonally opposite subunits have been labelled with the donor and acceptor, respectively. A cartoon of this is shown in Figure 3.5.

As the distance between donor and acceptor dyes is shorter in the proximal scheme than in the distal, E^* (FRET efficiency) will be higher and thus the two populations can be distinguished on the E^*-S histogram, as illustrated in Figure 3.4. The relevant (three-dimensional) donor-acceptor distances for KirBac1.1 in the *closed* state (calculated from PDB entry 2WLL) are given below in Table 3.1, and the locations illustrated in Figure 3.6.

[4]Förster radius: distance at which energy transfer is 50% efficient, or 50% of donors are deactivated by FRET rather than direct decay emission [1].

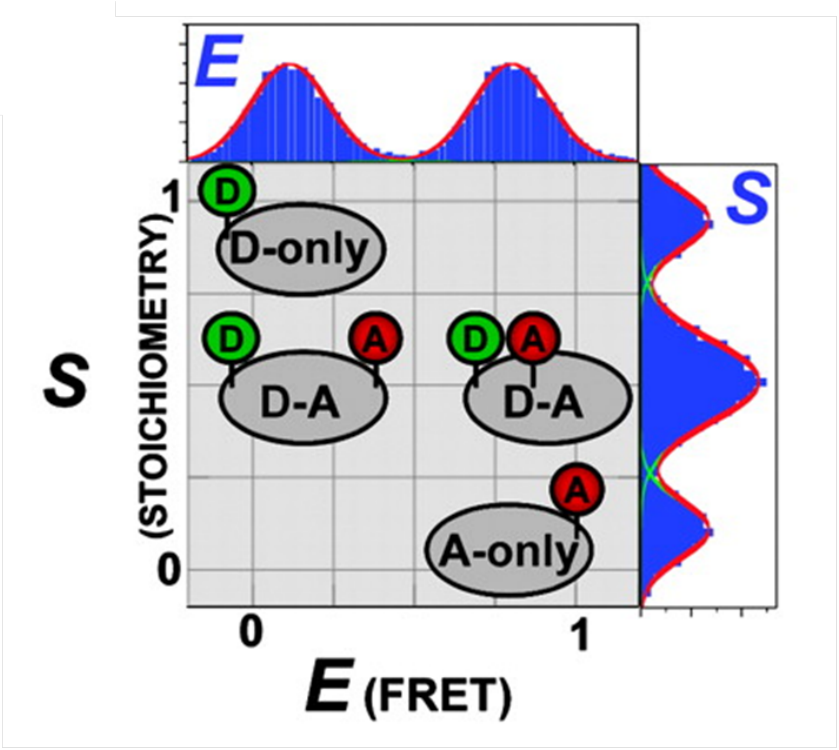


FIGURE 3.4: A stereotypical histogram showing the characteristic E^* and S values of D-only, A-only, and D-A labelled single molecules. The two D-A species have different distances between the donor and acceptor, and thus have different E^*; a higher E^* (FRET) value is characteristic of a shorter D-A separation, *i.e.* more efficient FRET (adapted from Kapanidis *et al.* [72]).

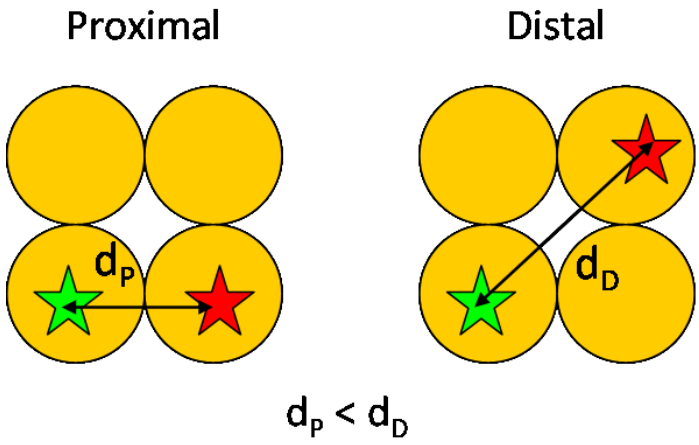


FIGURE 3.5: The two possibilities for doubly labelled KirBac1.1. In the proximal scheme, two adjacent subunits are labelled, there is a short D-A distance, and thus there will be a high E^* (FRET efficiency), whereas in the distal scheme, two subunits diagonally opposite are labelled, there is a longer D-A separation, and hence there will be lower E^*. This is the ideal situation arsing from substoichiometric labelling: three- or four-fold labelling, with more than one donor or acceptor per tetramer, is also possible.

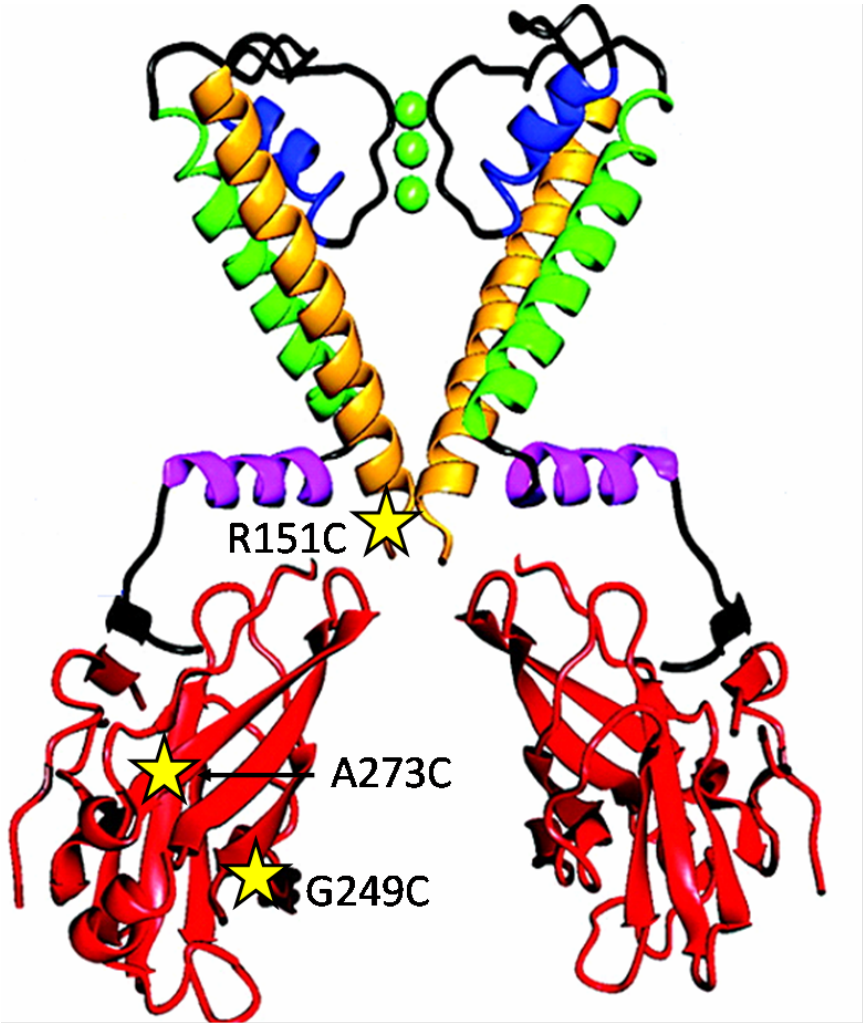


FIGURE 3.6: The location of the cysteine mutations made in KirBac1.1 in order to facilitate cysteine-maleimide labelling. The sites are clustered in or near the cytoplasmic domain, and are hence solvent-accessible (adapted from [74]).

	Proximal	Distal
R151C	16.02 Å	22.77 Å
G249C	44.34 Å	64.22 Å
A273C	34.43 Å	48.07 Å

TABLE 3.1: The donor-acceptor inter-fluorophore distances for three cysteine reporter mutants of KirBac1.1.

The differences between these distances are well within the detectable range of the dye pair, which has a Förster radius of ~ 65 Å, and will therefore appear as distinct populations in the FRET histogram. However, this is the ideal situation resulting from substoichiometric labelling: it is possible that there could be more than one donor or acceptor molecule in each tetramer, resulting in three- or four-fold labelling. This would create complications when considering the collated results of such experiments, but such events are usually excluded by the data processing algorithms.

3.2.3 Data analysis

Photon arrival times were recorded and analysed using software written by Johannes Hohlbein and Joseph Torella using LabVIEW (National Instruments) and MATLAB (MathWorks, Natick) [107]. As previously mentioned, ALEX produces four photon streams, the signals from which can be used to calculate apparent FRET efficiency, E^*, and Stoichiometry, S. Photon bursts were identified using the algorithm described in Kapanidis *et al.* (2008) [109] and Lee *et al.* (2005) [78], which acknowledges photons arriving at the APDs accompanied by a certain number of neighbouring photons arriving within a threshold time interval, and a filter for $F_{Aex,Aem}$ was applied to ensure that only bursts with an activated acceptor fluorophore were examined. E^* and S were collated into two-dimensional E^*-S histograms.

Peak positions of the two FRET populations were obtained by fitting the E^* histograms to double-Gaussian functions. The software also calculated the standard deviation of E^* of each fluorescence burst using a sliding window of twenty photons along the donor excitation stream ($F_{Dex,Dem} + F_{Dex,Aem}$): this was compared to the shot noise limit for each burst, and a standard deviation greater than the shot noise limit was determined to be indicative of protein dynamics, rather than an intrinsic property of the APDs.

3.3 Results: smFRET observations

3.3.1 First observations

Detergent-solubilised purified KirBac1.1 was doubly labelled with Cy3B and AlexaFluor®647 maleimides in observation buffer (20 mM HEPES pH = 7.5, 150 mM KCl, 5 mM EDTA) and observed using confocal-in-solution microscopy with ALEX at 10 kHz between 532 nm (Cy3B, donor excitation, 120 μW CW) and 635 nm (AlexaFluor®647, acceptor excitation, 30 μW CW). The resulting data showed that smFRET was taking place in these samples: a representative example is given in Figure 3.7. Due to the nature of the process, smFRET will not be seen unless the protein in the observation volume is labelled with at least one fluorophore. Comparing the exemplary data to the stereotypical histogram in Figure 3.4, it is likely that regions A and D correspond to acceptor-only and donor-only fluorescence, respectively, whereas B and C are likely to be populations with suboptimal labelling stoichiometry, *e.g.* a deviation from one donor:one acceptor/tetramer. Although it is difficult to distinguish from the other fluorescence populations, it is possible that region E does correspond to donor-acceptor fluorescence, implying that at least a subset of channels in the sample have labelled with the desired stoichiometry. The labelling procedure (described in the previous chapter) was therefore adjusted until a more favourable outcome was achieved, but the smFRET collection procedure itself also required optimisation (described below).

These initial observations confirmed that smFRET was taking place within the samples, and despite the difficulty in distinguishing unambiguous features relating to the subpopulations, they represent the first smFRET observations of an inwardly rectifying potassium channel in solution. It can be seen from Figure 3.7 that while smFRET is occurring, subpopulations that may be distinguishable in E^* have a large spread in S, and *vice versa*. It was therefore highly desirable to optimise the procedure in order to resolve the proximally and distally labelled subpopulations, as this would form a useful control for future measurements.

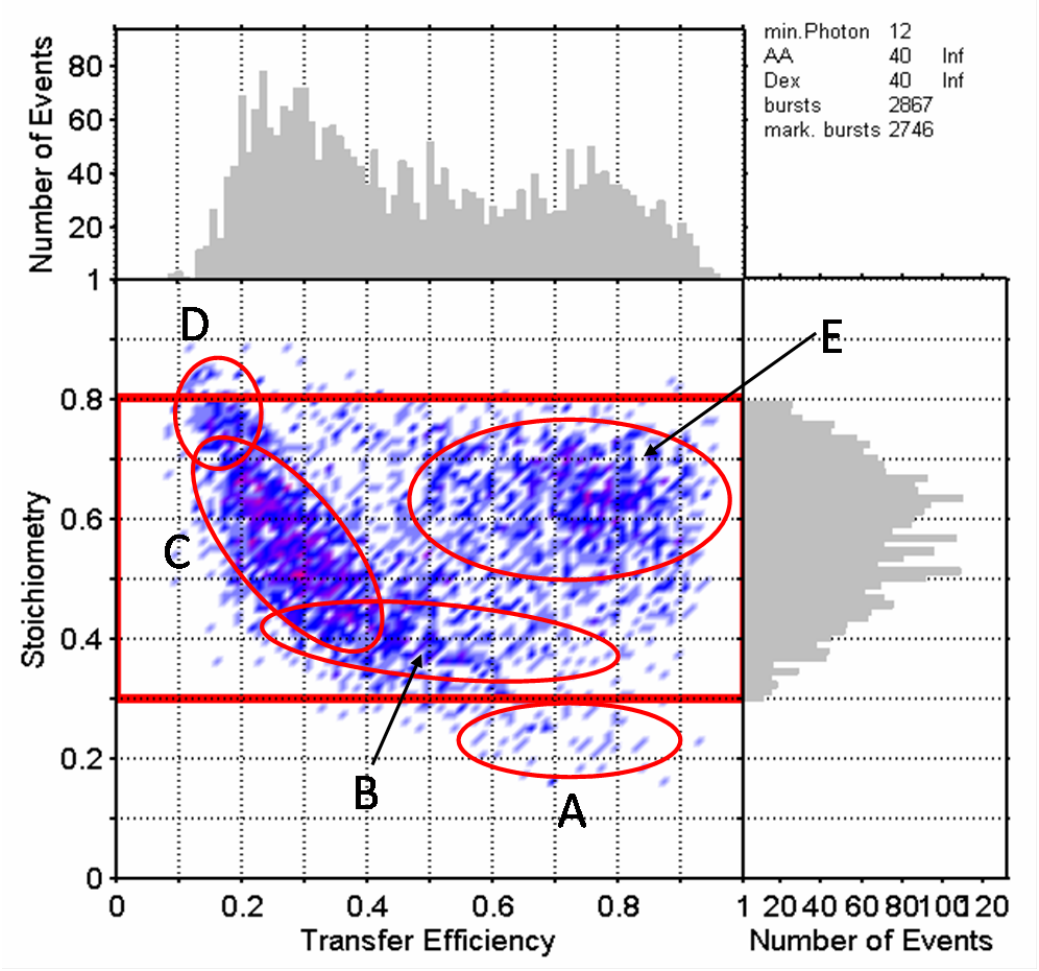


FIGURE 3.7: The initial signals observed from doubly labelled KirBac1.1 (R151C, in this case) implied that smFRET was occurring, but it is difficult to unambiguously distinguish separate populations and make further inferences about the protein subpopulations until further optimisation is undertaken. However, comparison to the stereotypical histogram in Figure 3.4 can help with putative identifications. A: acceptor-only fluorescence. B and C: channels with suboptimal labelling stoichiometry. D: donor-only fluorescence. E: possible donor-acceptor fluorescence.

3.3.2 Optimisation of signal

Optimisation was performed by iterating adjustments of the sample concentration and observation time, with optimal results typically being obtained by observing samples at 5-20 nM for 600-900 seconds with a frame rate of 1 ms, assuming that a single labelled channel in a detergent micelle would diffuse across the femtolitre observation volume in a time of $\sim$ 10 ms (this is relatively trivial to calculate[5]).

However, small deviations from optimal alignment of the microscope (particularly of the detection pathways) can affect the ability of the APDs to detect fluorescence bursts. In order to confirm that the alignment was optimal, and consistent between experimental sessions, a piece of doubly labelled double-stranded DNA was observed. The construct used is T1B17: the upper strand has a donor fluorophore (Cy3B) attached at one end, and a biotin molecule at the other; and the lower strand has an acceptor fluorophore (Atto647N) attached 16 base pairs from the donor, illustrated in Figure 3.8. The peak in the E^*-S histogram should be a symmetric Gaussian, and should be consistent to $\sim$1% between sessions. This is also shown in Figure 3.8, with E = $\sim$0.51 and S = $\sim$0.68.

3.3.3 Resolution achieved

Iteration of the adjustments required for optimising smFRET signal collection resulted in being able to obtain data sets for all three cysteine mutants where the proximally and distally labelled protein populations can be distinguished. This is illustrated in Figure 3.9, where two clearly defined fluorescence populations can be seen in the smFRET histograms for the R151C, G249C, and A273C reporter mutations. These results are the first smFRET

[5] A rough estimate can be obtained using the Einstein relation and assuming only translational diffusion (*i.e.* disregarding rotational diffusion of the micelle). The Einstein relation defines:

$$D = \frac{k_B T}{6\pi\eta r} \tag{3.4}$$

Where $k_B T \sim 4x10^{-21}$ J at room temperature; dynamic viscosity of water $\eta = 8.90x10^{-4}$ Pa s; and the radius of the protein-detergent complex is assumed to be $\sim$ 20 nm. This results in a coefficient of diffusion $D \sim 1.2x10{-}12$ $m^2 s^{-1}$.

For three-dimensional diffusion:

$$\langle z^2 \rangle = 6Dt \tag{3.5}$$

Assuming $\langle z^2 \rangle = 10^{-12}$ m^2 (for a femtolitre observation volume assumed to be a cube), this results in $t \sim 10$ ms.

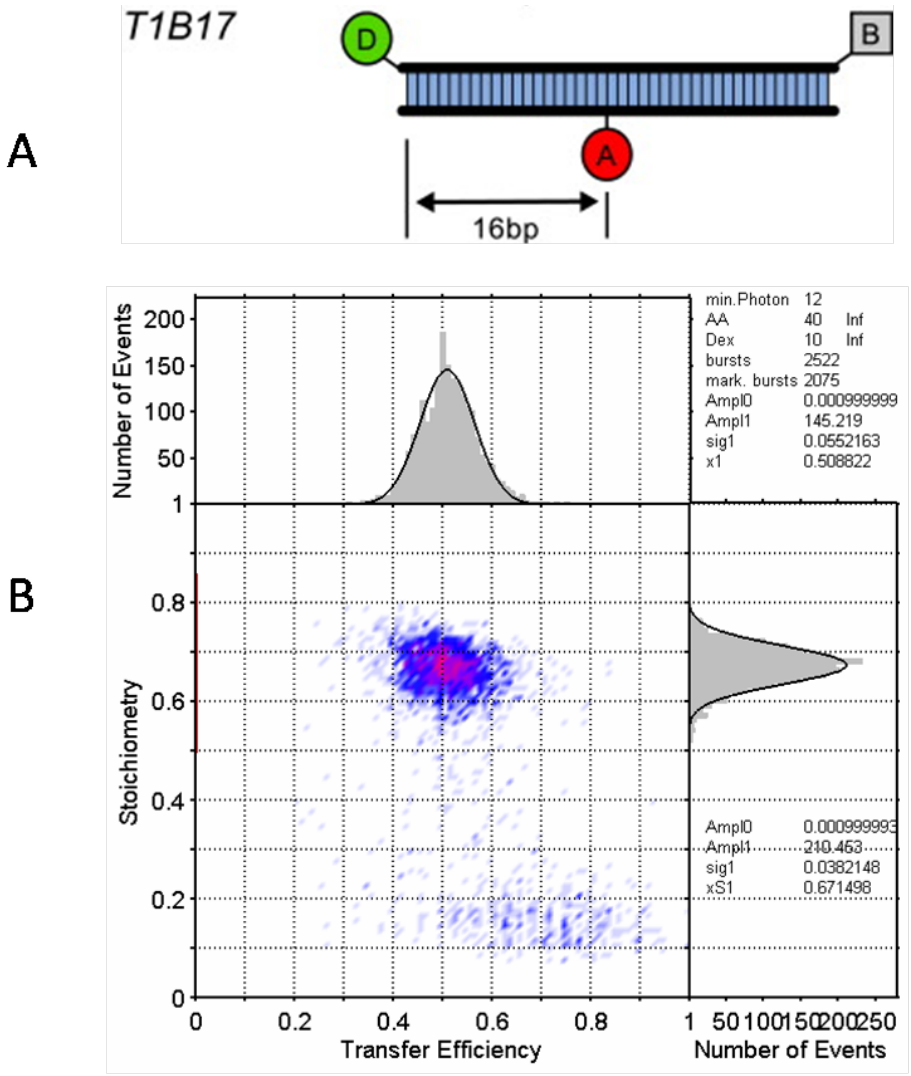


FIGURE 3.8: The smFRET signal for a doubly labelled piece of double-stranded DNA should have consistent values of E^* and S between experimental sessions if the detection path of the microscope has remained in optimal alignment.
(A) T1B17 is the construct used in this study. The upper strand has the donor (D: Cy3B) attached at one end, and a biotin molecule (B in the figure) at the other. The bottom strand has the acceptor (A: Atto647N) attached 16 base pairs away from the donor.
(B) The control sample should produce a symmetric Gaussian peak with $[E^*, S] = [0.51, 0.68]$. There is a small amount of acceptor-only fluorescence in the bottom right-hand corner of the histogram.

observations of an inwardly rectifying potassium channel in solution, and therefore represent a notable achievement with respect to experimental treatment of these channels.

3.4 Conclusions

This chapter describes the protocol for smFRET recordings of KirBac1.1, and presents the first observations of single-molecule fluorescence from an inwardly rectifying potassium channel in solution. This has been performed for all three cysteine reporter mutations made on KirBac1.1. The signals observed reliably and repeatably distinguished the proximally and distally labelled populations present in the samples, and will therefore form the basis of the control measurements for future investigations.

However, it is also necessary to demonstrate that these are true smFRET signals from the channel, rather than artefacts of some sort. This was done by modifying the dynamic equilibrium of the channel by making changes to the gating state in a predictable way which matches observations made in functional studies, with the aim of producing a predictable and repeatable shift in E^* corresponding to the known conformational changes of KirBac1.1 upon gating. Several modulatory factors were explored: point mutations known to correspond to activatory point mutations of KirBac1.1 [95]; changing the pH of the buffer; and adding a lipid ligand such as PIP_2. These attempts, and the resulting smFRET data, are presented and discussed in Chapter 4.

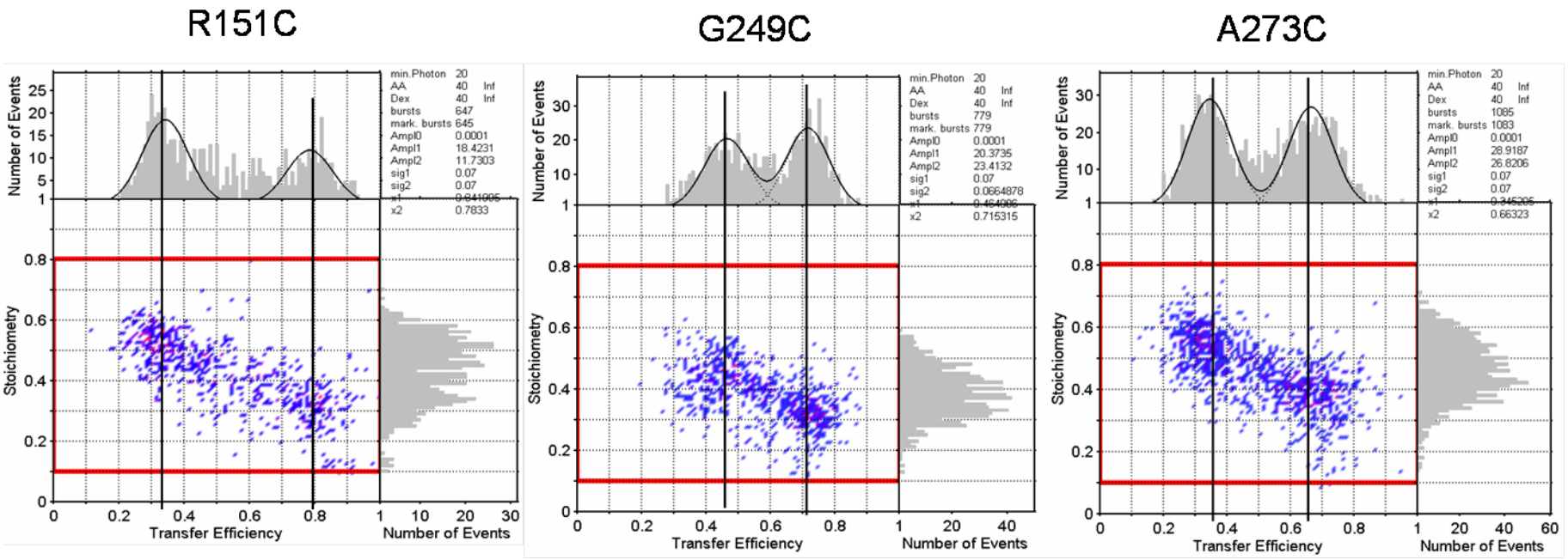


FIGURE 3.9: Post-optimisation smFRET histograms for all three cysteine mutants of KirBac1.1. The proximally (higher E^*) and distally (lower E^*) labelled populations can be distinguished, and the fitted Gaussian curves are distinct.

Chapter 4

Monitoring conformational changes in KirBac1.1 using smFRET

4.1 Introduction

The first smFRET observations of an inwardly rectifying potassium channel in solution have been obtained, and are presented in the previous chapter. However, in order to fully validate these results it is necessary to be able to modulate this signal in a repeatable manner. This can be done by changing the open-closed state dynamic equilibrium using point mutations and well-known modulatory factors such as pH and PIP_2. The aim was to be able to observe a repeatable and predictable change in E^* corresponding to known conformational effects of the perturbatory factors on KirBac1.1 gating, hence confirming that the fluorescence observed originates from KirBac1.1. This has indeed been achieved for doubly labelled KirBac1.1 in detergent micelles, and in addition, evidence for a common conformational mechanism for both pH- and PIP_2-modulated inhibition has been obtained.

For all modulatory attempts, codon-optimised KirBac1.1 with a single cysteine mutation was expressed, purified, and doubly labelled with Cy3B and AlexaFluor®647 as described in Chapter 2, and confocal-in-solution smFRET microscopy with ALEX between the donor and acceptor wavelengths performed as described in Chapter 3. There were some variations in the minor details of the experimental techniques depending on the method of perturbation being investigated; these are described in the relevant sections below.

4.1.1 Chapter summary

This chapter is divided into three sections, each separately dealing with the perturbatory factors upon the open-closed dynamic equilibrium examined in this thesis, and thereby the smFRET histograms and FRET efficiency:

- Role of activatory gating mutants;
- Changes in pH: inhibition by H^+;
- Addition of inhibitory PIP_2.

4.2 Activatory gating mutations

4.2.1 Selection and creation of mutations

Random mutagenesis followed by potassium uptake assays performed by Paynter *et al.* identified potential activatory mutations in KirBac1.1, hypothesised to be caused by gating modulations, possibly by increasing the open probability of the channel [95]. These mutations were mainly clustered near the slide helix and helix bundle crossing (HBC), and were used as the starting point for this study: the mutations in KirBac1.1 chosen, including the cysteine reporter mutations, are listed in Table 4.1 and illustrated in Figure 4.1.

	Mutation	Location
Labelling site	R151C	HBC
	G249C	cytoplasmic domain
	A273C	cytoplasmic domain
Activatory site	S136P	HBC
	G143E	HBC
	L144P	HBC
	V145L	HBC

TABLE 4.1: Mutations – both cysteine reporter and activatory – made in KirBac1.1.

All activatory mutations have been made in conjunction with one of the cysteine mutations required for labelling, and all fifteen possible combinations were made by PCR using the codon-optimsed KirBac1.1 as the template. Construction of these mutations was facilitated by use of the codon-optimised gene, rather than the original G-C rich gene. Following creation of the point mutations, the protein was expressed, purified, and doubly

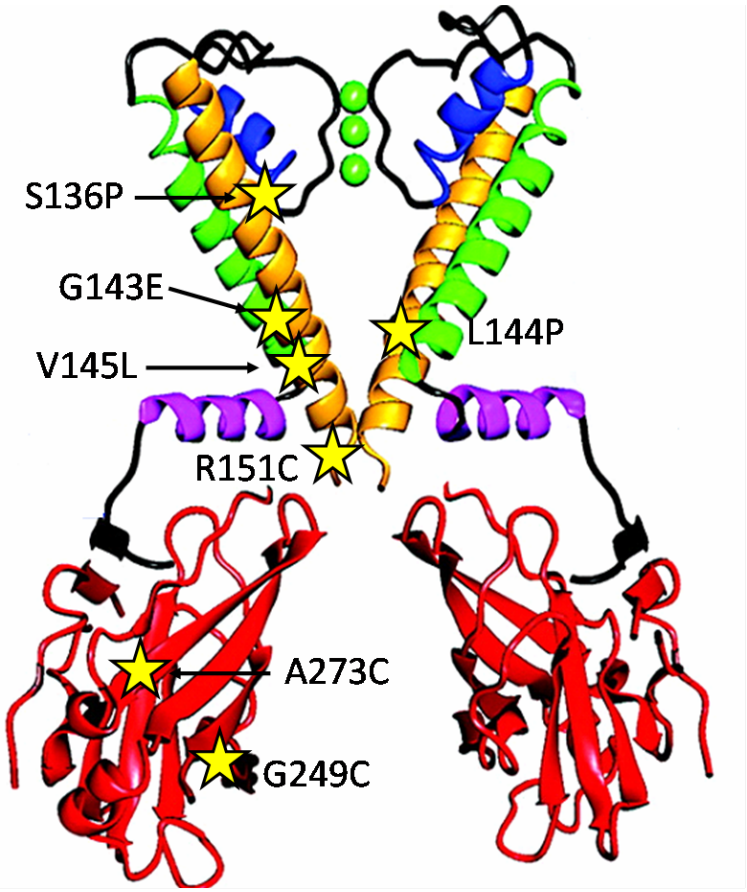


FIGURE 4.1: The location of each point mutation made in KirBac1.1. The cysteine reisdues are clustered in or near the cytoplasmic domain, are therefore solvent-accessible, and hence accessible to labelling substrates, whereas the activatory mutations are clustered near the helix bundle crossing (figure adapted from [74]).

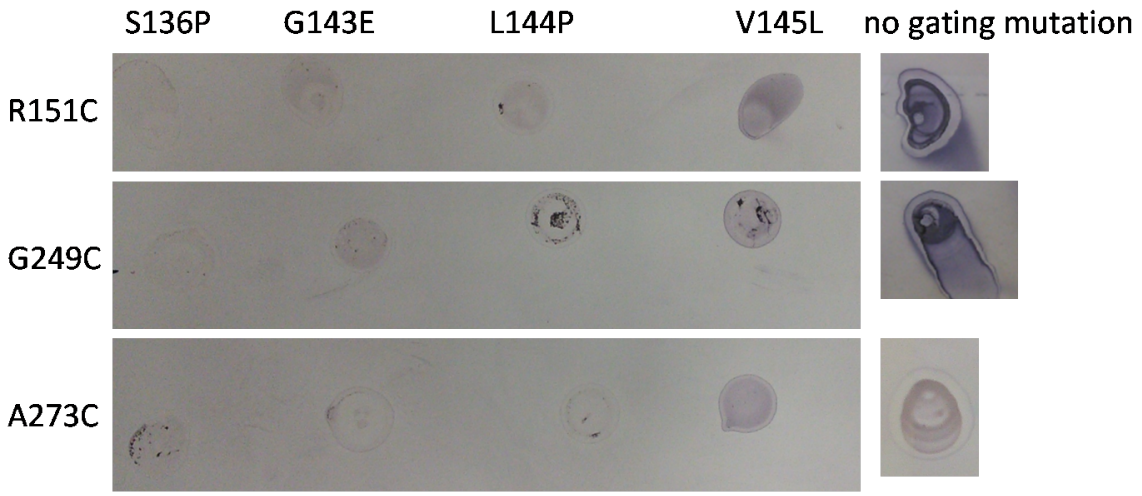


FIGURE 4.2: A dot blot expression test for the five activatory point mutations upon templates already containing the cysteine mutations. A clear purple spot indicates a satisfactory level of expression: it can be seen that while V145L is expressed with a high yield, there is a poor yield of S136P.

labelled with Cy3B and AlexaFluor®647 maleimides in the same way as the cysteine-only versions. The reporter cysteine residues used in this study have all been shown to be solvent-accessible and capable of being labelled [123].

4.2.2 Expression levels of gating mutants

Protein expression was tested by making a dot blot of the whole cell lysate using Anti-His antibody: results are shown in Figure 4.2. The S136P mutant was deemed to produce too low a yield for further experiments, and as the yield of V145L was particularly high compared to the other gating mutations, work therefore focused on the use of V145L as a perturbatory mutation applied to KirBac1.1.

4.2.3 Functional studies of KirBac1.1 (V145L)

To verify the presence of V145L, electrophysiological studies were performed by Marc Szabo[1]): the results are shown in Figure 4.3. These recordings were taken using the patch clamp method applied to channels inserted into a droplet-hydrogel bilayer (DHB) [19]. The reversal of the current direction upon reversal of the polarity of the applied voltage suggests the presence of a channel. The V145L mutation is thought to increase activity of KirBac1.1 based upon the results potassium uptake studies performed by Paynter *et al.* [95].

[1]Wallace group, Chemistry Research Laboratory, University of Oxford

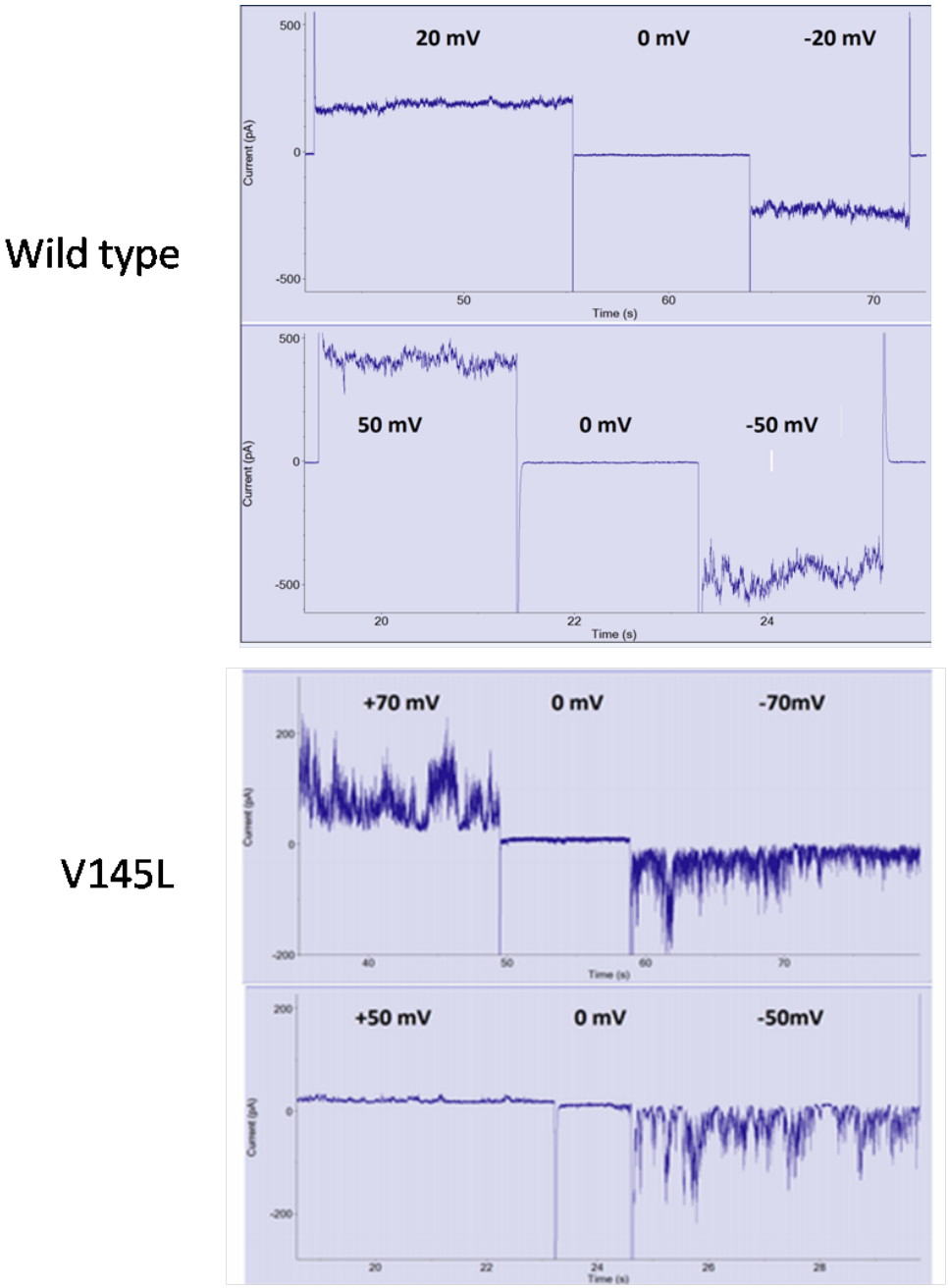


FIGURE 4.3: An I-V trace of a KirBac1.1-V145L channel (bottom), compared with the wild type (top). The reversal of current direction upon reversal of the polarity of the applied voltage suggests that a channel may be present. These experiments were performed by Marc Szabo, of the Wallace group.

4.2.4 Labelling and smFRET

Labelling of the mutant channels was successfully performed according to the protocols described in Chapter 2. The doubly labelled detergent-solubilised KirBac1.1 with gating mutants in buffer (20 mM HEPES pH = 7.5, 150 mM KCl, 0.5 mM EDTA) was observed using confocal-in-solution microscopy with ALEX at 10 kHz between 532 nm (Cy3B, donor excitation, 120 μW CW) and 635 nm (AlexaFluor®647, acceptor excitation, 30 μW

CW). Data was obtained for the cysteine/gating mutation combinations marked in Table 4.2.

	R151C	G249C
S136P	X	
G143E		X
V145L	X	X

TABLE 4.2: Cysteine/gating mutation combinations for which smFRET data was obtained.

4.2.5 Results: exemplary raw data

In order to obtain a reliable value for the shift in the smFRET histogram population peaks, it is necessary to be able to resolve the two peaks corresponding to the distal labelling population (denoted x_1) and the proximal labelling population (denoted x_2). This is illustrated using a 'raw' data set in Figure 4.4. If the two population peaks cannot be resolved, a shift in the E^* of the peaks will not be resolved upon attempting to modulate the signal, so the acquired data cannot be used. An exemplary E^*-S histogram for each experimental condition is given in the Appendices (Section A.3) for illustrative purposes.

4.2.6 Results: exemplary smFRET shift data

The shift in E^* of each peak is plotted on a scatter/bar graph, where the height of the bar represents the mean shift, and the error bars correspond to the standard deviation. This is illustrated using artificially generated data in Figure 4.5 (all figures were created using GraphPad Prism 6). The overall shift is deemed to be the difference between the mean FRET efficiency for each population peak (with and without the modulatory factor), and p-values are calculated for each population using the automatic unpaired t-test function included in the software.

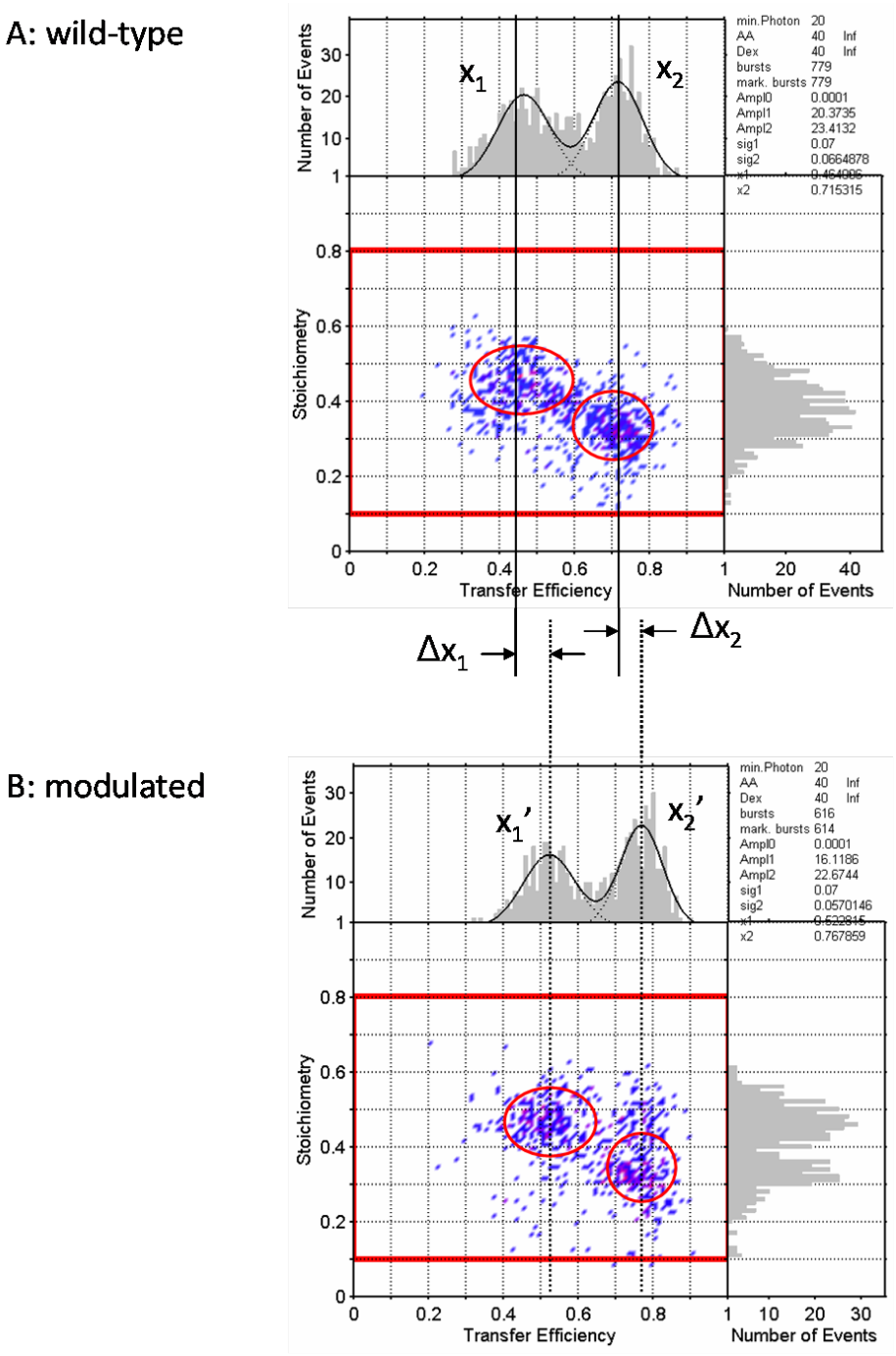


FIGURE 4.4: An examplary smFRET histogram, illustrating the notation used in determining peak E^* shift. The distally labelled (low transfer efficiency) population peak is referred to as x_1, and the proximally labelled (higher transfer efficiency) population peak is denoted by x_2. (A) wild-type, unmodulated KirBac1.1. (B) KirBac1.1 with the application of a modulatory factor, demonstrating a shift in E^* ($x_1' - x_1 = \Delta x_1$, $x_2' - x_2 = \Delta x_2$) to higher values.

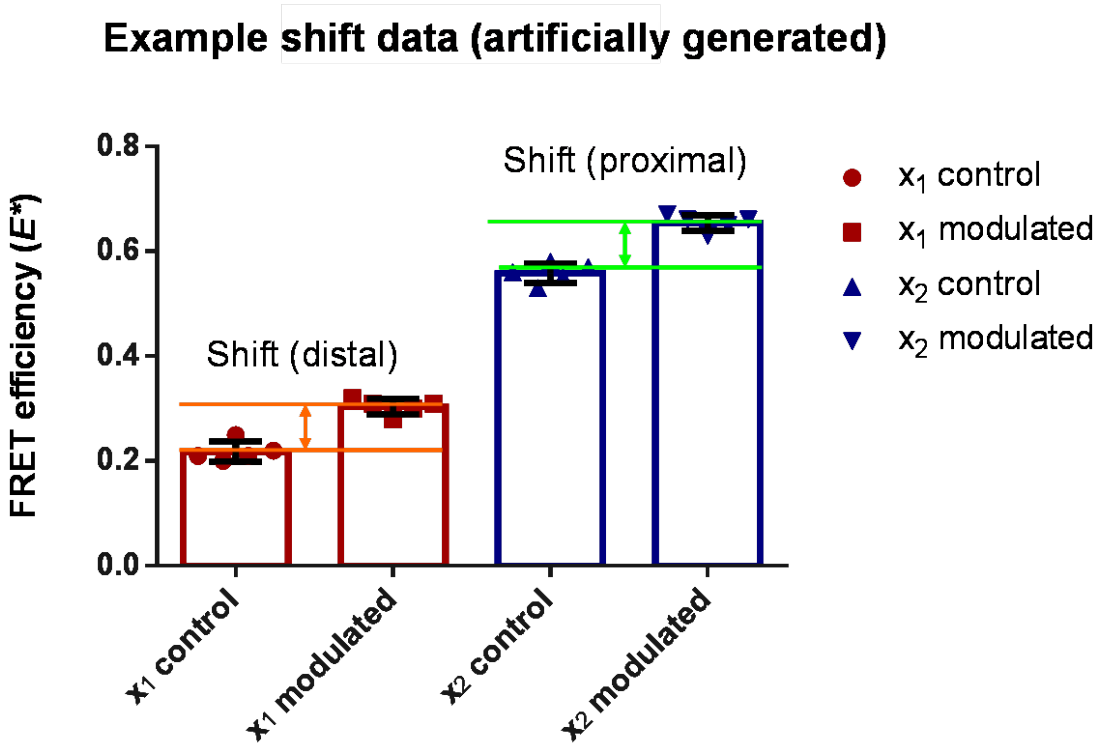


FIGURE 4.5: An exemplary graph showing how the shifts in E^* are calculated, made by plotting artificially generated data. The height of the bar represents the mean shift for the population, and the error bars correspond to standard deviation. The shift in E^* for each labelling population is the difference between the mean FRET efficiencies.

4.2.7 Results: R151C as the reporter site

Although smFRET recordings were attempted for all the mutation combinations listed above in Table 4.2, the only combination which was found to produce fluorescence data with sufficiently distinct histogram populations to enable the detection of a shift in E^* was R151C/V145L, which produced a slight shift to higher E^*, therefore reporting a *decrease* in the inter-fluorophore distance. However, it can be seen from the values of E^* obtained (from the Gaussian fitting algorithm applied to the fluorescence bursts, given in Table 4.3 and illustrated in Figure 4.6), that although this shift showed some degree of repeatability, it was not necessarily reliably so, and the errors were relatively large[2]. Indeed, when all experiments were collated, the data had a p-value of 0.686 and 0.177, for the distal (x_1) and proximal (x_2) peaks, respectively[3]. This is well above the $p < 0.05$ required for statistical significance.

Sample		R151C only	R151C + V145L	Shift in E^*
α	x_1	0.218 ± 0.004	0.235 ± 0.012	0.017 ± 0.013
	x_2	0.454 ± 0.023	0.539 ± 0.031	0.085 ± 0.039
		n = 3	n = 7	
β	x_1	0.229 ± 0.012	0.226 ± 0.008	-0.003 ± 0.014
	x_2	0.469 ± 0.052	0.478 ± 0.017	0.009 ± 0.055
		n = 3	n = 4	
γ	x_1	0.245 ± 0.012	0.269 ± 0.004	0.024 ± 0.013
	x_2	0.481 ± 0.007	0.512 ± 0.005	0.031 ± 0.009
		n = 2	n= 3	
δ	x_1	0.306 ± 0.010	0.316 ± 0.005	0.010 ± 0.011
	x_2	0.526 ± 0.015	0.525 ± 0.011	-0.001 ± 0.019
		n = 7	n= 5	
Mean	x_1	0.250 ± 0.040	0.262 ± 0.041	0.012 ± 0.012
	x_2	0.483 ± 0.031	0.513 ± 0.025	0.031 ± 0.038

TABLE 4.3: smFRET shifts for the R151C reporter mutation with and without the activatory V145L mutation. There is a modest shift to higher FRET efficiency.

[2]All errors on E^* values in this thesis are the standard deviation of the values obtained from the Gaussian fits. "n" denotes the number of trials during each acquisition session (denoted by the Greek letters). Errors on the mean values are the standard deviation of the means for all sessions. Errors on the shifts were obtained by root squared addition of these standard deviations.

[3]All p-values in this thesis were calculated using the unpaired t-test function of GraphPad Prism 6. A p-value is defined as the probability of observing a result as extreme as the one actually obtained, when assuming the null hypothesis (no change, in this case). It is generally considered that $p < 0.05$ represents an acceptable degree of statistical significance.

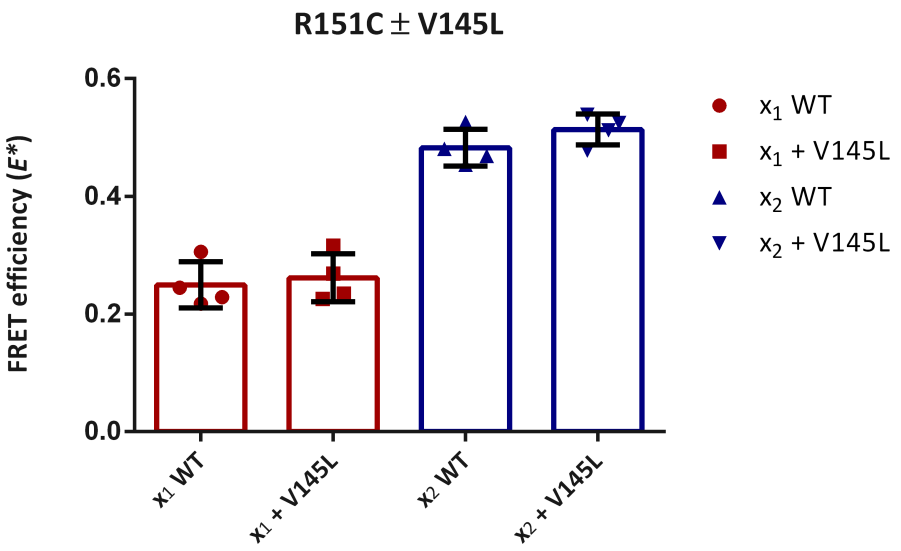


FIGURE 4.6: smFRET shifts for the R151C reporter mutation with and without ("WT") the activatory point mutation V145L. There is a modest shift to a higher FRET efficiency for both peaks, but this is obscured by a large error on the data.

4.2.8 Discussion: activatory mutations

It is possible that a channel solubilised in detergent micelles might not produce the most reproducible data. In addition to the non-ideal physical properties of the micelles themselves, such as their tendency to aggregate, and to autofluoresce which may interfere with the detected signal, a detergent micelle is an energetically unfavourable environment for a membrane protein. This consequently may hinder the gating mechanism, not only because the protein may be less stable, but also because membrane lipids themselves may be required to interact with the protein and stabilise its conformational states: this is thought to be essential for gating due to PIP_2 and other phospholipids [62, 127]. Repeating this experiment with KirBac1.1 reconsituted into nanodiscs would hopefully produce better quality results as the channel will be solubilised in a more favourable, native-like environment: this is presented and discussed in Chapter 5.

Although observations of other reporter/gating mutant combinations were attempted, it was not possible to detect a shift in E^*, in part because the two distinct labelling populations could not be resolved. This is potentially either because those mutants have no effect on the conformational states of KirBac1.1, or, more interestingly, they do not have an effect on the conformation *at the location of the cysteine reporter mutation*, and therefore any

conformational change that might be taking place is effectively undetectable. It would be interesting to re-examine these mutants after reconstitution into nanodiscs has eliminated the problem of the unfavourable solubilisation into detergent. Indeed, these experiments with the V145L mutation were performed in nanodiscs with G249C as the reporter mutation, and an effect was observed (see Chapter 5).

4.3 Inhibition by H^+

4.3.1 Sample preparation

KirBac1.1 is known to be inhibited by low pH [13, 24, 67], and as buffer exchange is a relatively trivial procedure to perform upon a protein sample, investigating whether a change in pH would produce a modulation of the smFRET signal was an obvious investigation to perform.

All smFRET experiments were performed as described in Chapter 3, with the exception of the observation buffer, which instead used 50 mM MES pH = 5.5 (in substitution for 20 mM HEPES pH = 7.5 control), constituting a change towards more acidic pH. As the protein is diluted in the observation buffer ~100 times to achieve the concentration required for resolving the fluorescence bursts, it was therefore unnecessary to perform buffer exchange on the protein sample itself.

The doubly labelled detergent-solubilised KirBac1.1 was observed using confocal-in-solution microscopy with ALEX at 10 kHz between 532 nm (Cy3B, donor excitation, 120 μW CW) and 635 nm (AlexaFluor®647, acceptor excitation, 30 μW). Data was obtained for both the R151C and G249C cysteine reporter mutations, but A273C did not produce resolvable peaks.

4.3.2 Results: R151C as the reporter site

As can be seen from the FRET efficiency values given below in Table 4.4 (taken from the Gaussian algorithm fitting applied to the burst data and smFRET histograms), a shift towards *lower E** (of magnitude ~0.05, on average) was observed upon a change to more acidic pH when R151C is used as the reporter mutation, illustrated in Figure 4.7.

Sample		pH = 7.5	pH = 5.5	Shift in *E**
α	x_1	0.261 ± 0.006	0.254 ± 0.006	-0.007 ± 0.008
	x_2	0.525 ± 0.037	0.468 ± 0.011	-0.057 ± 0.039
		n = 3	n = 4	
β	x_1	0.256 ± 0.007	0.247 ± 0.009	-0.009 ± 0.011
	x_2	0.490 ± 0.033	0.469 ± 0.014	-0.021 ± 0.036
		n = 6	n = 7	
γ	x_1	0.326 ± 0.054	0.238 ± 0.008	-0.088 ± 0.055
	x_2	0.558 ± 0.069	0.438 ± 0.030	-0.12 ± 0.075
		n = 9	n = 6	
Mean	x_1	0.281 ± 0.039	0.246 ± 0.008	-0.035 ± 0.046
	x_2	0.524 ± 0.034	0.458 ± 0.018	-0.066 ± 0.050

TABLE 4.4: smFRET shifts for the R151C reporter mutation upon a change to a more acidic (inhibitory) pH when the protein is solubilised in detergent micelles. There is a repeatable shift to lower *E**.

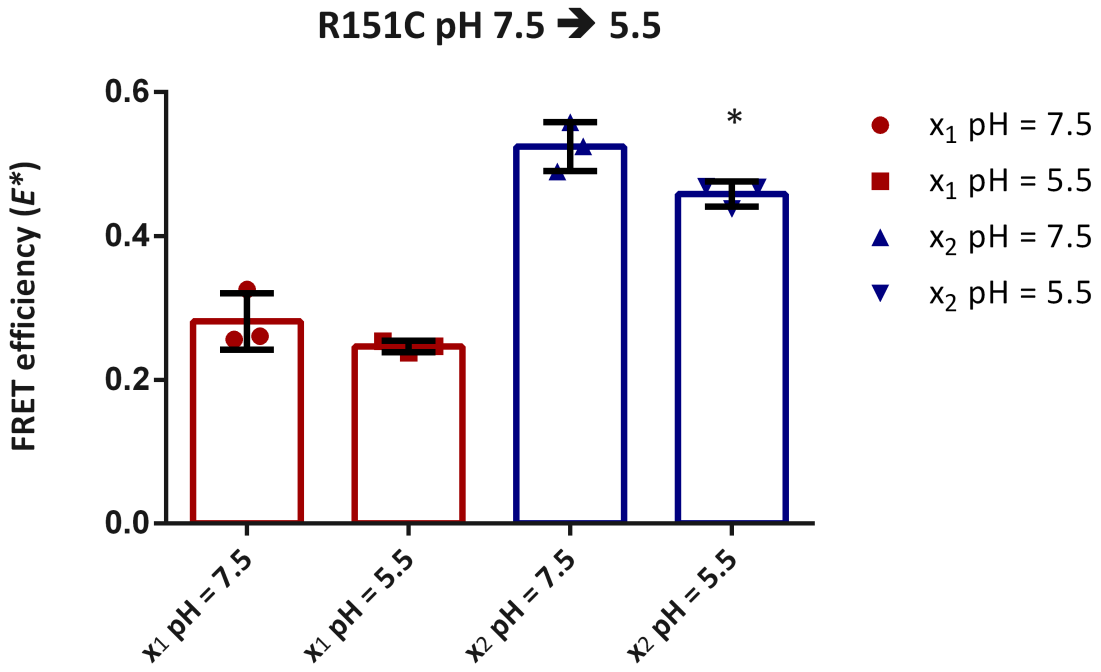


FIGURE 4.7: smFRET shifts for the reporter mutation R151C upon a change to a more acidic (inhibitory) pH when KirBac1.1 is solubilised in detergent micelles. There is a distinct shift to lower E^* for both population peaks.

This effect also appears to be rather variable (standard deviation of shifts ~0.04), but may again be due to the unfavourable environment of the detergent micelle. Indeed, the p-values of the x_1 and x_2 peaks, respectively, were $p = 0.207$ and $p = 0.041$, not representing a truly statistically significant result. However, despite this, it might be said that there is a decrease in FRET efficiency for both labelling populations.

4.3.3 Results: G249C as the reporter site

As can be seen from the FRET efficiency values given in Table 4.5 (taken from the Gaussian fitting algorithm applied to the fluorescence burst data and smFRET histograms), a shift towards *higher* E^* (of magnitude ~0.04, on average) was observed upon a change to more acidic pH when G249C is the dye-labelled reporter mutation. This is also illustrated in Figure 4.8.

Sample		pH = 7.5	pH = 5.5	Shift in E^*
α	x_1	0.382 ± 0.010	0.471 ± 0.006	0.089 ± 0.012
	x_2	0.690 ± 0.013	0.727 ± 0.025	0.037 ± 0.028
		n = 5	n = 3	
β	x_1	0.410 ± 0.009	0.458 ±0.010	0.048 ± 0.013
	x_2	0.725 ± 0.008	0.741 ± 0.012	0.016 ± 0.014
		n = 6	n = 4	
γ	x_1	0.460 ± 0.030	0.559 ± 0.034	0.099 ± 0.045
	x_2	0.733 ± 0.005	0.773 ± 0.010	0.040 ± 0.051
		n = 3	n = 4	
δ	x_1	0.522 ± 0.023	0.604 ± 0.001	0.082 ± 0.023
	x_2	0.741 ± 0.022	0.748 ± 0.010	0.007 ± 0.024
		n = 3	n = 2	
ϵ	x_1	0.482 ± 0.018	0.519 ± 0.018	0.037 ± 0.025
	x_2	0.707 ± 0.006	0.728 ± 0.005	0.021 ± 0.008
		n = 3	n = 2	
ζ	x_1	0.485 ± 0.004	0.522 ± 0.004	0.037 ± 0.006
	x_2	0.717 ± 0.013	0.760 ± 0.023	0.043 ± 0.026
		n = 5	n = 3	
η	x_1	0.500 ± 0.008	0.510 ± 0.006	0.010 ± 0.010
	x_2	0.710 ± 0.019	0.751 ± 0.025	0.040 ± 0.031
		n = 4	n = 2	
Mean	x_1	0.463 ± 0.050	0.520 ± 0.050	0.057 ± 0.033
	x_2	0.718 ± 0.017	0.747 ± 0.017	0.029 ± 0.014

TABLE 4.5: smFRET shifts for the reporter mutation G249C upon a change to a more acidic (inhibitory) pH when the protein is solubilised in detergent micelles. There is a repeatable shift to a higher FRET efficiency.

Similar to the data obtained for the R151C reporter mutation, these results also exhibit some variability (standard deviation of shifts ~0.03), despite the greater number of trials. However, the p-values for this set of data are significantly lower than for the R151C: $p = 0.053$ for x_1, and $p = 0.007$ for x_2, representing a statistically signficant result. Therefore, it can be said that these data show a reasonably convincing shift to a higher FRET efficiency.

Interestingly, this shift in FRET efficiency is in the opposite direction from that observed with the R151C mutation. This has great significance as it suggests the conformational changes underlying the gating mechanism are arising due to specific effects of H^+ inhibition.

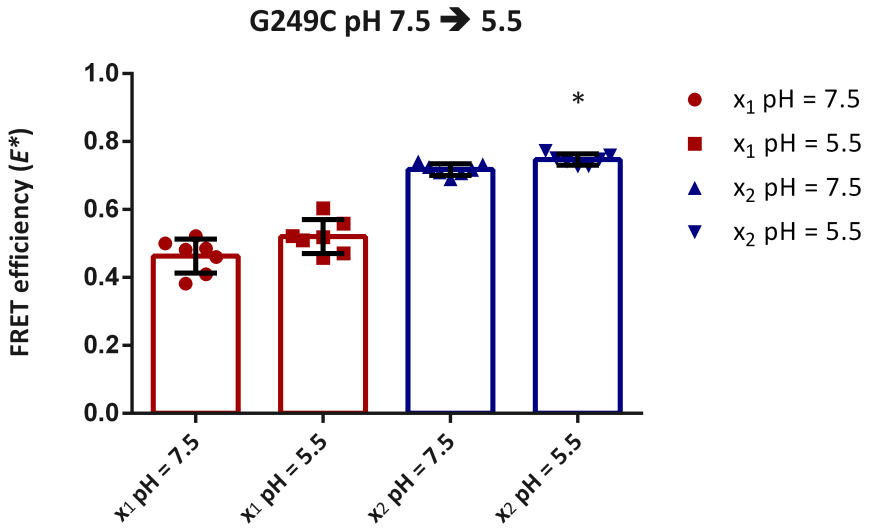


FIGURE 4.8: smFRET shifts for the reporter mutation G249C upon a change to more acidic (inhibitory) pH when KirBac1.1 is solubilised in detergent micelles. There is a small but repeatable shift to higher E^*.

4.3.4 pH does not affect the fluorescent dyes

It is a valid concern that the change in E^* observed upon a change in pH was due to an effect on the dyes themselves, rather than a true effect upon the protein's dynamic equilibrium. Control experiments were therefore performed where a solution of doubly labelled DNA (with some residual free dye present) was observed using the standard confocal-in-solution with ALEX configuration and conditions for the protein measurements. No effect could be observed upon changing pH: as illustrated in Figure 4.9, both conditions produced a transfer efficiency E^* ~0.46, and there was no variation despite repeating this several times. This is in accordance with the manufacturers' specifications which implied that the fluorescence of the dyes should not be variable by a detectable amount within this pH range [2].

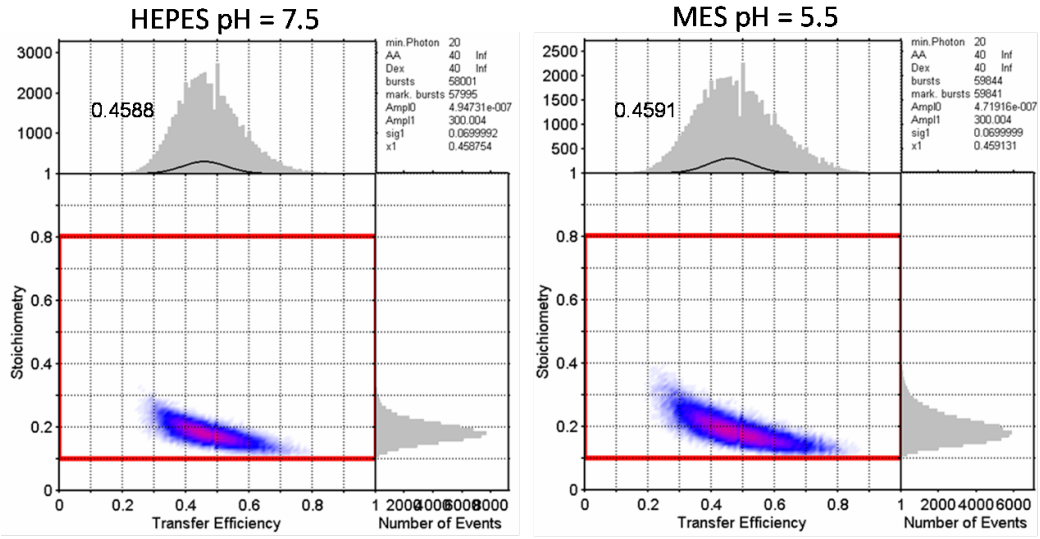


FIGURE 4.9: Representative histograms for the dye-only control measurements at the two different experimental pH points. There is essentially no difference between the conditions: both produced a E^* ~0.46.

4.3.5 Discussion: inhibition by H^+

These experiments were approached with some reservations as previous studies have shown that KirBac1.1 required a non-physiological pH of <5 to exhibit any inhibitory effect [50], but as can be seen in this thesis, a pH of 5.5 still produced a detectable effect while remaining just within the range of what may be experienced by a bacterium *in vivo*.

The above results show that upon lowering the pH of the observation buffer, a condition under which KirBac1.1 has been shown to be inhibited [13, 24, 67], the E^* of both subpopulation peaks in the resultant smFRET histogram is shifted to *lower* E^* for R151C, but *higher* E^* for G249C. Notably, these reporter mutations are in different domains of the protein: R151C is located at the base of one of the transmembrane helices, near the helix bundle crossing, whereas G249C is located near the bottom of the cytoplasmic domain. This therefore suggests that the different domains of KirBac1.1 may move in different directions upon a pH-induced conformational change, a conclusion also reached by Wang *et al.* in their study of the inhibition of KirBac1.1 by PIP_2 [123]. The translations of the cytoplasmic domain and helix bundle crossing in opposing directions could also imply a rotation of the cytoplasmic domain with respect to the transmembrane domain upon gating, a mechanism which has been proposed by several crystallographic studies [13, 37], as well as ensemble-based fluorescence studies by Wang *et al.* [123].

4.4 Inhibition by PIP_2

In an attempt to reproduce the findings of Wang *et al.* with respect to PIP_2 [123], PIP_2 was added to KirBac1.1 with the aim of observing an effect on the smFRET signals.

Wang *et al.* used diC8-PIP_2 at a concentration of 1.25% of total lipid content in their liposome reconstitution [123]. For this study, diC8-phosphatidylinositol 4,5-bisphosphate (PIP_2) (Avanti Polar Lipids) was added to the observation buffer at an equivalent concentration, corresponding to ~20 μM.

Doubly labelled detergent-solubilised KirBac1.1 in buffer (20 mM HEPES pH = 7.5, 150 mM KCl, 0.5 mM EDTA) + 20 μM diC8-PIP_2 was measured using confocal-in-solution microscopy with ALEX at 10 kHz between 532 nm (Cy3B, donor excitation, 120 μW CW), and 635 nm (AlexaFluor®647, acceptor excitation, 30 μW CW), in accordance with the established protocol.

There was no detectable effect[4] on the FRET efficiencies of any of the three cysteine reporter mutations. However, as PIP_2, and related lipid ligands, although producing their effect on Kir and KirBac channels by direct binding, are thought to require some degree of mediation *via* neighbouring membrane lipids [62, 127, 128], such effects are clearly limited when the target protein is solubilised in a detergent micelle.

4.5 Summary of findings

Table 4.6 is a summary of the findings from the study described in this chapter: the direction of the shift in E^* upon perturbation of the dynamic equilibrium of the channel is given. The modulatory factors used in this thesis are known from other studies to affect the gating of the channel: activatory point mutations [95]; inhibition by acidic pH [13, 24, 67]; and inhibition by PIP_2 [62, 127, 128].

It was reassuring to note that the FRET efficiency shift was in opposing directions for the activatory mutation, and for H^+ inhibition for the R151C reporter. Furthermore, the pH-induced shift for the two different cysteine reporter mutations (R151C and G249C) was in opposite directions, reflecting the conformational changes seen by Wang *et al.* [123]. How-

[4] with respect to the resolvability of the proximally and distally labelled smFRET populations

	R151C	G249C
V145L (activatory)	increase x_1: $p = 0.686$ x_2: $p = 0.177$	not measured
acidic pH (inhibitory)	decrease x_1: $p = 0.207$ x_2: $p = 0.041$	increase x_1: $p = 0.053$ x_2: $p = 0.007$
PIP_2 (inhibitory)	no effect (not presented)	no effect (not presented)

TABLE 4.6: A summary of the smFRET data obtained using detergent-solubilised KirBac1.1. The direction of the shifts in E^* relative to the control measurements are given.

ever, the p-values of the collated data show that these results are not particularly significant, with $p > 0.05$ for most shifts in E^* quantified. Addition of PIP_2 had no detectable effect, but this may be due to the requirement for an interaction with the membrane lipids for KirBac1.1 [62, 127, 128].

These studies were therefore repeated with KirBac1.1 solubilised into a more native-like environment. This work is presented in the next chapter, where the channel is reconstituted into nanodiscs and the examinations of the perturbation of the dynamic equilibrium through measurements of the changes in FRET efficiency carried out.

Chapter 5

Nanodisc reconstitution

5.1 Introduction

Nanodiscs consist of two amphipathic alpha-helical membrane scaffold proteins (based on apolipoprotein A-I) each wrapped around one leaflet of a bilayer lipid membrane [14, 18], as illustrated in Figure 5.1. The fact that the nanodisc is stabilised by the bounding protein belt means that a reconstituted protein sample could be stable at room temperature for several days, the nanodiscs' size is monodisperse within a sample, and their size is consistent between sample preparations [14, 87, 103]. Nanodiscs are also thought to reflect the phase behaviour of the membrane more accurately than other lipid reconstitution systems, and certainly more accurately than detergent micelles, which will of course have an influence on the conformational dynamics of an integral membrane protein [20, 44, 110].

It is clear that nanodiscs are more likely to accurately reflect the *in vivo* behaviour of an intergral membrane protein such as an ion channel; not only is the protein going to remain more stable, whereas a detergent-solubilised sample might degrade or aggregate [11], the presence of membrane lipids are thought to play a mediating role in processes such as gating regulation by certain ligands, for example PIP_2 [51]. As regulation of both eukaryotic Kir and prokaryotic KirBac activity is thought to be associated with tethering of the cytoplasmic domains of the membrane through an interaction between the membrane lipids and slide helix [51], this approach could provide new insights into structural aspects of the gating mechanism that are not possible using detergent-solubilised samples.

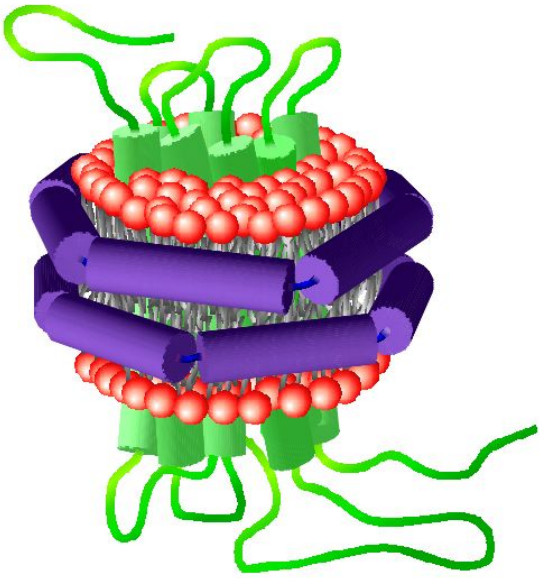


FIGURE 5.1: A cartoon of a nanodisc containing a reconsituted membrane protein with six transmembrane alpha helices. The "double belt" amphipathic alpha-helical membrane scaffold proteins are shown in purple, the lipids in red, and the reconstituted membrane protein in green (from S. Sligar's webpage).

It was therefore hoped that reconstitution into nanodiscs might lead to more reliable and repeatable data than for detergent solubilisation. Successful reconstitution would also act as proof that this technique is viable for future examinations of Kir (and other potassium-selective) channels. In solution, nanodiscs can be treated in the same manner as detergent micelles [18], the fluorescence microscope procedures for which have already been optimised and described in detail in this thesis (particularly in Chapter 3). It is therefore unnecessary to modify the experimental procedure in order to acquire smFRET observations of KirBac1.1 reconstituted into nanodiscs.

This chapter presents the successful expression and purification of membrane scaffold protein (MSP) which hence enabled the successful optimisation of a protocol for the reconstitution of doubly labelled KirBac1.1 into nanodiscs. Confocal-in-solution smFRET microscopy with ALEX was performed, as described in Chapter 3, and fluorescence data acquired in order to make a comparison of this technique with standard detergent solubilisation. If the nanodisc system is an effective alternative to detergent solubilisation for inwardly rectifying potassium channels, this would represent a useful addition to the many extant applications of nanodiscs to other target proteins, and attempts to make single-molecule observations of ion channels.

5.1.1 Chapter summary

This chapter is divided into several sections, each separately dealing with a different aspect of the reconstitution of protein into nanodics in relation to the smFRET experiments detailed in the previous chapters:

- Methods for MSP expression and purification, and nanodisc reconstitution;
- Successful reconstitution of KirBac1.1 into nanodiscs;
- Modulation of smFRET from KirBac1.1 in nanodiscs, using inhibitory H^+ and PIP_2, and an activatory gating mutation;
- Comparison of smFRET results from KirBac1.1;
- Reconstitution of TREK-2 into nanodiscs.

5.2 Methods

5.2.1 Membrane scaffold protein (MSP)

Expression of MSP

Nanodiscs require a constraining and supportive amphipathic alpha-helical membrane scaffold protein (MSP) which is based on apolipoprotein A-I [14, 18]: the construct used in this study was the gene MSP1E3D1[1] and was obtained from Addgene[2]. A schematic representation of its structure in comparison with apolipoprotein A-I and the shorter MSP1D1 is given in Figure 5.2.

The MSP1E3D1 gene was subcloned into the kanamycin-resistant pET28a vector, then transformed into BL21-Gold (DE3)pLysS (*E. coli*) and an overnight starter culture (15 mL/L) used to inoculate 2 L Terrific Broth (TB) (Merck) kanamycin (Apollo Scientific Ltd.) (0.05% w/v), which was incubated at 37°C and 190 rpm until OD_{600} >1.4. Expression

[1] Originally developed by the Sligar lab, University of Illinois, Urbana-Champaign

[2] Described on their website as "A non-profit global plasmid repository" which "facilitates the exchange of genetic material between laboratories by storing plasmids and their associated cloning data".

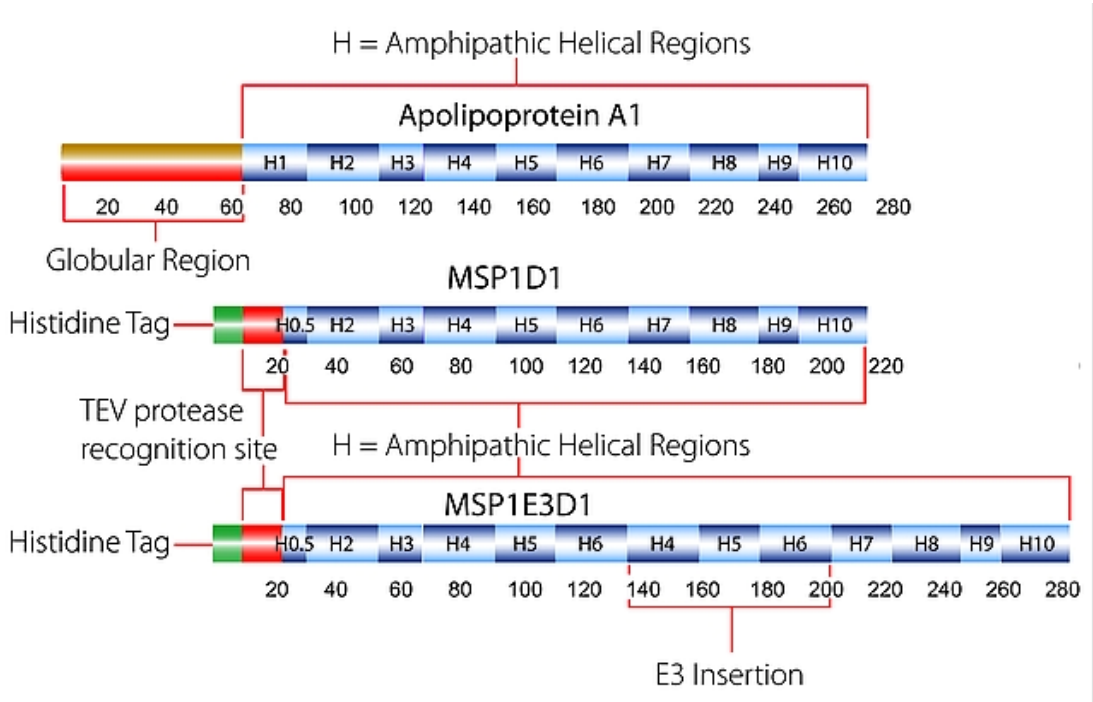


FIGURE 5.2: The membrane scaffold proteins (MSPs) are based on apolipoprotein A-I: the amphipathic alpha-helical regions of MSP are identical to those of apolipoprotein A-I, and the globular region of apolipoprotein A-I has been replaced by a histidine tag and TEV protease cleavage site in the MSP constructs. In the case of MSP1E3D1, an extra repeat of three of the alpha-helical domains has been inserted in the course of its development from MSP1D1 (figure from sigmaaldrich.com).

was induced by adding 1 mM IPTG and incubating for 3 hours at 37°C and 190 rpm. Cells were harvested by centrifugation at 16,000 *g* for 15 minutes and the pellets frozen at -80°C for future use.

Purification of MSP

Pellets were thawed and resuspended in 50 mL phosphate buffered saline (PBS, Sigma-Aldrich), 1% Triton X-100 (VWR International Ltd.), Hen Egg White Lysozyme (Fluka), EDTA-free protease inhibitor (Roche), and DNaseI (Sigma Aldrich). Cells were lysed using a French press homogeniser (4-6 passes) (Stansted Fluid Power Ltd.), and the lysate centrifuged at 70,000 *g* for 30 minutes to extract cell debris. The supernatant was added to washed and equilibrated cobalt resin[3] (Amintra Co-His Resin, Expedeon) (equilibration buffer: 40 mM Tris-HCl pH = 8.0, 300 mM NaCl) and incubated at 4°C for 1 hour to facilitate binding in preparation for affinity purification, performed using the buffers listed in Table 5.1.

[3]Suspension of beads with hexaaquacobalt(II) $[Co(H_2O)_6]^{2+}$

	Tris-HCl pH = 8.0	NaCl	
Wash 1 (W1)	40 mM	300 mM	1% Triton X-100
Wash 2 (W2)	40 mM	300 mM	-
Wash 3 (W3)	40 mM	300 mM	10 mM imidazole
Elution	40 mM	300 mM	500 mM imidazole

TABLE 5.1: MSP purification wash buffers

The unbound fraction was collected and the resin washed with 20 volumes W1 buffer, followed by 20 volumes W2 buffer, and 20 volumes W3 buffer. Elution was performed using 10 volumes Elution buffer after a 20 minute incubation.

Buffer exchange of the eluted fraction to 20 mM Tris-HCl pH = 7.8, 100 mM NaCl, 0.5 mM EDTA was performed, and the elute concentrated to ~2 mg/ml using a 10 kDa cut-off centrifugal filter device (Millipore) before filtering with a 0.22 μm membrane (VWR). SDS-PAGE was used to visualise the final purification product, shown in the third lane of the gel in Figure 5.4.

5.2.2 Nanodisc assembly

Reagents were mixed in the quantities listed in Table 5.2 below, including (doubly labelled) KirBac1.1:MSP in a 2:1 mass ratio, roughly corresponding to a 1:1 molecule number ratio (both from stock concentrations of 2 mg/mL). Stock concentrations of lipids were 10 mM, and the final cholate concentration was ~22.5 mM. Buffer recipes are given in Table 5.3.

KirBac1.1 (2mg/mL)	200 μL (0.4 mg)
MSP (2mg/mL)	100 μL (0.2 mg)
10 mM POPE	100 μL
10 mM POPG	34 μL
Cholate buffer	166 μL
MSP standard buffer	200 μL
Total volume	800 μL

TABLE 5.2: Nanodisc assembly mixture

	MSP standard buffer	Cholate buffer
Tris-HCl pH = 7.8	20 mM	20 mM
NaCl	100 mM	100 mM
EDTA	0.5 mM	0.5 mM
Cholate	-	100 mM

TABLE 5.3: Nanodisc assembly buffer recipes

The mixture was incubated overnight at 4°C with gentle agitation. It was then added to Bio-Beads (Bio-Rad) equilibrated with MSP standard buffer and incubated at 4°C for 6-8 hours. The sample was loaded onto a size exclusion column (Superdex 200 10/300, GE Healthcare) equilibrated with MSP standard buffer for purification and visualisation. Buffer for size-exclusion chromatography had been filtered using a 0.22 μm membrane and degassed by vacuum pump for >3 hours.

5.2.3 smFRET of KirBac1.1 in nanodiscs

Confocal-in-solution smFRET microscopy was performed as for the detergent-solubilised samples. Purified KirBac1.1 labelled with Cy3B and AlexaFluor®647 maleimides in buffer (20 mM Tris pH = 7.8, 100 mM NaCl, 0.5 mM EDTA) was observed with ALEX at 10 kHz between 532 nm (Cy3B, donor excitation, 120 μW CW) and 635 nm (AlexaFluor®647, acceptor excitation, 30 μW CW), and the resulting fluorescence bursts analysed using the Gaussian fitting algorithms described in Chapter 3 [78, 107, 109].

5.3 Results: reconstitution of KirBac1.1 into nanodiscs

The reconstitution process was optimised to arrive at the protocol described above. This entailed several iterations of varying protein:MSP:lipid ratios to arrive at the mixture given in Table 5.2.

Doubly labelled KirBac1.1 was determined to have been successfully reconstituted into MSP-bounded nanodiscs *via* size-exclusion chromatography and SDS-PAGE. Size-exclusion chromotography shows a peak that is shifted from that of tetrameric KirBac1.1 by an amount which corresponds to the mass of the extra compenents required for an assembled nanodisc (*i.e.* MSP and lipids): this is shown in Figure 5.3, where peaks from assembled nanodiscs and unassimilated KirBac1.1 are highlighted.

The relatively low sample concentrations arising from the small protein volumes used means that that the chromatography trace would be expected to display a low intensity peak, but SDS-PAGE gels were also run to confirm the presence of labelled KirBac1.1 (A273C reporter, in this case), a representative example of which is shown in Figure 5.4. The lane corresponding to the nanodisc sample appears to contain both MSP and a low concentration of doubly labelled KirBac1.1. This is a denaturing gel: hence only the monomeric forms of all constituent proteins can be detected, as opposed to the fully assembled nanodisc product.

Although the concentration appears to be very low, few molecules are required for successful smFRET measurements, so fluorescence data can still be acquired from a sample which appears to contain all components as smFRET signal cannot be obtained from a degraded channel, ruling out the possibility of unwanted signal from unassembled reactants. A low sample concentration was typical for all samples upon which smFRET experiments were performed in this thesis.

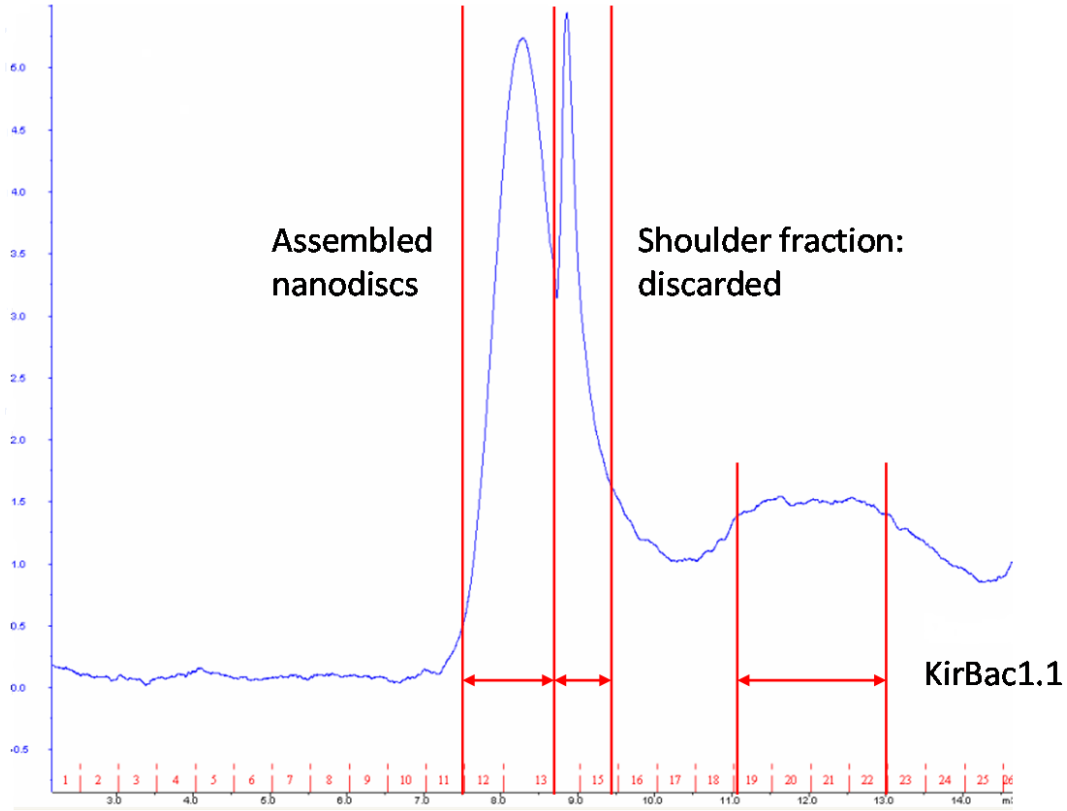


FIGURE 5.3: Size-exclusion chromatography (FPLC) trace of a reconsitution of KirBac1.1 into nanodiscs. Although the peak intensity is low, it is still non-zero, and shifted to a higher molecular mass from the position expected for tetrameric KirBac1.1 by an amount consistent with a successful reconstitution.

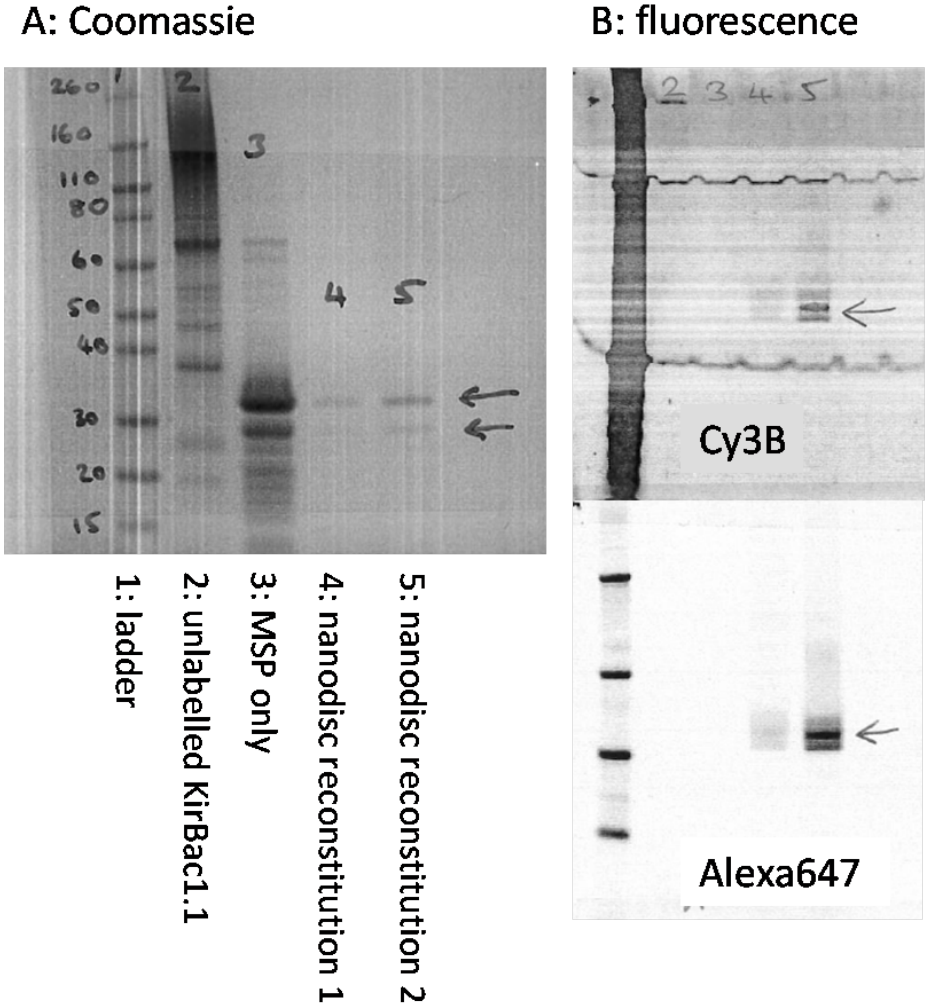


FIGURE 5.4: SDS-PAGE of nanodisc assembly products. The presence of both MSP and doubly labelled KirBac1.1 in lane (5) indicates the probable success of the reconstitution. (A) SDS-PAGE + Coomassie stain: (1) ladder; (2) unlabelled KirBac1.1; (3) MSP only; (4) nanodisc reconstitution attempt 1; (5) nanodisc reconstitution attempt 2. (B) The same gel as in (A), but scanned using the Pharos FX™Molecular Imager to visualise the labelled KirBac1.1 (highlighted by the arrow).

5.4 smFRET from KirBac1.1 reconstituted in nanodiscs

Purified KirBac1.1 doubly labelled with Cy3B and AlexaFluor®647 maleimides reconstituted into nanodiscs in buffer (20 mM Tris pH = 7.8, 100 mM NaCl, 0.5 mM EDTA) was observed using confocal-in-solution microscopy with ALEX at 10 kHz between 532 nm (Cy3B, donor excitation, 120 μW CW) and 635 nm (AlexaFluor®647, acceptor excitation, 30 μW CW). The resulting data resembled that obtained for detergent micelle-solubilised KirBac1.1, and confirmed that smFRET was taking place in the nanodisc-reconstituted sample. A representative smFRET histogram is presented in Figure 5.5. It can be seen that it was possible for the Gaussian fitting to clearly resolve the proximally and distally labelled subpopulation peaks.

These preliminary data were exceptionally promising, not only for the increased clarity compared to detergent solubilisation, but also as they represented the first observations of confocal-in-solution smFRET from KirBac1.1 reconstituted into nanodiscs, or indeed, the first fluorescence observations of any inwardly rectifying potassium channel reconstituted into nanodiscs.

5.5 Modulation of smFRET of KirBac1.1 in nanodiscs

The previous chapter described modulation of smFRET obtained from detergent-solubilised KirBac1.1 by perturbing the gating of the channel, and thereby the dynamic equilibrium, *i.e.* the physical property upon which smFRET reports. This confirmed that the observed smFRET signal was most likely to be originating directly from the labelled KirBac1.1. The attempts were successful, and provided evidence for a structural and/or conformational effect of an activatory mutation (V145L), and H^+-induced inhibition. However, the quality of the data from the detergent-solubilised KirBac1.1 was suboptimal and it was also not possible to investigate the effect of any regulatory mechanisms which require the interaction of the protein with the membrane, such as phospholipids [42, 52, 51, 62, 123]. As phospholipids such as PIP_2 are a major class of gating regulators in Kir and KirBac channels [50, 61, 101, 102], consideration of more native-like lipid-based forms of solubilisation are important. No effect could be seen using detergent-solublised protein; however, the

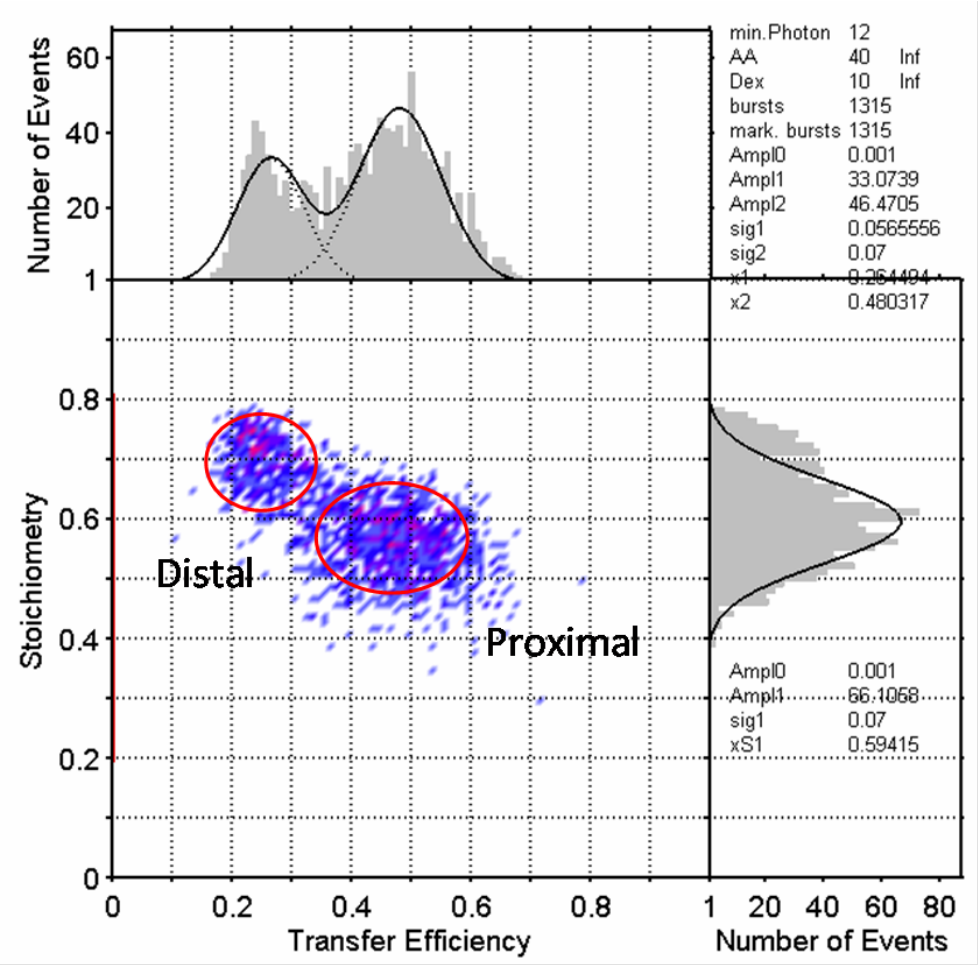


FIGURE 5.5: A representative smFRET histogram for KirBac1.1 reconstituted into nanodiscs. It is possible to clearly resolve the two separate proximally and distally labelled subpopulation peaks.

nanodisc environment represents a better choice of system to explore PIP_2 regulation.

Furthermore, as the protein is in a more native-like environment in a nanodisc, it is also possible that the conformational changes seen as a result of perturbing the channel *via* inhibitory H^+ and activatory point mutations will be more pronounced.

Illustrative *E**-*S* histograms for each of the experimental conditions are given in Section A.3.

5.6 Effect of the V145L activatory gating mutation

The activatory mutation V145L described in the previous chapter was inserted into KirBac1.1, and the protein expressed, purified, and doubly labelled before successful reconstitution into nanodiscs. Single-molecule FRET studies were then performed.

All smFRET experiments were performed as described in Chapter 3, with the exception of the observation buffer, which was instead MSP standard buffer (20 mM Tris-HCl pH = 7.8, 100 mM NaCl, 0.5 mM EDTA) to facilitate stability of the nanodiscs. The doubly labelled nanodisc-reconstituted KirBac1.1 was observed using confocal-in-solution microscopy with ALEX at 10 kHz between 532 nm (Cy3B, donor excitation, 120 μW CW) and 635 nm (AlexaFluor®647, acceptor excitation, 30 μW CW). Fluorescence data were obtained which was analysed using the fitting algorithms described in Chapter 3.

5.6.1 Results: R151C as the reporter site

As can be seen from the FRET efficiency values listed in Table 5.4 and illustrated in Figure 5.6 (taken from the Gaussian fitting algorithm applied to the fluorescence burst data and *E**-*S* histograms), an *increase* in *E** (of magnitude ~0.09, on average) was observed upon the addition of the activatory gating mutant V145L when compared to the wild type controls.

The same shift was observed for the R151C/V145L channel solubilised in detergent micelles, although the statistical significance of the shifts obtained using nanodisc reconsitution was considerably greater: $p = 0.0001$ for the distally labelled population peaks (x_1); and $p < 0.0001$ for the proximally labelled population peaks (x_2).

Sample		R151C only	R151C + V145L	Shift
α	x_1	0.273 ± 0.011	0.353 ± 0.014	0.080 ± 0.018
	x_2	0.516 ± 0.017	0.610 ± 0.031	0.094 ± 0.035
		n = 7	n = 4	
β	x_1	0.280 ± 0.013	0.353 ± 0.015	0.073 ± 0.020
	x_2	0.502 ± 0.015	0.558 ± 0.045	0.056 ± 0.047
		n = 4	n = 4	
γ	x_1	0.276 ± 0.014	0.377 ± 0.014	0.101 ± 0.020
	x_2	0.484 ± 0.013	0.601 ± 0.024	0.117 ± 0.027
		n = 8	n = 7	
δ	x_1	0.296 ± 0.011	0.370 ± 0.014	0.074 ± 0.018
	x_2	0.500 ± 0.012	0.583 ± 0.009	0.083 ± 0.015
		n = 9	n = 7	
ϵ	x_1	0.302 ±, 0.005	0.380 ± 0.010	0.078 ± 0.011
	x_2	0.490 ± 0.005	0.600 ± 0.033	0.110 ± 0.033
		n = 6	n = 8	
Mean	x_1	0.285 ± 0.013	0.367 ± 0.013	0.081 ± 0.011
	x_2	0.498 ± 0.012	0.590 ± 0.021	0.092 ± 0.024

TABLE 5.4: smFRET shifts for the R151C reporter mutation with and without the activatory V145L mutation, with the protein reconstituted into nanodiscs. There is a marked shift to higher FRET efficiency.

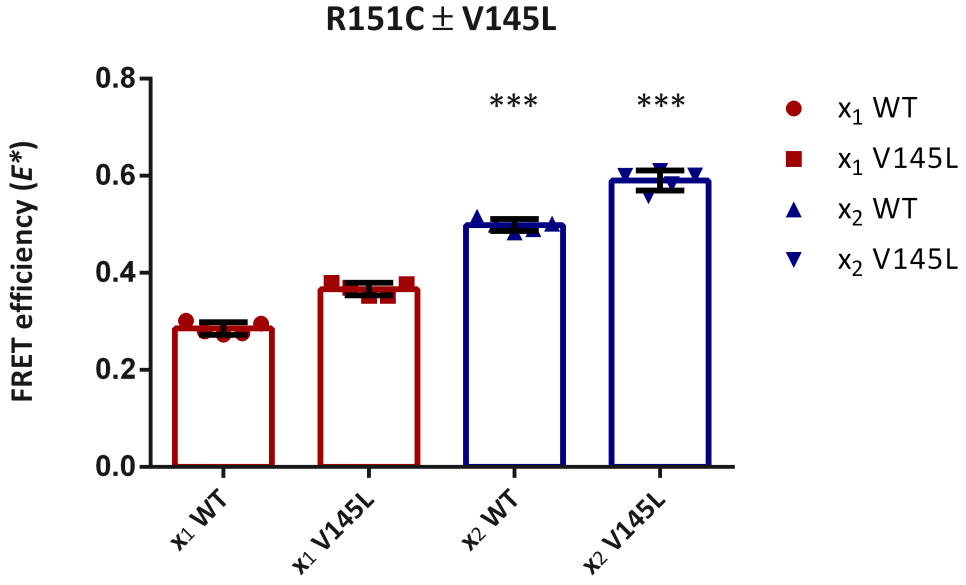


FIGURE 5.6: smFRET shifts for the R151C reporter mutation with (V145L) and without (WT) an activatory point mutation, with KirBac1.1 reconstituted into nanodiscs. There is a marked shift to higher E^* for both labelling population peaks.

5.6.2 Results: G249C as the reporter site

Single-molecule FRET experiments performed using KirBac1.1 with the G249C cysteine reporter mutation and the V145L activatory mutation produced a viable smFRET signal. This represented a major improvement because the G249C/V145L mutation combination did not produce viable smFRET data using the detergent-solubilised channels, suggesting that nanodiscs may present an improvement in the ease of data collection with respect to the stability of purified KirBac channels.

As can be seen from the FRET efficiency values given in Table 5.5, a shift towards *lower* E^* of magnitude ~0.05 on average was observed upon addition of the V145L activatory mutation compared to the cysteine reporter-only control, also illustrated in Figure 5.7. The collated data also showed a high degree of statistical significance, with $p \ll 0.05$ for the distally labelled population peak (x_1), and $p < 0.05$ for the proximally labelled population peak (x_2).

This shift to a *lower* E^* is in the opposite direction to the that observed upon lowering the pH of the observation solution (see previous chapter and below), which is an *inhibitory* gating modulation, whereas this is an *activatory* modulation.

In addition, this shift in E^* is in the opposite direction to that observed when R151C is used as the reporter mutation. This is perhaps to be expected as it has been shown by Wang *et al.*'s studies of PIP_2-induced inhibition [123] that the R151C and G249C residues move in opposite directions during the conformational changes associated with inhibition: it is interesting to note that the converse appears to be the case for an activatory perturbation of the channel's dynamic equilibrium.

Sample		G249C only	G249C + V145L	Shift
α	x_1	0.366 ± 0.016	0.280 ± 0.027	-0.086 ± 0.031
	x_2	0.508 ± 0.015	0.433 ± 0.031	-0.075 ± 0.028
		n = 4	n = 5	
β	x_1	0.368 ± 0.022	0.329 ± 0.022	-0.039 ± 0.031
	x_2	0.509 ± 0.016	0.461 ± 0.038	-0.048 ± 0.041
		n = 4	n = 6	
γ	x_1	0.358 ± 0.027	0.289 ± 0.033	-0.070 ± 0.043
	x_2	0.478 ± 0.017	0.415 ± 0.049	-0.063 ± 0.052
		n = 6	n = 5	
δ	x_1	0.335 ± 0.071	0.292 ± 0.034	-0.043 ± 0.036
	x_2	0.466 ± 0.026	0.469 ± 0.076	0.003 ± 0.080
		n = 5	n = 3	
ϵ	x_1	0.362 ± 0.017	0.283 ± 0.029	-0.079 ± 0.034
	x_2	0.485 ± 0.036	0.469 ± 0.023	-0.016 ± 0.045
		n = 4	n = 3	
Mean	x_1	0.358 ± 0.013	0.295 ± 0.020	-0.063 ± 0.021
	x_2	0.489 ± 0.019	0.449 ± 0.024	-0.040 ± 0.033

TABLE 5.5: smFRET shifts for the G249C reporter mutation with and without the activatory V145L mutation, with the protein reconstituted into nanodiscs. There is a marked shift to lower FRET efficiency.

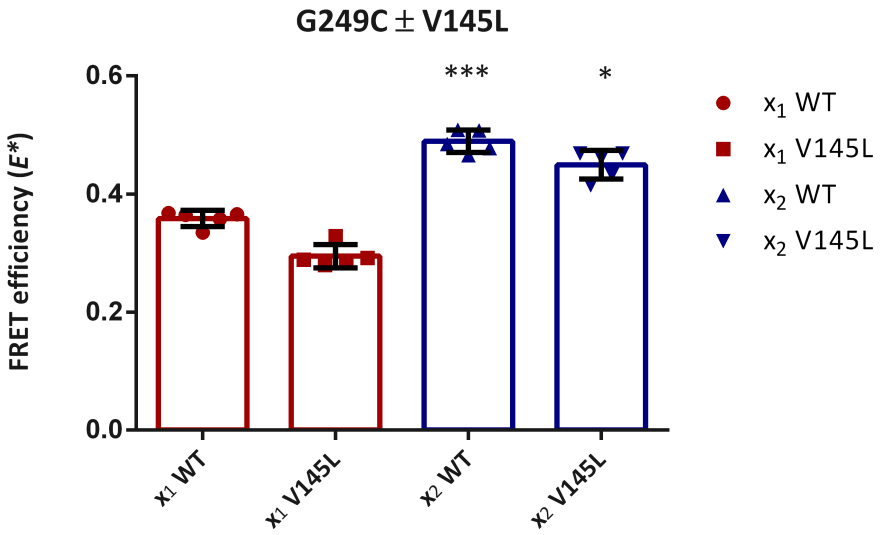


FIGURE 5.7: smFRET shifts for the G249C reporter mutation with (V145L) and without (WT) an activatory point mutation, with KirBac1.1 reconstituted into nanodiscs. There is a distinct and repeatable shift to lower FRET efficiency for both labelling population peaks.

5.7 Inhibition by H^+

All smFRET experiments were performed as described in Chapter 3, with the exception of the observation buffers: control experiments were performed in MSP standard buffer (20 mM Tris-HCl pH = 7.8, 100 mM NaCl, 0.5 mM EDTA); and the low pH measurements were performed with the sample in two parts MSP standard buffer and one part 'low pH buffer' (20 mM MES pH = 5.0, 100 mM NaCl, 0.5 mM EDTA). This corresponded to a final solution pH = 5.5.

The doubly labelled nanodisc-reconstituted KirBac1.1 was observed using confocal-in-solution microscopy with ALEX at 10 kHz between 532 nm (Cy3B, donor excitation, 120 μW CW) and 635 nm (AlexaFluor®647, acceptor excitation, 30 μW CW). Both the R151C and G249C cysteine reporter mutations were studied in order to facilitate comparison with the results obtained for detergent-solubilised samples.

5.7.1 Results: R151C as the reporter site

As shown by the FRET efficiency values listed in Table 5.6 and illustrated in Figure 5.8, a shift towards a *lower E** of magnitude ~0.07, on average, was observed upon a change to a more acidic pH when R151C was used as the dye-labelled reporter mutation.

This shift to *lower E** is consistent with the findings from the equivalent experiments with detergent-solubilised protein, but appears to be somewhat more pronounced as the magnitude of the shift is generally greater, and the error considerably lower (0.07 ± 0.02, as opposed to 0.050 ± 0.046). Indeed, this is reflected in the high degree of statistical significance of the collated shifts: $p = 0.0004$ for the distal labelling population peak (x_1); and $p = 0.020$ for the proximal labelling population peak (x_2).

The shift observed from R151C when considering inhibition by H^+ is in the opposite direction to that from G249C (see below). This result is consistent with those of the previous chapter, where the effect of inhibitory H^+ on detergent-solubilised protein was investigated. In addition, the shift observed here due to H^+ inhibition is in the opposite direction from that induced *via* the activatory point mutation (see above).

Sample		pH = 7.8	pH = 5.3	Shift
α	x_1	0.298 ± 0.035	0.252 ± 0.017	-0.046 ± 0.039
	x_2	0.537 ± 0.025	0.474 ± 0.021	-0.063 ± 0.033
		n = 8	n = 9	
β	x_1	0.338 ± 0.020	0.261 ± 0.018	-0.077 ± 0.027
	x_2	0.558 ± 0.020	0.462 ± 0.022	-0.096 ± 0.030
		n = 8	n = 7	
γ	x_1	0.367 ± 0.026	0.282 ± 0.029	-0.085 ± 0.039
	x_2	0.584 ± 0.022	0.495 ± 0.043	-0.089 ± 0.048
		n = 7	n = 12	
δ	x_1	0.284 ± 0.024	0.260 ± 0.035	-0.024 ± 0.042
	x_2	0.529 ± 0.010	0.450 ± 0.040	-0.079 ± 0.041
		n = 5	n = 6	
ϵ	x_1	0.357 ± 0.028	0.274 ± 0.024	-0.083 ± 0.037
	x_2	0.556 ± 0.027	0.471 ± 0.024	-0.085 ± 0.036
		n = 6	n = 10	
Mean	x_1	0.329 ± 0.036	0.266 ± 0.012	-0.063 ± 0.027
	x_2	0.553 ± 0.021	0.470 ± 0.017	-0.082 ± 0.012

TABLE 5.6: smFRET shifts for the R151C reporter mutation upon a change to a more acidic (inhibitory) pH when the protein is reconstituted into nanodiscs. There is a marked shift to lower FRET efficiency.

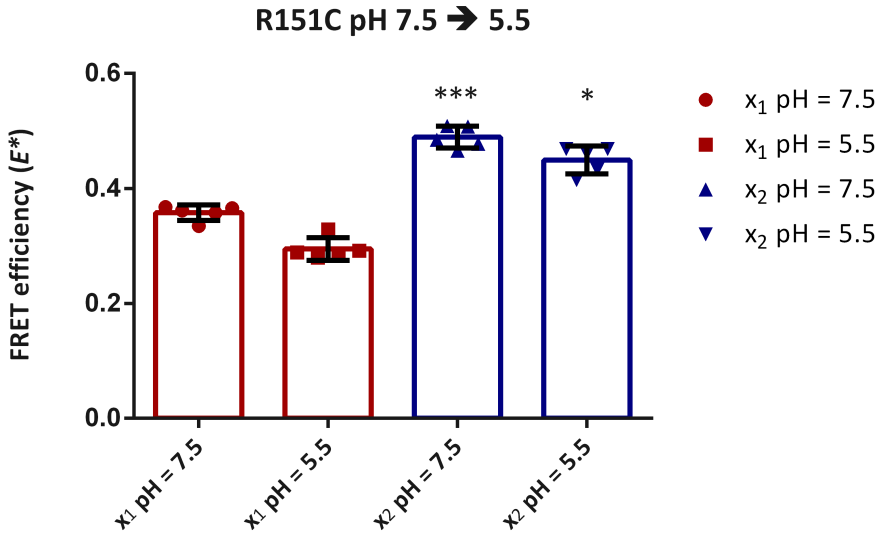


FIGURE 5.8: smFRET shifts for the R151C reporter mutation upon a change to more acidic (inhibitory) pH when KirBac1.1 is reconstituted into nanodiscs. There is a distinct shift to lower FRET efficiency for both labelling population peaks.

5.7.2 Results: G249C as the reporter site

As can be seen from the FRET efficiency values listed in Table 5.7 and illustrated in Figure 5.9 (taken from the Gaussian fitting algorithm applied to the fluorescence burst data and smFRET histograms), a shift towards *higher E** of magnitude ~0.065, on average, was observed upon a change to more acidic pH when using G249C as the dye-labelled reporter mutation.

This marked shift to a higher FRET efficiency verifies what was observed during H^+ inhibition of the detergent-solubilised protein. Also, the error on this shift is considerably lower than was obtained for the detergent-solubilised sample (0.065 ± 0.025, as opposed to 0.04 ± 0.03) with a smaller number of experimental repeats, representing an improvement in the quality of the data obtained. Indeed, there is a much greater degree of statistical significance compared to the results from detergent solubilisation: $p = 0.0003$ for both the proximally and distally labelled population peaks from the nanodisc-reconstituted samples, as opposed to $p = 0.053$ and $p = 0.007$ for detergent-solubilisation.

This shift is also in the opposite direction to that observed when the V145L activatory mutation is combined with the G249C reporter mutant. This is consistent with acidic pH being *inhibitory* [13, 24, 67], whereas the V145L mutation is *activatory* [95]. Notably, this positive shift upon H^+ inhibition of the G249C reporter is in the opposite direction to the shift observed when using R151C as the reporter, consistent with the findings of Wang *et al.* in their study of PIP_2 inhibition of KirBac1.1 [123].

Sample		pH = 7.8	pH = 5.5	Shift
α	x_1	0.332 ± 0.015	0.375 ± 0.022	0.043 ± 0.027
	x_2	0.457 ± 0.014	0.515 ± 0.008	0.058 ± 0.016
		n = 4	n = 3	
β	x_1	0.335 ± 0.013	0.368 ± 0.021	0.033 ± 0.025
	x_2	0.466 ± 0.026	0.516 ± 0.016	0.050 ± 0.031
		n = 5	n = 6	
γ	x_1	0.304 ± 0.039	0.343 ± 0.027	0.039 ± 0.047
	x_2	0.408 ± 0.046	0.472 ± 0.037	0.064 ± 0.059
		n = 5	n = 6	
δ	x_1	0.309 ± 0.030	0.355 ± 0.021	0.046 ± 0.037
	x_2	0.415 ± 0.020	0.504 ± 0.049	0.089 ± 0.053
		n = 6	n = 8	
ϵ	x_1	0.286 ± 0.026	0.372 ± 0.017	0.086 ± 0.031
	x_2	0.396 ± 0.026	0.493 ± 0.016	0.097 ± 0.031
		n = 7	n = 8	
ζ	x_1	0.288 ± 0.016	0.362 ± 0.019	0.074 ± 0.025
	x_2	0.399 ± 0.022	0.506 ± 0.026	0.107 ± 0.034
		n = 8	n = 6	
Mean	x_1	0.309 ± 0.021	0.363 ± 0.012	0.054 ± 0.021
	x_2	0.424 ± 0.030	0.501 ± 0.016	0.078 ± 0.023

TABLE 5.7: smFRET shifts for the G249C reporter mutation upon a change to a more acidic (inhibitory) pH when the protein is reconstituted into nanodiscs. There is a marked shift to higher FRET efficiency.

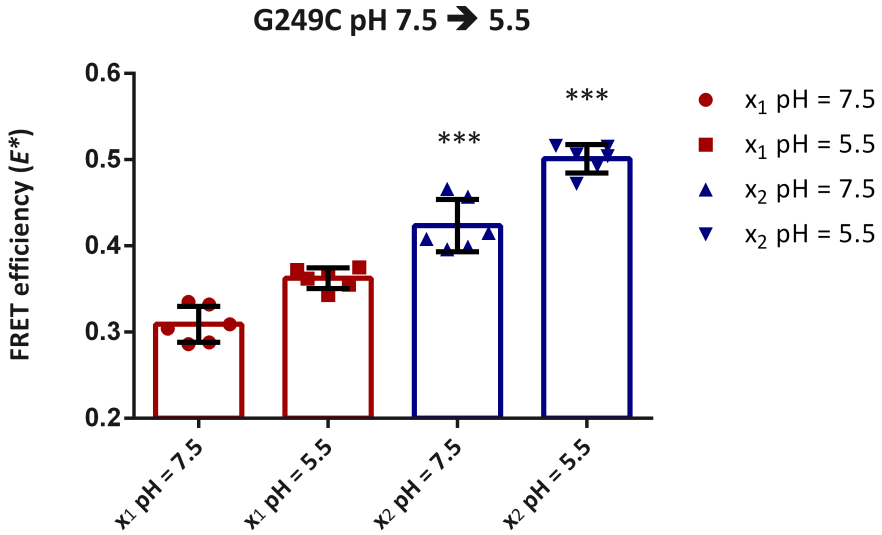


FIGURE 5.9: smFRET shifts for the G249C reporter mutation upon a change to a more acidic (inhibitory) pH when KirBac1.1 is reconstituted into nanodiscs. There is a marked shift to higher E^* for both labelling population peaks.

5.8 Inhibition by PIP_2

All smFRET experiments were performed as described in Chapter 3: purified doubly labelled KirBac1.1 reconstituted into nanodiscs was observed using confocal-in-solution microscopy with ALEX at 10 kHz between 532 nm (Cy3B, donor excitation, 120 μW CW), and 635 nm (AlexaFluor®647, acceptor excitation, 30 μW CW). Buffer for the control measurements was the standard MSP buffer (20 mM Tris-HCl pH = 7.8, 100 mM NaCl, 0.5 mM EDTA), and the same buffer with the addition of ~20 μM diC8-PIP_2 for the ligand-modulated measurements. Data was obtained for both the R151C and G249C cysteine reporter mutations.

5.8.1 Results: R151C as the reporter site

As shown by the FRET efficiency values listed in Table 5.8 (calculated using the Gaussian fitting algorithm applied to the fluorescence burst data and resulting E^*-S histograms), a shift towards *lower* E^* of magnitude 0.043 ± 0.010 was observed upon addition of 20 μM diC8-PIP_2 when using R151C as the cysteine reporter mutation. This is also illustrated in Figure 5.10.

Importantly, the collated shifts in E^* also demonstrate an extremely high degree of statistical significance, with $p < 0.0001$ for both population peaks. This shift is also notably in the same direction as that observed for a change to more acidic pH, a change which, like the addition of PIP_2, is thought to be inhibitory. This could suggest that the mechanism for inhibition by ligand binding share common conformational transitions which are independent of the bound ligand species.

Sample		MSP buffer	+ 20 μM PIP_2	Shift
α	x_1	0.328 ± 0.029	0.294 ± 0.021	-0.034 ± 0.036
	x_2	0.523 ± 0.025	0.486 ± 0.019	-0.037 ± 0.031
		n = 12	n = 21	
β	x_1	0.337 ± 0.024	0.304 ± 0.019	-0.033 ± 0.036
	x_2	0.535 ± 0.026	0.488 ± 0.017	-0.047 ± 0.031
		n = 16	n = 16	
γ	x_1	0.336 ± 0.017	0.300 ± 0.017	-0.036 ± 0.024
	x_2	0.521 ± 0.014	0.493 ± 0.021	-0.028 ± 0.025
		n = 16	n = 14	
δ	x_1	0.340 ± 0.015	0.287 ± 0.018	-0.053 ± 0.023
	x_2	0.547 ± 0.018	0.490 ± 0.025	-0.057 ± 0.031
		n = 12	n = 16	
ϵ	x_1	0.363 ± 0.010	0.310 ± 0.019	-0.053 ± 0.021
	x_2	0.546 ± 0.023	0.491 ± 0.017	-0.055 ± 0.029
		n = 12	n = 16	
ζ	x_1	0.344 ± 0.016	0.303 ± 0.013	-0.041 ± 0.021
	x_2	0.534 ± 0.015	0.488 ± 0.009	-0.046 ± 0.017
		n = 10	n = 12	
Mean	x_1	0.341 ± 0.012	0.300 ± 0.008	-0.042 ± 0.009
	x_2	0.534 ± 0.011	0.489 ± 0.003	-0.045 ± 0.011

TABLE 5.8: smFRET shifts for the reporter mutation R151C with and without the addition of PIP_2 with the protein reconstituted into nanodiscs. There is a repeatable shift to lower FRET efficiency.

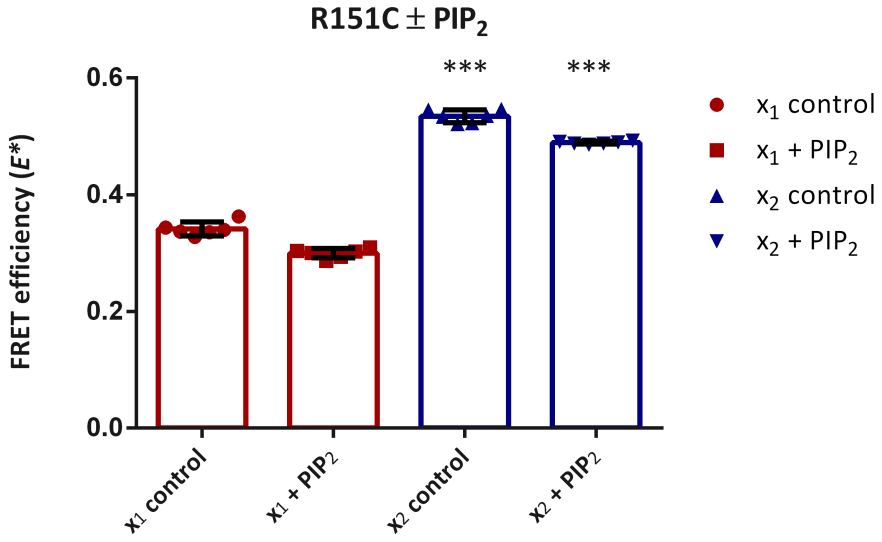


FIGURE 5.10: smFRET shifts for the reporter mutation R151C with and without PIP_2 with KirBac1.1 reconstituted into nanodiscs. There is distinct and repeatable shift to lower E^* for both labelling population peaks.

5.8.2 Results: G249C as the reporter site

As shown by the FRET efficiency values given in Table 5.9 (calculated using the Gaussian fitting algorithm applied to the fluorescence burst data and smFRET histograms), a shift towards *higher E** of magnitude 0.059 ± 0.018 was observed upon addition of 20 μM diC8-PIP_2 when using G249C as the reporter mutation. This is also illustrated graphically in Figure 5.11.

The p-values of the collated shifts in *E** demonstrated a very high degree of statistical significance: $p = 0.0002$ for the distally labelled population peak, x_1; and $p < 0.0001$ for the proximally labelled population peak, x_2.

This shift is in the opposite direction to that observed when PIP_2 was added to the R151C reporter sample, consistent with the findings of both H^+ inhibition, and V145L *activation*. The similarities between the H^+ and PIP_2 modulations, both inhibitory regulators, are particularly interesting as they suggest shared elements in the conformational mechanism associated with inhibition. In addition, Wang *et al.* also found that the R151C and G249C reporters produced FRET shifts in opposite directions [123].

Sample		MSP buffer	+ 20 μM PIP_2	Shift
α	x_1	0.326 ± 0.032	0.372 ± 0.034	0.046 ± 0.047
	x_2	0.471 ± 0.041	0.538 ± 0.028	0.067 ± 0.050
		n = 8	n = 6	
β	x_1	0.305 ± 0.016	0.365 ± 0.020	0.060 ± 0.026
	x_2	0.470 ± 0.029	0.544 ± 0.030	0.074 ± 0.042
		n = 9	n = 6	
γ	x_1	0.292 ± 0.022	0.348 ± 0.014	0.056 ± 0.026
	x_2	0.472 ± 0.033	0.534 ± 0.020	0.062 ± 0.039
		n = 5	n = 10	
δ	x_1	0.292 ± 0.017	0.343 ± 0.017	0.051 ± 0.024
	x_2	0.482 ± 0.019	0.542 ± 0.023	0.060 ± 0.030
		n = 7	n = 10	
ϵ	x_1	0.292 ± 0.012	0.360 ± 0.013	0.068 ± 0.018
	x_2	0.475 ± 0.021	0.553 ± 0.013	0.078 ± 0.025
		n = 9	n = 7	
Mean	x_1	0.301 ± 0.015	0.358 ± 0.012	0.056 ± 0.008
	x_2	0.474 ± 0.005	0.542 ± 0.007	0.068 ± 0.008

TABLE 5.9: smFRET shifts for the reporter mutation G249C with and without PIP_2 with the protein reconstituted into nanodiscs. There is a shift to higher FRET efficiency for both peaks.

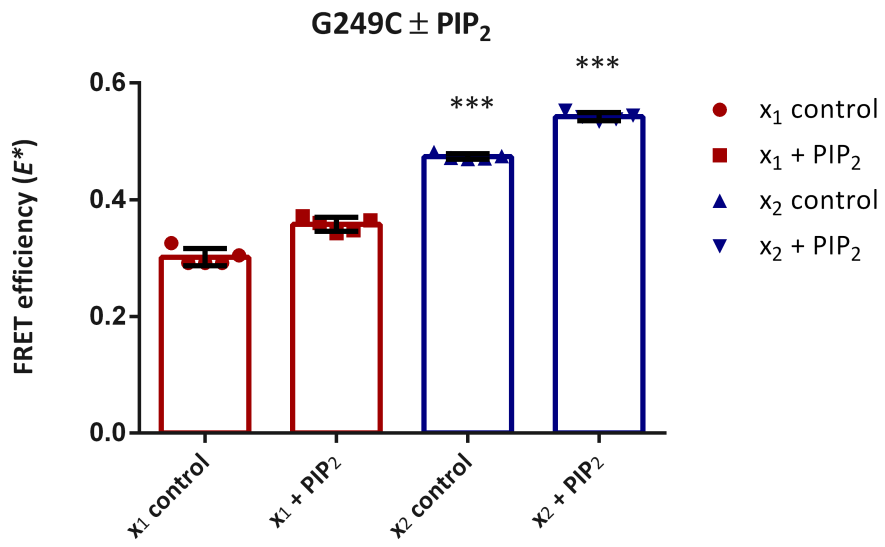


FIGURE 5.11: smFRET shifts for the reporter mutation G249C with and without PIP_2 with KirBac1.1 reconstituted into nanodiscs. There is a shift to higher E^* for both labelling population peaks.

5.9 Summary of results for nanodisc-reconstituted KirBac1.1

Table 5.10 is a summary of the findings from the study described in this chapter: the direction of the shift in E^* upon perturbation of the dynamic equilibrium of the channel is given. The properties used in this study are known from other studies to affect the gating of the channel: an activatory point mutation; inhibition by H^+; and addition of inhibitory PIP_2. All p-values demonstrate statistical significance ($p < 0.05$).

A summary chart of the mean shifts (with standard deviations) obtained for each modulatory factor acting upon KirBac1.1 solubilised in nanodiscs is given in Figure 5.12. This clearly shows that the change in smFRET efficiency was in opposite directions for the activatory *vs* inhibitory modulations, and was consistently in opposite directions for the two cysteine reporter sites.

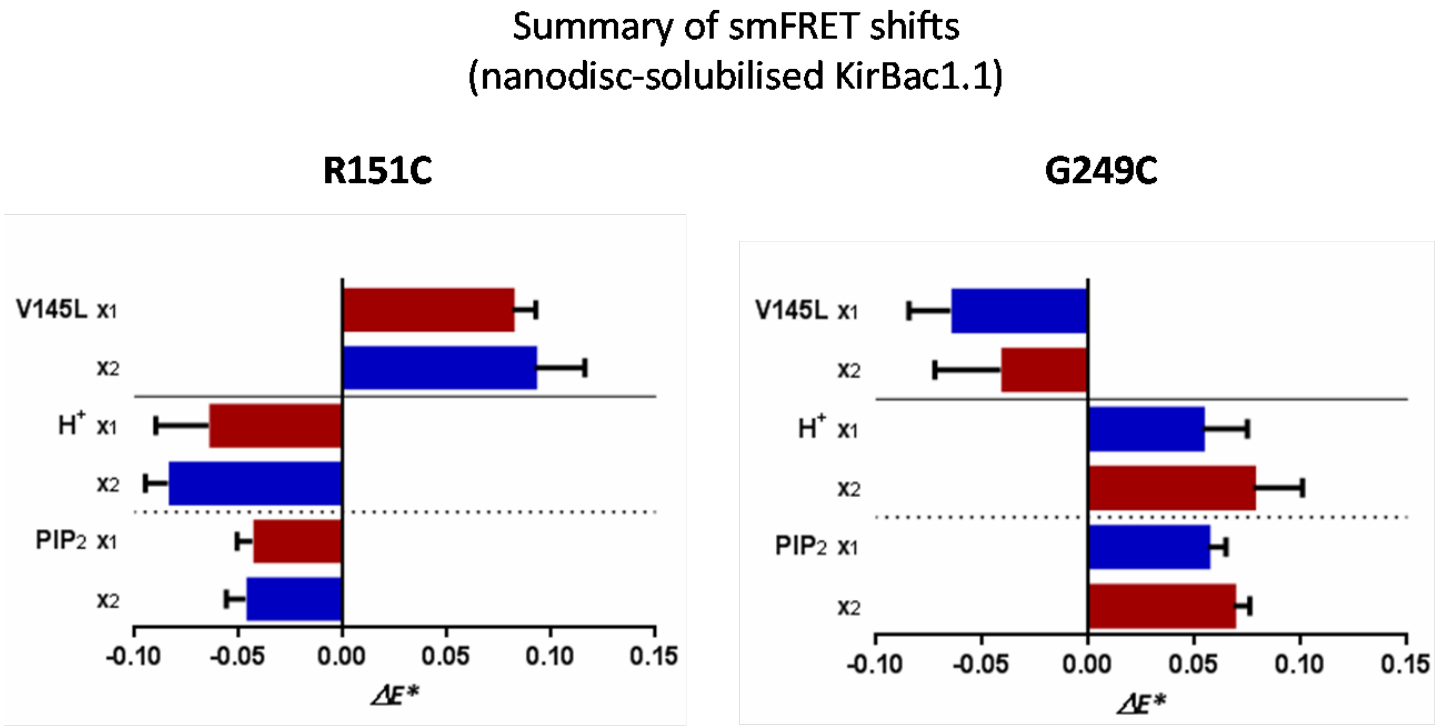


FIGURE 5.12: Summary of the mean (plus standard deviation) of the shifts in smFRET efficiency observed upon modulation of KirBac1.1 solubilised into nanodiscs. This shows that the changes in E^* are in opposite directions for the activatory *vs* inhibitory modulations, and that the shifts are consistently in opposite directions for the two cysteine reporter sites.

	R151C	G249C
V145L (activatory)	increase x_1: $p = 0.0001$ x_2: $p < 0.0001$	decrease x_1: $p = 0.0003$ x_2: $p = 0.020$
acidic pH (inhibitory)	decrease x_1: $p = 0.0004$ x_2: $p = 0.020$	increase x_1: $p = 0.0003$ x_2: $p = 0.0003$
PIP_2 (inhibitory)	decrease x_1: $p < 0.0001$ x_2: $p < 0.0001$	increase x_1: $p = 0.0002$ x_2: $p < 0.0001$

TABLE 5.10: A summary of the smFRET data obtained using KirBac1.1 reconstituted into nanodiscs.

5.10 Comparison of the modulatory factors

An examination of the effects of several factors known to modulate KirBac1.1 gating has been carried out using two different cysteine reporter mutations located in different regions of the protein: R151C (near the helix bundle crossing); and G249C (in the cytoplasmic domain). The effects of inhibition by H^+, addition of inhibitory PIP_2, and an activatory gating mutation (V145L) have been investigated using KirBac1.1 both solubilised in detergent micelles and reconstituted into lipid nanodiscs: results are consistent between the two solubilisation methods.

An interesting finding is that the shifts induced for the two reporter mutations were in opposite directions. This is in accordance with the findings of Wang *et al.* [123] who mapped the conformational changes of doubly labelled KirBac1.1 reconsituted into liposomes upon addition of the inhibitory ligand PIP_2 [62, 127, 128] for a series of different cysteine reporter mutations. This showed FRET shifts which corresponded to the distances between the fluorescence dyes increasing at the cytoplasmic domain and decreasing at the helix bundle crossing: the current study observed equivalent shifts but in opposing directions for R151C (at the helix bundle crossing), and G249C (in the cytoplasmic domain). Moreover, these shifts were consistently in opposite directions to each other regardless of the modulatory factor used, for both inhibitory perturbations and *vice versa* with respect to directionality for activatory mechanisms.

It is also interesting to note that both acidic pH (*i.e.* increased $[H^+]$) and PIP_2, factors which are known from functional studies to be inhibitory [13, 24, 62, 67, 127, 128],

produced smFRET shifts for the fluorescent populations in the same direction (consistent for both cysteine reporter mutations), and of approximately the same magnitude (shifts are listed in Table 5.11). These results suggest a common conformational mechanism for inhibition of KirBac1.1 by charged ligands, whether they be protons or lipids.

As might be expected from the fact that it is an *activatory* mutation [95], the point mutation V145L produced smFRET shifts of the fluorescence populations in the opposite direction from H^+ and PIP_2. Again, this was in opposite directions for the two cysteine reporter mutations, but consistent with respect to a conformational change in the opposite direction to that for inhibition. It is reassuring to note that the global conformational change involved in activation by a point mutation appears to be the approximate inverse of that produced by environmental inhibition. This suggests that that the conformational changes are transduced throughout the protein to the locations of the cysteine reporters: this would not necessarily be expected to be the case for an activatory mutation which is far removed from both the reporter sites, and the putative inhibitory ligand binding site.

5.11 Comparison of solubilisation methods

Some of the improvement noticed upon introducing the nanodisc reconstitution method was qualitative rather than quantitative. It was much faster to acquire sufficient readings using nanodisc-reconstituted protein than detergent-solubilised KirBac1.1, mostly because of the lack of aggregation events which produce a massive fluorescence burst without distinct single-molecule signals: an example of such an event is shown in Figure 5.13. As nanodiscs are known to be robust with respect to their resistance to aggregation, this was a promising confirmation of the enthusiasm surrounding the system.

The nanodisc-reconstited samples also appeared to have a longer 'shelf life' than their detergent-solubilised counterparts: satisfactory fluorescence data could be acquired from samples which had been stored at 4° for three months, whereas detergent-solubilised samples would typically be discarded after 3-4 weeks due to micelle aggregation. In one case, it was even noticed that a sample left on a coverslip on the microscope set-up overnight, which had serendipitously not completely dried out, was still producing a viable smFRET

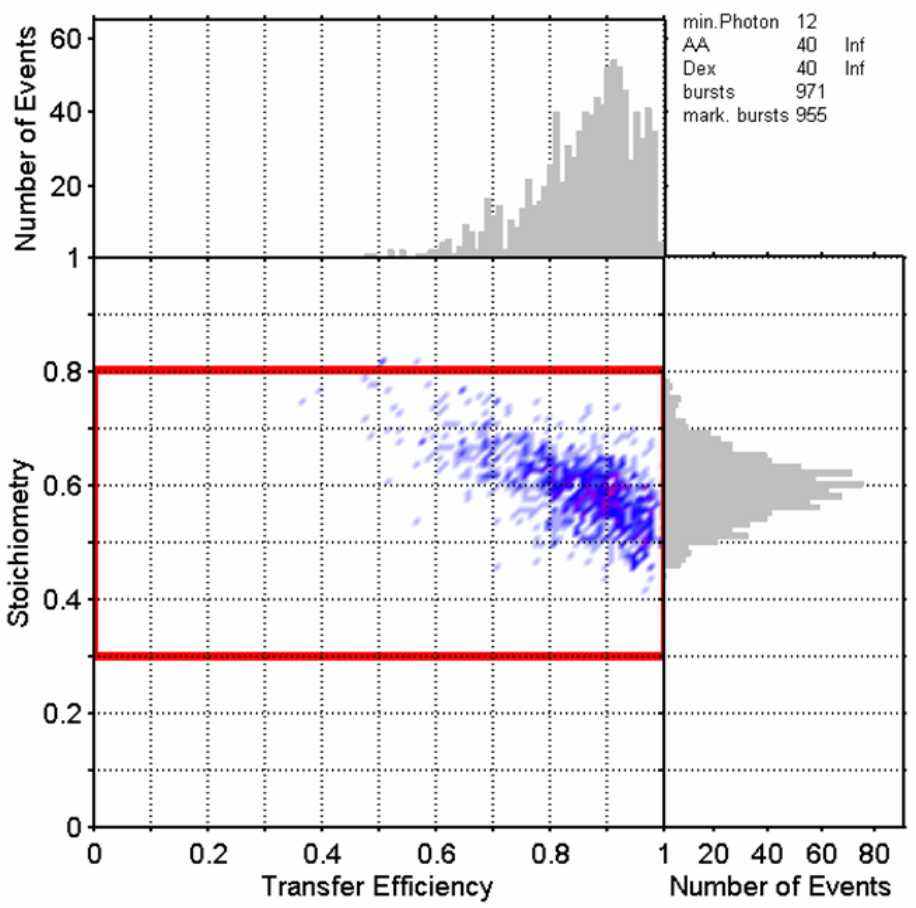


FIGURE 5.13: An example of a fluorescence burst in which single-molecule signals could not be discerned, most likely due to protein aggregation.

signal the following morning, after ~16 hours at room temperature. As detergent-solubilised samples either degrade or aggregate within a couple of hours at room temperature, this therefore represents a vast improvement in sample stability. This illustrates that previous reports of the increased stability of nanodisc samples are well-founded, and the major limiting factor for fluorescence experiments may be photodestruction of the dyes rather than degradation or aggregation of the target protein.

Another advantage was the ability to obtain quality data from all samples reconstituted into nanodiscs. This is in marked contrast to the previous chapter, in which it was not possible to obtain smFRET data for all reporter/perturbatory combinations using detergent-solublised protein. This could be because KirBac1.1 was not stable enough when solubilised in detergent micelles, but the more native-like environment of the lipid nanodisc was more favourable. Interestingly, the most obvious example of this was for the effect of PIP_2: no detectable effect of PIP_2 was observed using detergent-solubilised protein, but

it was possible to acquire data of sufficient quality to confirm the findings of Wang *et al.* [123] using a sample reconstituted into nanodiscs. As there is some debate about whether PIP_2 interactions with KirBac proteins are mediated by the membrane lipids, this is an interesting finding, although more study would be required to determine whether this is due to the different environments, or whether KirBac1.1 is merely too unstable for these measurements when solubilised in detergent micelles.

In addition to these qualitative findings, the difference between the two solubilisation methods can also be quantified by examining the mean and standard deviations of the sm-FRET shifts produced, which are summarised in Table 5.11, and the p-values, given in Table 5.12.

It can be seen that the nanodisc method appeared to result in shifts of greater magnitude and less variability (*i.e.* greater consistency) than detergent micelles, presumably due to the more favourable environment being experienced by KirBac1.1. In addition, the collated data showed a much higher degree of statistical significance when the equilibirum of the nanodisc-solubilised protein was being perturbed by a modulatory factor. This suggests that although the repeatability of the results imply that the results obtained using detergent micelle-solubilised protein were valid, the data obtained using nanodisc-reconstituted samples are more convincing. In summary, the nanodisc-reconsitution method therefore represents a considerable improvement in the both the methodology and quality of single-molecule fluorescence measurements of KirBac1.1, and potentially other potassium channels.

		Detergent	Nanodiscs
V145L	R151C	0.022 ± 0.028	0.087 ± 0.019
(activatory)	G249C	-	-0.052 ± 0.029
acidic pH (H^+)	R151C	-0.050 ± 0.046	-0.073 ± 0.022
(inhibitory)	G249C	0.043 ± 0.028	0.066 ± 0.025
PIP_2	R151C	-	-0.043 ± 0.009
(inhibitory)	G249C	-	0.062 ± 0.010

TABLE 5.11: A summary and comparison of the smFRET shifts obtained from detergent-solubilised KirBac1.1, and from nanodisc-reconstituted protein. In general, the nanodisc method resulted in shifts of a greater magnitude with less variability. It was also not possible to acquire smFRET data for all the reporter/perturbation combinations using the detergent-solubilisation method.

			Detergent	Nanodiscs
V145L (activatory)	R151C	x_1	$p = 0.686$	$p = 0.0001$
		x_2	$p = 0.177$	$p < 0.0001$
	G249C	x_1	-	$p = 0.0003$
		x_2	-	$p = 0.020$
acidic pH (H^+) (inhibitory)	R151C	x_1	$p = 0.207$	$p = 0.0004$
		x_2	$p = 0.041$	$p = 0.020$
	G249C	x_1	$p = 0.053$	$p = 0.0003$
		x_2	$p = 0.007$	$p = 0.0003$
PIP_2 (inhibitory)	R151C	x_1	-	$p < 0.0001$
		x_2	-	$p < 0.0001$
	G249C	x_1	-	$p = 0.0002$
		x_2	-	$p < 0.0001$

TABLE 5.12: A summary and comparison of the p-values of the collated shifts in E^* obtained using detergent-solubilised and nanodisc-reconstituted KirBac1.1. It is clear that the nanodisc method of solubilisation generated smFRET shifts upon equilibrium perturbation with a modulatory factor with a much higher degree of statistical significance than the samples solubilised into detergent micelles.

5.12 Reconstitution of TREK-2 into nanodiscs

5.12.1 Introduction

Mammalian potassium channels can be divided into three structural categories based on their number of transmembrane (TM) domains [92, 93, 94]. These TM segments are usually the TM alpha helices, such as the two (inner and outer) helices of the Kir and KirBac channels [13, 74]. In fact, the inwardly rectifying channels, examined in great detail in this thesis, are partially defined by their possession of two TM segments, whereas the outwardly rectifying voltage-gated potassium channels, such as the *Shaker*-related $K_V1.1$, belong to the 6-TM segment branch, where the pore domain also possesses an additional 4-TM voltage sensing module [60, 94].

A third and structurally distinct group is comprised of subunits with four TM segments, where each subunit contains two 2-TM pore modules. These channels assemble as a dimer to form a pseudotetrameric pore, and are hence known as the "K2P" channels [12, 93, 94]. Notable members of this group include TREK[4]-1, TREK-2, and TRAAK[5] [12, 92].

Like the other K2P channels, TREK-2 is highly multimodal, and is regulated by membrane stretch, acidosis, heat, and anionic fatty acids (which make up the majority of cellular lipids) such as arachidonic acid, as well as being a target for volatile anaesthetics such as the halothanes [12, 58, 80, 92, 93, 94]. TREK-2 is highly expressed in the central nervous system (CNS) and peripheral nervous system (PNS), particularly in the hippocampus, cerebral cortex, and cerebellum, suggestive of a role in cognition [92, 93]. Additionally, TREK-2 is expressed in the pancreas and kidneys [80].

K2P channels are highly unusual in that the X-ray crystal structures do not possess a helix bundle crossing, implying that the section of the pore nearest the cytoplasmic face of the membrane is constitutively "open" at all times [30, 86, 98]. This is consistent with the hypothesis that gating occurs entirely at the filter [97, 98]. In addition, recent structures of TREK-2 from the Structural Genomics Consortium (Oxford)[6] (and also of TRAAK from

[4]TREK: TWIK-related potassium channel (TWIK: twin-pore inwardly rectifying potassium channel).

[5]TRAAK: TWIK-related arachidonic acid-activated potassium channel.

[6]unpublished data

MacKinnon *et al.* [30]) suggest that large structural changes occur within the lower TM segments during gating. Understanding these conformational changes is vital to elucidating the mechanism of TREK-2 gating, and hence K2P gating, so TREK-2 is an attractive target for smFRET solution-based studies of conformational transitions similar to those of KirBac1.1 presented in this thesis. To this end, optimisation of reconstitution of TREK-2 into nanodiscs was undertaken.

5.12.2 Methods

Purification

TREK-2 expressed in insect cells was purified by Alexandra MacKenzie[7]. The protein was solubilised using the detergents Octyl Glucose Neopentyl Glycol (OGNG) and Cholesteryl Hemisuccinate Tris Salt (CHS), and affinity purification performed *via* His-tag binding to TALON® Metal Affinity Resin[8] (Clontech). Further purification was performed *via* size-exclusion gel filtration using a Superose 6 10/300 GL column (GE Healthcare). The chromatography trace is given in Figure 5.14: the peak used for the reconstitution experiments is highlighted, at ~15.5 mL.

Nanodisc assembly

To optimise incorporation into nanodiscs, several different ratios of TREK-2 and MSP were examined. The combinations are given in Table 5.13 below. The stock concentration of TREK-2 was 2.06 mg/mL, and that of MSP was 2.05 mg/mL. The final cholate concentration was ~22.5 mM. Buffer recipes are given in Table 5.14.

The mixture was incubated overnight at 4°C with gentle agitation. It was then added to Bio-Beads (Bio-Rad) equilibrated with MSP standard buffer and incubated at 4°C for 8 hours. The sample was loaded onto a size exclusion column (Superdex 200 10/300, GE Healthcare) equilibrated with MSP standard buffer for purification and visualisation. Buffers for size-exclusion chromatography had been filtered using a 0.22 μm membrane

[7]Member of the Integral Membrane Proteins group led by Liz Carpenter at the Structural Genomics Consortium (SGC) Oxford, Old Road Campus Research Building, Headington, Oxford

[8]Suspension of beads with hexaaquacobalt(II) $[Co(H_2O)_6]^{2+}$.

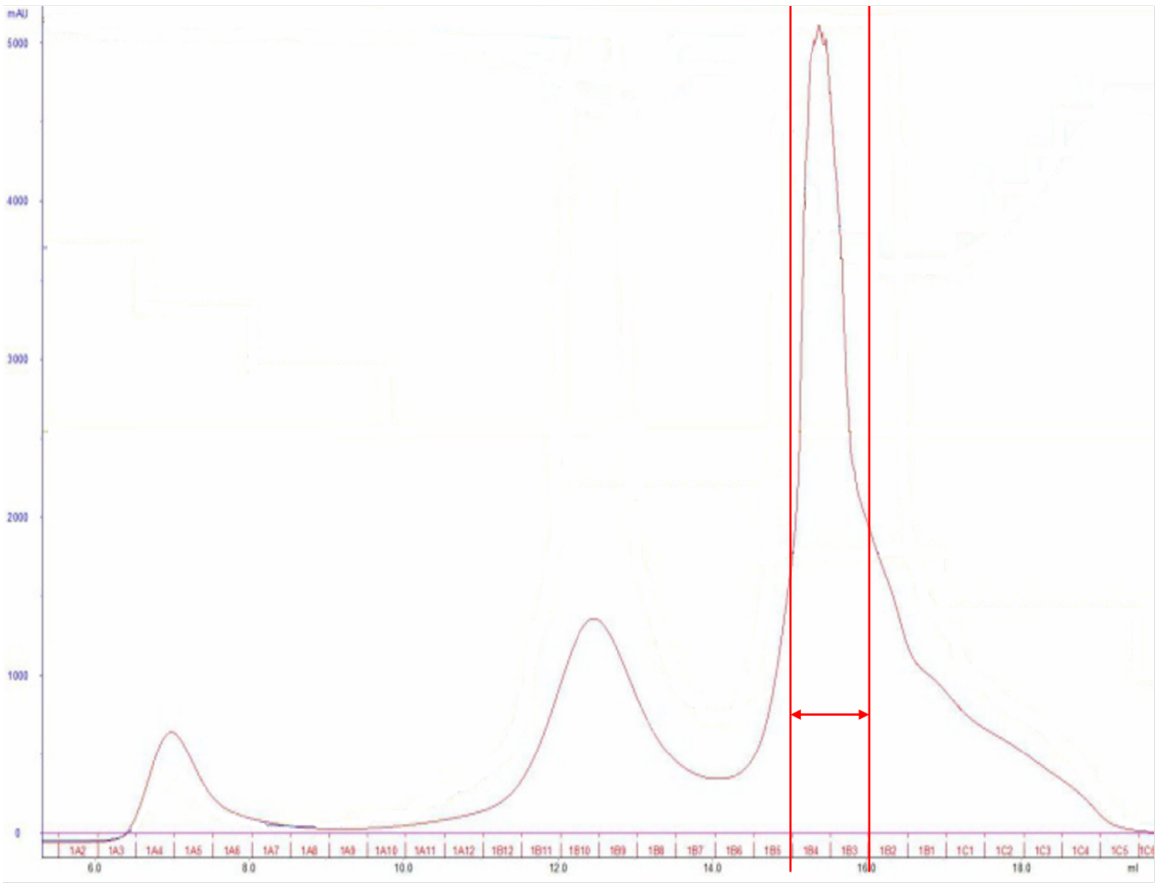


FIGURE 5.14: Size-exclusion chromatography of purified TREK-2; purification performed by Alexandra MacKenzie. The peak used for nanodisc reconstitution is highlighted (~15.5 mL).

	nano1	nano2	nano3	nano4
TREK-2/μL	97	97	194	194
MSP/μL	98	196	98	196
10 mM POPE/μL	100	100	100	100
10 mM POPG/μL	34	34	34	34
Cholate buffer/μL	166	166	166	166
MSP standard buffer/μL	305	207	208	110
Total volume/μL	800	800	800	800
TREK-2:MSP ratio	1:1	1:2	2:1	2:2

TABLE 5.13: Nanodisc assembly mixtures for TREK-2 reconstitution trials

	MSP standard buffer	Cholate buffer
Tris-HCl pH = 7.8	20 mM	20 mM
NaCl	100 mM	100 mM
EDTA	0.5 mM	0.5 mM
Cholate	-	100 mM

TABLE 5.14: Nanodisc assembly buffer recipes

and degassed by vacuum pump for >3 hours.

5.12.3 Results

The results of the optimisation procedures were visualised using size-exclusion chromatography, an example of which is given in Figure 5.15. The blue trace corresponds to a TREK-2 + MSP samples (sample "nano2"), and the red trace corresponds to MSP only. The green arrow marks the position at which monomeric TREK-2 would be expected to appear using the same column: dimeric (assembled) TREK-2 would be expected to occur in region γ. Regions γ and δ correspond to dimeric and monomeric MSP, respectively, whereas region β corresponds to aggregated multimeric MSP and/or TREK-2. Region α corresponds to complexes of the correct molecular weight to be assembled nanodiscs, although it is also possible that these could merely be aggregates, particularly of TREK-2 which is in a highly suboptimal buffer during nanodisc reconstitution.

All four TREK-2:MSP ratios were visualised using size-exclusion chromatography, with a little variation between the results. These are presented in Figure 5.16, where the blue traces represent the nanodisc reconstitution samples and the red traces correspond to MSP only. It can be seen that samples "nano2" and "nano4" both have a considerable shoulder at a molecular weight which is suggestive of TREK-2 and/or MSP aggregation. The single peak in samples "nano1" and "nano3" may be indicative of a greater degree of success, but also of aggregation, particularly of TREK-2 which was in an unfavourable buffer solution during these reconstitutions. SDS-PAGE showed that there was both TREK-2 and MSP present in the size exclusion chromatography peaks, shown in Figure 5.17. These results are therefore promising, but require optimisation before successful assembly can be verified unambiguously.

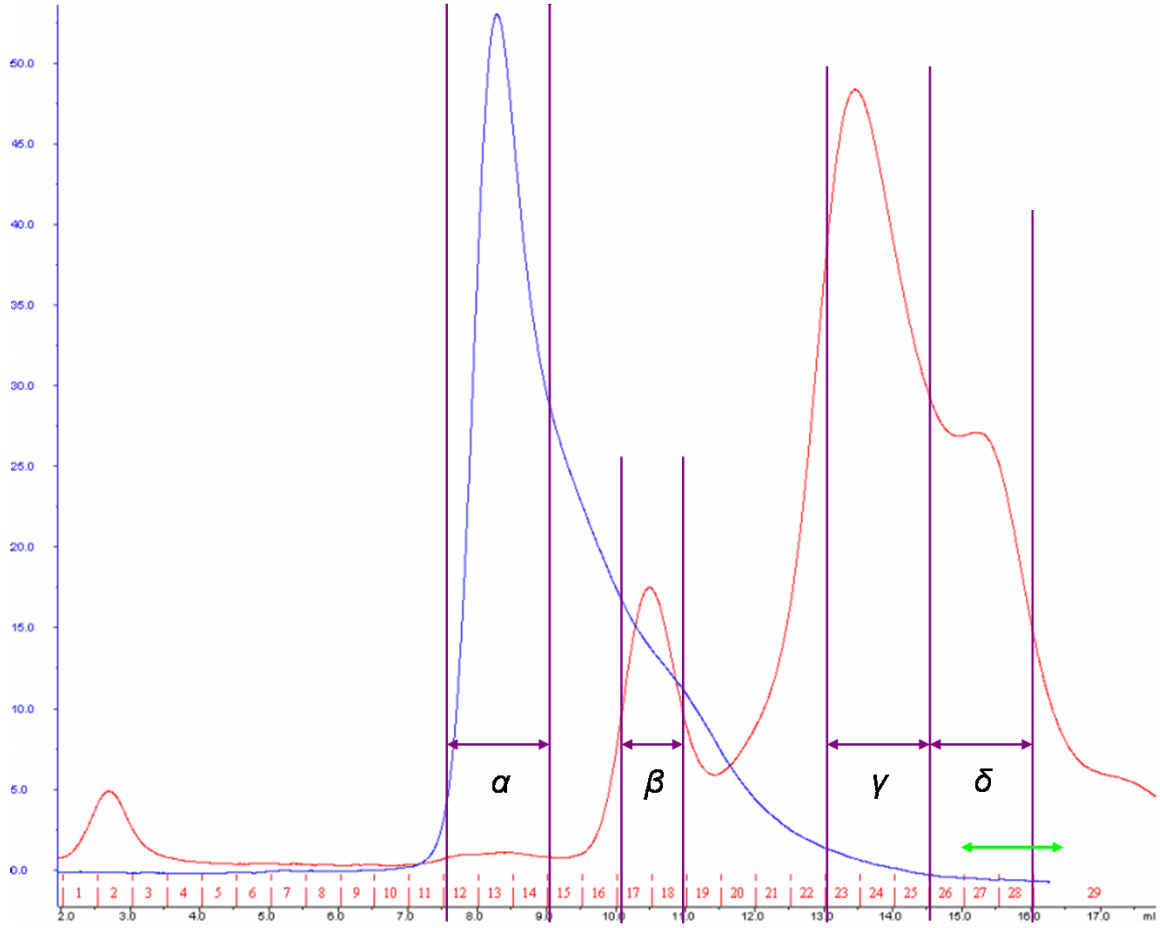


FIGURE 5.15: Exemplary size-exclusion chromatography trace of TREK-2 reconstitution. The blue trace represents the TREK-2 + MSP sample, and the red trace corresponds to MSP only. The green arrow marks the position at which monomeric TREK-2 would be expected to appear using the same column: dimeric (assembled) TREK-2 would be expected to occur in region γ. Regions γ and δ correspond to dimeric and monomeric MSP, respectively, whereas region β corresponds to aggregated multimeric MSP and/or TREK-2. Region α may represent assembled nanodiscs, or aggregated TREK-2.

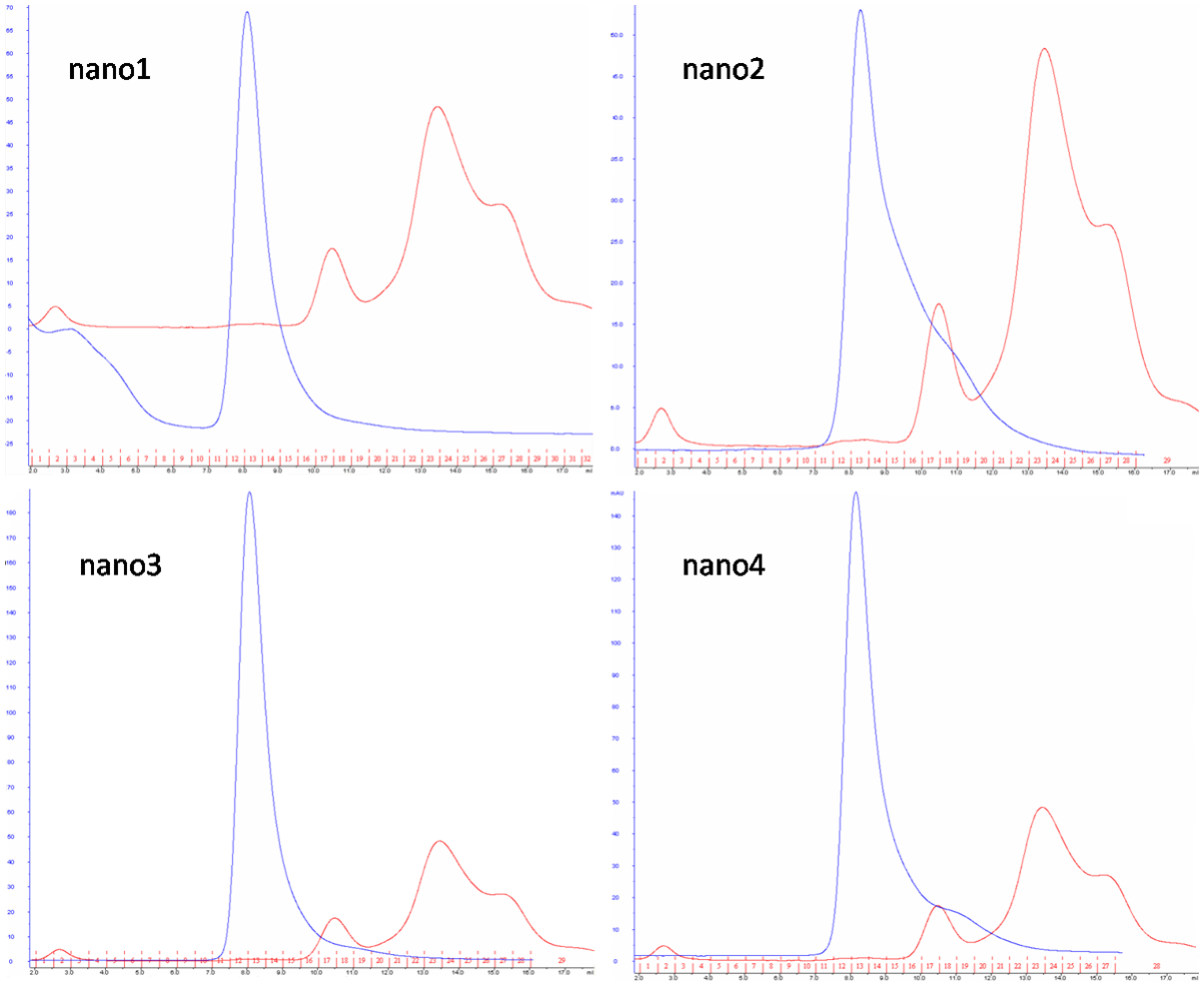


FIGURE 5.16: Size-exclusion chromotography of the optimisation of the reconstitution of TREK-2 into nanodiscs. The trace corresponding to the mixture mixture is shown in blue, and a trace for MSP only is shown in red. Samples nano1 and nano3 appear to be the most promising as the peaks lack the shoulder, presumed to correspond to aggregated MSP and/or TREK-2.

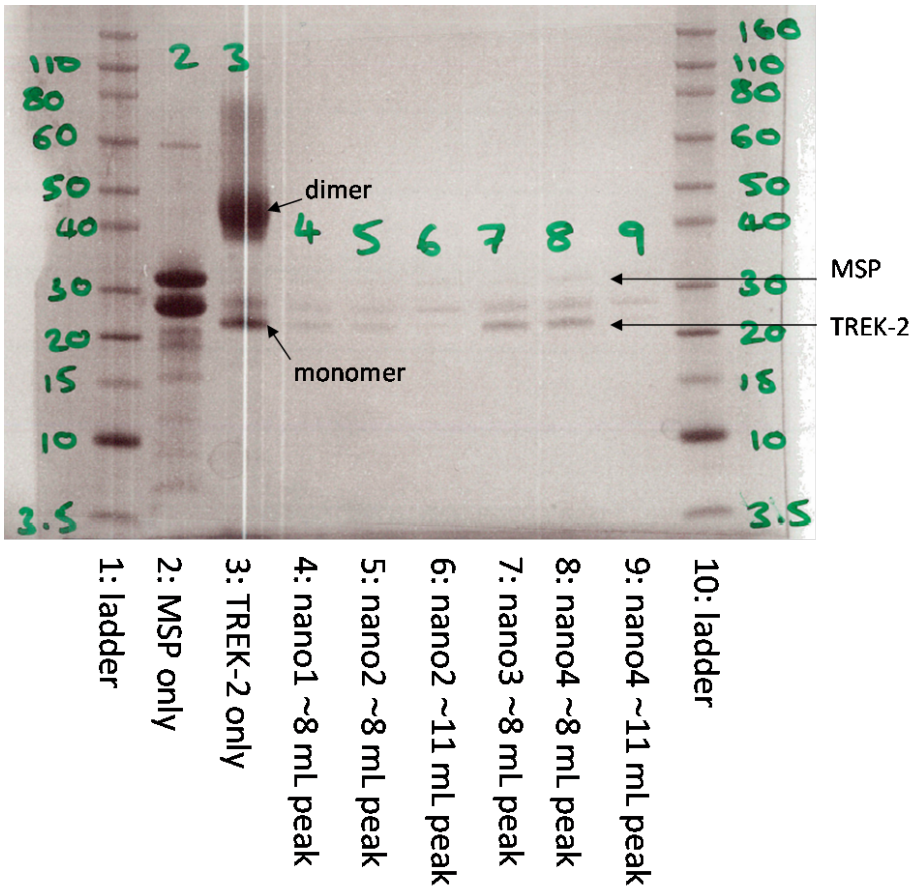


FIGURE 5.17: SDS-PAGE of the reconstitution of TREK-2 into nanodiscs. The samples correspond to the samples from FPLC traces, shown in Figure 5.16. There is both MSP and TREK-2 visible in the samples, particularly in nano3 and nano4 (sample concentration is much lower than stock concentrations of MSP and TREK-2 only, hence the lower intensity).

5.12.4 Discussion and conclusions

Although there appears to have been some success in the attempts to reconstitute TREK-2 into lipid nanodiscs, it is not clear whether the reconstitutions were successful due to the possible presence of aggregated TREK-2 protein in the relevant peak. The TREK-2 protein used in this study is truncated as the construct was originally designed for X-ray crystallography trials, and has a tendency to form highly multimeric complexes, with up to ten monomers, although this is vastly more likely when using the construct with the His tag still attached, which was not the case in this study (personal communication with A. MacKenzie).

In addition, most previous lipid-based reconstitutions of TREK (and other K2P) channels have used cholesterol and soybean-derived lipids such as azolectin as the reconstitutory lipids, rather than members of the phosphatidyl family as in this study [22, 31]. It is therefore highly likely that optimisation of the lipid environment is required.

However, while the results presented here show that more optimsation will be necessary, there is some promise that further work will result in the unambiguously successful reconstitution of TREK-2 into nanodiscs. This strongly suggests the possibility of smFRET studies of conformational transitions of TREK-2, as well as highlighting the wide applicability of nanodiscs as a tool for the study of a variety of ion channels, not just the inwardly rectifying potassium channels.

Chapter 6

Conclusions and future directions

6.1 Summary of findings

This thesis is based upon a series of single-molecule fluorescence studies of KirBac1.1. In order to perform these, KirBac1.1 was successfully expressed in *E. coli*, purified into detergent micelles, and labelled with donor and acceptor dyes using a cysteine-maleimide reaction. Initial smFRET observations of the detergent-solubilised protein using confocal-in-solution microscopy with ALEX were obtained and optimised, representing the first single-molecule fluorescence studies of a member of the inwardly rectifying potassium channel family.

When the smFRET measurements had been sufficiently optimised to enable resolution of the two labelling populations, the signals were validated by the use of modulatory factors (inhibitory [H^+] and PIP_2, and an activatory point mutation) known to perturb the open-closed dynamic equilibrium of KirBac1.1. These produced a shift in the FRET efficiency (E^*) of the fluorescence populations, suggesting a conformational change which produces an intra-protein movement at the location of the cysteine reporter sites. However, detergent micelles are a suboptimal solubilisation system for membrane proteins, so a more native-like alternative was investigated: nanodiscs.

Labelled KirBac1.1 was successfully reconstituted into nanodiscs, and the smFRET measurements repeated, including those in which a modulation of the dynamic gating equilibrium was performed. The results of these investigations were consistent with those using

detergent micelles, but were more distinct and reproducible in the lipid-based nanodisc system.

It was found that the two cysteine reporter sites, located in different domains of the protein, produced a FRET shift in opposite directions, suggesting that the residues themselves are moving in opposite directions upon a change in gating state. This is consistent with the results of Wang *et al.* in their mapping of the conformational changes in KirBac1.1 upon PIP_2 inhibition [123]. Furthermore, the current study found that the shifts produced by PIP_2 and H^+, both inhibitory ligands, are in the same directions and of approximately the same magnitude, suggesting common conformational changes associated with inhibition in KirBac channels.

In addition, it was seen that the *activatory* point mutation produced smFRET shifts, and therefore residue movement, in the opposite direction to the inhibitory factors. This suggests that the conformational changes induced by this mutation are approximately the converse of those implicated in the inhibitory mechanism.

Finally, results have been obtained which suggest that it will be possible to reconstitute other potassium channels into nanodiscs. This thesis presents one of the first demonstrations of the solubilisation of a human K2P channel (TREK-2) in this manner, further highlighting the utility of nanodiscs in future studies of a potassium channel where smFRET would be particularly helpful to address its unique gating mechanism.

6.2 Cautions and caveats

6.2.1 Detergent micelles *vs* nanodiscs

It is clear from many sources that detergent micelles are a suboptimal environment for integral membrane proteins. Detergent micelles are highly prone to aggregation and instability [11], making functional or structural studies more challenging. It is also clear that the detergent micelle is an environment far removed from that experienced by an integral membrane protein in the phospholipid membrane, thereby raising questions about the validity of results obtained in the non-native environment. For example, Akyuz *et al.* and Erkens *et al.* both examined the transporter Glt_{Ph}, but one study was performed using detergent-solubilised protein, and the other with the protein reconstituted into lipid vesicles: this difference is thought to have led the groups to reach different conclusions about the dynamic behaviour of the protein [3, 53]. In addition, detergent micelles have non-ideal optical properties which could produce artefacts in fluorescence measurements [18]. For these reasons, it was desirable to optimise the nanodisc system as an alternative method of solubilisation.

Nanodiscs, effectively a small section of lipid bilayer bounded by a scaffold protein [14, 18], are soluble and can therefore be treated in the same manner as detergent micelles with respect to confocal-in-solution microscopy. The bounding membrane scaffold protein means that a nanodisc-reconstituted sample is more stable [14], and the nanodiscs themselves are monodisperse, with nanodisc size being consistent between preparations [14, 87, 103].

The more native-like environment of the nanodisc means that the conformational changes observed can be more reliably interpreted as coresponding to those which might occur in the protein's native environment in the membrane, and processes which are thought to depend on or be mediated by membrane lipids, such as the interaction of PIP_2 with KirBac1.1 [62, 127, 128], can be examined. Nanodiscs are also thought to reflect the phase behaviour of the membrane more accurately [44, 110], and as the membrane is a dynamic, fluid environment, such perturbations would be expected to affect protein conformational changes [20]. Membrane lipid dynamics are clearly absent in detergent micelles.

However, consideration of the limitations of the nanodisc environment highlights some valid concerns. In order to form an optimally stable protein-nanodisc system, it is desirable for the diameter of the assembled disc to be as close to the diameter of the transmembrane region of the protein as possible, accommodating a single annulus of lipid molecules, but this could impose a constraint on the dynamics of the transmembrane region of the protein, particularly in KirBac1.1 which is expected to undergo a significiant change in diameter upon gating [13]. Reassuringly, nanodiscs have been previously exploited to study the dynamics of the membrane, and protein-lipid interactions, suggesting that the environment possesses enough fluidity and flexibility for this to be a minor concern; this has additionally been confirmed by MD simulations of lipid dynamics in nanodiscs [44, 46, 110, 111].

In addition, it is possible that oxidation reactions of the nanodisc constituent lipids may mean that the composition of the membrane surrogate is different from that intended. However, the stability of the nanodisc-KirBac1.1 system over time with respect to its reaction to perturbation suggests that this process has either reached an equilibrium early in the lifetime of the nanodisc, or is not a concern for this study. Unfortunately, from the data available, there is no way of establishing which scenario is correct.

Another pertinent effect of nanodiscs in this study was the ease of collecting data. Both the sample quality, in terms of the frequency of aggregation events, and the extended stable lifetime, were vastly improved compared to samples of KirBac1.1 solubilised in detergent micelles. The evidence that nanodiscs are a viable solubilsation method for confocal-in-solution smFRET studies of inwardly rectifying channels is in itself significant, and the finding that a member of the two-pore potassium channel family can also be stably reconstituted into nanodiscs additionally highlights their potential utility as a tool for examining the dynamic behaviour of ion channels, and potassium channels in particular.

6.2.2 Eukaryotic *vs* prokaryotic channels

Although it is ideal to study eukaryotic channels when considering channel families which are widely implicated in physiology and pathology, eukaryotic Kir channels can be challenging to express and purify, so the prokaryotic homologue KirBac1.1 was used in this study. Although Kir and KirBac channels are genetically homologous [34], share significant structural homology [24, 74, 113], and are functionally homologous to a great degree [95, 113], there are some differences in their regulation which must be considered.

Most notably, while eukaryotic Kir channels are known for their inward rectification, prokaryotic KirBac channels do not rectify under physiological conditions, although they can be made to do so by the addition of point mutations [34]. In addition, both eukaryotic Kir and prokaryotic KirBac are inhibited by H^+ [50, 61, 101, 102], but whereas negatively charged lipid ligands such as PIP_2 have an activatory effect on eukaryotic Kir channels [50, 61, 101, 102], they have an *inhibitory* effect on KirBac channels [34, 42, 52, 123], thought to be due to subtle structural differences near the face of the cytoplasmic membrane [42, 52, 62, 123]. This striking difference emphasises the caveat that while studying prokaryotic channels is undoubtedly valuable, one must exercise due caution when trying to apply conclusions drawn from studies of bacterial channels to their eukaryotic homologues.

6.2.3 Relevance of crystal structures to native conformation

As a study examining the dynamic equilibrium of the gating states of KirBac1.1 by exploiting the power of smFRET to detect small distances changes, this thesis would not have been possible without a structurally-derived model for the conformational changes involved in gating. The model used for this study was based on X-ray crystal structures of KirBac3.1 in the closed and open states, with some interpolation between the two structures [13]. However, this requires several assumptions, the first of which is that the model of the open state made using KirBac3.1 will be valid for KirBac1.1. The crystal structures of both KirBac1.1 and KirBac3.1 show an exceptionally high degree of structural homology, so the model based on KirBac3.1 is likely to be reasonably accurate [13, 47, 74, 113]. However, a greater concern is that the crystal structures used to create the proposed gating mechanism

do not necessarily reflect the native structure of the protein under physiological conditions. Interestingly, nearly all Kir and KirBac structures have been crystallised in the closed state, suggesting that this is the state of lowest energy of the purified protein once extracted from the membrane [13, 136], but this does not necessarily correspond to the *native* state of the protein in the membrane.

Under the right circumstances, examination of crystal structures can be extremely useful: Bollepalli *et al.* studied crystal structure-based models of Kir1.1 in the open and closed states, and compared these to functional data gathered from >190 mutants to model a network of interacting residues which stabilised the open states, particularly with respect to pH regulation [28]. This was a major advance in the understanding of the gating mechanism of Kir1.1, and inwardly rectifying potassium channels more generally. However, although myriad different crystal structures of Kir in many different conformations were examined in that study, the question of how these map onto a functional gating scheme remains, and the situation outlined in that study is one where the power of smFRET as a tool for detecting (and quantifying) intra-protein distance changes, paired with the more native-like environment of nanodiscs could be a powerful new method for elucidating conformational mechanisms and interaction networks.

In addition, the current models of KirBac gating acknowledge only two states – open and closed – whereas the reality is likely to be more complicated, with additional intermediate states and movements of individual intra-protein domains. The power of smFRET to quantify these motions could be applied to explore the conformational landscape traversed by KirBac channels during their gating and regulatory processes.

The current thesis has shown that it is possible to use smFRET to detect conformational changes in an ion channel, whether in detergent micelles or in lipid nanodiscs, and it is only a matter of refinement to be able to apply this technique to other channels, or indeed to be able to accurately quantify specific distances produced by intra-protein conformational changes.

6.2.4 Limitations of smFRET data

Although the studies presented in this thesis have highlighted the power of smFRET studies of membrane proteins, the technique has not been fully exploited. Differences in the physical properties of the fluorophores – transfer/excitation efficiency, detection efficiency, and environmental variations in quantum yield – mean that the smFRET values presented in this thesis require the application of corrections such as the γ factor [78] to obtain 'accurate' smFRET values. It is possible to use the histograms already acquired to perform these corrections, and estimates of the accurate smFRET efficiences are outlined in the appendices (section A.3). Reassuringly, while the absolute efficiencies are very different from the uncorrected values, there is no significant difference in the shifts in E^*, the principal property examined in this thesis, hence the conclusions reached can still be considered valid.

However, the non-zero size of the fluorophores and their linkers means that the distances and distance changes being reported *via* smFRET, even when the correction factors have been applied, are not the true distances between the residues. Flexibility of the linkers mean that the distances reported will be within the range spanning the possible positions of the dyes, which can be detected as a broadening of the peaks in the smFRET histogram with respect to E^*. However, in certain positions in the protein it is possible that the dye movement could be *more* constricted compared to a free linker, hence narrowing the range of motion. As long as it can be assumed that the dye/linker will be equally motile in both the open and closed states, it is still possible to draw conclusions based on the centre of the fitted Gaussian peaks, provided that the population peaks can be resolved with respect to E^*, and therefore the shifts in FRET efficiency upon modulation calculated. However, this may be complicated by the concern that the accurately resolved structure of the open state is unknown, and even the X-ray crystal structure of the closed state may not be representative of the channel in the environment it experiences in these studies.

Further complications arise when considering the possibility of fluorescence anisotropy: emitted fluorescence intensity may vary with the alignment of the fluorophore with respect to the axis of observation, and additionally the efficiency of the dipole-dipole interaction in FRET depends on the relative orientations of the donor and acceptor fluorophores. If the

motion and orientation of the dye is restricted in at least one state and/or reporter position, then the observed smFRET and fluorescence intensities will be reduced relative to freely motile dyes. As stated above, it has been assumed that the dyes are equally motile in both the open and closed states, but no measurements have been performed to quantify this. As well as these such a study being desirable in order to justify the conclusions reached in this thesis, these measurements could additionally facilitate formation of a more accurate model of KirBac1.1 gating as differences in spatial restrictions of the dyes between gating states would assist in further mapping of the conformational changes taking place.

Examination of the fitted peak widths may also reveal obscured molecular heterogeneity: if an observed peak appears to be much wider than predicted, this could an indication that the population in question is actually formed of two poorly resolved populations. However, more than 95% of the peaks observed in the studies presented in this thesis were consistent with each other. In addition, a large discrepancy in peak intensity between populations can also highlight the existence of unresolved subpopulations, hence revealing molecular heterogeneity. Consideration of 'hiddden' heterogeneity is relevant to this thesis as there were concerns that both labelling populations of the R151C reporter were present in the high E^* peak. However, rough calculation of the expected FRET efficiencies when considering the dyes and linkers which match the 'corrected' efficiencies (given in the appendices, section A.3), and the fact that the low E^* population was shifted by the applied gating modulations suggests that the two peaks are the resolved proximally and distally labelled populations for R151C.

An additional concern is that the Förster radius, R_0 of the Cy3B/AlexaFluor®647 dye pair under the relevant experimental conditions is not the expected 65 Å: the physical properties of fluorophores are sensitive to the chemical environment, and a change in R_0 would also affect the absolute FRET efficiencies. To calculate R_0, it would be necessary to make control measurements of the FRET pair. However, this is only relevant when considering absolute FRET efficiencies, and is superfluous when considering only the direction and approximate magnitude of shifts in FRET efficiency.

6.3 Implications of smFRET studies of KirBac1.1

6.3.1 Possible structural interpretations

Effect of the V145L activatory mutation

The activatory mutation V145L produced a shift in the smFRET efficiency to *higher E** for the R15C reporter, and *lower E** for the G249C reporter. The form of fluorescent donor/fluorescent acceptor FRET used in this study means that an increase in transfer efficiency is due to a decrease in the distance between the dyes, and *vice versa*. Therefore, the shifts observed in this thesis are thought to correspond to a decrease in the inter-dye distance at the location of the R151C reporter, and an increase in the inter-dye distance at the location of the G249C residue, suggesting a structural change whereby the R151C residues are moving closer together, and the G249C residues further apart.

Interestingly, the shift in FRET efficiency is in opposite directions for each reporter site, implying that these residues – and therefore the region near the helix bundle crossing/C-linker and the region near the G-loop in the cytoplasmic domain – are moving in opposite directions during these conformational changes. An opposing movement of these regions is also consistent with what was observed by Wang *et al.* in their study of KirBac1.1 [123].

Effect of H^+ and PIP_2 inhibition

Both inhibitory factors examined in this thesis – acidic pH and PIP_2 – produced shifts in *E** in the same direction for both reporter sites. This could suggest either a common conformational mechanism for ligand-induced inhibition, or shared elements of a similar mechanism for inhibition by both regulators.

Inhibitory H^+ and PIP_2 both induced a *decrease* in transfer efficiency for the R151C reporter site, and an *increase* for the G249C reporter site, suggesting an *increase* in the inter-dye distance at R151C, and a *decrease* in the inter-dye distance at G249C. The fact that the reporter sites R151C and G249C appear to be moving in opposite directions is consistent both with the investigations using the activatory mutation V145L, and the study of PIP_2 inhibition by Wang *et al.* [123].

However, the shifts observed to be induced by inhibitory PIP_2 or H^+ in this thesis are the inverse of what was found by Wang *et al.*: the authors of the Wang *et al.* study concluded that the distance between the R151C reporters is *decreasing* upon inhibition by PIP_2, whereas that between the G249C reporters is *increasing* [123]. This apparent inconsistency is discussed in more detail below.

Activation *vs* inhibition

It would initially appear to make sense that the structural changes induced by activation and inhibition are roughly the inverse of each other, despite the difference with the results of Wang *et al.* [123]. This supports the simplistic picture of channel gating as a transition between a single open state and a single closed state. However, the reality is undoubtedly more complicated, with the presence of additional intermediate states and transitions.

Interestingly, the magnitude of the smFRET shifts associated with the G249C reporter site also appear to be larger than for the R151C reporter site, possibly supporting the concept of 'gearing' of the global conformational changes, as the G249C site in the cytoplasmic domain is further away from the putative 'pivot', the helix bundle crossing, than R151C. However, without an accurately resolved structure of both the open and closed states of KirBac1.1, this is purely speculative.

6.3.2 Comparison with the findings of Wang *et al.*

It is interesting to compare the findings presented here to the results of Wang *et al.* (2012) [123]. In that study, the authors measured the change in (bulk) FRET efficiency upon binding of PIP_2 to KirBac1.1 reconstituted into liposomes, and repeated this for a series of reporter cysteine point mutations. The group reported an increase in the FRET efficiency (ΔE >0 in their notation) for R151C of magnitude ~0.03, and a decrease (ΔE <0) for G249C of magnitude ~0.03, *i.e.* the inverse of the current study[1].

The study by Wang *et al.* therefore suggests conformational movements where the distance between the dyes is *decreasing* for the R151C reporter site, and *increasing* for the G249C reporter site. The authors proposed that this corresponded to a narrowing at the helix bundle crossing, and a dilation in the cytoplasmic domain (with a possible rotation with respect to the transmembrane domain); this is shown in Figure 6.1. PIP_2 is known to have an inhibitory effect on the activity of KirBac1.1 [62, 127, 128], and the results of Wang *et al.* hence represent a proposed conformational mechanism for PIP_2 inhibition.

However, these shifts are the opposite of those observed in this thesis, raising a major point of interest. Among several other factors, it is notable that the study by Wang *et al.* used an ensemble, rather than a single-molecule FRET-based technique, unlike the studies presented in this thesis.

[1] For Wang *et al.* [123]:

$$E_{app} = \frac{F_{max} - F_o}{F_{max}} \tag{6.1}$$

where F_{max} is the fluorescence after proteinase digestion and is assumed to be constant, and F_o is the observed (bulk) fluorescence. Upon a FRET shift, $F_o \rightarrow F_o + \delta = F'_o$ and $\delta = F'_o - F_o$. This means that

$$\Delta E = \frac{-\delta}{F_{max}} \tag{6.2}$$

Wang *et al.* used a quencher for the acceptor in the FRET pair, so $\Delta E < 0$ corresponds to $\delta > 0$ and $F'_o > F_o$, *i.e. less* fluorescence transfer, suggesting $\Delta x > 0$, an outward motion of the fluorophores (and *vice versa* for $\Delta E > 0$).

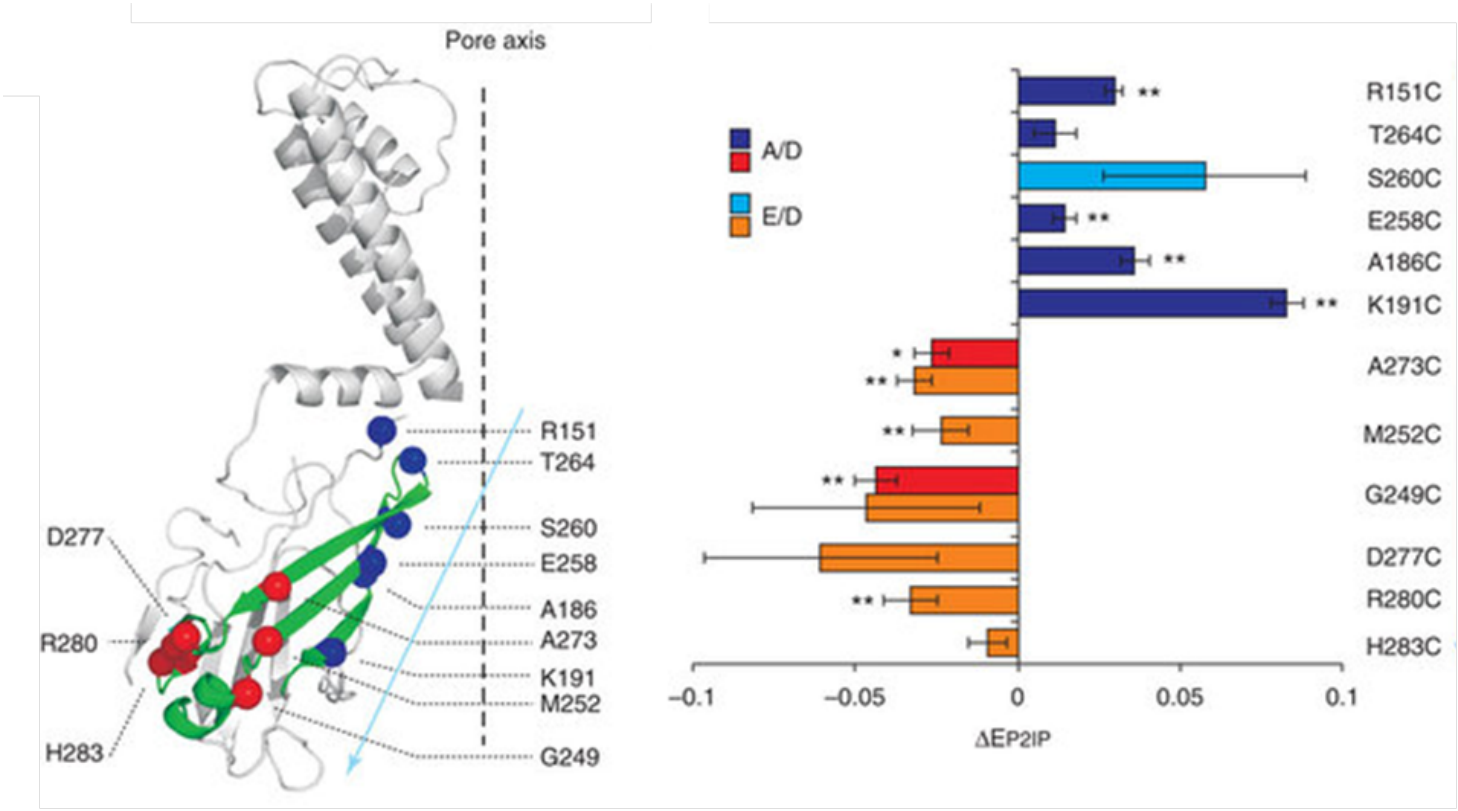


FIGURE 6.1: Wang *et al.* (2012) measured the FRET changes for a series of cysteine reporter point mutations in KirBac1.1 and used these values to map the conformational changes of the protein upon PIP_2, illustrating the proposed mechanism for inhibition by PIP_2 and related ligands (adapted from [123]). It can be seen that R151C residues, at the helix bundle crossing, will move closer to each other, whereas G249C residues, near the base of the cytoplasmic domain, will move further apart. This would correspond to a narrowing of the channel pore at the helix bundle crossing, and a dilation with a potential rotation of the cytoplasmic domain with respect to the transmembrane domain.
("A/D" and "E/D" refer to the fluorescent dye pairs used by the authors.)

6.3.3 Inconsistencies with Wang *et al.*: possible reasons

As stated above, this thesis presents observations which suggest that the R151C reporters are moving further apart and the G249C reporters closer together upon binding of inhibitory ligands (compared to the unmodified wild type channel), and *vice versa* for an activatory mutation. However, the examination of PIP_2 inhibition by Wang *et al.* led the authors to the inverse conclusion, where their *ensemble*-based FRET measurements suggested a *decrease* in the inter-residue distance at R151C, and an *increase* at G249C [123]. There are several possible explanations of this apparent inconsistency.

Forming a gating model

The gating model used as the starting point for this thesis was based on the X-ray crystal structures of KirBac3.1 in the open and closed state[2], solved to 3.65 Å by Bavro *et al.* [13]: the proposed gating mechanism was then based upon an interpolation between these open and closed states.

However, taking two static X-ray crystal structures and interpolating between them to obtain a dynamic mechanism is far from ideal, as there is no direct evidence for the structural intermediates. As described in Section 6.2.3, it is possible that these X-ray crystal structures do not precisely reflect the native structure of the protein when in the membrane.

However, the gating model proposed by Wang *et al.*, and used as the basis of the structural interpretation of their results, was based *only* on the (closed) structure of KirBac1.1 elucidated by Kuo *et al.* in 2003[3] [74]: the authors generated a model of the open structure by a rigid body rotation of the C-terminal domain and kinking of the second transmembrane helix at the glycine hinge [123].

The twisting of the cytoplasmic domain proposed by Bavro *et al.* [13] could conceivably produce shifts in transfer efficiency in either direction for both reporter sites, depending on the details of the structural models used. This is particularly pertinent for R151C, which is located *near* the helix bundle crossing, but actually *below* the helix bundle crossing in the C linker between the cytoplasmic domain and transmembrane domain [74, 123].

[2]PDB structure reference 3ZRS, solved using homology modelling based on the partial structures 2WLJ and 2X6C.

[3]PDB structure reference 1P7B

These linkers are located at the protein-solution interface and appear to lack secondary structural motifs, making their structure particularly difficult to solve due to their inherently disordered nature. Indeed, G249C also appears to be located in such a loop, being in the G-loop in the cytoplasmic domain [74, 123].

It is likely that structural modelling exhibits the highest degree of accuracy within the transmembrane domains, as the trade-off between optimal packing and steric clashes between the helices means that the available conformational space for transmembrane domains is much more limited than for soluble domains [41]. Indeed, the vast majority of gating mechanisms of homomeric ion channels resemble the opening of an iris with some helical translation, highlighting the importance of the transmembrane packing for quaternary structure [41]. However, as transmembrane regions are by definition not solvent-accessible, their motions cannot be easily examined using fluorescent labelling studies such as those described here, as labelling of membrane-bound domains is challenging. Indeed, many of the sites within the transmembrane helices of KirBac1.1 have been shown to be inaccessible to fluorescent labelling in the study of Wang *et al.* [123], and smFRET studies of similar channels such as KcsA have limited labelling sites to sites near the membrane-solution interface, such as in the study by Blunck *et al.* which utilised labels near the extracellular end of the transmembrane helices, and at sites near the helix bundle crossing [25]. However, Wang *et al.* and Akyuz *et al.* have utilised sites within the transmembrane domains in their studies of the mechano-sensitive channel MscL [125] and the glutamate transporter Glt_{Ph} [3], respectively.

Gating models and structural ambiguity

The gate at the helix bundle crossing is thought to be the F146 residue, which forms a steric constriction in the pore at its narrowest point (highlighted in yellow in Figure 6.2 and 6.3) [24, 67, 74, 106]. It is clear from these structures that R151 (highlighted in pink) is located below the helix bundle crossing gate [37]. As stated above, it is likely that the structural and conformational modelling of these looped regions are less accurate than for the more constrained and intrinsically ordered transmembrane domains [41], so it is not necessarily clear in which direction the R151 residues would move relative to F146 upon the channel

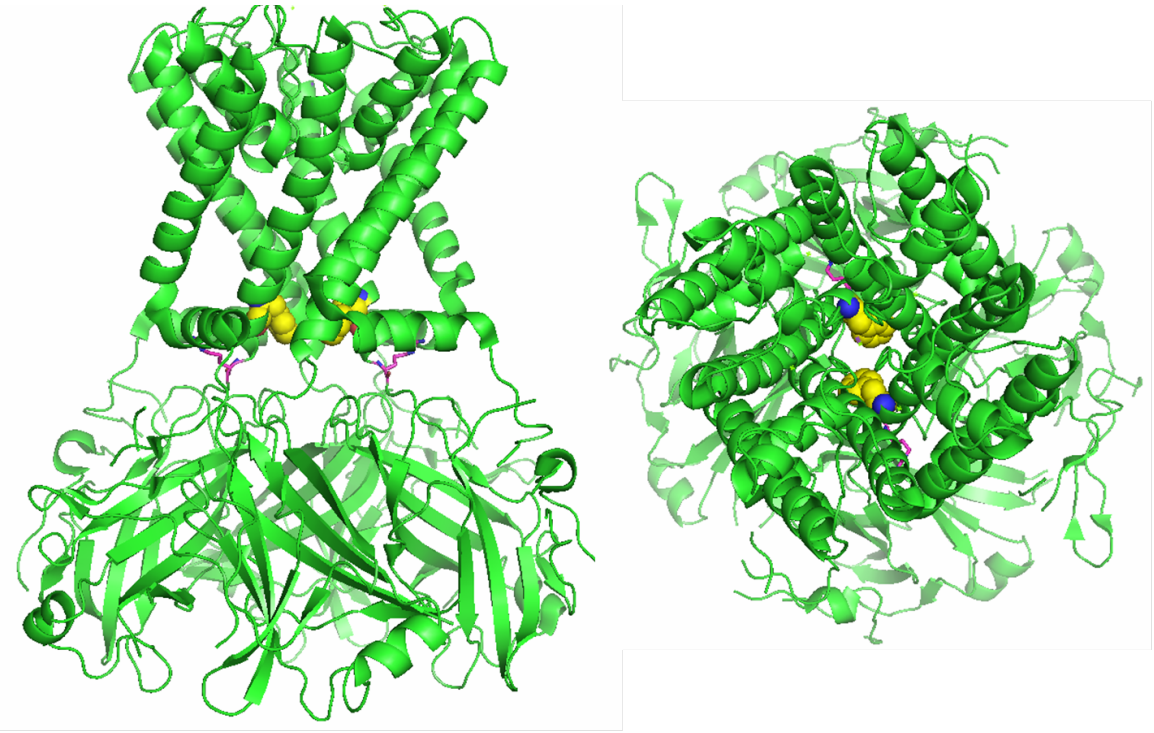


FIGURE 6.2: Structure of KirBac1.1, using PDB file 2WLL [37]: side view (left) and bird's eye view along the pore, in the extra- to intracellular direction (right). The steric gating residue F146 is highlighted in yellow, and R151 is highlighted in pink. The residues highlighted in this diagram are on diagonally opposite subunits and hence would correspond to the 'distal' labelling scheme. It can be seen that R151 is not located directly on the helix bundle crossing, but is in one of the interdomain loops between the transmembrane domain and the cytoplasmic domain.

undergoing a gating transition.

Without an accurately resolved structural model of the open and closed states of KirBac1.1, as well as a detailed model of the gating intermediates, it is not possible to predict in which direction the R151 residue will move upon an inhibitory conformational change. Determination of this *via* interpolation of static X-ray crystal structures would be highly dependent on the structures and assumptions used to generate the models.

Although existing evidence clearly implies a constriction of the helix bundle crossing during closure [13, 24, 37, 67, 74, 106], it is conceivable that the R151 residues could move further apart upon an inhibitory gating motion that also causes a constriction of the pore at the helix bundle crossing, particularly if this conformational change is associated with a twisting of the cytoplasmic domain like that observed for KirBac3.1 by Bavro *et al.* and proposed as a general gating mechanism for the KirBac family [13].

There are several proposed models for the movement of the transmembrane helices during potassium channel gating, and while the model including translational motion of

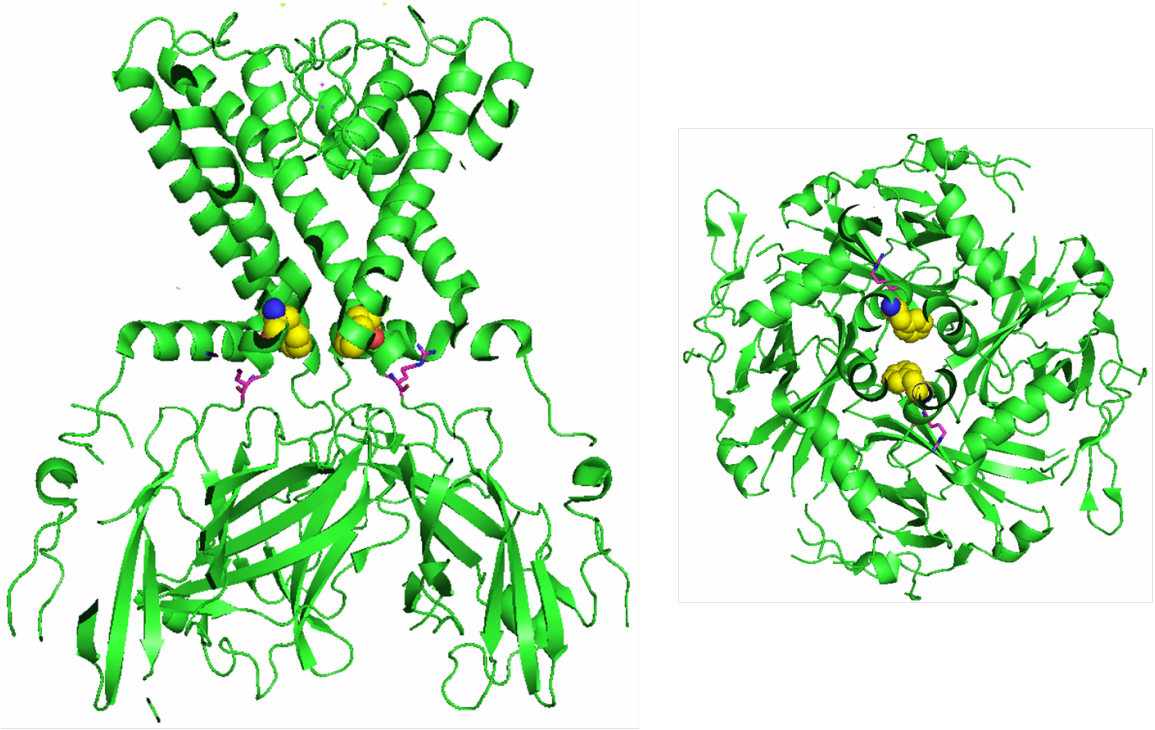


FIGURE 6.3: The same structure of KirBac1.1 as in Figure 6.2, with cross sections taken on the vertical (left) and horizontal (right) planes. This enables a clearer view of the F146 (yellow) and R151 (pink) residues. It can be seen that the F146 steric gating residue forms a constriction in the pore pathway at the helix bundle crossing, whereas R151 is located in the interfacial loop at the cytoplasmic face of the membrane. It is perhaps reasonable to surmise that if there is a twisting motion associated with the cytoplasmic domain as proposed by Bavro *et al.* [13], the R151 residues could move further apart upon inhibition, while the F146 residues move closer together, further constricting the pore.

the helices (illustrated in Figure 6.4 A) results in a decrease in the distance between positions on the helices away from the helix bundle crossing, a model with rotation as well as translation of the helices (Figure 6.4 B), resulting in a tighter 'crossing', produces the opposite scenario: $d_{open} < d_{closed}$. This second model is very similar to the "twist-to-shrink" model[4] proposed by Yao and Olvera de la Cruz [133] which suggests that a rotation of the transmembrane helices that produces a constriction at the helix bundle crossing could produce an increase in the distance between two points on different helices located away from the helix bundle crossing, illustrated in Figure 6.5. The possibility for $d_{open} < d_{closed}$ at the R151 site, located below the helix bundle crossing, fits with the smFRET shifts observed in this thesis, despite being the opposite of what was observed by Wang *et al.* [123].

It is clearly necessary to generate a more accurate picture of the motions occurring in this interfacial region upon gating than those which can be obtained through X-ray crystallographic studies. It would therefore be desirable to exploit the power of smFRET to detect and quantify these movements to resolve these structural and transitional ambiguities.

[4]Originally formulated for KcsA but applicable to other potassium channels, including KirBac1.1.

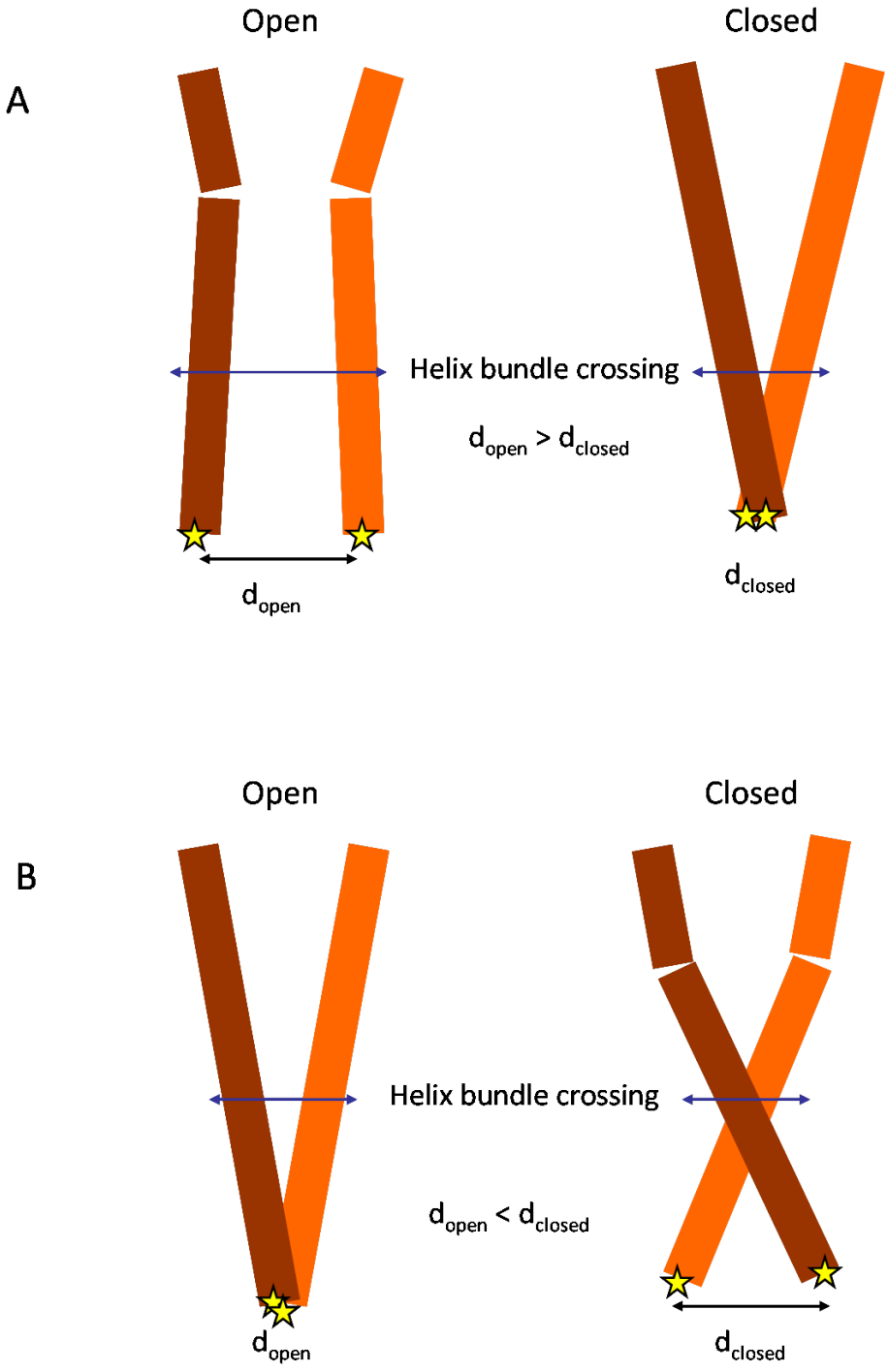


FIGURE 6.4: Cartoon of the two possible models of the helix bundle crossing during gating.
A: The lower portions of the transmembrane helices move translationally to produce a dilation or constriction upon gating, often by means of a kink in the transmembrane helices. This leads to $d_{open} > d_{closed}$, as proposed by Wang *et al.* [123].
B: The transmembrane helices rotate as well as translate, producing an overall 'twisting' of the transmembrane domain relative to the cytoplasmic domain. This leads to $d_{open} < d_{closed}$, as suggested by this thesis.

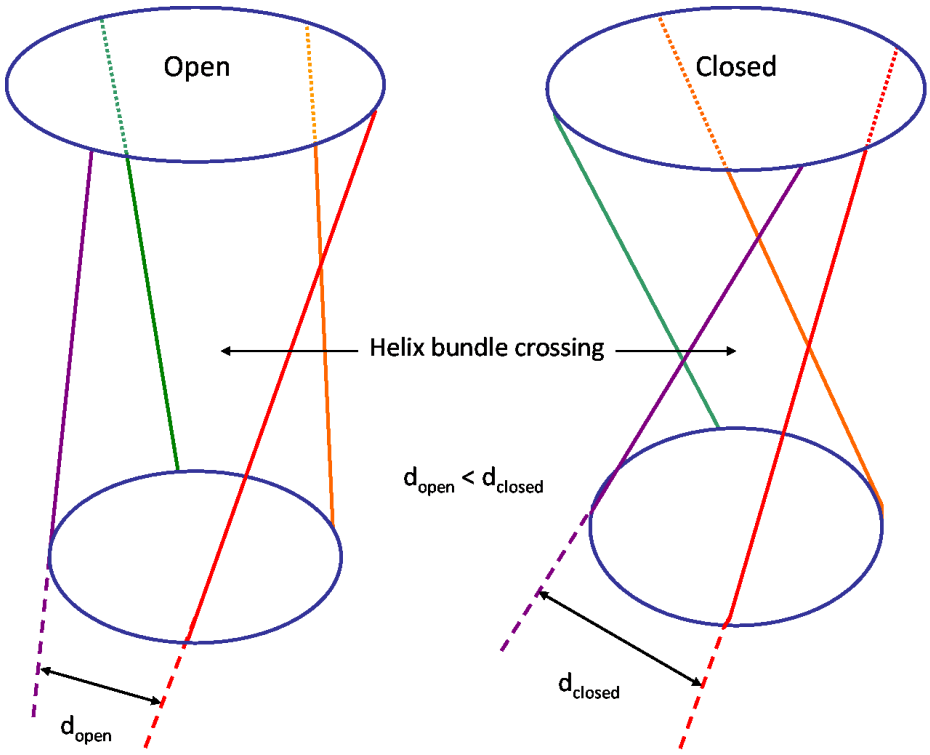


FIGURE 6.5: Illustration of the helix bundle crossing "twist-to-shrink" model of gating [133]. A rotation of the transmembrane helices (represented by the coloured lines) produces a constriction at the helix bundle crossing, but may produce an increase in the distance between the helices away from the helix bundle crossing. The hypothesis that $d_{open} < d_{closed}$ further along the helices is proposed as an explanation of the smFRET shifts observed for the R151C site in this thesis.

Mechanism and functionality

Both R151 and G249 are highly conserved residues within the KirBac family, suggesting they may have a crucial role in the structure and function of the channels.

R151 is located very near the putative lipid binding site, itself thought to be near the highly dynamic interfacial region containing the helix bundle crossing and C-linker [59, 95, 97]. It might be expected that mutation of this residue would therefore have an effect on the function of the channel. However, it has been demonstrated that the R151C mutation (and also the G249C mutation) did not affect the basic functional properties of KirBac1.1 when examined using a rubidium flux assay with the protein reconstituted into liposomes [123]. In addition, this thesis has also presented results showing that an activatory point mutation, made at a location distant from the putative ligand binding site, produces shifts in E^* that are approximately equal to and in the opposite direction to those due to inhibitory ligands, suggesting that at least parts of the regulatory mechanisms of the protein are intact.

Solubilisation methods

The primary conclusions of this thesis were obtained using KirBac1.1 solubilised *via* reconstitution into lipid nanodiscs (described in detail in this thesis), whereas the study of Wang *et al.* (2012), with which the results are being compared, used KirBac1.1 reconstituted into liposomes [123]. Both the nanodiscs used in this thesis and the liposomes of Wang *et al.* were formed from the same lipid ratio of 3:1 POPE:POPG: indeed, the lipid content of the nanodiscs was chosen to match that of the Nichols group's work. Notwithstanding the possibility of lipid oxidation, this means that KirBac1.1 experienced the same lipid environment – with respect to lipid chemistry – in both cases.

As discussed above, it is possible that the relatively small diameter of a nanodisc could constrain the movement of KirBac1.1, meaning that the full range of motion is not accessible, and hence creating a discrepancy between the results of this thesis and those of Wang *et al.*, but it is also conceivable that the curvature of a liposome could have a similar effect. Without a direct comparison of the two solubilisation methods incorporating structural information, this issue cannot be resolved.

Fluorescence methods

This thesis presents data obtained using *single-molecule* FRET: the small confocal volume combined with an optimal sample concentration meant that only one channel was traversing the observation volume at a time. Furthermore, the nature of the method of alternating laser excitation coupled with the two channel fluorescence detection enabled the filtering of fluorescence events which did not correspond to donor-excitation/acceptor-emission.

However, the study by Wang *et al.* was based upon *bulk* measurements of the *ensemble* fluorescence resulting from FRET events [123], and hence was not a single-molecule method. As fluorescence was measured using a spectrophotometer, all fluorescence events were effectively 'binned' together and there was no way of filtering out signals which did not originate from one donor/one acceptor proteoliposomes. A model for E_{app} was used which could account for tetramers with more than one donor and/or acceptor, outlined by Cheng *et al.* [35], which was in turn based on the rate theory outlined by Lakowicz [76]. However, the model of Cheng *et al.* makes the assumptions that the tetrameric protein in question is perfectly four-fold symmetric, and that the FRET pathways are independent and additive [35], neither of which are necessarily valid.

Although the single-molecule method outlined in this thesis is not perfect (*e.g.* events from proteins with more than one donor and/or acceptor are not necessarily excluded from the summary histograms), it could still be considered to be a more accurate observation method than using bulk fluorescence, and one only originating from the donor fluorophores at that (as the FRET used by Wang *et al.* employs a quenching acceptor). Therefore, the smFRET measurements generated in the studies in this thesis require fewer assumptions to determine structural and functional implications than that of Wang *et al.*.

6.4 Concluding remarks and future directions

This thesis has presented confocal-in-solution smFRET studies reporting on the conformational transitions of KirBac1.1 associated with gating regulated by inhibitory H^+ and PIP_2, and an activatory point mutation. Data were obtained from the channel solubilised in detergent micelles and reconstituted into lipid nanodiscs.

Solution-based studies of detergent-solubilised proteins appeared feasible, but were also challenging, and additionally the detergent environment had a profoundly detrimental effect on the protein itself. Single-molecule fluorescence studies are rapidly becoming a gold standard for examining conformational changes in real time, reporting on intermediate states which cannot be detected *via* X-ray crystallography, so it is important to develop a reliable technique for examining membrane proteins in an environment which more closely approximates their native state.

Lipid nanodiscs have here been demonstrated to be a viable solubilisation method for obtaining smFRET data reporting on the conformational changes of KirBac1.1 associated with gating regulation. I was also able to successfully reconstitute the TREK-2 channel into nanodiscs, demonstrating that this technique is applicable to other potassium channels, and therefore highlighting the versatility of what is still a relatively new approach to the examination of membrane proteins.

6.4.1 KirBac1.1

It is an obvious extension of this thesis to examine the effect of the activatory and inhibitory regulators in combination with other cysteine reporter mutations in order to more fully explore the conformational landscape of KirBac1.1. As mentioned above in the discussion of the inconsistencies of the results presented in this thesis with those already published by Wang *et al.*, there is a great deal of ambiguity in the structural, and hence gating, models of KirBac1.1, particularly with respect to the loops in the interfacial region between the transmembrane and cytoplasmic domains: depending on the model used, it could be argued that the R151 residues would move either in the same as or opposite directions to the steric gating residues upon an inhibitory conformational transition. In addition, the loop regions

of the cytoplasmic domains are more ambiguous than the more constrained alpha-helical and beta sheet motifs of the protein. The power of smFRET to detect and quantify intra-protein distance changes would therefore be highly applicable to investigations forming a detailed map of the conformational changes of KirBac1.1.

However, one of the limitations of the technique presented in this thesis is the ability to resolve the population peaks in the smFRET histograms, and therefore to resolve small changes in E^*, which could be improved by having a single labelling population to which a Gaussian is fitted. KirBac1.1 is a homotetramer, with four possible cysteine/maleimide reaction sites per assembled channel, so it would be necessary to make a chimeric homodimer of KirBac1.1, in which only one monomer contains a cysteine mutation: this would result in a tetrameric protein which only contains two possible labelling sites. The use of this construct would exclude the possibility of smFRET signal from proteins labelled with more than one donor and more than one acceptor, and the two-donor and two-acceptor proteins which produce donor-only and acceptor-only signals, respectively, would be clearly distinguishable on the resulting smFRET histograms.

6.4.2 Other channels

The successful reconstitution of KirBac1.1 into nanodiscs for smFRET studies implies that it is likely that this could be achieved for other members of the KirBac, and indeed eukaryotic Kir, family. However, the results using the K2P channel TREK-2 demonstrate that this is also possible for other channel superfamilies.

Considering just TREK-2, this protein is involved in a wide range of physiological functions, and implicated in many pathologies, yet much still remains unknown about its gating mechansim, so it is desirable to obtain information about its conformational transitions. Merely relying on electrophysiological and X-ray crystallographic studies is clearly a limitation when it could be possible to label TREK-2 to enable single-molecule fluorescence studies of this channel reconstituted into nanodiscs. Additionally, it is also notable that TREK-2 is a homo*dimer*, so only one point subsitution is required to obtain a channel with only two cysteine-maleimide labelling sites. Doubly labelling the channel would enable the acquisition of vital data to correlate structural changes with its function, particu-

larly when coupled with the relatively large movements thought to occur in the lower parts of the transmembrane domains upon gating, making TREK-2 ideally suited to smFRET studies. However, TREK-2 contains a large number of endogenous cysteine residues, and it is unlikely that all of these can be removed without altering the function of the protein, so it would also be necessary to optimise a form of labelling not based on the cysteine-maleimide reaction, such as the use of non-native amino acids.

Since this thesis was initiated over three years ago, it is now commonplace to to express and purify mammalian Kir channels for biochemical assays, such as the studies of the PIP_2-induced activation of Kir2.1 and Kir2.2 by D'Avanzo *et al.* [42]. It would therefore also be desirable to exploit such advances to reconstitute eukaryotic Kir channels into nanodiscs for smFRET, an essential undertaking if a complete understanding of the inwardly rectifying potassium channels is to be obtained.

Appendix A

Appendices

A.1 KirBac1.1 amino acid sequence

The sequence is listed from the start codon to the 6-His tag at the C-terminal end. The selectivity filter sequence is highlighted in red.

MGNVD PFSPH SSDSF AQAAS PARKP PRGGR RIWSG TREVI AYGMP ASVWR DLYYW ALKVS WPVFF ASLAA LFVVN NTLFA LLYQL GDAPI ANQSP PGFVG AFFFS VETLA TVGYG DMHPQ TVYAH AIATL EIFVG MSGIA LSTGL VFARF ARPRA KIMFA RHAIV RPFNG RMTLM VRAAN ARQNV IAEAR AKMRL MRREH SSEGY SLMKI HDLKL VRNEH PIFLL GWNMM HVIDE SSPLF GETPE SLAEG RAMLL VMIEG SDETT AQVMQ ARHAW EHDDI RWHHR YVDLM SDVDG MTHID YTRFN DTEPV EPPGA APDAQ AFAAK PGEGD ARPVL VPRGS RS HHHHHH

A.2 Original *vs* codon-optimised KirBac1.1

As stated in earlier chapters, the original KirBac1.1 sequence was highly G-C rich (67.53%), so a codon-optimised version of the gene was synthesised (which has 56.42% G-C content). An alignment of the original sequence and the codon-optimised gene is presented here in Figure A.1.

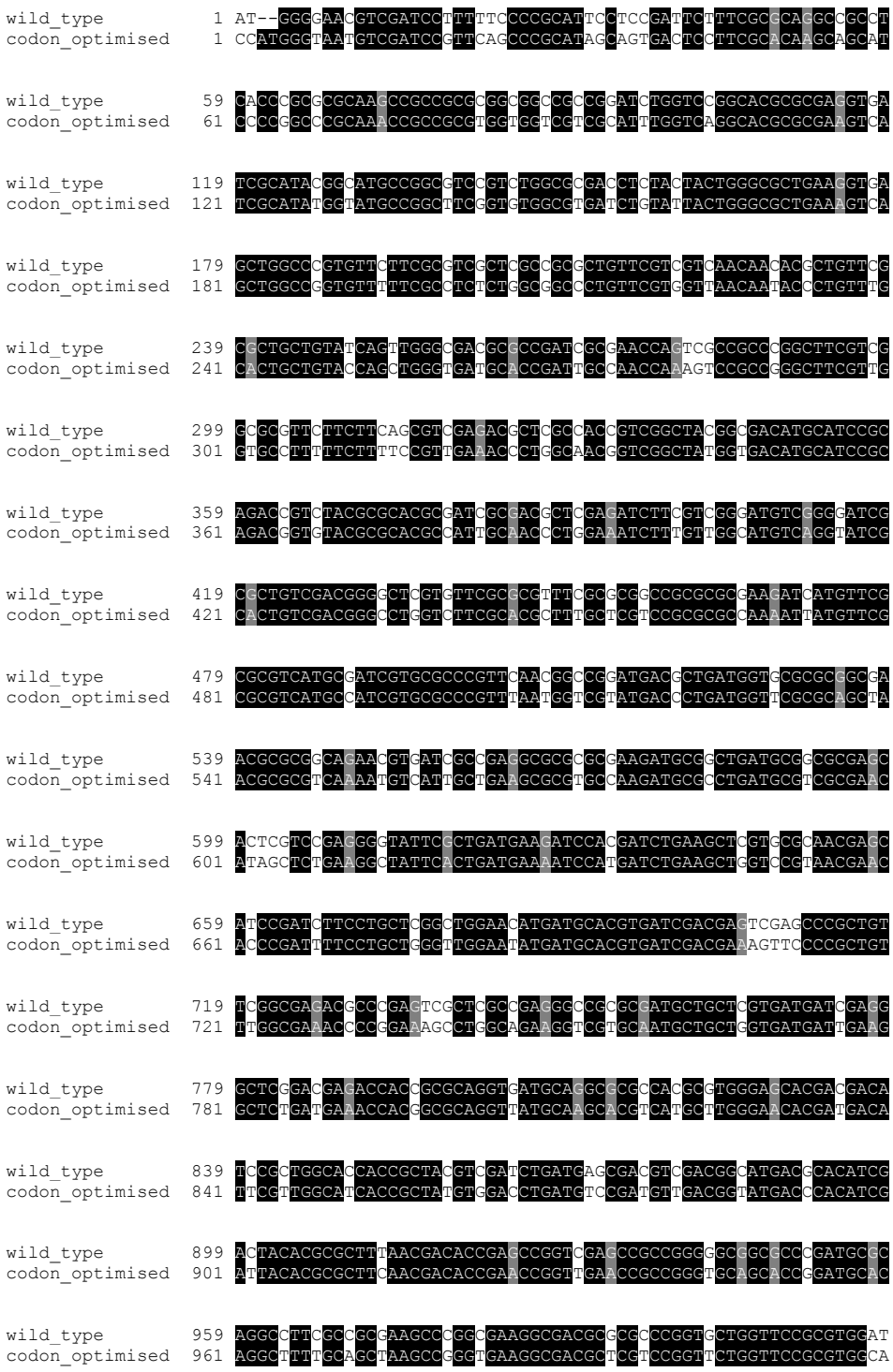


FIGURE A.1: An alignment of the original (highly G-C-rich, 67.53%) KirBac1.1 gene with the synthesised codon-optimised version (56.42% G-C).

A.3 Exemplary *E**-*S* histograms

A.3.1 Detergent-solubilised KirBac1.1

R151C reporter site

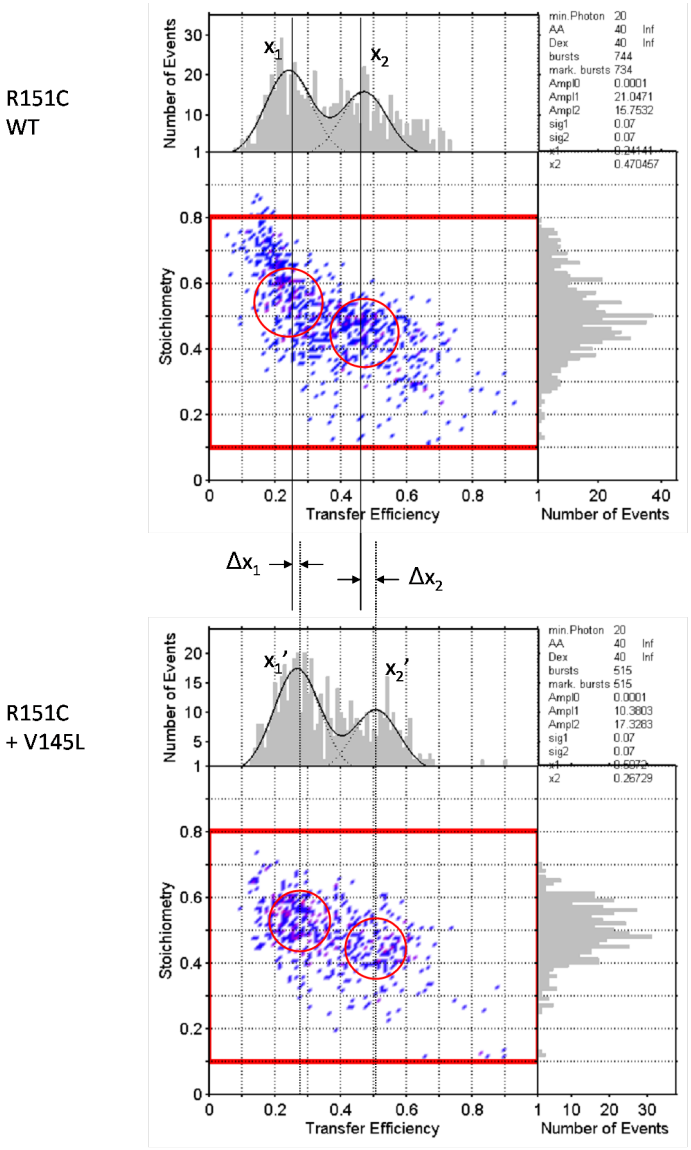


FIGURE A.2: Illustrative *E**-*S* histograms for the R151C reporter site with KirBac1.1 solubilised in detergent micelles showing the small increase in FRET efficiency upon inclusion of the activatory point mutation V145L.

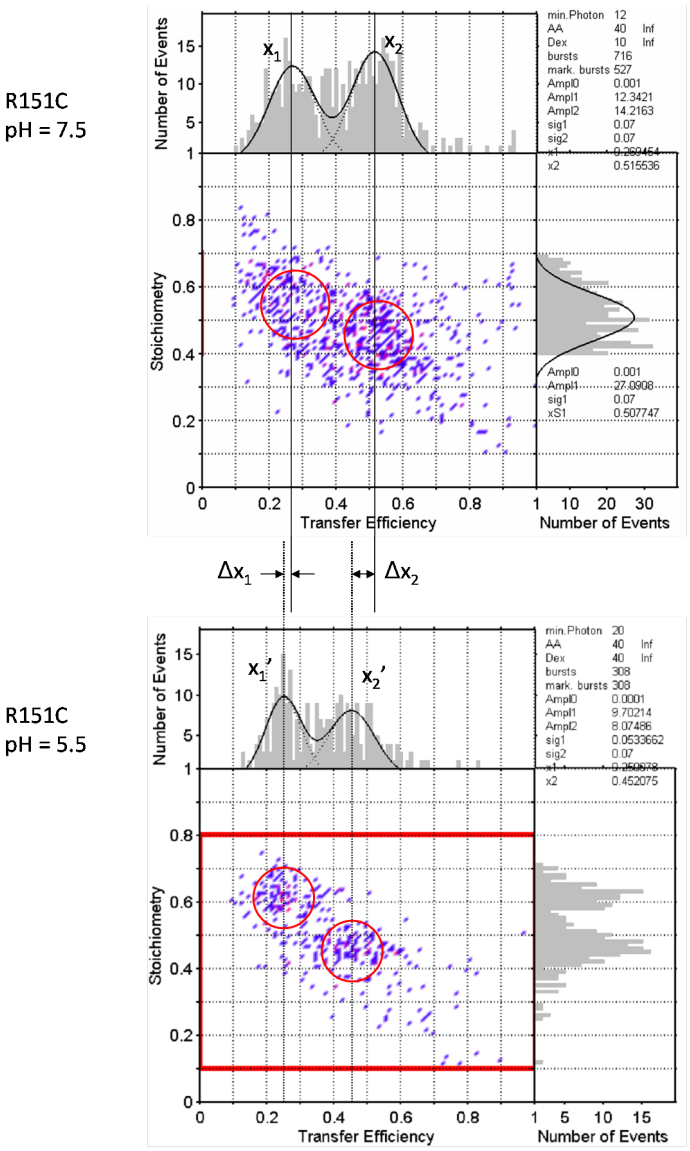


FIGURE A.3: Illustrative *E**-*S* histograms for the R151C reporter site with KirBac1.1 solubilised in detergent micelles showing the small decrease in FRET efficiency upon a change in pH.

G249C reporter site

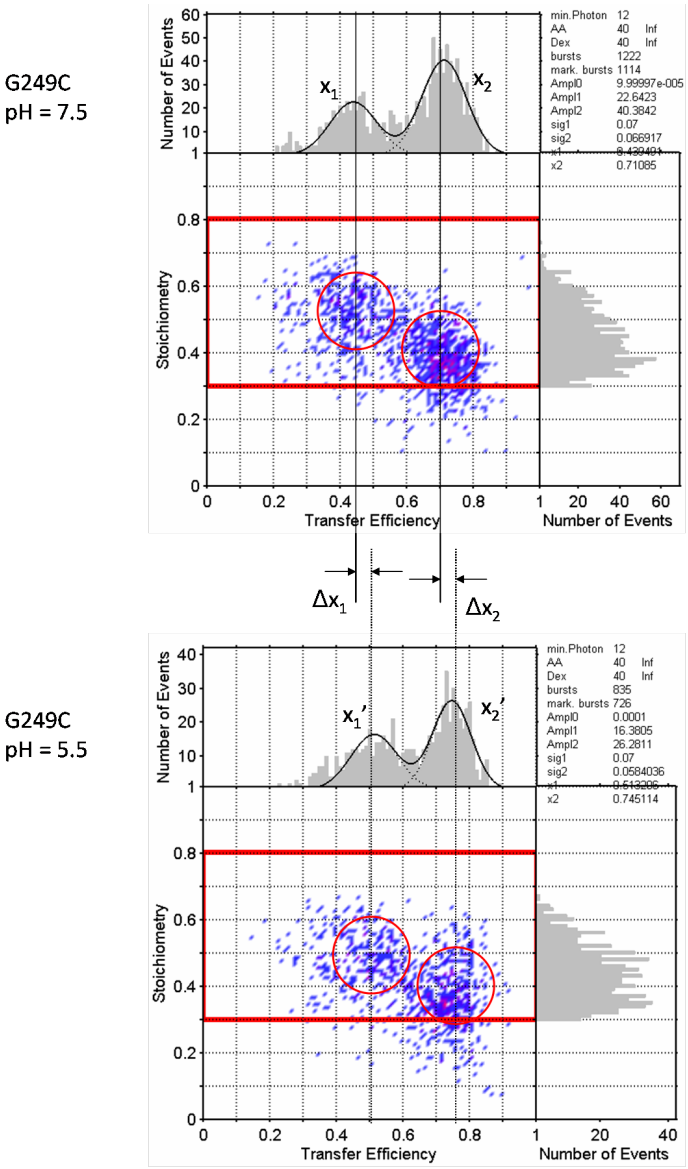


FIGURE A.4: Illustrative *E**-*S* histograms for the G249C reporter site with KirBac1.1 solubilised in detergent micelles showing the small increase in FRET efficiency upon a change in pH.

A.3.2 Nanodisc-reconstituted KirBac1.1

R151C reporter site

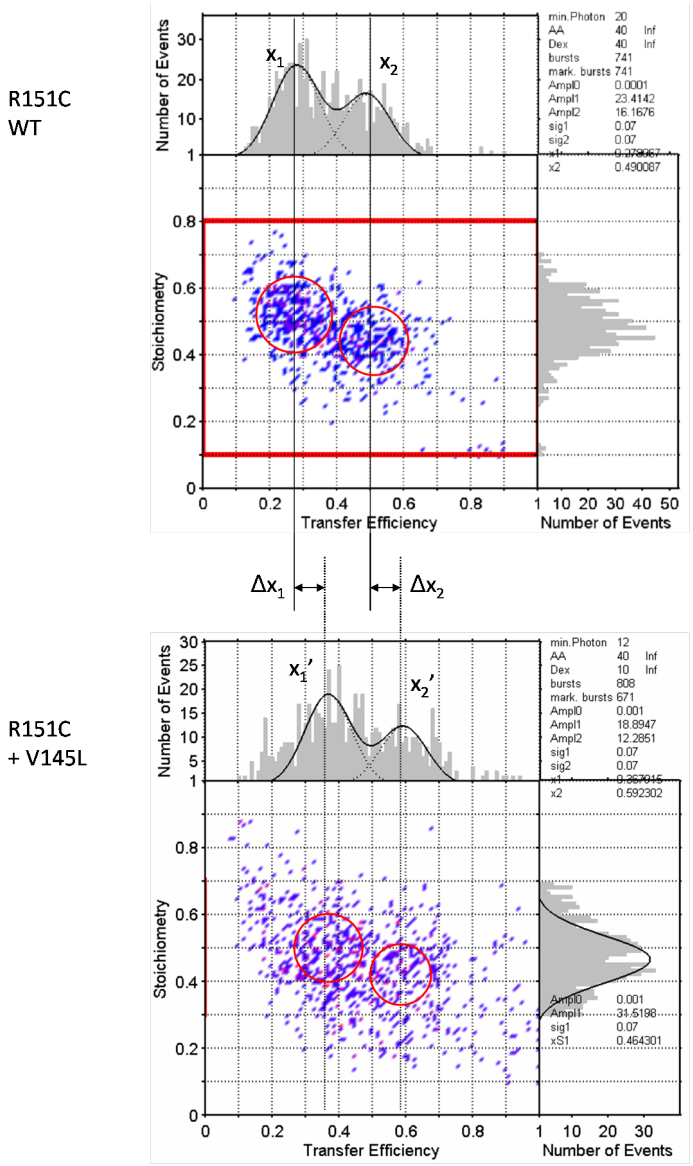


FIGURE A.5: Illustrative *E**-*S* histograms for the R151C reporter site with KirBac1.1 reconstituted into nanodiscs showing the increase in FRET efficiency upon inclusion of the activatory point mutation V145L.

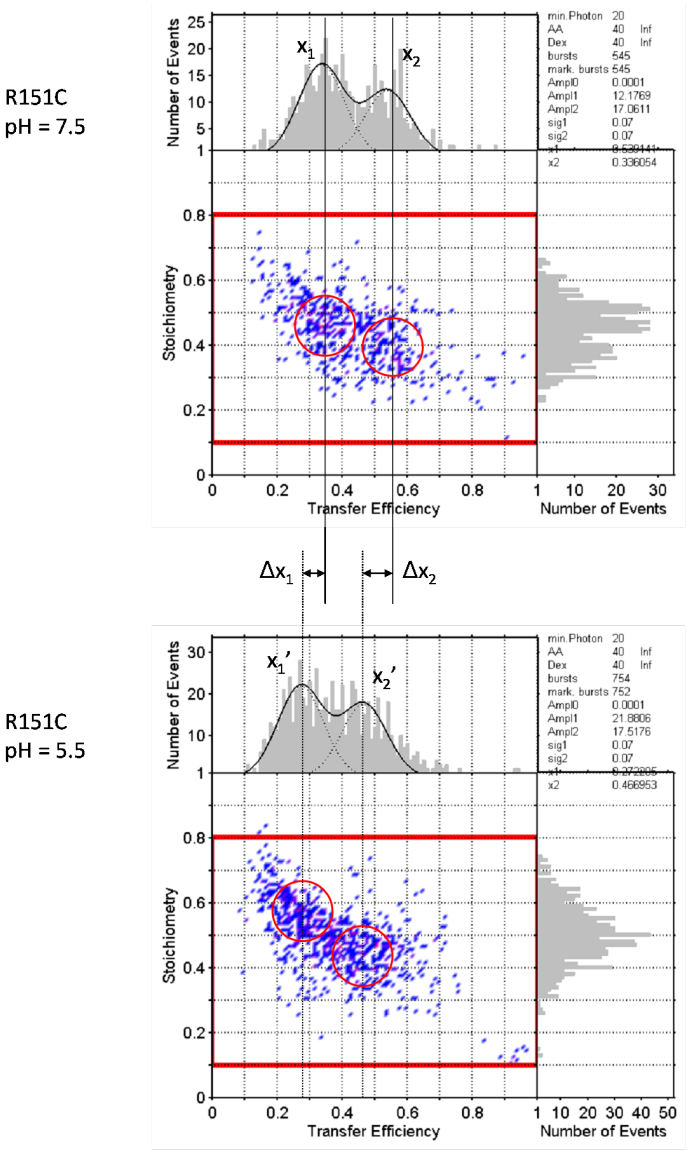


FIGURE A.6: Illustrative *E**-*S* histograms for the R151C reporter site with KirBac1.1 reconstituted into nanodiscs showing the small decrease in FRET efficiency upon a change in pH.

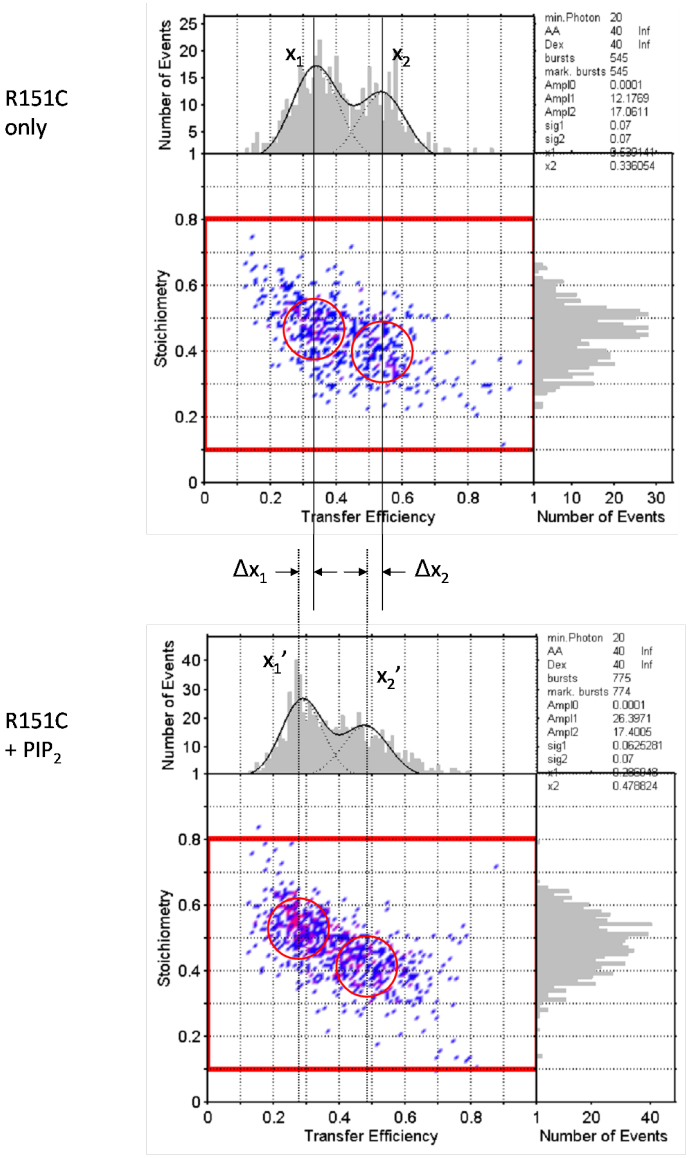


FIGURE A.7: Illustrative *E**-*S* histograms for the R151C reporter site with KirBac1.1 reconstituted into nanodiscs showing the small decrease in FRET efficiency upon addition of PIP_2.

G249C reporter site

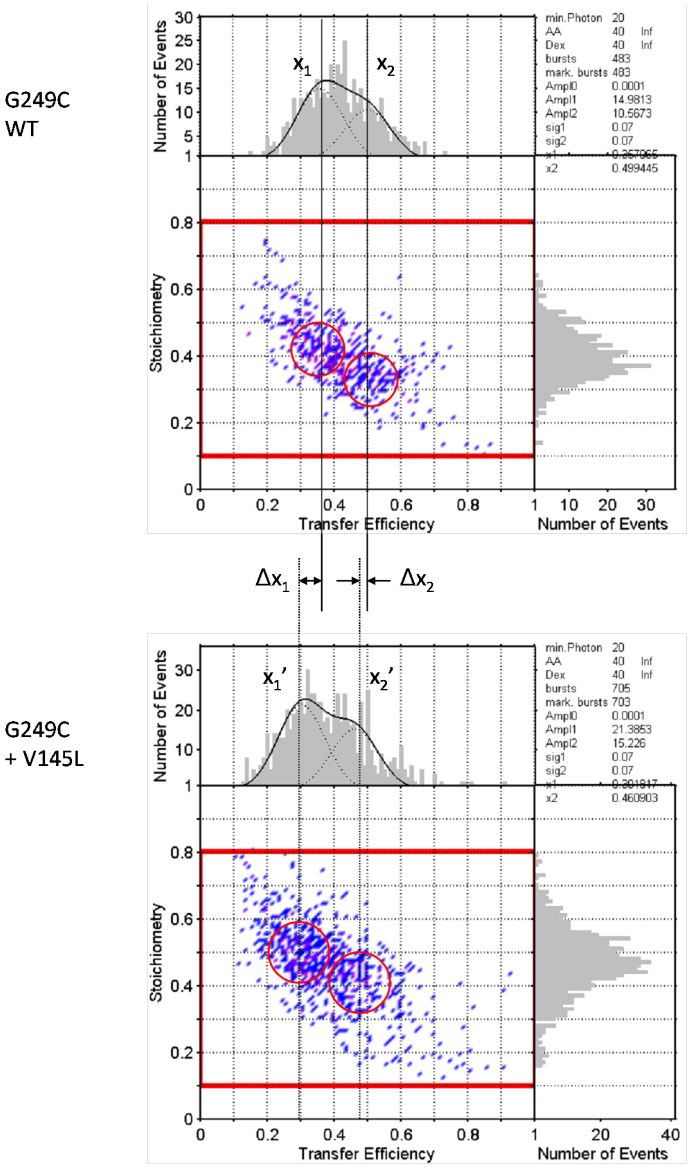


FIGURE A.8: Illustrative *E**-*S* histograms for the G249C reporter site with KirBac1.1 reconstituted into nanodiscs showing the small decrease in FRET efficiency upon inclusion of the activatory point mutation V145L.

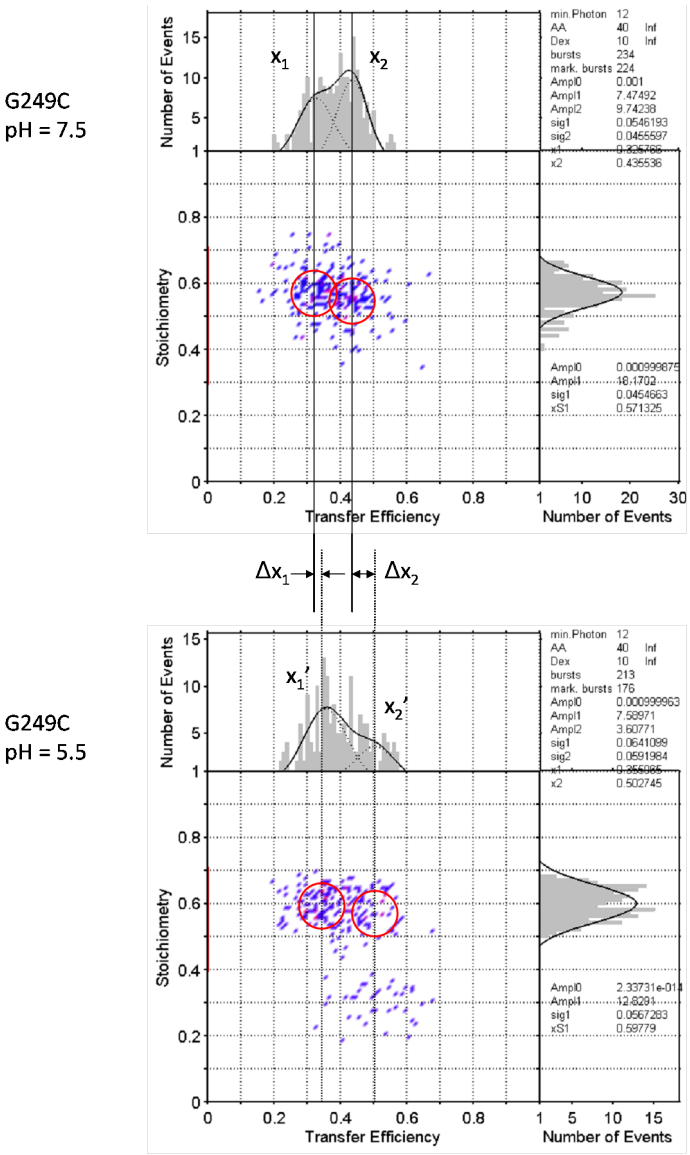


FIGURE A.9: Illustrative *E**-*S* histograms for the G249C reporter site with KirBac1.1 reconstituted into nanodiscs showing the small increase in FRET efficiency upon a change in pH.

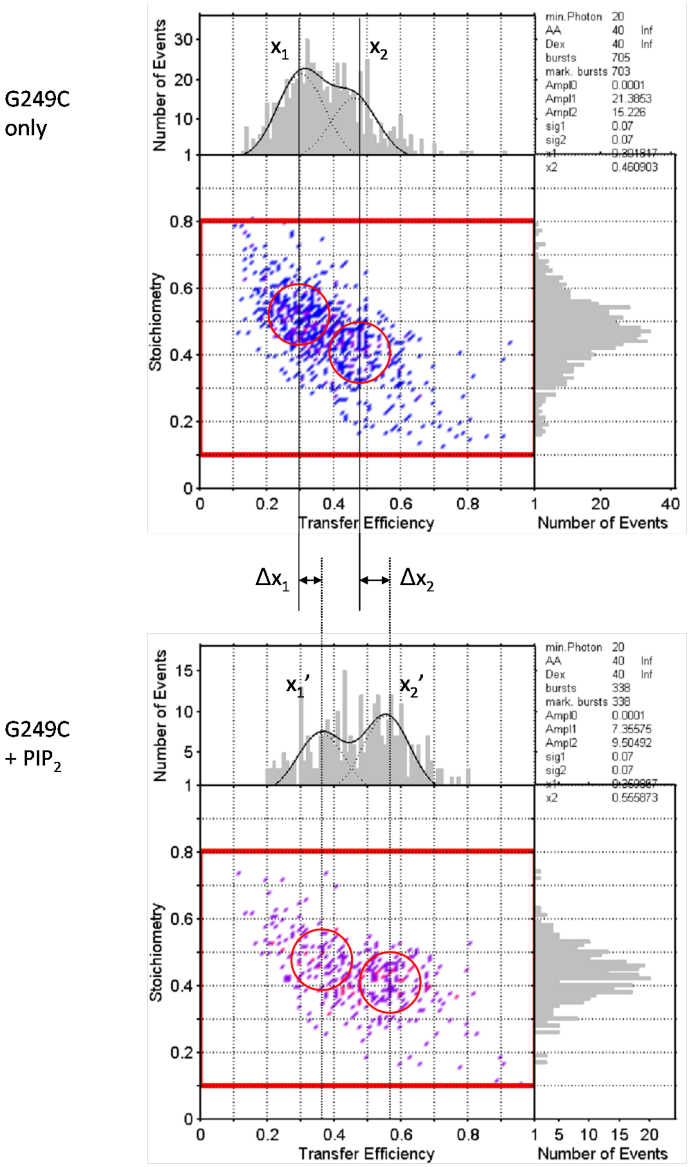


FIGURE A.10: Illustrative *E*-S* histograms for the G249C reporter site with KirBac1.1 reconstituted into nanodiscs showing the increase in FRET efficiency upon addition of PIP_2.

A.4 Corrected smFRET values

The smFRET values presented previously in this thesis are *uncorrected* values, as opposed to *corrected* absolute smFRET efficiencies. Cross-talk between the donor and acceptor channels, differences in efficiency of fluorescence transfer and collection efficiency, and differences in quantum yield between the donor and acceptor fluorophores can account for significant discrepancies in absolute values compared to 'raw' values. However, *relative* efficiencies (*i.e.* shift in E^*), the salient property for this thesis, should remain unchanged.

More accurate estimates of smFRET efficiencies can be obtained by following the approach outlined by Lee *et al.* [78]. It can be seen from the tables in Sections A.3.2 and A.3.3 that the direction of the shifts in E^* is unchanged, and the magnitude of the shifts is approximately unchanged relative to uncorrected values, meaning that the conclusions of this thesis are still valid. It should be noted that this method of correction assumes that the two smFRET species are well-separated in E^* and independent [78]: as the two D-A distances are due to the proximal and distal labelling arrangements by donor and acceptor fluorophores, and hence arise during the labelling process, this is a legitimate assumption.

A.4.1 Calculation of corrected smFRET efficiencies

In order to calculate the correction factor γ, it is necessary to visualise a sample with two smFRET populations which are resolved in E^*: serendipitously, the proximal/distal labelling schemes of doubly labelled KirBac1.1 mean that such samples are already being measured during the studies presented in this thesis. It can be seen from Figure A.11 that these populations are displaced slightly in Stoichiometry, S, and it is hence possible to construct a straight line through the centre of both populations which has the equation $S = \Sigma E + \Omega$, where Σ is the gradient and Ω the intercept.

Following Lee *et al.* [78], the equation of this line and the correction factors are related through the following:

$$\Omega = 1 + \beta\gamma \tag{A.1}$$

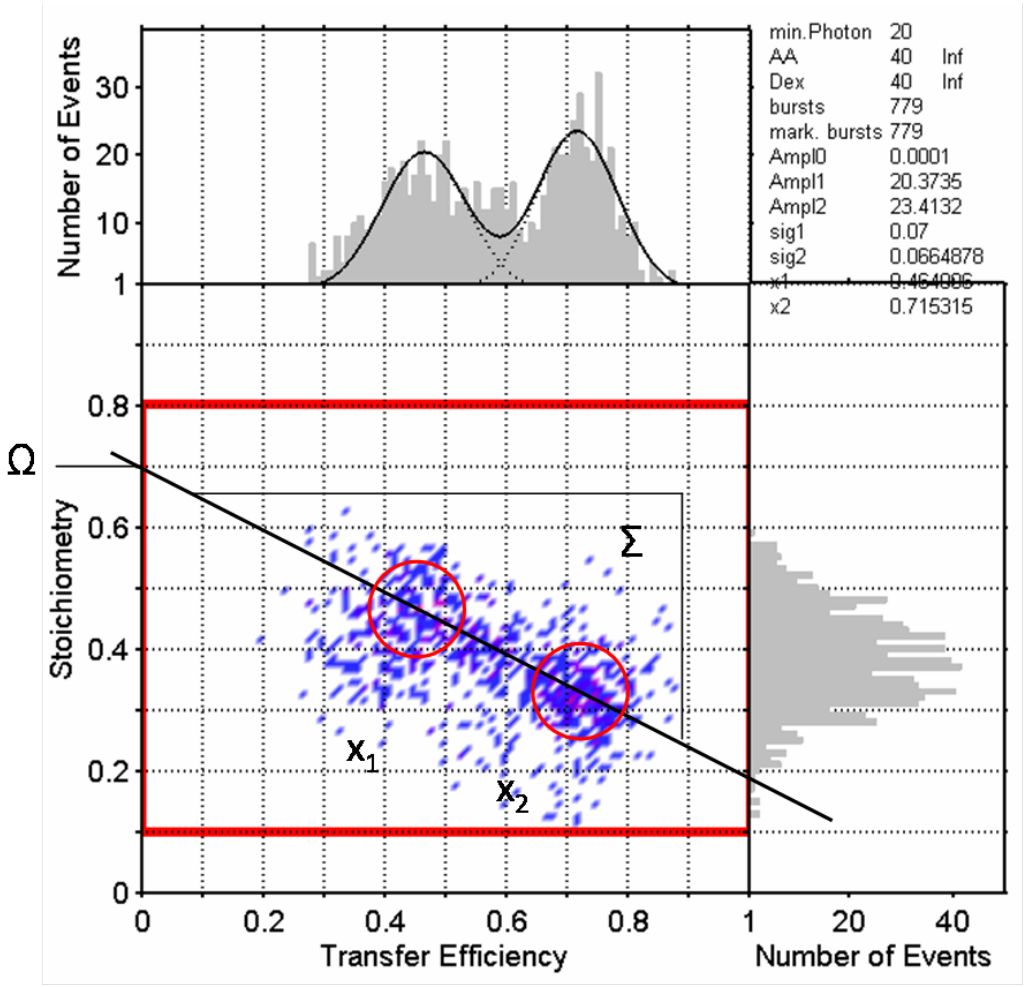


FIGURE A.11: Due to differences in the physical properties of the fluorphores, two populations which differ in E^* may also be separated in S. A straight line can be constructed through the centre of the populations with equation $S = \Sigma E + \Omega$, and Σ and Ω used to calculate the correction factors β and γ.

$$\Sigma = \beta(1 - \gamma) \tag{A.2}$$

Where the excitation correction factor $\beta = \frac{I_{Aex}\sigma^A_{Aex}}{I_{Dex}\sigma^D_{Dex}}$, and the detection correction factor $\gamma = \frac{\phi_A \eta^A_{Aem}}{\phi_D \eta^D_{Dem}}$. I_{Xex} is the laser intensity for the donor/acceptor excitation wavelength, σ^X_{Xex} is the absorption cross section of the fluorophore at the donor/acceptor excitation wavelength, ϕ_X is the quantum yield of the donor/acceptor, and η^X_{Xem} is the detection efficiency of the APDs at the donor/acceptor emission wavelength.

With some rearrangement:

$$\beta = \Omega + \Sigma - 1 \tag{A.3}$$

$$\gamma = \frac{\Omega - 1}{\Omega + \Sigma - 1} \tag{A.4}$$

It is hence possible to calculate absolute 'accurate' smFRET efficiency:

$$E = \frac{E_r}{\gamma - (\gamma - 1)E_r} \tag{A.5}$$

where E_r is the 'raw' efficiency taken from experiment.

The subsections below give the resulting corrected smFRET efficiencies calculated from the data presented in this thesis.

A.4.2 Detergent-solubilised KirBac1.1: corrected values

R151C reporter site

R151C	(detergent)
Σ	-0.43
Ω	0.66
γ	0.44

Table A.1: Correction factors: detergent-solubilised R151C

		R151C only	R151C + V145L	Shift
R151C	x_1	0.4289 ± 0.050	0.444 ± 0.052	0.016 ± 0.015
± V145L	x_2	0.629 ± 0.027	0.706 ± 0.022	0.027 ± 0.033

Table A.2: Corrected smFRET values: detergent-solubilised R151C ± V145L

		pH = 7.5	pH = 5.5	Shift
R151C	x_1	0.469 ± 0.047	0.426 ± 0.011	-0.043 ± 0.056
pH 7.5 → 5.5	x_2	0.714 ± 0.028	0.658 ± 0.016	-0.056 ± 0.042

Table A.3: Corrected smFRET values: detergent-solubilised R151C at pH = 7.5 and pH = 5.5

G249C reporter site

G249C	(detergent)
Σ	-0.42
Ω	0.63
γ	0.47

TABLE A.4: Correction factors: detergent-solubilised G249C

		pH = 7.5	pH = 5.5	Shift
G249C	x_1	0.646 ± 0.047	0.696 ± 0.042	0.051 ± 0.029
pH 7.5 → 5.5	x_2	0.844 ± 0.011	0.863 ± 0.010	0.019 ± 0.009

TABLE A.5: Corrected smFRET values: detergent-solubilised G249C at pH = 7.5 and pH = 5.5

A.4.3 Nanodisc-reconstituted KirBac1.1: corrected values

R151C reporter site

R151C	(nanodiscs)
Σ	-0.64
Ω	0.77
γ	0.26

TABLE A.6: Correction factors: nanodisc-reconstituted R151C

		R151C only	R151C + V145L	Shift
R151C	x_1	0.606 ± 0.015	0.690 ± 0.012	0.084 ± 0.012
± V145L	x_2	0.793 ± 0.008	0.848 ± 0.012	0.055 ± 0.014

TABLE A.7: Corrected smFRET values: nanodisc-reconstituted R151C ± V145L

		pH = 7.5	pH = 5.5	Shift
R151C	x_1	0.652 ± 0.038	0.582 ± 0.015	-0.070 ±0.027
pH 7.5 → 5.5	x_2	0.826 ± 0.012	0.773 ± 0.011	-0.053 ± 0.008

TABLE A.8: Corrected smFRET values: nanodisc-reconstituted R151C at pH = 7.5 and pH = 5.5

		MSP buffer	+ 20 μM PIP_2	Shift
R151C	x_1	0.666 ± 0.012	0.622 ± 0.009	-0.044 ± 0.009
± PIP_2	x_2	0.815 ± 0.007	0.787 ± 0.002	-0.029 ± 0.007

TABLE A.9: Corrected smFRET values: nanodisc-reconstituted R151C ± PIP_2

G249C reporter site

G249C	(nanodiscs)
Σ	-0.52
Ω	0.81
γ	0.27

TABLE A.10: Correction factors: nanodisc-reconstituted G249C

		G249C only	G249C + V145L	Shift
G249C	x_1	0.673 ± 0.013	0.607 ± 0.022	-0.067 ± 0.023
± V145L	x_2	0.780 ± 0.013	0.751 ± 0.019	-0.029 ± 0.024

TABLE A.11: Corrected smFRET values: nanodisc-reconstituted G249C ± V145L

		pH = 7.5	pH = 5.5	Shift
G249C	x_1	0.623 ± 0.023	0.678 ± 0.012	0.055 ± 0.023
pH 7.5 → 5.5	x_2	0.731 ± 0.024	0.788 ± 0.011	0.058 ± 0.019

TABLE A.12: Corrected smFRET values: nanodisc-reconstituted G249C at pH = 7.5 and pH = 5.5

		MSP buffer	+ 20 μM PIP_2	Shift
G249C	x_1	0.615 ± 0.017	0.673 ± 0.012	0.058 ± 0.009
± PIP_2	x_2	0.769 ± 0.003	0.814 ± 0.004	0.045 ± 0.005

TABLE A.13: Corrected smFRET values: nanodisc-reconstituted G249C ± PIP_2

Bibliography

[1] Life Technologies *Molecular Probes: The Handbook*. http://www.lifetecnhnologies.com/uk/en/home/references/molecular-probes-the-handbook/technical-notes-and-product-highlights/fluorescence-resonance-energy-transfer-fret.html, Accessed: 2014-08-10.

[2] Life Technologies *Molecular Probes: The Handbook*. http://www.lifetechnologies.com/uk/en/home/references/molecular-probes-the-handbook/fluorophores-and-their-amine-reactive-derivatives/alexa-fluor-dyes-spanning-the-visible-and-infrared-spectrum.html, Accessed: 2014-08-10.

[3] Nurunisa Akyuz, Roger B Altman, Scott C Blanchard, and Olga Boudker. Transport dynamics in a glutamate transporter homologue. *Nature*, 2013.

[4] EJ Ambrose. A surface contact microscope for the study of cell movements. *Nature*, 178:1194, 1956.

[5] David L Andrews. A unified theory of radiative and radiationless molecular energy transfer. *Chemical physics*, 135(2):195–201, 1989.

[6] David L Andrews and David S Bradshaw. The role of virtual photons in nanoscale photonics. *Annalen der Physik*, 526(3-4):173–186, 2014.

[7] Frances M Ashcroft. *Ion channels and disease*. Academic Press, 1999.

[8] David Atkinson and Donald M Small. Recombinant lipoproteins: implications for structure and assembly of native lipoproteins. *Annual review of biophysics and biophysical chemistry*, 15(1):403–456, 1986.

[9] Daniel Axelrod. Cell-substrate contacts illuminated by total internal reflection fluorescence. *The Journal of cell biology*, 89(1):141–145, 1981.

[10] Bradley J Baas, Ilia G Denisov, and Stephen G Sligar. Homotropic cooperativity of monomeric cytochrome P450 3A4 in a nanoscale native bilayer environment. *Archives of biochemistry and biophysics*, 430(2):218–228, 2004.

[11] Sourabh Banerjee and Crina M Nimigean. Non-vesicular transfer of membrane proteins from nanoparticles to lipid bilayers. *The Journal of general physiology*, 137(2):217–223, 2011.

[12] Hyoweon Bang, Yangmi Kim, and Donghee Kim. TREK-2, a new member of the mechanosensitive tandem-pore K^+ channel family. *Journal of Biological Chemistry*, 275(23):17412–17419, 2000.

[13] Vassiliy N Bavro, Rita De Zorzi, Matthias R Schmidt, João RC Muniz, Lejla Zubcevic, Mark SP Sansom, Catherine Vénien-Bryan, and Stephen J Tucker. Structure of a KirBac potassium channel with an open bundle crossing indicates a mechanism of channel gating. *Nature structural & molecular biology*, 19(2):158–163, 2012.

[14] Timothy H Bayburt, Yelena V Grinkova, and Stephen G Sligar. Self-assembly of discoidal phospholipid bilayer nanoparticles with membrane scaffold proteins. *Nano Letters*, 2(8):853–856, 2002.

[15] Timothy H Bayburt, Yelena V Grinkova, and Stephen G Sligar. Assembly of single bacteriorhodopsin trimers in bilayer nanodiscs. *Archives of biochemistry and biophysics*, 450(2):215–222, 2006.

[16] Timothy H Bayburt, Andrew J Leitz, Guifu Xie, Daniel D Oprian, and Stephen G Sligar. Transducin activation by nanoscale lipid bilayers containing one and two rhodopsins. *Journal of biological chemistry*, 282(20):14875–14881, 2007.

[17] Timothy H Bayburt and Stephen G Sligar. Self-assembly of single integral membrane proteins into soluble nanoscale phospholipid bilayers. *Protein science*, 12(11):2476–2481, 2003.

[18] Timothy H Bayburt and Stephen G Sligar. Membrane protein assembly into nanodiscs. *FEBS letters*, 584(9):1721–1727, 2010.

[19] Hagan Bayley, Brid Cronin, Andrew Heron, Matthew A Holden, William L Hwang, Ruhma Syeda, James Thompson, and Mark Wallace. Droplet interface bilayers. *Molecular BioSystems*, 4(12):1191–1208, 2008.

[20] Howard C Berg. *Random walks in biology*. Princeton University Press, 1993.

[21] Simon Bernèche and Benoît Roux. A gate in the selectivity filter of potassium channels. *Structure*, 13(4):591–600, 2005.

[22] Catherine Berrier, Alexandre Pozza, Agnes de Lacroix de Lavalette, Solenne Chardonnet, Agnes Mesneau, Christine Jaxel, Marc le Maire, and Alexandre Ghazi. The purified mechanosensitive channel TREK-1 is directly sensitive to membrane tension. *Journal of Biological Chemistry*, 288(38):27307–27314, 2013.

[23] Georgi Beschiaschvili and Joachim Seelig. Peptide binding to lipid bilayers: binding isotherms and zeta-potential of a cyclic somatostatin analog. *Biochemistry*, 29(49):10995–11000, 1990.

[24] Delphine Bichet, Friederike A Haass, and Lily Yeh Jan. Merging functional studies with structures of inward-rectifier K^+ channels. *Nature Reviews Neuroscience*, 4(12):957–967, 2003.

[25] Rikard Blunck, Julio F Cordero-Morales, Luis G Cuello, Eduardo Perozo, and Francisco Bezanilla. Detection of the opening of the bundle crossing in KcsA with fluorescence lifetime spectroscopy reveals the existence of two gates for ion conduction. *The Journal of general physiology*, 128(5):569–581, 2006.

[26] Rikard Blunck, Hugo McGuire, H Clark Hyde, and Francisco Bezanilla. Fluorescence detection of the movement of single KcsA subunits reveals cooperativity. *Proceedings of the National Academy of Sciences*, 105(51):20263–20268, 2008.

[27] Thomas Boldog, Stephen Grimme, Mingshan Li, Stephen G Sligar, and Gerald L Hazelbauer. Nanodiscs separate chemoreceptor oligomeric states and reveal their signaling properties. *Proceedings of the National Academy of Sciences*, 103(31):11509–11514, 2006.

[28] Murali K Bollepalli, Philip W Fowler, Markus Rapedius, Lijun Shang, Mark SP Sansom, Stephen J Tucker, and Thomas Baukrowitz. State-dependent network connectivity determines gating in a K^+ channel. *Structure*, 22(7):1037–1046, 2014.

[29] V Borisenko, T Lougheed, J Hesse, E Füreder-Kitzmüller, N Fertig, JC Behrends, GA Woolley, and GJ Schütz. Simultaneous optical and electrical recording of single gramicidin channels. *Biophysical journal*, 84(1):612–622, 2003.

[30] Stephen G Brohawn, Josefina del Mármol, and Roderick MacKinnon. Crystal structure of the human K2P TRAAK, a lipid-and mechano-sensitive K^+ ion channel. *Science*, 335(6067):436–441, 2012.

[31] Stephen G Brohawn, Zhenwei Su, and Roderick MacKinnon. Mechanosensitivity is mediated directly by the lipid membrane in TRAAK and TREK-1 K^+ channels. *Proceedings of the National Academy of Sciences*, 111(9):3614–3619, 2014.

[32] Oliver K Castell, James Berridge, and Mark I Wallace. Quantification of membrane protein inhibition by optical ion flux in a droplet interface bilayer array. *Angewandte Chemie International Edition*, 51(13):3134–3138, 2012.

[33] Albert Cha, Gregory E Snyder, Paul R Selvin, and Francisco Bezanilla. Atomic scale movement of the voltage-sensing region in a potassium channel measured *via* spectroscopy. *Nature*, 402(6763):809–813, 1999.

[34] Wayland WL Cheng, Decha Enkvetchakul, and Colin G Nichols. KirBac1.1:

it's an inward rectifying potassium channel. *The Journal of general physiology*, 133(3):295–305, 2009.

[35] Wei Cheng, Fan Yang, Christina L Takanishi, and Jie Zheng. Thermosensitive TRPV channel subunits coassemble into heteromeric channels with intermediate conductance and gating properties. *The Journal of general physiology*, 129(3):191–207, 2007.

[36] Senyon Choe, Susan Cushman, Kent A Baker, and Paul Pfaffinger. Excitability is mediated by the T1 domain of the voltage-gated potassium channel. In *Ion Channels: From Atomic Resolution Physiology to Functional Genomics: Novartis Foundation Symposium 245*, pages 169–177. Wiley Online Library, 2002.

[37] Oliver B Clarke, Alessandro T Caputo, Adam P Hill, Jamie I Vandenberg, Brian J Smith, and Jacqueline M Gulbis. Domain reorientation and rotation of an intracellular assembly regulate conduction in Kir potassium channels. *Cell*, 141(6):1018–1029, 2010.

[38] Ben Corry, Annette C Hurst, Prithwish Pal, Takeshi Nomura, Paul Rigby, and Boris Martinac. An improved open-channel structure of MscL determined from FRET confocal microscopy and simulation. *The Journal of general physiology*, 136(4):483–494, 2010.

[39] Ben Corry, Dylan Jayatilaka, and Paul Rigby. A flexible approach to the calculation of resonance energy transfer efficiency between multiple donors and acceptors in complex geometries. *Biophysical journal*, 89(6):3822–3836, 2005.

[40] Ben Corry, Paul Rigby, Zhen-Wei Liu, and Boris Martinac. Conformational changes involved in MscL channel gating measured using FRET spectroscopy. *Biophysical journal*, 89(6):L49–L51, 2005.

[41] Jian Dai and Huan-Xiang Zhou. General rules for the arrangements and gating motions of pore-lining helices in homomeric ion channels. *Nature communications*, 5, 2014.

[42] Nazzareno D'Avanzo, Wayland WL Cheng, Declan A Doyle, and Colin G Nichols. Direct and specific activation of human inward rectifier K^+ channels by membrane phosphatidylinositol 4, 5-bisphosphate. *Journal of biological chemistry*, 285(48):37129–37132, 2010.

[43] Dmitri R Davydov, Harshica Fernando, Bradley J Baas, Stephen G Sligar, and James R Halpert. Kinetics of dithionite-dependent reduction of cytochrome P450 3A4: heterogeneity of the enzyme caused by its oligomerization. *Biochemistry*, 44(42):13902–13913, 2005.

[44] IG Denisov, YV Grinkova, AA Lazarides, and SG Sligar. Directed self-assembly of monodisperse phospholipid bilayer nanodiscs with controlled size. *Journal of the American Chemical Society*, 126(11):3477–3487, 2004.

[45] Ilia G Denisov, Yelena V Grinkova, Bradley J Baas, and Stephen G Sligar. The ferrous-dioxygen intermediate in human cytochrome P450 3A4 substrate dependence of formation and decay kinetics. *Journal of biological chemistry*, 281(33):23313–23318, 2006.

[46] Alexander D Dergunov, Josee Taveirne, Berlinda Vanloo, Hans Caster, and Maryvonne Rosseneu. Structural organization of lipid phase and protein-lipid interface in apolipoprotein-phospholipidrecombinants: influence of cholesterol. *Biochimica et Biophysica Acta (BBA)-Lipids and Lipid Metabolism*, 1346(2):131–146, 1997.

[47] Declan A Doyle, João Morais Cabral, Richard A Pfuetzner, Anling Kuo, Jacqueline M Gulbis, Steven L Cohen, Brian T Chait, and Roderick MacKinnon. The structure of the potassium channel: molecular basis of K^+ conduction and selectivity. *science*, 280(5360):69–77, 1998.

[48] Jürgen Drews. Drug discovery: a historical perspective. *Science*, 287(5460):1960–1964, 2000.

[49] Hui Duan, Natanya R Civjan, Stephen G Sligar, and Mary A Schuler. Co-incorporation of heterologously expressed *Arabidopsis* cytochrome P450 and P450

reductase into soluble nanoscale lipid bilayers. *Archives of biochemistry and biophysics*, 424(2):141–153, 2004.

[50] Decha Enkvetchakul, Jaya Bhattacharyya, Iana Jeliazkova, Darcy K Groesbeck, Catherine A Cukras, and Colin G Nichols. Functional characterization of a prokaryotic Kir channel. *Journal of Biological Chemistry*, 279(45):47076–47080, 2004.

[51] Decha Enkvetchakul, Iana Jeliazkova, Jaya Bhattacharyya, and Colin G Nichols. Control of inward rectifier K^+ channel activity by lipid tethering of cytoplasmic domains. *The Journal of general physiology*, 130(3):329–334, 2007.

[52] Decha Enkvetchakul, Iana Jeliazkova, and Colin G Nichols. Direct modulation of Kir channel gating by membrane phosphatidylinositol 4, 5-bisphosphate. *Journal of Biological Chemistry*, 280(43):35785–35788, 2005.

[53] Guus B Erkens, Inga Hänelt, Joris MH Goudsmits, Dirk Jan Slotboom, and Antoine M van Oijen. Unsynchronised subunit motion in single trimeric sodium-coupled aspartate transporters. *Nature*, 502(7469):119–123, 2013.

[54] John BC Findlay and Michael A Harrison. A protein chemical approach to channel structure and function: The proton channel of the vacuolar H^+-ATPase. In *Ion Channels: From Atomic Resolution Physiology to Functional Genomics: Novartis Foundation Symposium 245*, pages 207–222. Wiley Online Library, 2002.

[55] Ulrik Gether, Sansan Lin, Pejman Ghanouni, Juan A Ballesteros, Harel Weinstein, and Brian K Kobilka. Agonists induce conformational changes in transmembrane domains III and VI of the β2 adrenoceptor. *The EMBO Journal*, 16(22):6737–6747, 1997.

[56] Pejman Ghanouni, Zygmunt Gryczynski, Jacqueline J Steenhuis, Tae Weon Lee, David L Farrens, Joseph R Lakowicz, and Brian K Kobilka. Functionally different agonists induce distinct conformations in the G protein coupling domain of the β2 adrenergic receptor. *Journal of Biological Chemistry*, 276(27):24433–24436, 2001.

[57] Kathi S Glauner, Lydia M Mannuzzu, Chris S Gandhi, and Ehud Y Isacoff. Spectroscopic mapping of voltage sensor movement in the *Shaker* potassium channel. *Nature*, 402(6763):813–817, 1999.

[58] Wenli Gu, Günter Schlichthörl, Jochen R Hirsch, Hartmut Engels, Christine Karschin, Andreas Karschin, Christian Derst, Ortrud K Steinlein, and Jürgen Daut. Expression pattern and functional characteristics of two novel splice variants of the two-pore-domain potassium channel TREK-2. *The Journal of physiology*, 539(3):657–668, 2002.

[59] Sayan Gupta, Vassiliy N Bavro, Rhijuta D'Mello, Stephen J Tucker, Catherine Vénien-Bryan, and Mark R Chance. Conformational changes during the gating of a potassium channel revealed by structural mass spectrometry. *Structure*, 18(7):839–846, 2010.

[60] George A Gutman, K George Chandy, Stephan Grissmer, Michel Lazdunski, David Mckinnon, Luis A Pardo, Gail A Robertson, Bernardo Rudy, Michael C Sanguinetti, Walter Stühmer, et al. International union of pharmacology. LIII: Nomenclature and molecular relationships of voltage-gated potassium channels. *Pharmacological reviews*, 57(4):473–508, 2005.

[61] Liora Guy-David and Eitan Reuveny. PIP_2 - the master key. *Neuron*, 55(4):537–538, 2007.

[62] Scott B Hansen, Xiao Tao, and Roderick MacKinnon. Structural basis of PIP_2 activation of the classical inward rectifier K^+ channel Kir2.2. *Nature*, 477(7365):495–498, 2011.

[63] Lydia M Harriss, Bríd Cronin, James R Thompson, and Mark I Wallace. Imaging multiple conductance states in an alamethicin pore. *Journal of the American Chemical Society*, 133(37):14507–14509, 2011.

[64] Minna Hassinen, Jaakko Haverinen, and Matti Vornanen. Electrophysiological properties and expression of the delayed rectifier potassium (ERG) channels in the heart

of thermally acclimated rainbow trout. *American Journal of Physiology-Regulatory, Integrative and Comparative Physiology*, 295(1):R297–R308, 2008.

[65] Andrew T Hattersley and Frances M Ashcroft. Activating mutations in Kir6.2 and neonatal diabetes new clinical syndromes, new scientific insights, and new therapy. *Diabetes*, 54(9):2503–2513, 2005.

[66] Andrew J Heron, James R Thompson, Brid Cronin, Hagan Bayley, and Mark I Wallace. Simultaneous measurement of ionic current and fluorescence from single protein pores. *Journal of the American Chemical Society*, 131(5):1652–1653, 2009.

[67] Hiroshi Hibino, Atsushi Inanobe, Kazuharu Furutani, Shingo Murakami, Ian Findlay, and Yoshihisa Kurachi. Inwardly rectifying potassium channels: their structure, function, and physiological roles. *Physiological reviews*, 90(1):291–366, 2010.

[68] Bertil Hille. *Ion channels of excitable membranes*, volume 507. Sinauer Sunderland, MA, 2001.

[69] Kevin Ho, Colin G Nichols, W Jonathan Lederer, Jonathan Lytton, Peter M Vassilev, Marie V Kanazirska, and Steven C Hebert. Cloning and expression of an inwardly rectifying ATP-regulated potassium channel. 1993.

[70] Alan L Hodgkin and Andrew F Huxley. A quantitative description of membrane current and its application to conduction and excitation in nerve. *The Journal of physiology*, 117(4):500, 1952.

[71] Akihiko Ishijima and Toshio Yanagida. Single molecule nanobioscience. *Trends in biochemical sciences*, 26(7):438–444, 2001.

[72] Achillefs N Kapanidis, Nam Ki Lee, Ted A Laurence, Sören Doose, Emmanuel Margeat, and Shimon Weiss. Fluorescence-aided molecule sorting: analysis of structure and interactions by alternating-laser excitation of single molecules. *Proceedings of the National Academy of Sciences of the United States of America*, 101(24):8936–8941, 2004.

[73] Anling Kuo, Carmen Domene, Louise N Johnson, Declan A Doyle, and Catherine Vénien-Bryan. Two different conformational states of the KirBac3.1 potassium channel revealed by electron crystallography. *Structure*, 13(10):1463–1472, 2005.

[74] Anling Kuo, Jacqueline M Gulbis, Jennifer F Antcliff, Tahmina Rahman, Edward D Lowe, Jochen Zimmer, Jonathan Cuthbertson, Frances M Ashcroft, Takayuki Ezaki, and Declan A Doyle. Crystal structure of the potassium channel KirBac1.1 in the closed state. *Science*, 300(5627):1922–1926, 2003.

[75] Harley T Kurata, L Revell Phillips, Thierry Rose, Gildas Loussouarn, Stefan Herlitze, Hariolf Fritzenschaft, Decha Enkvetchakul, Colin G Nichols, and Thomas Baukrowitz. Molecular basis of inward rectification polyamine interaction sites located by combined channel and ligand mutagenesis. *The Journal of general physiology*, 124(5):541–554, 2004.

[76] JR Lakowicz. Principles of fluorescence spectroscopy, 2nd edit., 1999.

[77] Mark C Leake. *Single-Molecule Cellular Biophysics*. Cambridge University Press, 2013.

[78] Nam Ki Lee, Achillefs N Kapanidis, You Wang, Xavier Michalet, Jayanta Mukhopadhyay, Richard H Ebright, and Shimon Weiss. Accurate FRET measurements within single diffusing biomolecules using alternating-laser excitation. *Biophysical Journal*, 88(4):2939–2953, 2005.

[79] Andrew J Leitz, Timothy H Bayburt, Alexander N Barnakov, Barry A Springer, and Stephen G Sligar. Functional reconstitution of β2 adrenergic receptors utilizing self-assembling nanodisc technology. *Biotechniques*, 40(5):601, 2006.

[80] Florian Lesage, Cécile Terrenoire, Georges Romey, and Michel Lazdunski. Human TREK2, a 2P domain mechano-sensitive K^+ channel with multiple regulations by polyunsaturated fatty acids, lysophospholipids, and G_s, G_i, and G_q protein-coupled receptors. *Journal of Biological Chemistry*, 275(37):28398–28405, 2000.

[81] Hui-hua Li, Douglas S Lyles, Michael J Thomas, Wei Pan, and Mary G Sorci-Thomas. Structural determination of lipid-bound ApoA-I using fluorescence resonance energy transfer. *Journal of Biological Chemistry*, 275(47):37048–37054, 2000.

[82] Xiao-Dan Li, Anthony Villa, Colleen Gownley, Myong Jin Kim, Jinmei Song, Manfred Auer, and Da-Neng Wang. Monomeric state and ligand binding of recombinant GABA transporter from *Escherichia coli*. *FEBS letters*, 494(3):165–169, 2001.

[83] Anatoli N Lopatin, Elena N Makhina, and Colin G Nichols. Potassium channel block by cytoplasmic polyamines as the mechanism of intrinsic rectification. *Nature*, 372(6504):366–369, 1994.

[84] Dale DO Martin, Madhu S Budamagunta, Robert O Ryan, John C Voss, and Michael N Oda. Apolipoprotein AI assumes a “looped belt" conformation on reconstituted high density lipoprotein. *Journal of Biological Chemistry*, 281(29):20418–20426, 2006.

[85] Junichiro Miake, Eduardo Marbán, H Bradley Nuss, et al. Functional role of inward rectifier current in heart probed by Kir2.1 overexpression and dominant-negative suppression. *The Journal of clinical investigation*, 111(10):1529–1536, 2003.

[86] Alexandria N Miller and Stephen B Long. Crystal structure of the human two-pore domain potassium channel K2P1. *Science*, 335(6067):432–436, 2012.

[87] Abhinav Nath, William M Atkins, and Stephen G Sligar. Applications of phospholipid bilayer nanodiscs in the study of membranes and membrane proteins. *Biochemistry*, 46(8):2059–2069, 2007.

[88] CG Nichols and AN Lopatin. Inward rectifier potassium channels. *Annual Review of Physiology*, 59(1):171–191, 1997.

[89] Motohiko Nishida and Roderick MacKinnon. Structural basis of inward rectification: cytoplasmic pore of the G protein-gated inward rectifier GIRK1 at 1.8 Å resolution. *Cell*, 111(7):957–965, 2002.

[90] R Ohashi, H Mu, X Wang, Q Yao, and C Chen. Reverse cholesterol transport and cholesterol efflux in atherosclerosis. *Qjm*, 98(12):845–856, 2005.

[91] Stacey E Panagotopulos, Erica M Horace, J Nicholas Maiorano, and W Sean Davidson. Apolipoprotein AI adopts a belt-like orientation in reconstituted high density lipoproteins. *Journal of Biological Chemistry*, 276(46):42965–42970, 2001.

[92] Amanda Patel and Eric Honoré. The TREK two P domain K^+ channels. *The Journal of physiology*, 539(3):647–647, 2002.

[93] Amanda J Patel and Eric Honoré. Properties and modulation of mammalian 2P domain K^+ channels. *Trends in neurosciences*, 24(6):339–346, 2001.

[94] Amanda J Patel, Michel Lazdunski, and Eric Honoré. Lipid and mechano-gated 2P domain K^+ channels. *Current opinion in cell biology*, 13(4):422–428, 2001.

[95] Jennifer J Paynter, Isabelle Andres-Enguix, Philip W Fowler, Stephen Tottey, Wayland Cheng, Decha Enkvetchakul, Vassiliy N Bavro, Yoshio Kusakabe, Mark SP Sansom, Nigel J Robinson, Colin G Nichols, and Stephen J Tucker. Functional complementation and genetic deletion studies of KirBac channels: Activatory mutations highlight gating-sensitive domains. *Journal of biological chemistry*, 285(52):40754–40761, 2010.

[96] Gadi Peleg, Pejman Ghanouni, Brian K Kobilka, and Richard N Zare. Single-molecule spectroscopy of the β2 adrenergic receptor: Observation of conformational substates in a membrane protein. *Proceedings of the National Academy of Sciences*, 98(15):8469–8474, 2001.

[97] L Revell Phillips, Decha Enkvetchakul, and Colin G Nichols. Gating dependence of inner pore access in inward rectifier K^+ channels. *Neuron*, 37(6):953–962, 2003.

[98] Paula L Piechotta, Markus Rapedius, Phillip J Stansfeld, Murali K Bollepalli, Gunter Erhlich, Isabelle Andres-Enguix, Hariolf Fritzenschaft, Niels Decher, Mark SP Sansom, Stephen J Tucker, et al. The pore structure and gating mechanism of K2P channels. *The EMBO journal*, 30(17):3607–3619, 2011.

[99] Peter Proks, Jennifer F Antcliff, Jonathan Lippiat, Anna L Gloyn, Andrew T Hattersley, and Frances M Ashcroft. Molecular basis of Kir6.2 mutations associated with neonatal diabetes or neonatal diabetes plus neurological features. *Proceedings of the National Academy of Sciences of the United States of America*, 101(50):17539–17544, 2004.

[100] Matthias Quick and Jonathan A Javitch. Monitoring the function of membrane transport proteins in detergent-solubilized form. *Proceedings of the National Academy of Sciences*, 104(9):3603–3608, 2007.

[101] Markus Rapedius, Philip W Fowler, Lijun Shang, Mark SP Sansom, Stephen J Tucker, and Thomas Baukrowitz. H bonding at the helix-bundle crossing controls gating in Kir potassium channels. *Neuron*, 55(4):602–614, 2007.

[102] Markus Rapedius, Jennifer J Paynter, Philip W Fowler, Lijun Shang, Mark SP Sansom, Stephen J Tucker, and Thomas Baukrowitz. Control of pH and PIP. *Channels*, 1(5):327–330, 2007.

[103] TK Ritchie, YV Grinkova, TH Bayburt, IG Denisov, JK Zolnerciks, WM Atkins, and SG Sligar. Reconstitution of membrane proteins in phospholipid bilayer nanodiscs. *Methods in enzymology*, 464:211–231, 2009.

[104] Inbal Riven, Eli Kalmanzon, Lior Segev, and Eitan Reuveny. Conformational rearrangements associated with the gating of the G protein-coupled potassium channel revealed by FRET microscopy. *Neuron*, 38(2):225–235, 2003.

[105] Benoît Roux. What can be deduced about the structure of *Shaker* from available data? In *Ion Channels: From Atomic Resolution Physiology to Functional Genomics: Novartis Foundation Symposium 245*, pages 84–108. Wiley Online Library, 2002.

[106] Henry Sackin, Mikheil Nanazashvili, Lawrence G Palmer, M Krambis, and DE Walters. Structural locus of the pH gate in the Kir1.1 inward rectifier channel. *Biophysical journal*, 88(4):2597–2606, 2005.

[107] Yusdi Santoso, Catherine M Joyce, Olga Potapova, Ludovic Le Reste, Johannes Hohlbein, Joseph P Torella, Nigel DF Grindley, and Achillefs N Kapanidis. Conformational transitions in DNA polymerase I revealed by single-molecule FRET. *Proceedings of the National Academy of Sciences*, 107(2):715–720, 2010.

[108] Jere P Segrest, Stephen C Harvey, and Vassilis Zannis. Detailed molecular model of apolipoprotein AI on the surface of high-density lipoproteins and its functional implications. *Trends in cardiovascular medicine*, 10(6):246–252, 2000.

[109] Paul R Selvin and Taekjip Ha. *Single-molecule techniques: a laboratory manual*. Cold Spring Harbor Laboratory Press Cold Spring Harbor, NY:, 2008.

[110] Andrew W Shaw, Mark A McLean, and Stephen G Sligar. Phospholipid phase transitions in homogeneous nanometer scale bilayer discs. *FEBS letters*, 556(1):260–264, 2004.

[111] Amy Y Shih, Ilia G Denisov, James C Phillips, Stephen G Sligar, and Klaus Schulten. Molecular dynamics simulations of discoidal bilayers assembled from truncated human lipoproteins. *Biophysical journal*, 88(1):548–556, 2005.

[112] Alois Sonnleitner, Lidia M Mannuzzu, Susumu Terakawa, and Ehud Y Isacoff. Structural rearrangements in single ion channels detected optically in living cells. *Proceedings of the National Academy of Sciences*, 99(20):12759–12764, 2002.

[113] Si Sun, Jo Han Gan, Jennifer J Paynter, and Stephen J Tucker. Cloning and functional characterization of a superfamily of microbial inwardly rectifying potassium channels. *Physiological genomics*, 26(1):1–7, 2006.

[114] Gayathri Swaminath, Yang Xiang, Tae Weon Lee, Jacqueline Steenhuis, Charles Parnot, and Brian K Kobilka. Sequential binding of agonists to the β2 adrenoceptor kinetic evidence for intermediate conformational states. *Journal of Biological Chemistry*, 279(1):686–691, 2004.

[115] Ignacio Tinoco and Ruben L Gonzalez. Biological mechanisms, one molecule at a time. *Genes & development*, 25(12):1205–1231, 2011.

[116] M Alejandra Tricerri, Andrea K Behling Agree, Susana A Sanchez, Jared Bronski, and Ana Jonas. Arrangement of apolipoprotein AI in reconstituted high-density lipoprotein disks: an alternative model based on fluorescence resonance energy transfer experiments. *Biochemistry*, 40(16):5065–5074, 2001.

[117] Martin Tristani-Firouzi, Judy L Jensen, Matthew R Donaldson, Valeria Sansone, Giovanni Meola, Angelika Hahn, Said Bendahhou, Hubert Kwiecinski, Anna Fidzianska, Nikki Plaster, et al. Functional and clinical characterization of KCNJ2 mutations associated with LQT7 (Andersen syndrome). *The Journal of clinical investigation*, 110(3):381–388, 2002.

[118] Stephen J Tucker and Thomas Baukrowitz. How highly charged anionic lipids bind and regulate ion channels. *The Journal of general physiology*, 131(5):431–438, 2008.

[119] Serdar Uysal, Luis G Cuello, D Marien Cortes, Shohei Koide, Anthony A Kossiakoff, and Eduardo Perozo. Mechanism of activation gating in the full-length KcsA K^+ channel. *Proceedings of the National Academy of Sciences*, 108(29):11896–11899, 2011.

[120] Pavel Vesely and James B. Pawley (editor). *Handbook of Biological Confocal Microscopy*. Springer Science Business Media, 2007.

[121] James T Vivian and Patrik R Callis. Mechanisms of tryptophan fluorescence shifts in proteins. *Biophysical journal*, 80(5):2093–2109, 2001.

[122] Erik Wallin and Gunnar Von Heijne. Genome-wide analysis of integral membrane proteins from eubacterial, archaean, and eukaryotic organisms. *Protein Science*, 7(4):1029–1038, 1998.

[123] Shizhen Wang, Sun-Joo Lee, Sarah Heyman, Decha Enkvetchakul, and Colin G Nichols. Structural rearrangements underlying ligand-gating in Kir channels. *Nature communications*, 3:617, 2012.

[124] Shizhen Wang, Elena N Makhina, Ricard Masia, Krzysztof L Hyrc, Mary Lynn Formanack, and Colin G Nichols. Domain organization of the ATP-sensitive potassium channel complex examined by fluorescence resonance energy transfer. *Journal of Biological Chemistry*, 288(6):4378–4388, 2013.

[125] Yong Wang, Yanxin Liu, Hannah A DeBerg, Takeshi Nomura, Melinda Tonks Hoffman, Paul R Rohde, Klaus Schulten, Boris Martinac, and Paul R Selvin. Single molecule FRET reveals pore size and opening mechanism of a mechano-sensitive ion channel. *eLife*, 3, 2014.

[126] Cindy Weitzman, Thomas G Consler, and H Ronald Kaback. Fluorescence of native single-Trp mutants in the lactose permease from *Escherichia coli*: Structural properties and evidence for a substrate-induced conformational change. *Protein Science*, 4(11):2310–2318, 1995.

[127] Matthew R Whorton and Roderick MacKinnon. Crystal structure of the mammalian GIRK2 K^+ channel and gating regulation by G proteins, PIP_2, and sodium. *Cell*, 147(1):199–208, 2011.

[128] Matthew R Whorton and Roderick MacKinnon. X-ray structure of the mammalian GIRK2-G-protein complex. *Nature*, 498(7453):190–197, 2013.

[129] David S Wishart, Craig Knox, An Chi Guo, Savita Shrivastava, Murtaza Hassanali, Paul Stothard, Zhan Chang, and Jennifer Woolsey. Drugbank: a comprehensive resource for in silico drug discovery and exploration. *Nucleic acids research*, 34(suppl 1):D668–D672, 2006.

[130] Jianhua Wu, Stathis Frillingos, John Voss, and H Ronald Kaback. Ligand-induced conformational changes in the lactose permease of *Escherichia coli*: Evidence for two binding sites. *Protein Science*, 3(12):2294–2301, 1994.

[131] Jianhua Wu and H Ronald Kaback. Cysteine 148 in the lactose permease of *Escherichia coli* is a component of a substrate binding site: Site-directed fluorescence studies. *Biochemistry*, 33(40):12166–12171, 1994.

[132] Xiaojie Yao, Charles Parnot, Xavier Deupi, Venkata RP Ratnala, Gayathri Swaminath, David Farrens, and Brian Kobilka. Coupling ligand structure to specific conformational switches in the β2-adrenoceptor. *Nature chemical biology*, 2(8):417–422, 2006.

[133] Zhenwei Yao and Monica Olvera de la Cruz. Ruled surface underlying KcsA potassium channels. *Soft matter*, 10(4):540–543, 2014.

[134] Wei Zhou and Lily Jan. A twist on potassium channel gating. *Cell*, 141(6):920–922, 2010.

[135] Yufeng Zhou, Joao H Morais-Cabral, Amelia Kaufman, and Roderick MacKinnon. Chemistry of ion coordination and hydration revealed by a K^+ channel–Fab complex at 2.0 Å resolution. *Nature*, 414(6859):43–48, 2001.

[136] Lejla Zubcevic, Vassiliy N Bavro, Joao RC Muniz, Matthias R Schmidt, Shizhen Wang, Rita De Zorzi, Catherine Vénien-Bryan, Mark SP Sansom, Colin G Nichols, and Stephen J Tucker. Control of KirBac3.1 potassium channel gating at the interface between cytoplasmic domains. *Journal of Biological Chemistry*, 289(1):143–151, 2014.